

MICHAEL BRAIAN

DIGITAL DENTISTRY

Studies on the trueness and precision of additive manufacturing and intraoral scanning



DIGITAL DENTISTRY

Malmö University, Faculty of Odontology
Doctoral Dissertation 2018

© Copyright Michael Braian 2018
Photographs and illustrations: Michael Braian
ISBN 978-91-7104-940-7 (print)
ISBN 978-91-7104-941-4 (pdf)
Holmbergs, Malmö 2018

MICHAEL BRAIAN
DIGITAL DENTISTRY

Studies on the trueness and precision of additive
manufacturing and intraoral scanning

Malmö University, 2018
Department of fixed prosthodontics
Faculty of Odontology

The publication is also available in electronic format at
muep.mau.se

“Set your goal and conquer it”
Mohsen and Parvin Braian

TABLE OF CONTENTS

LIST OF PUBLICATIONS	11
THESIS AT A GLANCE	12
ABSTRACT	14
POPULÄRVETENSKAPLIG SAMMANFATTNING	17
ABBREVIATIONS AND DEFINITIONS	19
INTRODUCTION	21
Metrology	21
Accuracy and Precision	21
Repeatability and Reproducibility	22
Validation	23
Measurements	23
Tolerance, allowance and clearance	24
CONVENTIONAL WORKFLOW FOR FIXED PROSTHODONTICS	26
Conventional impression	26
Stone model	28
Die processing	28
Wax up	29
Investment	29
Casting	30
Post-processing	30
PARTIALLY DIGITAL WORKFLOW FIXED PROSTHODONTICS ..	31
Extraoral scanner	31
Hardware	31
Performance	32

COMPLETELY DIGITAL WORKFLOW FOR FIXED PROSTHODONTICS	33
Intraoral scanner	33
History	33
Light source	33
Working principles	34
Triangulation	34
Confocal microscopy	35
Data processing	35
Point cloud	35
Post-processing	36
Scanning strategy	38
Accuracy of intraoral scanners	40
Computer-aided design	41
Design perimeters	42
Computer-aided manufacturing	43
Subtractive manufacturing	44
Accuracy of subtractive manufacturing	46
Additive manufacturing	46
History	46
Product development	47
The STL file	48
Fabrication principles	48
Additive manufacturing applications in dentistry	49
Accuracy of additive manufacturing of polymer constructions ..	50
Build orientation	51
Accuracy of additive manufacturing of metallic constructions ..	52
DIGITAL VERSUS CONVENTIONAL WORKFLOW	53
Production tolerances in dentistry	54
Marginal fit	54
Final remarks	55
HYPOTHESIS	56
SPECIFIC AIM	57
MATERIALS AND METHODS	58
Study I	58
Study II	62
Study III	67
Study IV	70

RESULTS	73
Study I	73
Study II.....	75
Study III.....	80
Study IV	89
DISCUSSION.....	95
Discussion on methods	95
Study I	95
Studies II and III.....	101
Study IV	110
Discussions on results	117
Study I	117
Studies II and III.....	118
Linear measurements	118
Degree and corner radius measurements	122
Inter-observatory variability	125
Study IV	126
CONCLUSIONS.....	130
ACKNOWLEDGEMENTS	131
REFERENCES	132
PAPERS I-IV.....	143

LIST OF PUBLICATIONS

- I. Tolerance measurements on internal- and external-hexagon implants. Braian M, De Bruyn H, Fransson H, Christersson C, Wennerberg A. *Int J Oral Maxillofac Implants*. 2014 Jul-Aug;29(4):846-52.
- II. Production tolerance of additive manufactured polymeric objects for clinical applications. Braian M, Jimbo R, Wennerberg A. *Dent Mater*. 2016 Jul;32(7):853-61
- III. Geometrical accuracy of metallic objects produced with additive or subtractive manufacturing: A comparative in vitro study. Braian M, Jönsson D, Kevci M, Wennerberg A. *Dent Mater*. 2018 Jul;34(7):978-993
- IV. Trueness and precision of five intraoral scanners on scanning edentulous and dentated full arch mandibular casts: A comparative in vitro study. Braian M. DDS, CDT, Wennerberg A, DDS, Ph.D. Accepted, *journal of prosthetic dentistry*

THESIS AT A GLANCE

I

To present the horizontal clearance of the interface between internal-hexagon and external-hexagon implants and analogues with corresponding cylindric gold and plastic abutments upon delivery from the implant manufacturer.

II

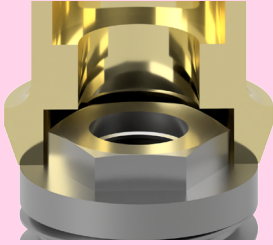
To determine the production accuracy of four commercially available polymeric additive manufacturing systems by reverse engineering two geometrical objects.

III

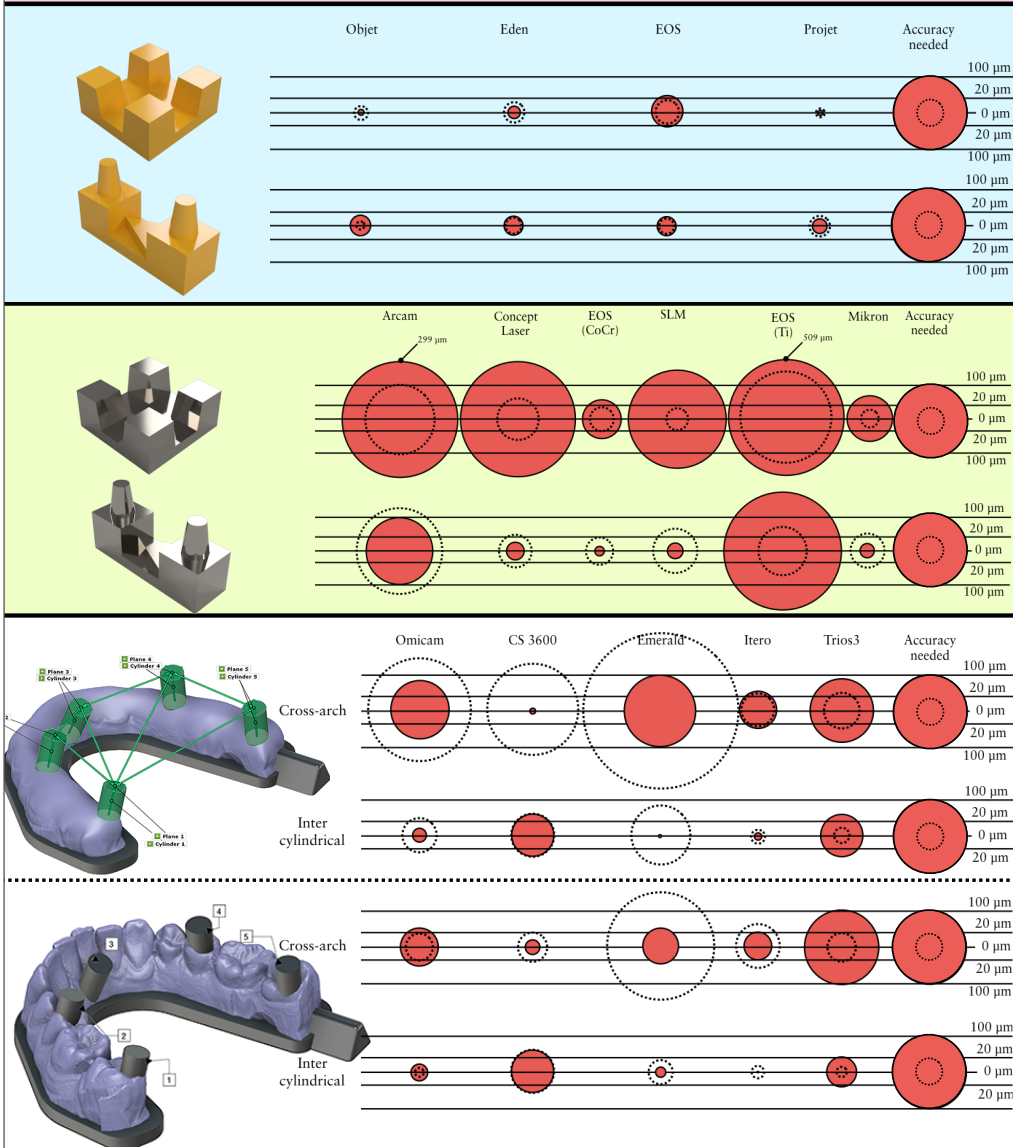
To evaluate the production accuracy of five additive manufacturing systems and one subtractive manufacturing system for the production of metallic components by reverse engineering two geometrical objects

IV

To study the accuracy of four different intraoral scanners for full-arch scanning of one edentulous model and one dentated model.



Prefabricated gold abutment on internal-hexagon implants showed tolerances $<90 \mu\text{m}$. In contrast, prefabricated plastic cylinders showed errors of $<100 \mu\text{m}$ for external-hexagon implants and $<130 \mu\text{m}$ for internal-hexagon implants.



ABSTRACT

Artificial designs and features usually control production workflows in the industry. The operator has the freedom to adapt designs to achieve the desired function; when the operator is satisfied, mass production of the two objects is possible. The production workflow for prosthetic restorations in dentistry is a fairly complicated procedure that requires several well-controlled processes, and each unit is individually adapted to one unique situation. The aim of the final restoration is to replace damaged or missing soft and hard tissue, and to restore function, phonetics and aesthetics. The restoration has high material property requirements in order to withstand high forces, thermal changes, aging and humidity. If the fit of the reconstruction is insufficient there is a high probability for clinical failures ranging from inflammatory processes to reconstruction fractures. The grading of perfect, sufficient and insufficient fit is unknown although the definition clinically acceptable fit has been used to describe and control a reconstruction that is well seated and controllable by the clinician. Study I in this thesis focuses on the clearance (play) between different implant components in order to achieve a threshold value for how accurate the production in dentistry needs to be. We found that metallic components on external hex connections have a clearance of approximately 50 μm .

Not only is every case individually designed and manufactured, but the receiving intraoral part also needs to be replicated into an extraoral part ahead of production, a procedure that has been possible with different impression materials. Subsequently, the production

goes through a series of controlled compensations to fit the intraoral situation. The conventional workflow starts by the selection of an impression tray, ranging from custom-made trays to plastic stock trays. The ideal trays are rigid, thereby minimising flexure during the impression taking. There are several types of impression materials with different properties regarding setting time, volume changes and mechanical properties. The next step in the conventional workflow is the casting of the impression. There are various types of gypsum products utilised in dentistry, and they require different amounts of water. The differences depend on the shape and compactness of the crystals. Type IV dental stone gypsum is often used in reconstructive dentistry with a typical setting expansion of 0.10%. For the partial digital workflow the same volume changes can be seen for the conventional impression, the stone model production and the die processing. In order to design the intended construction digitally instead of using wax, the model needs to be digitised in an extraoral scanner, also known as desktop scanner.

The fully digital workflow consists of a direct digitisation of the oral cavity utilising intraoral scanning devices. All intraoral scanners have the same goal, to digitise the size, shape and surface of a physical object into a geometrical virtual shape. This acquisition needs to be repeatable, reproducible and accurate. The IOS manufacturers try to achieve these goals with different hardware and software setups. Study IV focuses on the acquisition accuracy of five different intraoral scanners for the digitisation of edentulous and dentated models. The results suggest that the devices had lower accuracy for the digitisation of the edentulous models when compared to the dentated model. Furthermore, Study IV presented observations suggesting that full-arch scans had lower accuracy when compared to shorter arch scans on both models. For the cross-arch measurements on the edentulous scans, the trueness values ranged from 6 μm to 193 μm , and, for the shorter arch measurements, the results ranged from 2 μm to 103 μm . For the dentated cast, the cross-arch trueness values ranged from 6 μm to 150 μm , and, for the shorter arch measurements, the results ranged from 4 μm to -56 μm .

The digitised file is then utilised as a virtual model by a computer-aided designer in order to virtually design the intended reconstruction. The designed file is then manufactured utilising computer-aided manufacturing, which can be performed either by a subtractive machine (milling) or by additive systems (3D printing). Study II and Study III explore the production tolerances for producing polymeric and metallic objects from additive systems. Study III also contained a subtractive group. The results from these two studies suggest that all tested additive systems for producing polymeric objects were, on average, $<20\ \mu\text{m}$ for both precision and trueness, and the additive systems for manufacturing metallic objects ranged from $>500\ \mu\text{m}$ to $<30\ \mu\text{m}$ in trueness, with precision values of $<100\ \mu\text{m}$. The subtractive system showed trueness values of $<25\ \mu\text{m}$ with a precision around $20\ \mu\text{m}$.

POPULÄRVETENSKAPLIG SAMMANFATTNING

Vid mindre tandskador och hål i tänderna, kan tandläkaren laga dessa direkt inne i munnen med plastfyllningar. Men om skadan är större, eller om tanden är så pass skadad att den måste dras ut, måste tandvården använda sig av andra material för att återskapa den förlorade tanden. Vid större skador får man oftast tillverka en krona eller en bro, en krona ersätter skador på en tand och en bro ersätter en eller flera förlorade tänder. Kronor och broar kan inte tillverkas direkt i munnen, dessa måste framställas av en tandtekniker i ett tandtekniskt laboratorium. För att kunna göra detta måste tandteknikern ha en gipsmodell av patientens tänder. I decennier har tandläkarna tagit avtryck med en metallsked i patientens mun och sedan skickat det avtrycket till tandteknikern som i sin tur hållt i gips för att framställa modellen. Därefter använder tandteknikern vax för att bygga upp det som saknas och med hjälp av gjutning kan man sedan få fram ett metallskelett. På metallskelettet lägger man porslin för att efterlikna vanliga tänder. Idag finns det modernare tekniker för tandvården att använda, både för tillverkningen och för avtrycket. En studie i avhandlingen har undersökt hur pass bra en 3D scanner kan avbilda patientens tänder. I stort sett filmar då tandläkaren tänderna från alla möjliga vinklar, sedan sätts filmen ihop till en tredimensionell digital modell, som skickas över internet till tandteknikern. Tandteknikerna kan sedan forma kronan eller bron direkt i datorn, när formen är klar kan denna framställas i en datorstyrd fräsmaskin eller av en 3D printer. Två av avhandlingens

studier har tittat på hur pass bra olika 3D printrar är på att framställa relevanta former. Ingen av studierna har gjorts inne i munnen på patienter, så man bör vara lite försiktig med att dra för stora slutsatser. Avhandlingen visar dock på att både 3D scanningen och 3D printrarna har stor potential att kunna ersätta eller komplettera det traditionella sättet att framställa kronor och broar.

ABBREVIATIONS AND DEFINITIONS

Accuracy	Closeness of agreement between a measured quantity value and a true quantity value of a measurement
Allowance	Amount of designed intentional deviation
AM	Additive manufacturing
CAD	Computer-aided design or computer-assisted design
CAM	Computer-aided manufacturing or computer-assisted manufacturing
Clearance	The distance between two mating dimensions
DLP	Digital light processing
DMLS	Direct metal laser sintering
IOS	Intraoral scanner
Precision	Closeness of agreement between measured quantity values obtained by replicate measurements on the same or similar objects under specified conditions
Repeatability	Condition of measurement, out of a set of conditions that includes the same measurement procedure, operators, measuring system, operating conditions and location, and replicates measurements on the same or similar objects over a short period of time
Reproducibility	Condition of measurement, out of a set of conditions that includes different locations, operators, measuring systems, and replicate measurements on the same or similar objects
SLA	Stereolithography
SLM	Selective laser melting

SLS	Selective laser sintering
SM	Subtractive manufacturing
STL	Standard tessellation language or stereolithography
STEP	Standard for the exchange of product model data
Tolerance	Total amount that a specific dimension is permitted to vary
Traceability	Property of a measurement result whereby the result can be related to a reference through a documented unbroken chain of calibrations, each contributing to the measurement uncertainty
Trueness	Closeness of agreement between the average of an infinite number of replicate measured quantity values and a reference quantity value

INTRODUCTION

Metrology

Metrology is the science of measurement and its applications. The measure is used to communicate size, quantity, position, condition and time.

Accuracy and Precision

Two terms are central to understanding metrology: accuracy and precision. Accuracy relates to the closeness of a measured value to a standard or a known (true) value, whereas precision pertains to the closeness of measured values to each other. Figure 1 illustrates the correlation between these two terms, if the centre of the target would be referred to as the true value or the standard, then Figure 1a shows a result that has both low accuracy and precision. In contrast, Figure 1d illustrates results that are both accurate and precise. When conducting research, it is normal to calculate the standard deviation (SD) and the mean value of a measurement (mean). Relating these two terms to the metrological nomenclature would correlate the mean value as accuracy and the standard deviation to precision. ISO 5725-1[1] uses two terms to describe accuracy; the first is precision and the second is trueness. Trueness is described as closeness of agreement between the calculated mean from several measurements in comparison with a true or accepted reference value. If ISO 5725-1 is used as reference, then all accuracy legends in Figure 1 would change to trueness and image d) would be regarded as accurate and a) as not accurate, meanwhile image b) would be described as having a low trueness; the shooter is precise but not accurate. Only Study IV in this thesis has used the ISO 5725-1 definition.

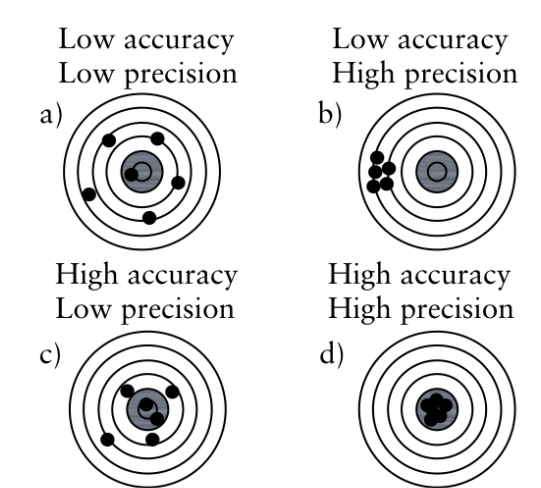


Figure 1. Illustration of the correlation between accuracy and precision.

Repeatability and Reproducibility

The typical term for irregularity between repeated measurements is precision. For describing the irregularity of a measurement method two conditions of precision have been found necessary, termed repeatability and reproducibility. Under repeatability conditions, the following factors:

1. Operator
2. Equipment used
3. Equipment calibration
4. Environment (temperature, humidity, air pollution, and so forth)
5. Time elapsed between measurements

are considered constants and do not contribute to the variability, while, under reproducibility conditions, they vary and do contribute to the irregularity of the test results. Hence, repeatability and reproducibility are the two extremes of precision, with the first describing the lowest and the second the highest variability in results [1].

Validation

Figure 1a would illustrate measuring equipment that has low accuracy and precision for measuring that specific object. It could also mean that the objects being measured are both manufactured inaccurately and imprecisely. To remove one of these errors, the measurement equipment should be validated if the true value (bull's eye) is exactly $10 \text{ mm} \pm 0.10 \text{ mm}$, the measuring device should be validated to be greater. The validation is also referred to as quality assurance or quality control. The process of quality assurance would require the operator to measure an object with known dimensions to validate the measuring equipment. One example of objects with known dimensions is gauge blocks; the reason why their dimensions are referred to as known is that they have been measured by measuring equipment with extreme accuracy, generally on an $\leq 1 \text{ }\mu\text{m}$ level.

Measurements

The core challenge of metrology is that the measuring tool used to measure an object must have a reference of greater accuracy, this is referred to as traceability. Without traceability, measurements are meaningless at best and could even be misleading. This means that the tool being used to measure an object requires the capability to measure that specific object with higher accuracy than the process in which it is going to be used. All measurements consist of the part, the measuring device and the standard or the known value, see Figure 2.

No measurements can be made with perfect accuracy. An instrument, when repeatedly subjected to the same input, may not indicate the same output. Response of an instrument may change with time due to wear. Environmental conditions such as temperature, pressure and humidity could affect the outcome. To achieve a reliable measurement, the operator needs to decrease possible errors by measuring room temperature, heat transformations, equipment conditions, and so forth.

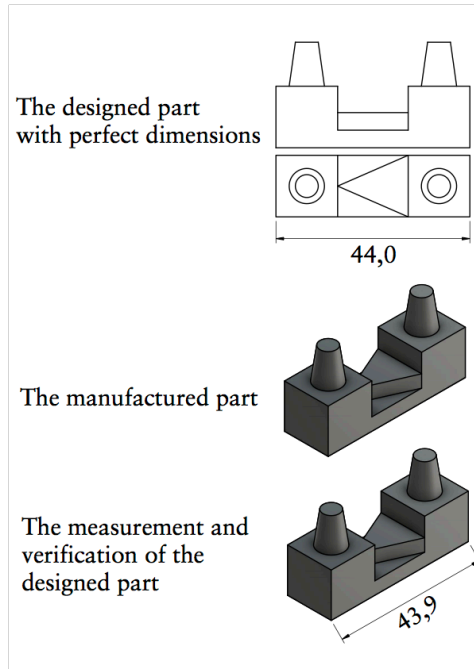


Figure 2. All measurements require these three elements.

Tolerance, allowance and clearance

Tolerance could also be described as “good enough”, i.e. all manufactured parts can vary in size or shape but still be satisfactory for their purpose. Tolerance is the total amount that a certain dimension is allowed to vary. Many objects such as drills, gears, threads and screws have specific tolerance requirements that are described by different standardisation organisations (United States Y14.5M and International Standards Organisation). Tolerance in manufacturing is strongly correlated to function, and the intended object should have good enough tolerances in order to function properly. On the contrary, allowance is when an operator intentionally over- or under-sizes a design in order to compensate for forthcoming machining procedures. One example would be the intended under-sizing of an object that will expand during a heat-treatment process. Clearance could be described as the air or space between two manufactured parts, as shown in Figure 3.

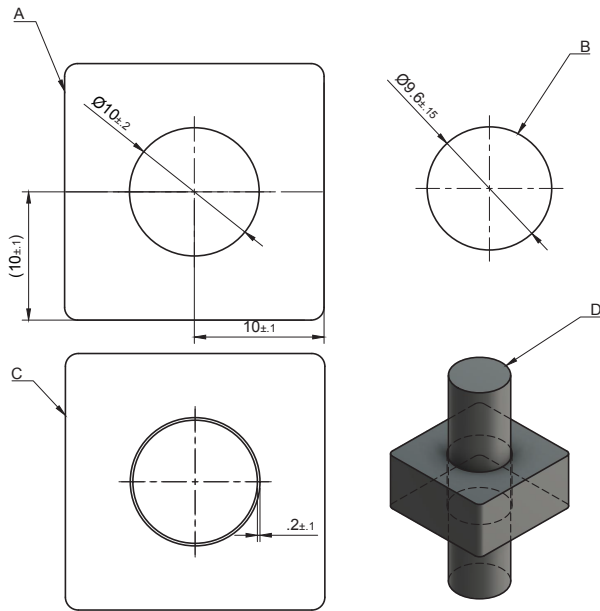


Figure 3. Example of the tolerance between a cylinder and a hole. The cylinder (D and B) is designed to move freely in the axial direction. In order to achieve this, there are production tolerance requirements for the manufacturing of the cylinder and the counterpart (A and C). In this example, clearance would be the air between the cylinder and the hole, while tolerance would be all the \pm markings.

CONVENTIONAL WORKFLOW FOR FIXED PROSTHODONTICS

Artificial designs and features usually control production workflows in the industry; Figure 3 shows a two-part object in which both the product features are designed and controlled digitally. The operator has the freedom to adapt both designs to achieve the desired function; when the operator is satisfied, mass production of the two objects is possible. In the field of dentistry, the construction manufacturing is adapted to a specific case individually. Not only is every case individually designed and manufactured, but the receiving intraoral part also needs to be replicated into an extraoral part ahead of production, a procedure that has been possible with different impression materials. Subsequently, the production goes through a series of controlled compensations to fit the intraoral situation (Figure 4).

Conventional impression

The conventional workflow is illustrated by green markings in Figure 4. The production starts by the selection of an impression tray, ranging from custom-made trays to plastic stock trays. The ideal trays are rigid, thereby minimising flexure during the impression taking[2]. There are several types of impression materials with different properties regarding setting time, volume changes and mechanical properties. Some of the elastomeric impression materials are made from polysulfide, condensation silicon, addition silicone or polyether materials. Studies have shown that different combinations of viscosity and impression techniques result in variances in accuracy. Satheesh

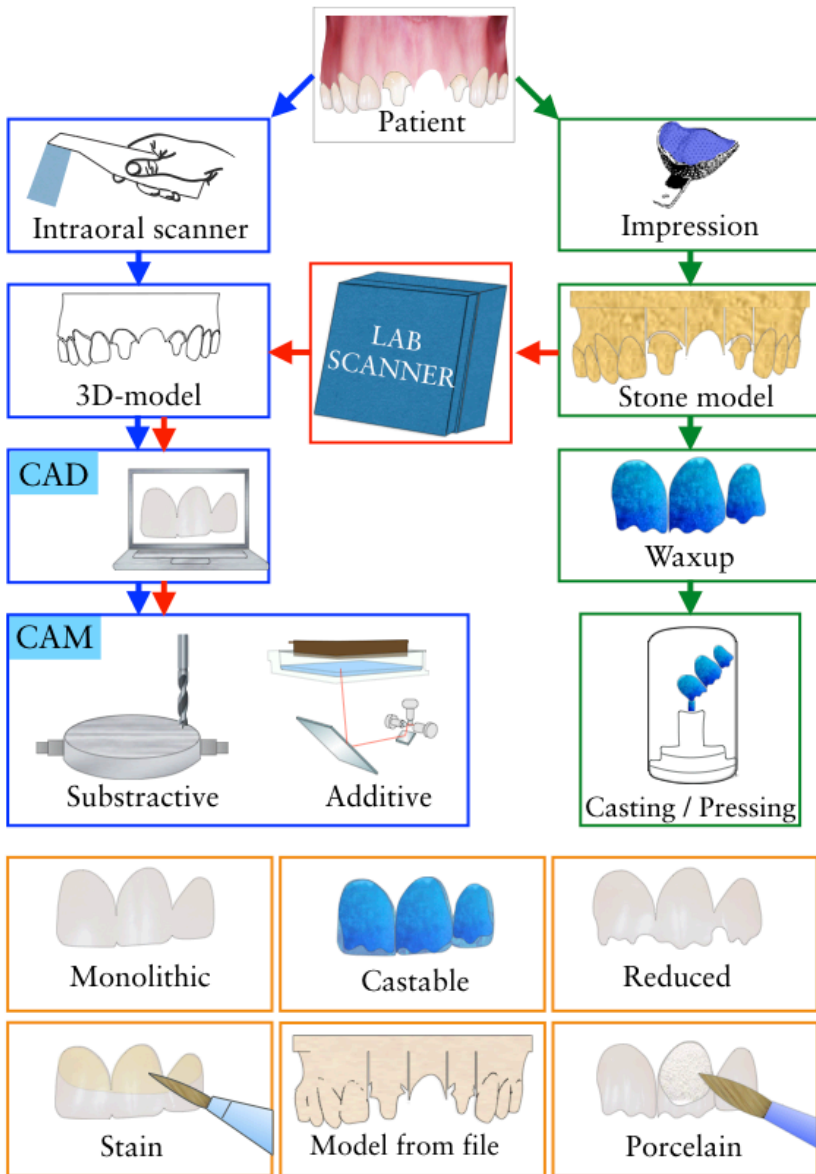


Figure 4. Production workflow illustration: the green markings illustrate the conventional workflow, the red markings, the partially digital workflow and the blue markings the digital workflow. The orange markings illustrate the outcome possibilities when utilising the different production techniques.

et al.[3] showed variations of volume changes ranging from 0.04% to 1.34% depending on impression material and impression technique utilised. The next step is the transportation of the impression to the dental technician. The findings from Murat *et al.*[4] suggest that storing time and humidity conditions affect the dimensional stability of the impression. One five-day test on an addition silicone material revealed mean differences immediately after impression at $43 \mu\text{m} \pm 162 \mu\text{m}$ to $0 \mu\text{m} \pm 191 \mu\text{m}$ five days later. Similar contraction settings after 24 hours could be found for polysulfide 0.40-0.45%, condensation silicone 0.38-0.60%, addition silicone 0.14-0.17% and for polyether 0.19-0.24%[5]

Stone model

The next step in the conventional workflow is the casting of the impression. There are various types of gypsum products utilised in dentistry, and they require different amounts of water. The differences depend on the shape and compactness of the crystals. The reaction between water and the crystals results in an exothermic heat reaction and expansion. Type IV dental stone gypsum is a strong material with minimal setting expansion, making it ideal as the foundation for the production of both fixed and removable prosthodontics. The required properties of type IV dental stone gypsum by the American Dental Association are a water powder ratio of 0.22-0.24 and a maximum two hour setting expansion of 0.10%[5]. After the setting of the stone model, the cast is segmented in one or several sections determined by the clinical case. Depending on the die system utilised, dimensional changes will occur ranging from 7 to 54 μm when comparing the pre-sectioning and post-sectioning dimensions of the stone model[6].

Die processing

When the sectioning is performed, the workflow continues with the addition of die hardener and spacer in order to achieve abrasion resistance and cement clearance between the die and intended construction. The die hardener could change the dimensions of the die by up to 0.16%[7]. The application of the die spacer is performed by painting on layers. The average thickness of one die spacer manufacturer (Nice Fit, gold; Shofu Inc. Kyoto, Japan) showed

a spacer thickness of $12.8 \pm 2.62 \mu\text{m}$ (2 coats), $26.80 \pm 3.90 \mu\text{m}$ (4 coats), and $38.09 \pm 4.26 \mu\text{m}$ (6 coats)[8].

Wax up

For indirect waxing technique, a type II wax is utilised. The wax is softened by heat, whereby it can be applied to the die. During the cooling and heating process the wax enters a liquid in a rigid state, at the same time it expands and contracts thermally pending between 0-1.0% [9]. When the desired shape of the reconstruction is achieved, the wax pattern is removed from the die. This procedure may result in a plastic deformation of the wax pattern most noticeable at the crown margin [10, 11].

Investment

There are two types of investment materials, based on gypsum or phosphate. Gypsum-based investment is used for the conventional casting of gold alloys, while phosphate bonded investment is used for metal ceramic constructions and for pressable ceramics. The investment materials are also sensitive to the water/powder ratios similar to the dental stone materials. Phosphate bonded investments undergo two dimensional changes – first there is a setting expansion and later a thermal expansion. Lloyd *et al.* [12] studied the setting expansion of different phosphate-based investments showing an expansion ranging from 0.78 to 3.3% depending on manufacturer, vacuum-mixing system and operator. Hutton *et al.* [13] studied the thermal expansion of phosphate bonded investments, finding expansions ranging from 1.01 to 1.71% depending on the manufacturer. The investment material is poured into a solid metal ring casting flask, and a ring liner is attached to the inside of the flask in order to allow expansion to the sides. The cylindrical openings allow expansion in the axial directions. This procedure is performed in order to allow a uniform expansion of the investment material (Figure 5).

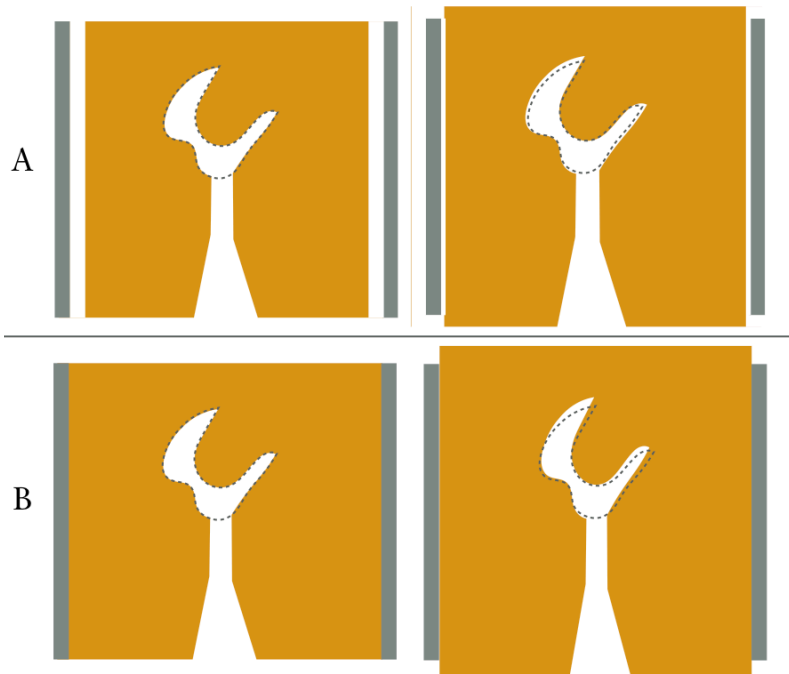


Figure 5. A) Illustrates a casting flask with liner. This allows for a uniform expansion. B) Illustrates the results without liner.

Casting

During the investment there are two steps of expansion, first a setting expansion and later a thermal expansion. Depending on investment material and temperatures, a linear expansion as high as 1.7% may be obtained. If the casted alloy has a casting shrinkage of less than 1.7%, the casted crown could be too large[14]. The volume compensations are dependent on investment material, setting expansion, thermal expansion, application of liner, and the casting shrinkage of the alloy.

Post-processing

The conventional workflow for fixed prosthodontics results in either a pressed ceramic core/full anatomic construction or an alloy-based core. For the production of core-based frameworks porcelain is added in order to achieve an aesthetic construction; full anatomic (monolithic) ceramic constructions could be stained for characteristics (Figure 4).

PARTIALLY DIGITAL WORKFLOW FIXED PROSTHODONTICS

Extraoral scanner

Figure 4 illustrates the conventional workflow for fixed prosthodontics in green, while the partially digital workflow is marked in red. For the partially digital workflow the same volume changes can be seen for the conventional impression, the stone model production and the die processing. It is also possible to scan the conventional impression directly, avoiding the stone model production. In order to design the intended construction digitally instead of using wax, the model needs to be digitised in an extraoral scanner, also known as a desktop scanner. There are two different types of extraoral digitising devices utilised to digitise dental stone models; optical and mechanical. The mechanical scanners collect data with a tactile method by touching the surface of the stone model, while the optical scanners employ a light source and cameras for triangulation. Accordingly, the optical scanner will be in focus.

Hardware

Extraoral dental laboratory scanners consist of a light source, receptor and a positioning system that orientate the object being digitised in different axes. The light source projects thin lines onto the object, when the light hits the surface it forms a profile; at the same time the receptor assesses the situation. In order to acquire a geometry with undercuts the object needs to be turned towards the light source, or vice versa[15]. The angle and distance between the light source and receptor are known, making it possible to measure objects

calculating the trigonometry, also known as triangulation[16]. The light source consists of either a laser or white light, the combination of light source and the reflective surface properties of the object being digitised are of importance for accuracy[17]. The extraoral scanners have a systematic digitising strategy because of the automatic surface projection, and the computer-controlled turntable that systematically coordinates the movement in collaboration with the receptor and the light source[18].

Performance

Several studies have tested the extraoral scanners utilised in dentistry for trueness and precision. Mandelli *et al.*[19] studied seven scanners utilising a standardised master model. Two of the scanners tested utilised lasers as a light source and the other five utilised structured light. All the tested scanners showed trueness values $<20\ \mu\text{m}$ with precision values ranging from 3.8 to 19.8 μm . Similar findings were shown by Luthardt *et al.*[20] with average trueness at 18.8 μm with a precision at 1 μm . Su *et al.* [21] compared intraoral scanning and extraoral scanning on five different reference models; their findings for the extra oral devices ranged from 8.67 to 24.33 μm (mean) with SD values ranging from 0.71 to 3.46 μm .

COMPLETELY DIGITAL WORKFLOW FOR FIXED PROSTHODONTICS

Intraoral scanner

History

In 1970, Francois Duret presented a concept of how to utilise scanning technologies from industry adapted for dentistry. His idea was to digitise preparations optically with a laser and then mill the final restoration, a process generally known as computer-aided design and computer manufacturing for dental restorations. The concept was further developed in the 1980s by Werner Mörmann and Marco Brandestini, who scanned their first patient in December the same year. Two years later (1982) the first handheld scanner for intraoral use was developed, and, by 1983, the first optical impression of an inlay was utilised. By 1985, the first functional intraoral scanner (IOS) was commercially available through CEREC 1 (Sirona, Bensheim, Germany)[22].

Light source

All intraoral scanners have the same goal, to digitise the size, shape and surface of a physical object into a geometrical virtual shape. This acquisition needs to be repeatable, reproducible and accurate. The IOS manufacturers try to achieve these goals with different hardware and software setups. There are two basic acquisition steps, firstly the scanner utilises some kind of optical light to capture the object. This light could either be active or passive. The passive light uses ambient light and is reliant on the texture of the object being digitised. The active light is either white, red or blue structured and is less reliant on

the texture of what is being digitised[16]. In the active technique, a luminous point is projected onto the object being digitised, this point is then captured by the receptor, making it possible to calculate the distance through triangulation. The surface acquisition consists of either images or a video (made from different frame rates). All these techniques are based on reflections from the surface of what is being scanned. For intraoral use there are many challenging surfaces such as blood, saliva, metals, composite surfaces, enamel, dentine, soft tissue and different light conditions depending on operator unit and office light[18]. Some manufacturers recommend the application of a powder on the surfaces before scanning. This procedure changes the reflective properties of the surfaces and simplifies the acquisition[23]. The powder application procedure could change the surface geometry by up to 40 μm depending on how the powder is applied[24]. Another strategy to overcome the reflective surfaces in the oral cavity is the use of polarizing filters[16].

Working principles

Triangulation

Also known as trigonometry, this is a measuring principle for optical systems to acquire the distance to the object being digitised. There are two types of triangulation, passive and active. The active method is the most utilised in dentistry because passive triangulation requires high contrast targets to work satisfactorily, and is thus not suitable for intraoral use[25]. In the active version a laser beam is deflected by a mirror, and the laser hits the surface and illuminates the object being digitised. A receptor registers the illuminated area; because of the fixed relation between laser and receptor a triangle is shaped and the distance to the object is possible to calculate. To speed up the process a series of patterns are projected onto the object instead of a laser dot. This is called the structured light method, consisting of an image of black and white lines that are projected onto the surface. If the scanned object is flat the receptor will register perfectly straight lines. If something is obstructing the lines the receptor will register deformed lines, thus making it possible to calculate the line deviations resulting in a surface topology[17]. Triangulation is not possible to conduct if the area being digitised is invisible to both, or either of, the laser or the receptor[26].

Confocal microscopy

This is a technique that acquires images on different focal depths. The lenses in confocal microscopy have a specific focal depth, and, when the digitised object is in focus, a 2D image is acquired. Then the camera is moved, thus a different area of the object will be in focus[16], resulting in several 2D images that are later software-processed. With mechanical systems adapting the lenses inside of the camera it is possible to acquire different focal depths faster, speeding up the acquisition process[26]. There are several other techniques utilised by different commercially available IOS devices.

Data processing

The digital data obtained from both intraoral scanners and extraoral scanners are represented by a point cloud; the digitising devices do not have the capability to acquire the whole surface of the object being digitised. Independent of light source and working principles, the virtual version of the digitised object will consist of points. The points represent the x, y and z coordinates of the digitised object.

Point cloud

The density of the point cloud depends on the digitising device and technique, operator, scan time, and software algorithms utilised by the manufacturer, along with the complexity and reflective properties of the geometry that is being digitised and many other parameters[17]. Figure 6 illustrates a test object digitised with a Trios (2nd generation 3Shape, Copenhagen, Denmark) the files have been manipulated for educational purposes. Figure 6a illustrates a very dense and unprocessed point cloud instantly after the acquisition, during calculation of the 2D images to 3D files. Each 2D image has to overlap the previous one; this procedure is often described as a stitching or the best fit algorithm. The alignment process is an important feature necessary to achieve an accurate 3D file. During this process unwanted scatter will ascend, because of dust, saliva, blood, reflections, humidity on the scanner mirrors and so forth. In the process of this sampling, the software tries to preserve the measured features by assessing the points and profile of surrounding points[27]. Figure 6b illustrates with red dots areas where the software algorithm has reduced deviant points in the cloud[18]. At the same

time areas missing point data will be calculated by the software and a polygonisation process will ensure that the surface is closed[17]. The intraoral scanners are not designed to assume specific shapes such as spheres or cylinders, with the exception of some scanners that adapt their reconstruction algorithm for scanning implant scan bodies. There are several types of reconstructive polygonisations but they all have one thing in common; they are estimating the geometry of the missing points[27].

The points in the cloud go through a triangulation process that converts the points to a polygonal model, also known as a mesh (Figure 6d, e). The mesh image from Figure 6d is simpler to observe compared to the dataset in Figure 6a. In Figure 6e the mesh model has a surface added, making it even easier to distinguish the geometries on that specific model. The surface texture of virtual 3D files simplifies for observers distinguishing between different shapes. Modern IOS has the possibility to colour the digitised version of whatever is scanned, making it even easier to distinguish between blood, saliva, enamel, dentine, and so forth.

Post-processing

There are several post-processing procedures available for the scanned virtual object. A virtual model with a high-density point cloud (Figure 6a, b), could display the scanned object sufficiently, but the file would be very big and difficult to work with without capable computers. This is an especially important aspect for scanners utilised in dentistry, because the file usually needs to be either sent to a dental technician or to a chairside manufacturing unit. If the files are too big they could obstruct a convenient workflow. At the same time, it is equally important that the file is accurate and reliable as a reference for the rest of the workflow. In order to reduce the file size and at the same time keep the 3D object intact, the IOS manufacturers utilise a polygon-editing operation, reducing the number of polygons and simultaneously preserving the shape of the object[27] Figures 6b and 6c illustrate the reduction of point cloud data. Flat surfaces require fewer polygons than curved surfaces to retain their shape. Typically, the areas with large 3D curvatures will keep many polygons after the polygon-editing process, which is illustrated in Figures 6h and 6i[16].

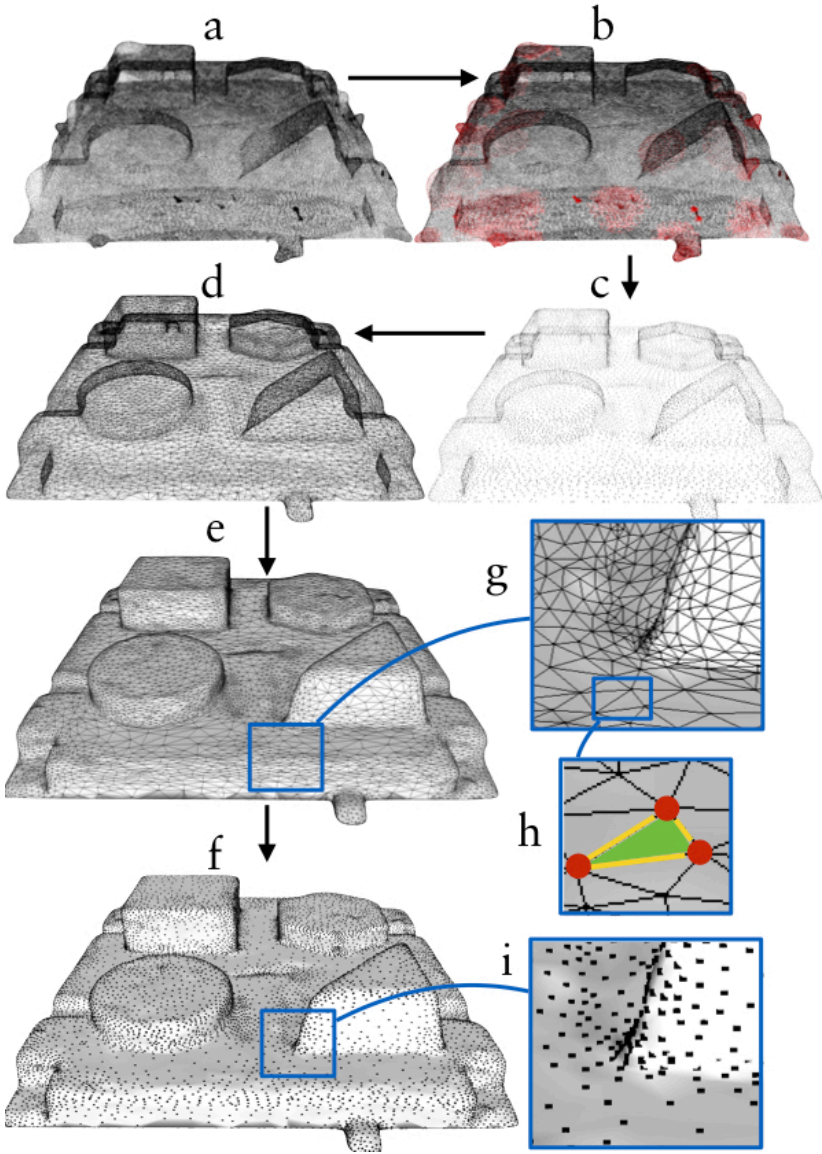


Figure 6. a) raw cloud file b) unnecessary cloud data (red) is removed c) simplified point cloud d) each point is bound by a line configuring a mesh of triangles e) a surface is added to each polygon (triangle) g) triangle shape h) red dots are vertices (points) yellow lines are edges f) combined image of surfaces and points (vertices) i) example of the software algorithm that keeps points in 3D curves and reduces them on moderate geometries.

One example of this feature is the software algorithm for the Trios (3Shape, Denmark, Copenhagen) scanners. At the beginning of the workflow the operator needs to decide on what type of reconstruction the intraoral impression will be utilised. If the operator selects, for instance, a crown preparation on tooth 11, the software will make sure to keep as many polygons in that area during the polygon-reduction process as possible, meanwhile the rest of the virtual model will have a reduced number of polygons[28].

Scanning strategy

Extraoral scanners usually have a disclosed chamber, where the object is placed inside of the chamber and the scanner is isolated. In this way, the environment can be controlled for temperature and light conditions. Furthermore, the digitisation is systematic and computer-controlled. When scanning a dental stone model, the lab scanners have the possibility to acquire large areas of the model on each image[29]. For intraoral scanning, however, this procedure is not possible. Instead, the operator needs to sweep over the tissues to acquire the images. Because of the optical technologies utilised in different intraoral scanners, the operator needs to keep a certain distance ranging from 5-30 mm to the tissues being digitised because of variations in focal depth [16]. The IOS heads are often small, thus each acquired image is small. Because of the stitching process described earlier, all the small images need to be aligned in order to achieve a full-scale model[16, 30]. The alignment of each image is achieved by software algorithms identifying comparable point cloud data on the two images. The alignment process is challenging if the operator scans a totally flat surface. In contrast, the alignment is easier to achieve if the surface has a complex organic shape, like an occlusal surface of a molar.

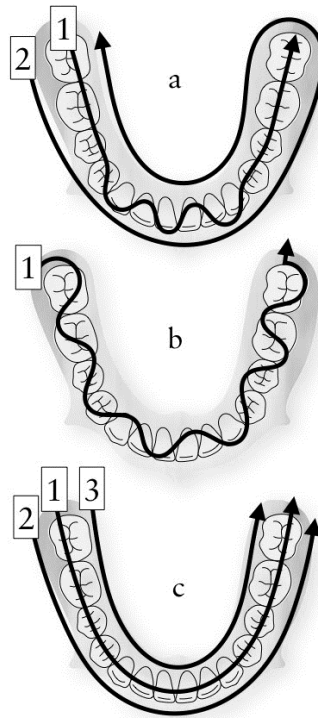


Figure 7. a) Scanning procedure with a wiggling motion in the incisal region. b) Zig-zag motion scanning. c) Occlusal, buccal and lingual procedure.

The scanning strategy, also known as scanning protocol or scan path, describes the acquisition process for intraoral scanning. One example would be to start scanning the occlusal surface in the maxilla from the posterior region to the incisal edge of the canine. Now the scanner is turned to acquire the buccal, incisal and palatal parts of the front teeth utilising a ‘wiggling’ motion (Figure 7a). When reaching the incisal part of the second canine the occlusal surfaces are acquired anterior to posterior. When reaching the last molar, the scanner tip is angled and the palatal and buccal surfaces are scanned respectively. Ender *et al.*[31] studied different scan strategies for full-arch scanning with different intraoral scanners, finding that the different strategies could impact upon the accuracy of the digital models up to almost 100%. Muller *et al.*[32] tested different scanning strategies. For one IOS system, they found that one of the three strategies (similar to the one described previously) had significantly better trueness and precision compared to other strategies.

Accuracy of intraoral scanners

In 2012, the International Organization for Standardisation published ISO 12836:2012 Dentistry - Digitizing devices for CAD/CAM systems for indirect dental restorations – Test methods for assessing accuracy (the document was revised in 2015 to ISO 12836 2015). The ISO describes a standardised way to test the trueness and precision of primarily extraoral digitising devices in dentistry. Regarding the validation process of intraoral scanners there are currently no standards. As a consequence of this, most of the studies published with regards to this topic have non-comparable methods, reference models and trueness validations (reference scanner or computer metric measurement system)[33]. Even if some studies are comparable, the IOS manufacturers upgrade their hardware and software continuously, making it even more challenging to compare new scanners from the same manufacturer to older generation scanners with different hardware and software architecture[34]. As previously described, the software algorithms have an impact on the final digital model, so changes in the algorithms could possibly have important effects on the final result. A standardised way of testing the accuracy is needed in order to compare different intraoral scanning devices.

Ender and Mehl[35] compared conventional and digital impressions for full-arch scans in vitro. The authors rejected the hypothesis that the conventional and digital impressions would be equally accurate. The models made with vinylsiloxanether (VSE) material showed the highest accuracy. Ender *et al.*[36] continued to study the conventional and digital impressions in vivo and in vitro for full-arch models. Once again they had to reject the same hypothesis, but this time they found precision differences between the groups. The digital impressions were significantly less precise compared to the VSE impressions. They also found that the digital impressions performed better in the in vitro group compared to the in vivo group. However, there were no differences between the in vitro and in vivo group for the VSE material. Malik *et al.*[37] compared full-arch digital and conventional impressions for trueness and precision, and had to reject the hypothesis that there would be no difference between the groups. The conventional polyvinyl siloxane (PVS) impression

presented significantly higher accuracy in comparison to the digital impression. While there were statistical differences, they also found that all the tested impression methods showed accuracy levels to be less than 100 μm .

It is evident that the intraoral scanners have difficulties scanning full arches with high trueness and precision, even when studying different digital impression without comparison to the conventional impressions[33, 38-41]. Ender *et al.*[42] studied the precision of several IOSs on scanning quadrants (short arches). They found the different impression systems displayed significantly different levels of precision. They also concluded that all the digital impressions tested were capable of digitising the quadrant with clinically satisfying precision (threshold value was not presented). They found the mean trueness to be between 10 and 48 μm , with precision values ranging from 4 to 16 μm depending on manufacturer and impression technique. Nedelcu *et al.*[43] studied accuracy and precision of digital impression systems in vivo, with the conclusion:

“Intraoral scanners can be used as a replacement for conventional impressions when restoring up to ten units without extended edentulous spans”.

Mangano *et al.*[44] studied trueness and precision for four IOSs on scanning two reference models with implant analogues, one partially edentulous and one totally edentulous. For the partially edentulous model the trueness ranged from 40.8 μm (SD 6.4) to 219.8 μm (SD 59.1), and, for the edentulous model, they presented trueness ranging from 55.2 μm (SD 10.4) to 204.2 μm (SD 22.7). The authors concluded that there was significant difference between the different IOSs, and this should be considered for the production of long-span prosthesis.

Computer-aided design

As seen in Figure 4, the next process in the digital workflow is computer-aided design (CAD). There are several dental-specific CAD software applications available, with different features and functions. Some of the features are universal for all types of dental

CAD software; these will now be described. The operator imports the scanned file either directly from an intraoral scan or indirectly from an extraoral scan. When the digital impression has finished with the previously described post-processing procedure, the virtual model is regarded as a master cast on which the restoration will be designed[45]. For the production of a one-unit full anatomic crown, the virtual master cast goes through a series of steps, usually starting with a clean-up stage where the operator can remove unnecessary mesh data. Regarding intraoral digital impressions, the unnecessary data could be information from the patient's tongue, cheeks, lips or any other structure captured from the scanner that has no meaning in the production steps to follow. When the operator is satisfied with the clean-up, the process continues by defining the preparation finish line; this could be done manually, automatically or a combination of both[46]. The next step is the adaptation of a library tooth with pre-defined anatomy[47]. The operator places the tooth as close as possible to the desired shape, with possibilities to morph the tooth in different directions, size changes and other shape-defining procedures[48]. The desired shape will then automatically adapt to the previously defined finish line[45]. The process continues with an adaptation to the antagonist either manually, automatically or a combination of both[46, 47].

Design perimeters

The digital workflow for designing constructions virtually not only consists of the actual anatomical designs, but also of design parameters that adapt the construction for the manufacturing unit and the final reconstruction material. Comparable to the conventional workflow, the cement spacer is added to the virtual die digitally. The operator can choose dimensions and cement spacer combinations, for example a 25 μm spacer in the first mm from the finish line and another cement space set to 50 μm for the rest of the die. The cement spacer in the virtual design has the same purpose as for the conventional workflow, intended as clearance for the cement. The operator also has the possibility to apply clearance features to the antagonist and adjacent teeth in order to adapt the design to the virtual environment of that specific situation. Some other parameters that most types of dental CAD software enable are the design parameters for edge

thickness, edge angles, undercut adaptation, milling diameter, minimal thickness warnings and connector dimensions (for fixed partial dentures). Depending on what material and manufacturing unit the reconstruction is going to be produced in, these parameters will vary. One example is the manufacturing parameters of IPS e-max CAD (Vivadent Ivoclar, Liechtenstein Schaan,) in the dental CAD software Exocad (Exocad GmbH, Germany, Darmstadt)[49]. Table 1 shows the recommended parameters from the manufacture for the production of crowns and bridges made from their lithium disilicate material. The parameters are defined for that specific dental CAD software (in this case Exocad), preparing the designed construction for the computer aided manufacturing (CAM) step to follow and post-production processes such as the crystallisation process. Similar parameters can be found from other manufacturers.

Table 1. Exocad production parameters for designing and manufacturing IPS e.max CAD constructions.

Software description	Cement spaces				External surfaces			Cross section of connector	
	Gap thickness of cement	Additional distance x/y	Beginning of cement	Minimal thickness	Horizontal crown margin	Angled crown margin Angle			
Single crown	anterior	0.06 mm	0.02 mm	1.20 mm	1.00 mm	0.20 mm	65°	0.10 mm	–
	premolar	0.06 mm	0.02 mm	1.20 mm	1.00 mm	0.20 mm	65°	0.10 mm	–
	molar	0.06 mm	0.02 mm	1.20 mm	1.00 mm	0.20 mm	65°	0.10 mm	–
	primary tele	0.06 mm	0.02 mm	1.20 mm	1.00 mm	0.20 mm	65°	0.10 mm	–
	Connector settings								
Minimum connector area / 2 crowns	anterior	0.06 mm	0.02 mm	1.20 mm	1.20 mm	0.20 mm	65°	0.10 mm	16 mm ²
	posterior	0.06 mm	0.02 mm	1.20 mm	1.50 mm	0.20 mm	65°	0.10 mm	16 mm ²
Minimum connector area / 1 pontic	anterior	0.06 mm	0.02 mm	1.20 mm	1.20 mm	0.20 mm	65°	0.10 mm	16 mm ²
	posterior	0.06 mm	0.02 mm	1.20 mm	1.50 mm	0.20 mm	65°	0.10 mm	16 mm ²
Milling parameters									
Anticipate milling	Yes								
Diameter	1.31 mm								

Computer-aided manufacturing

Figure 4 illustrates the next process for digital dentistry, namely the CAM step. In the production processes for dental application, computerised manufacturing is divided into two main groups, subtractive and additive. The subtractive group consists of machines that remove material from a solid body with rotating tools, in order to attain the designed shape. The additive group consist of machines that add material layer by layer, solidifying each layer or the end-product in order to attain the designed shape.

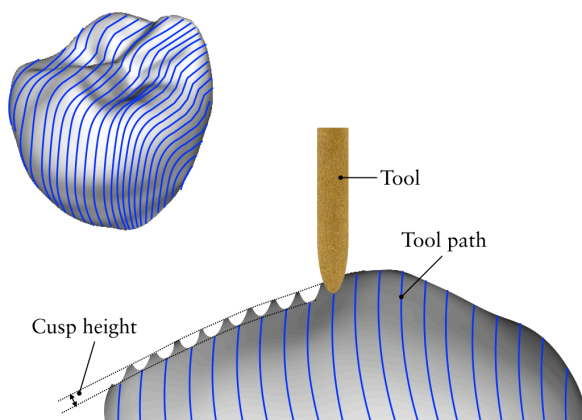


Figure 8. Illustration of the machining nomenclatures correlated to subtractive manufacturing.

Subtractive manufacturing

When the operator has completed the design procedure, the file will be processed by CAM software. The CAM software will calculate computerised numerical controlled (CNC) machining tool paths also known as G-codes[50] for the designed reconstruction. The tool paths consist of the object's profile data, and also contains the selection of cutting tool type for different parts of the design as well as the rotational speed of the cutting tool[18, 29, 51]. The G-code also contains information regarding cooling sequences during the manufacturing process. There are many subtractive manufacturing units available for dental application, ranging from small units for chairside use to machines for industrial use. A unit generally consists of a machine frame, a tool holder, a workpiece holder and rotational axis ranging from 3-5 axis[51]. The size and shape of the tool tip in correlation to the tool path will determine how closely the object will be manufactured to the designed geometry (Figure 8). If the tool tip has a high diameter with steps between the tool paths, the manufactured object will end up with a rough surface[18]. In mechanical engineering the surface roughness created by CNC machining is referred to as tool path cusp height[52]. To achieve a smooth surface the tool paths need to be close to each other and the diameter of the cutting tool needs to be as small as possible.

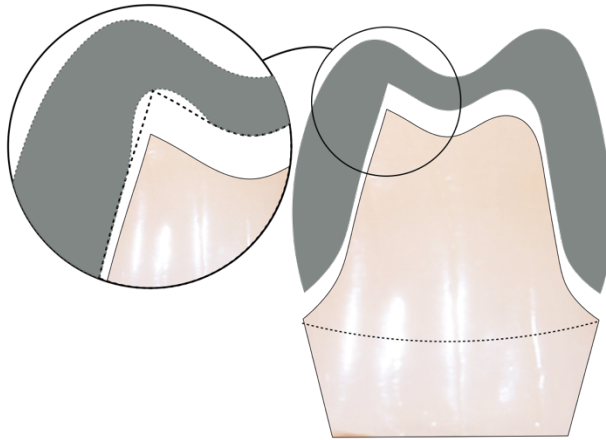


Figure 9. Illustration of drill compensation. The dotted lines illustrate the intended design, because of the tool dimension limitations the CAM procedure need to compensate in sharp areas.

The tools utilised for cutting the bulk material will be subject to wear; when the sharpness or abrasiveness is reduced, the surface roughness of the manufactured object will be affected. The wear of the tools utilised during the fabrication process is correlated to the hardness of the bulk material. If the bulk material is soft, the tools will be less affected[53]. Most dental CAM machines have the ability to change tools during the manufacturing process. Typically, the process starts with a highly abradant tool that has the ability to remove a high amount of material in the periphery – as the tool paths get closer to the intended design, the machine changes tool, to a smaller diameter. If the prepared tooth has sharp edges with an edge radius smaller than the smallest diameter of the machining tool, the design software will have to compensate for this in the design, also known as drill compensation (Figure 9).

For the milling of yttrium-stabilized tetragonal zirconia polycrystals (Y-TZP), or metallic materials, the bulk material could either be pre-sintered (green stage) or densely sintered. Both bulk versions have their advantages and disadvantages – as previously described, milling hard materials wears out the tools, something that would take place with the densely sintered version. Furthermore, the pre-sintered version

needs to go through a sintering process, leading to a shrinkage. For the pre-sintered version, the CAM software needs to compensate allowance for the shrinkage before the manufacturing[54].

Accuracy of subtractive manufacturing

Kirsch *et al.*[55] studied the manufacturing trueness for four different milling units, by designing different single unit constructions that were later manufactured in dental CAM machines. The manufactured objects were compared to the designs, a process also known as reverse engineering. They found an overall trueness in the range of $25,7 \mu\text{m} \pm 9,4 \mu\text{m}$ to $48,7 \mu\text{m} \pm 23,3 \mu\text{m}$. They concluded that the five-axis machines showed highest trueness, because these milling devices had the ability to process areas that were difficult for machines with less axes to reach. Bosch *et al.*[56] used a similar approach to investigate the dimensional accuracy on milled reconstructions. Their findings for trueness ranged from 42 to 76 μm in the occlusal areas and 41 to 96 μm in the inner areas (surface close to the preparation). They concluded that a five-axis milling machine accomplishes accurate reconstructions, and that a small diameter rotary tool resulted in more accurate milling. In a review based on 70 studies by Papadiochou *et al.*[57] marginal adaptations of different CAD/CAM technologies were evaluated. Their findings suggest that the majority of dental restorations produced with CAD/CAM presented marginal discrepancies $\leq 120 \mu\text{m}$.

Additive manufacturing

History

Also known as rapid prototyping, additive manufacturing (AM) is a manufacturing technology invented by Charles ‘Chuck’ Hull in 1984[58]. The invention describes a production process of producing solid plastic models by successively applying thin layers of curable material on a build plate. The build plate is then moved away from the liquid surface by a thickness of one layer and the layer-curing process starts all over again; this production process was named stereolithography (SLA). Hull also explains in his patent that the SLA process helps the operator to avoid the tool path processes otherwise necessary in subtractive manufacturing. He also describes the invention as a time- and material-saving process for part production.

Instead of weeks and months of production time, the part can be produced rapidly. The following citation describes the purpose of the patent;

“Hence, the stereolithographic apparatus of the present invention satisfies a long existing need for a CAD and CAM system capable of rapidly, reliably, accurately and economically designing and fabricating three-dimensional plastic parts and the like.”

The AM technology has been utilised just as Hull hoped in his patent, as the manufacturing sector has been using it for rapid-design purposes ahead of mass production. Meanwhile, one of the significant advantages with the additive technique has been the ability to produce almost any shape. This includes generic, biological shapes such as human organs. Thus, the technique has been adopted by scientists, medical doctors, artists, architects and other professionals in need of generic designs[59]. According to the Wholers report[60] from 2018, 135 companies around the world produced and sold AM systems in 2017. They also reported an increase of nearly 80% of sold metallic AM systems in 2017 (estimated to 1768 units). According to the same report from 2017[61], nearly half of the AM businesses use polymer manufacturing units. Currently, there are several versions of AM for light curable resins.

Product development

The product development for industrial AM processes starts with a design concept. During this process the operator needs to decide whether the concept is going to be manufactured subtractively or additively. The concept is later visualised and designed through CAD software – if SM is going to be used the designer needs to take this into account; as previously stated the SM technology has some limitations regarding design features because of the tactile five-axis movement technology. For AM production the operator has almost total design freedom. When the CAD is finished, the file goes through a software process preparing it for manufacturing. The SM units use the G-code preparation, while, for AM production, the pre-production process consists of a slicing algorithm that slices the 3D object into profile layers with a thickness defined by the operator with limitations of the capabilities of the specific AM machine being utilised.

The STL file

The original SLA approach to build parts was based on building walls (the profile of the object). This led to two types of problems: 1) weak structural strength because the object was hollow, and 2) failures in the layer-to-layer adhesion. Further developments of the SLA patent led to the invention of the STL file, also known as Standardised Tessellation Language file. The file structure describes the surface geometry of a design by triangulating the surface – the more triangles that are formed the better surface resolution. Data points representing the triangle coordinates in each slice are then transferred to the AM system for layering, making it possible to manufacture objects that are not only produced by a thin wall[62].

Fabrication principles

The operation of all AM systems is based on the same principles; the fabrication of parts layer-by-layer without the need for manufacturing tools. Furthermore, there are three basic fabrication stages, starting with the selection of build parameters, where the operator selects layer height (thickness) and placement of supporting structures so that the object being produced has limited movement and to support overhangs from distortion. The next phase consists of the manufacturing of the part; the SLA system utilises a light curable liquid resin, curing source utilising ultra violet (UV) light and an elevation platform. The three parts are coordinated in the fabrication process. When the UV light strikes the polymer surface, it cures one layer of polymer. The first layers adhere to the elevating platform, the elevator is lowered by one layer's height. A new layer of uncured resin is then recoated and polymerised with UV light, forming another layer on top of the previous layer. This process continues layer-by-layer until the part fabrication is completed[15]. The third and final stage is the post-production phase, consisting of cleaning, surface enhancements, and post-curing[15, 63]. The original patent for SLA described a laser as light source; however, today there are other light sources available. One system often seen for dental applications is the Digital Light Projection (DLP) technology, the light source in this case is a projector utilising UV light to cure the resin. For the production of metallic components, the fabrication principles are the same. Instead of a liquid light curable resin the AM of metallic components utilises a

fine metallic powder. One thin layer of the powder is coated onto the elevation platform, the object layers are then either melted (Selective Laser Melting, SLM)[64], sintered (Selective Laser Sintering, SLS for polymers, or Direct Laser Metal Sintering, DLMS) or merged utilising either a high-energy laser, electron beams (Electron Beam Melting, EBM) or some kind of binder[65]. The elevation platform is then lowered by one layer's height and the process starts all over again. The post-production phase for metallic components consists of cleaning, sintering or heat treatment and surface enhancements.

Additive manufacturing applications in dentistry

The limitation of use for dental application is correlated to materials that are biocompatible or bioinert; the continuing material development from additive manufacturers enables more dental applications. For the production of polymers, AM technologies are being used for the fabrication of dental models[66, 67], provisional reconstructions[68], surgical guides[69], occlusal devices[70], prosthetic metallic frameworks for both fixed[71] and removable prosthodontics[72]. For metallic applications AM technologies are being used for prosthetic frameworks in Ti-6Al-4V alloys, and Co-Cr. The metallic AM systems also have the ability to manufacture surgical Ti-6Al-4V alloy implants individualised for patient requirements[65]. For the additive production of metallic components, the dental field has predominantly utilised Direct Metal laser sintering and Selective Laser Melting. Both of these technologies are powder based, the main difference between the technologies is that the first one sinters the powder particles and the second melts it. The SLS technology has a limited use in dentistry today, primarily because of the higher surface roughness on the end products compared to SLA and DLP manufacturing. The SLS technology does not require support structures and the technology has the ability to manufacture tough objects with greater material properties compared to objects manufactured through SLA (Table 2).

Table 2. Table illustrating different additive technologies utilised in dentistry today.

Phase	Liquid		Powder	
Technique	Photopolymerization		Powder bed fusion	
Technology	SLA Stereolithography	DLP Digital Light Processing	DMLS / SLM Direct Metal Laser Sintering Selective Laser Melting	SLS Selective laser sintering
Material	Monomers	Monomers	Metals	Polymers
Solidification	Laser 	Projector 	Laser (high energy) 	Laser 
Postprocessing				
Surface cleaning	Yes	Yes	Yes	Yes
Post curing	Yes	Yes	No	No
Post heat treatment	No	No	Yes	No
Support removal	Yes	Yes	Yes	No
Dental application	Provisionals Dies & models Night guards Implant guides Castable framework Denture bases		Titanium and Cobalt Chromium framework for removable and fixed prosthodontics Surgical prosthesis	Models

Accuracy of additive manufacturing of polymer constructions

Salmi et al.[66] studied the accuracy of medical polymer models of human craniums, comparing three different AM technologies. They found that the model errors were in the range of 0.18% to 0.80% in deviation when compared to the original CAD model. Turbush et al.[73] compared the accuracy of implant placement by studying three different types of surgical implant guides made with SLA utilising cone beam computerized tomography (CBCT) as base. They found that the mean angular deviation was 2.2 ± 1.2 degrees, and the mean linear deviation was 1.18 ± 0.42 mm at the implant neck. They could not identify any significant differences among the guides, and they concluded that the average linear deviation was 1 mm between planned implant placement and the actual placement. Arnold et al.[74] studied the accuracy of producing removable partial dentures utilising five different methods: conventional, SLA (castable), SLM (direct) and two types of subtractive (direct and castable). They found that both of the AM groups exhibited the

highest discrepancies, whereas the subtractive group showed the best results. Fathi et al.[75] studied the marginal and internal fit of wax patterns produced by conventional, subtractive, and additive methods, finding that the additive wax patterns were more accurate ($36 \pm 5 \mu\text{m}$) than the conventional ($141 \pm 31 \mu\text{m}$) method. Other authors have compared marginal and internal fit on printed wax patterns to conventional and milled constructions, with differing results. Homsy et al.[76] concluded that the subtractive method of wax pattern fabrication presented better marginal and internal fit compared to the conventional and additively manufactured groups. Yau et al.[77] compared additive and subtractive manufacturing of models for orthodontic planning. They concluded that the subtractive five-axis machine produced models with an accuracy of 10-20 μm while the additive group had an accuracy ranging from 30-50 μm .

Build orientation

For the SLA approach different types of polymers are utilised. Ideally, the materials consist of monomers, comonomers and reactive oligomers. The resins should have a viscosity suitable for AM (not too high or too low). The balance between type of monomers, photo initiator concentration and curing intensity/speed gives the end product different properties[78]. Tahayeri et al.[68] studied additively manufactured provisionals for crown and bridge applications. They found that the provisionals had an elastic modulus close to 2000 MPa, comparable to conventional provisionals. They also found that the manufacturing orientation of the test objects affected the accuracy. When manufacturing the objects at a 90-degree orientation the length accuracy was 2% on average, while the thickness had a 20% error. When the orientation was changed to 0 degrees the thickness accuracy was reduced to 10% error. They also found that, depending on which colour setting was selected, they could see sample thickness variations of 41.5%. Alharbi et al.[79] studied the build angle and support structures of full anatomic polymer crowns made through SLA. They concluded that the build orientation should be 120 degrees with thin supports. Depending on support thickness and build orientation, the maximum deviation and minimum deviation ranged from 548 μm (210°-thick supports) to -548 μm (270°-thick supports). Osman et al.[80] also studied the correlation between

accuracy and build angle, with a similar approach as the previous study. They utilised a DLP system for production, concluding that the highest dimensional stability was achieved at 135 degrees.

Accuracy of additive manufacturing of metallic constructions

Huang et al.[81] studied the marginal fit of metal ceramic CoCr crowns manufactured with SLM. They compared the SLM group with a conventionally casted group, finding that mean marginal discrepancies of $75.6 \mu\text{m} \pm 32.6$ for the SLM group and $91 \mu\text{m} \pm 32.1$ for the casted CoCr group. They concluded that the marginal Co-Cr metal ceramic crowns had better marginal fit in comparison with the casted Co-Cr crowns. They also found that the SLM group had less accurate occlusal fit compared to the casted group. Kim et al.[82] compared the marginal and internal gaps of Co-Cr copings fabricated with SLM, subtractive manufacturing and conventional casting. Their findings showed that the mean of the marginal discrepancies for the SLM group was $239 \mu\text{m} \pm 126.0$ while the lost wax casted group had a marginal discrepancy of $91 \mu\text{m} \pm 80.9$ and the subtractive group $60 \mu\text{m} \pm 20.6$. Their findings also suggested that the SLM group had a higher occlusal gap compared to the other groups, when compared to the subtractive group, the occlusal gap was 4 times larger for the SLM group. Bae et al.[83] studied the production accuracy of subtractive manufacturing and two additive methods; SLM, and SLA. Their findings suggested that both of the additive systems had higher accuracy than the subtractive group. Örtorp et al.[84] studied the fit of Co-Cr three-unit frameworks, comparing four different manufacturing techniques. Two of the groups consisted of a milling group and a DLMS group. They found that the DLMS group had the lowest mean gap value ($<100 \mu\text{m}$).

DIGITAL VERSUS CONVENTIONAL WORKFLOW

The manufacturing of prosthetic restorations in dentistry is a fairly complicated procedure that requires several well-controlled processes. The aim of the final restoration is to replace damaged or missing soft and hard tissue, and to restore function, phonetics and aesthetics. The restoration has high material property requirements in order to withstand high forces, thermal changes, aging and humidity. If the fit of the reconstruction is insufficient there is a high probability for clinical failures ranging from inflammatory processes to reconstruction fractures[85-89]. The grading of perfect, sufficient and insufficient fit is unknown although the definition clinically acceptable fit has been used to describe and control a reconstruction that is well seated and controllable by the clinician. It is also unknown when a misfit of a reconstruction challenges biological and mechanical failures. When comparing the digital workflow to the conventional one there are several interesting aspects to consider:

1. Production time
2. Cost benefits
3. Material properties
4. Manufacturing tolerances, clearance and allowance
5. Environmental effect
6. Operator health aspects
7. Patient benefit and biological aspects

Henceforth, the comparison will focus on manufacturing tolerances and aspects related to geometrical accuracy and fit.

Production tolerances in dentistry

Using the nomenclature from the field of metrology, it would be interesting to know the tolerance, allowance and clearance when producing a prosthetic construction. When analysing publications in the dental field, there are some interesting reflections, such as “clinically acceptable fit” or “marginal adaptation” [84, 90, 91]. There are no clear distinctions between whether a construction is clinically acceptable or not. Some studies have used the dental probe size as a “measuring tool”[92] for assessing if the fit is acceptable or not. Other studies have utilised optical microscopy[93], scanning electronmicroscopy[94], silicone replica[95], triple 3D scanning[96] or micro-CT[97]. Even though there is no consensus regarding the threshold of the fit between the reconstruction and underlying support, some authors have utilised 120 μm as a baseline for an acceptable marginal fit[98-102]. One should remember that some of the gap between the reconstruction and underlying support is intentional. The cement spacer that is added manually in the conventional workflow and the digital cement spacer should be accounted for in the 120 μm gap in the final reconstruction. Furthermore, the internal dimensions need to be defined. On implant-supported constructions, the “one-screw test”[103, 104] has been a well-documented method to clinically test the fit. For implant components the implant manufacturer designs both the connecting and receiving parts of the constructions, thus they have the possibility to calculate tolerances and clearance for both parts. Some authors have investigated the clearance between different implant components ranging from 22-130 μm [105, 106].

Marginal fit

In a review by Boiltelle *et al.*[107] on fit of CAD/CAM restorations a total of 90 articles resulted in a marginal fit ranging from 39.1 to 201 μm and the internal fit varied from 23 to 230 μm . In an review based on 55 studies by Papadiochou *et al.*[57], marginal adaptation of different CAD/CAM technologies were evaluated. Their findings suggest that the majority of dental restorations produced with CAD/

CAM presented marginal discrepancies $\leq 120 \mu\text{m}$. Ueda *et al.*[108] compared fit of 4-unit reconstructions made from CoCr and zirconia after conventional and digital impression, the reconstruction fabrication was digital (subtractive). Their findings suggested that all reconstructions showed clinically satisfying results; nevertheless, the digital group showed better marginal fit when CoCr was used. Mean marginal openings for the digital group ranged from $32.05 \mu\text{m}$ to $62.85 \mu\text{m}$ while the conventional impressions ranged from $81.1 \mu\text{m}$ to $86.51 \mu\text{m}$. Jonathan *et al.*[109] studied the fabrication of crowns made from a digital workflow compared to a conventional workflow. They found that the digital workflow had a mean marginal gap of $48 \mu\text{m} \pm 25 \mu\text{m}$ in comparison to the conventional group, which demonstrated a gap in the range of $74 \mu\text{m} \pm 47 \mu\text{m}$. Still, if the threshold of $120 \mu\text{m}$ is to be used, both groups would be regarded as clinically acceptable. Pompa *et al.*[110] studied the marginal gap of reconstructions made from milling (Y-TZP), SLM (CoCr) and the conventional (Ni-Cr) lost wax method. They concluded that the SLM group had a better marginal fit compared to the two other groups. Regardless of manufacturing method and material, all measurements were below $80 \mu\text{m}$.

Final remarks

It is clear that the conventional and digital workflow for the manufacturing of reconstructions have comparable results, especially for crowns and short-arch bridges. Some researchers have presented similar results while others have found better-fitting reconstructions through the digital workflow. It seems like a manufacturing tolerance around $100 \mu\text{m}$ is sufficient in the dental field. This tolerance is noticeable clinically. As a point of reference, one human red blood cell is about $10 \mu\text{m}$ and a stray human hair has a thickness of about $30\text{-}70 \mu\text{m}$. New process technologies introduced in dentistry that have the capability to either digitise or manufacture subjects with a trueness about $50\text{-}100 \mu\text{m}$ and with precision values about $20 \mu\text{m}$ would, in theory, be sufficient for dental applications.

HYPOTHESIS

Subtractive manufacturing is superior to AM regarding accuracy and precision of the final product.

There would be no significant differences within each IOS system when scanning an edentulous arch compared to a dentated one.

SPECIFIC AIM

To present the horizontal clearance of the interface between internal-hexagon and external-hexagon implants and analogues with corresponding cylindric gold and plastic abutments upon delivery from the implant manufacturer.

To determine the production accuracy of four commercially available polymeric AM systems by reverse engineering two geometrical objects.

To evaluate the production accuracy of five AM systems and one subtractive manufacturing system for the production of metallic components by reverse engineering two geometrical objects.

To study the accuracy of four different intraoral scanners for full-arch scanning of one edentulous model and one dentated model.

MATERIALS AND METHODS

Study I

Part One

One implant with an internal-connection interface (Biomet 3i) with a corresponding prefabricated gold cylinder (PGC) and gold screw; an internal-connection implant analogue, prefabricated cylindrical plastic cylinder (PPC), and laboratory screw; one implant with an external-connection interface (Biomet 3i), corresponding PGC, and gold screw; and an external-connection implant analogue, PPC, and laboratory screw were used for this part of the study. These implant and analogue parts were used to capture the raw data needed to create CAD models. The implants' cylindrical parts were measured manually using a micrometer instrument (CEJ 101) and digitally with a Leica microscope using a $\times 50$ magnification and Leica computer software (Leica application suite version 3.7.0 2010).

All specimens were then embedded in epoxy (EpoFix Resin Hardener, Struers). After 24 hours, each specimen was cut and ground to the centre point using a grinder (Phoenix 4000 sample preparation system, Buehler), with the alignment centred and carefully controlled according to prior cylindrical measurements. On the implants and analogues, the centre point was located according to Figure 10. Digital measurements of all the connecting parts were made with a Leica microscope under $\times 50$ magnification and Leica computer software (Leica application suite, version 3.7.0 2010), and the equipment was calibrated before each measurement. The dimensions of all 12 components were then used to model 12 virtual three-dimensional objects using Autocad 2013 (Autocad 2013, version G.55.M.108

Mac, Autodesk Corp). In Part One, each component was measured separately, while in Part Two the fully assembled implant (analogue)/cylinder/screw specimens were measured.

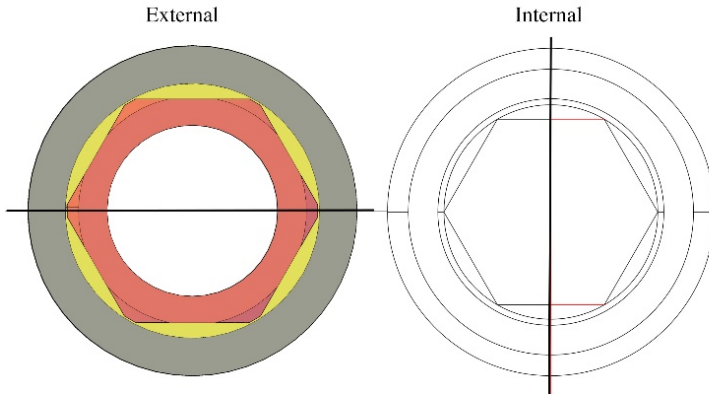


Figure 10. Optimal cut orientation on external- and internal-hexagon-connection implants and analogues.

Part Two

In this portion of the study, 12 commercial implant (analogue)/abutment connections were measured, six with external-hexagon connections and six with internal-hexagon connections. Each group included three implants and three analogues: internal implant (II) and internal analogue (IA) in the internal-hex group, and external implants (EI) and external analogues (EA) in the external hex group. A total of 12 cylindric abutments were retained with gold screws; on the implants, PGC abutments were used, and, on the analogues, PPC abutments were used. All the abutments were retained carefully with finger pressure calculated to 5 Ncm (W&H Elcomet), simulating the force a dental technician uses when making a framework. All specimens were then embedded in epoxy and positioned vertically. After 24 hours, each specimen was cut and ground to the centre point. A central position was regarded to be most representative of the fit of the connection. Digital measurements were made with a Leica microscope using $\times 50$ magnification. The distances between each abutment and its corresponding implant/analogue were measured on

the left and right sides of all the samples. Measurements for EA and EI were designated M1, and, for IA and II, the measurements were designated M2. The epoxy, abutments, and abutment screws were then removed from the implants/analogues, and measurements of the external hexagon and internal hexagon were made to orientate the direction of the cut (Figure 11).

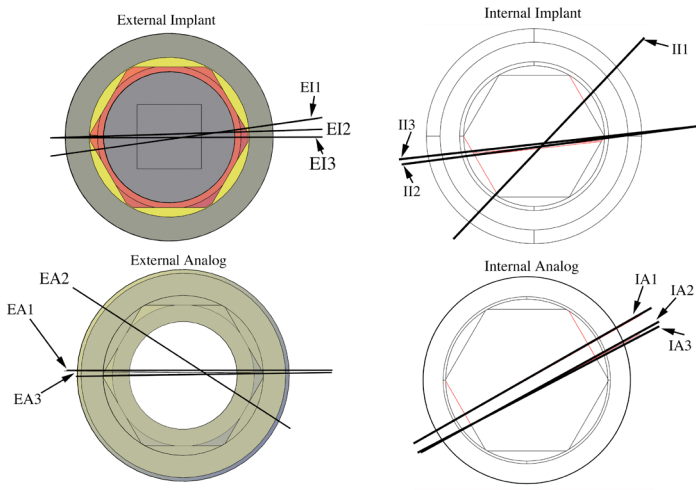


Figure 11. Orientation of cuts of specimens for internal- and external-hexagon implants and analogues. Note the divergence of EA2 and II1.

Part Three

The measurements of the cut assemblies obtained in Part Two were then used on the CAD objects to orientate and replicate the different cuts (Figure 12). The virtual objects were then cut digitally, and M1 and M2 were compared with the digital measurements (M1CAD and M2CAD). Threshold results were calculated from this comparison.

Part Four

The virtual model was then used to obtain optimally oriented cuts (Figure 10). M3CAD and measurements of the theoretical machining tolerances were made.

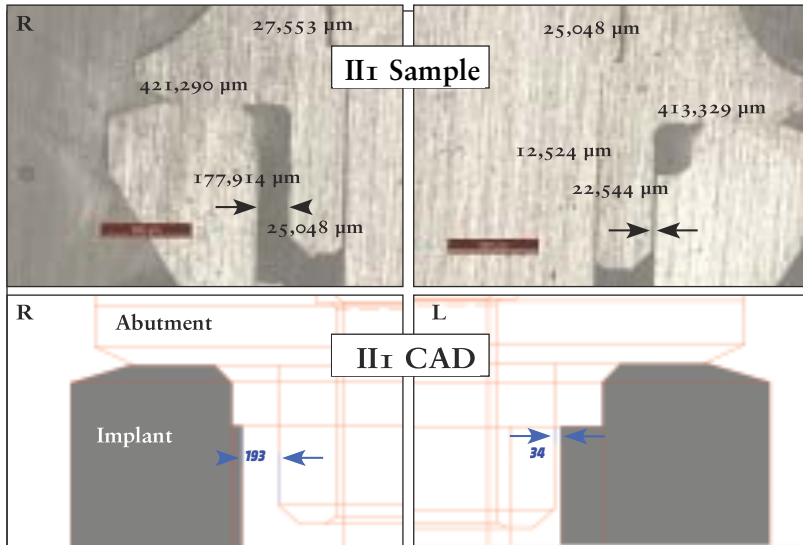


Figure 12. Comparison of left and right sides of an internal-hex implant sample and internal-hex implant CAD model.

Study II

ISO reference

The ISO 12836 “Dentistry – Digitising devices for CAD/CAM systems for indirect dental restorations – Test methods for assessing accuracy”. The ISO describes three geometrical figures, described as Annex A, B and C. The present study has utilised Annex A and B as reference, with the former specifying the measurement of an inlay-shaped object and the latter a multi-unit specimen to simulate a four-unit bridge model. Annex A and B from the ISO were the reference for the design of object A and B in the present study (Figure 13 and Figure 14). The CAD was designed as solids using 3D modelling software (Solidworks educational edition 2013) with an edge radius of 0.01 mm. Both CAD models were exported as standard tessellation language files (STL) and delivered together with production information to the manufacturers.

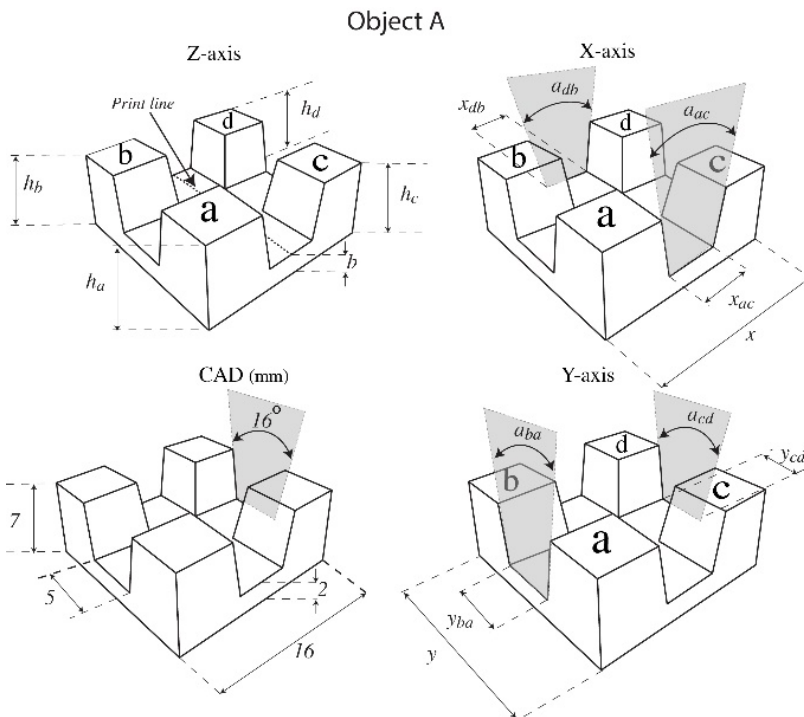


Figure 13. Figure illustrates object A (inlay shaped), the CAD illustration describes the dimensions designed in the computer, the x, y and z illustrations show the abbreviation measurements.

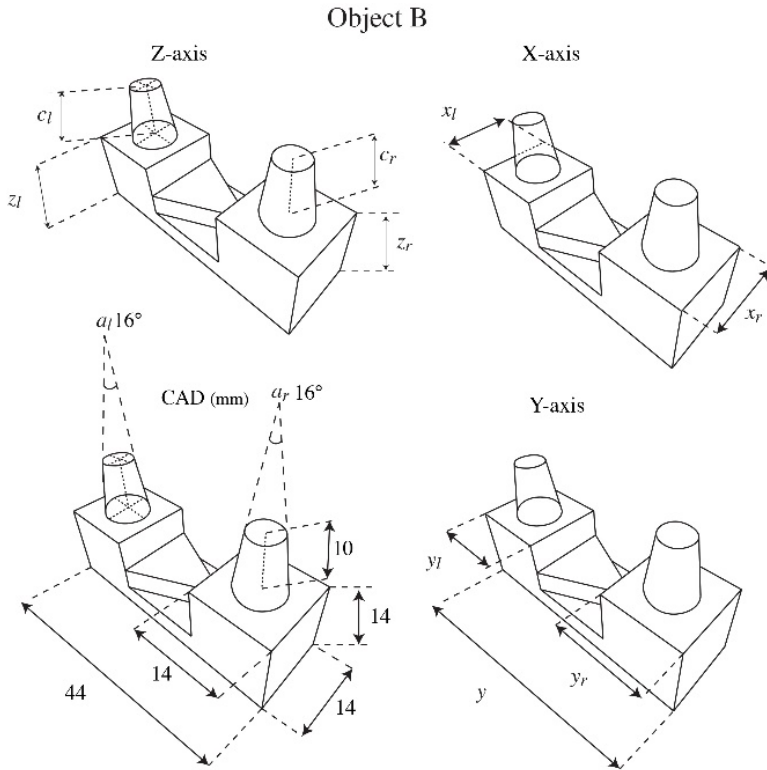


Figure 14. Illustration of object B (four unit bridge model) CAD illustration describes the dimensions designed in the computer, the x, y and z illustrations show the abbreviation measurements.

CAM

A total of four AM units were tested: EOS (Formiga P110) 3D Systems (Projet MP 3510), Stratasys (Objet30) and Stratasys (Objet Eden) (Table 3). Authorised personnel from each company manufactured all objects. All producers manufactured 10 sets for object A and 10 sets for object B on separate build plates. The geometries of both object A and object B have no undercuts, thus there was no need for support structures, allowing the objects to be manufactured directly onto the build plate. The person responsible for each production unit decided upon material and software settings to achieve accurate samples. All manufacturers had seen the protocol ahead of initiating the present study. It was clear that all objects would be tested for

geometrical accuracy. The manufacturers decided the best parameters for their specific machine, and price was not an evaluated parameter (Table 3). The material of choice was then specified together with information about the print resolution, specification of the production unit, software, and the manufacturing time (Table 3). The test samples went through the same process as for clinical dental products, regarding both production and shipment.

Measurements

The measurements for the inlay shaped geometry of object A was divided in x, y and z-axis. The geometrical measurements that were conducted consisted of linear parameters, angles and corner radius. Object A was divided into a total of 16 parameters (Figure 13) and object B was tested for 12 parameters (Figure 14). Each manufacturing unit produced 10 objects from each group; all parameters were measured five times for a total of 5,600 measurements. All the objects were measured within 7 days of arrival. All the measurements were conducted by one investigator.

Measurements parameters

The z-axis describes the height of the objects; this vertical dimension was perpendicular to the layering orientation and consisted of five linear measurements for object A and 4 for object B. The x and y-axis describe the horizontal dimensions and consist of three linear x-axis dimensions for object A and 2 for object B. Both objects A and B consisted of three y-axis dimensions. To orientate object A, the four cubic forms were named A-D, the placement of A was orientated in the top left corner in relation to the horizontal print lines (surface lines see Figure 13) on each object. Object B was divided in a left and right side, the tip of the triangle shaped geometry in the middle of the object points on the right side (Figure 14). All linear parameters were measured using tactile measurement equipment (digital micrometer C.E Johansson Jomic IP67, Eskilstuna, Sweden, and digital calliper Sylvac S Cal Pro IP67, Crissier, Switzerland). All the measurements were conducted in a stable temperature environment $20 \pm 1^\circ\text{C}$.

Table 3. Information about the four additive manufacturing units.

Information about the four additive manufacturing units.			
Manufacturer	EOS	3D Systems	Stratagys
Material	PA.2105	VISIJET	VeroWhite
Layer thickness/printing resolution	60 μ m	PEARLSTONE HIGH DEFINITION PLASTER (HDP) x-axis 375 dpi, y-axis 375 dpi, z-axis 790 dpi	16 μ m x-axis 600 dpi, y-axis 600 dpi, z-axis 1 600 dpi
Machine/model	FORMIGA P110	3D SYSTEMS PROJET MP 3510	Objet 30 Objet Eden 260 V
Production year	2013	2013	2013
Firmware	PSW 3.6.62	CONTROL VERSION 5.2.3540	V 27.0.1.16 V30.2.1.10908
Software/data preparation	Magics/Materialize 17.02.00, RPTools/EOS 06.01.08	PRINT3D 5.2.3540	Objet Studio 9.1.1.0 9.2.8.10
Build time (Part A – 10 parts)	3 h	2 h 8 min	34 min
Build time (Part B – 10 parts)	6 h 30 min	6 h 3 min	1 h 43 min
Effective build volumex, y, z in mm	200 \times 250 \times 330	298 \times 185 \times 203	255 \times 252 \times 200
Production technique	Selective Laser Sintering	Multi jet printing	Polyjet

Angle parameters/corner radius

A total of four angle parameters were measured for object A and two for object B. These measurements were conducted using a digital microscope (Dino-Lite Premier2 HR, polarisator, AM5018MT, Hsinchu, Taiwan) and computer software (DinoCapture 2.0 Version 1.5.5). The same method was conducted to measure corner radius.

Measurement equipment validation and test conditions

Validation of the micrometer and the calliper were conducted using measurement gauge blocks (Passbitsats Limit, Sweden, DIN 861/2, DIN 861/1). The micrometer equipment was validated with gauge blocks for 2, 5, 7 mm and the calliper for 20, 30 and 40 mm. These tests were conducted in a stable temperature environment 20 ± 1 C, the gauges were stabilised in a silicone form to avoid body heat transferred to the test objects. Each block was measured 50 times. Results for calliper validation for 20 mm blocks mean 20.001 ± 0.002 , for 30 mm blocks mean 29.998 ± 0.001 and for 40 mm blocks mean 30.998 ± 0.002 . Validation of the micrometer instrument showed mean 2.001 ± 0.001 for the 2 mm block, mean 5.003 ± 0.0005 for the 5 mm block and mean 7.006 ± 0.001 for the 7 mm block.

Study III

ISO reference

The ISO (the International Organization for Standardization) is an international federation of standardised ISO bodies. This paper utilises ISO 12836:2015 ‘Dentistry – Digitizing devices for CAD/CAM systems for indirect dental restorations – test methods for assessing accuracy’. Three geometrical figures were described by ISO as Annex A, B and C. In this paper, Annex A and B were utilised but not the method in the ISO (Figure 13 and 14). Annex A simulates the structures of an inlay-shaped object and Annex B simulates the structures of a four-unit bridge model. The CAD object was designed using 3D software (Solidworks educational edition 2013) with a corner radius of 0.01 mm set as 90° (Figure 13 and 14). The purpose of the objects’ geometry was to mimic linear, angle and corner radius measurements. Object A contained 16 measurements and object B 12 measurements. The standard tessellation language files (STL) for Annex A and B were exported and delivered to the manufacturers with information about the products and production.

Fabrication of specimens

Five AM units and one subtractive machine were tested. The additive machines tested were: Arcam®, Concept laser®, EOS®, SLM Solutions® and the subtractive machine was Mikron®. Every company manufacturing the objects and all their personnel were authorised and included in the protocol sent out at the start of the project. Ten sets were manufactured for object A and object B. The software settings were decided by authorised personnel for each production unit in order to achieve accurate samples. Arcam, Mikron, SLM solutions, Concept laser and EOS manufactured the objects in titanium. EOS also manufactured the objects in chrome cobalt. Upon delivery, the manufacturer decided the print resolution, specification of production unit, software and manufacturing time, based on the choice of alloy. All the samples went through the same process with regard to the delivery and manufacturing that is utilised for dental products.

Linear measurements

All the objects were divided into three different axes: X, Y and Z. The X-axis describes one of the horizontal dimensions for both objects. A total of three linear dimensions were measured in object A and two for object B. The Y-axis also measured horizontal dimensions for objects A and B, which consisted of three linear dimensions for each object. The Z-axis describes the vertical dimensions of the objects and a total of five linear measurements were performed for object A and four for object B. The linear dimensions of the objects were perpendicular to the layering orientation. To ease the orientation of object A, the four cubic forms were named a-d (Figure 13). The placement of the cube form a was orientated in the top-left corner in relation to the horizontal print lines on each object. Object B has a triangle shape in the middle; the tip of the triangle was defined as the right-hand side of the object and the opposite as the left-hand side (Figure 14). The tool for measuring all linear measurements was executed with a validated and calibrated digital calliper (Digital Sylvac S Cal Pro IP67, Crissier, Switzerland). While measuring the linear measurements of the objects, the examiner validated the digital calliper by using gauge blocks (Passbitsats Limit, Sweden, DIN 861/2, DIN 861/1). The digital calliper measured gauge blocks of 2, 5, 7, 20 and 40 mm in order to calibrate between the operators and the validation of the instrument. Each gauge block was measured 50 times. A calculation was then performed with standard error of measurement using Dahlberg's formula in order to control inter-observatory variations. This was done for all manufacturing groups before measuring objects A and B. In order to keep dimensional stability, the objects were placed on a silicone form and the measuring process was executed in a room with a stable temperature of $20 \pm 1^\circ\text{C}$; all the linear measurements were measured five times.

Angle parameters and corner radius

There were four measurements of angles for object A and two for object B. The angles and corner radius were measured using a validated and calibrated digital microscope (Dino-Lite Premier2 HR, polarisator, AM5018MT, DinoXcope Version 1.12, Hsinchu, Taiwan). Before measuring the angle parameters and corner radius

of the objects, a validation of the microscope was performed using a Dino-Lite calibration sample (Dino-lite calibration sample P/N TC2001Aug 2013). The validation sample had known measurements, with 1 mm intervals and a line was drawn on the validation sample in the measurement software to calibrate the microscope against the sample. In the computer software (DinoCapture 2.0), all the calibrations were saved in a calibration manager and were later used for each magnification (X30, X50 and X250). During the angle and corner radius measurements, a calibration was performed between the operators (Table 4). The result from Dahlberg's formula indicates that the error of measurement between the operators is negligible.

Table 4. Inter-observatory variability between the operators using digital calliper, calculated with Dahlberg's formula.

	X30	X50	X250
Error of measurement	0.0103	0.0050	0.0023

Study IV

Utilising 3Shape Trios 3 (Denmark, Copenhagen), an intraoral scan of a full-arch mandible was conducted; the scan was exported as STL (Standard Tessellation Language) and imported to CAD modelling software (Autodesk Fusion 360 2017 Version 2.0.3800). In Fusion 360, five cylinders were designed and placed axially onto the occlusion (Figure 15a,b). The locations of the cylinders were as follows: second molars, second premolars and one was placed lingually onto the front teeth (Figure 15c). The same cylinders were utilised for the edentulous mandible and the teeth were removed utilising mesh modelling software (Figure 15d) (Autodesk Meshmixer 2017 Version 3.4.35). Prior to manufacturing, the validation casts were hollowed and checked for errors utilising Materialise Magics (RP Version 13). The casts were produced additively utilising ConceptLaser M-lab 100W (Germany, Lichtenfels) and manufactured directly on the build plate without support structures. Remanium-Star-CL (Co 60.5%, Cr 28%, W 9%, Si 5%) material powder was utilised. The casts were treated according to ConceptLaser recommendations for heat treatment throughout post-processing. The casts were not removed from the build plate. Finally, the casts were sandblasted using aluminium oxide powder with a grain size of 250 µm until a non-reflective surface was achieved. The validation casts were measured with CMM equipment (Zeiss O-inspect, 153862, Germany) by authorised personnel at an ISO 13485:2016 validated institution (Elos MedTech AB, Gothenburg, Sweden). Table 5 shows the scanners tested, and provides information on the scan conditions, equipment and software related information. Each system was utilised to scan each cast 15 times (n=15 for dentated cast and n=15 for edentulous cast) by the same operator.

Although there was some difference between scan protocols between the systems, all scans started at position 1 (Figure 15c) and continued to positions 2-3-4-5. On some occasions there had to be a corrective scan in order to achieve a watertight (i.e. data without holes) scan file. Usually, these corrections were in correlation to the cylinders. The validation casts were fixated; only the ISO device was moved while scanning the casts, and there was a 10-minute break between each scan.

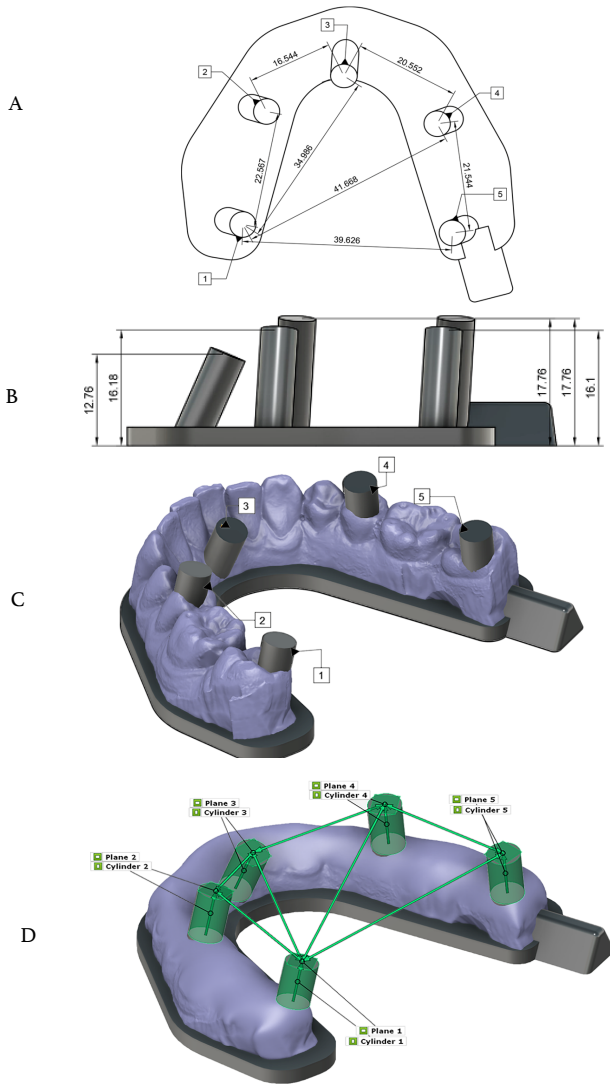


Figure 15. A) Occlusal view of the CAD sketch illustrating the cylinder orientations and abbreviations. The dimensions are from the CMM measurements. B) Lateral view of the CAD sketch illustrating the design without cast; the height dimensions are the designed dimensions. C) Angled view of the assembled dentate CAD cast with cylinder abbreviations. D) Angled view of the assembled edentulous CAD cast. It illustrates the placement of fitting cylinders, planes and their abbreviations. In the intersection of the cylinders and planes, a point is marked; these are the measuring points. The lines illustrate both the inter-cylindrical and cross-arch measurements.

We utilised 3D measuring data for the quality control software (Gom Inspect 2017 Hotfix 4 Rev. 106794 build 2018-01-18). All 150 intraoral scans were measured in the exact same way. Figure 15d illustrates the construction of fitting cylinders, fitting planes, the intersecting point between the constructed cylinders and planes, and, finally, the 2-point measurements between the intersecting points. The best Gaussian fit was utilised as the fitting algorithm for the cylinders and planes. The measurement data was exported to SPSS (IBM SPSS Statistics version 25) where calculations for mean, precision, trueness, two tailed independent student t-test and a Mann-Whitney test (<P.05) were carried out.

Table 5. IOS-related specifications, and applicable information. Scan protocol abbreviations O=occlusal, L=lingual, B=buccal, W=wiggling (scanning in a rocking manner incisal to the front teeth).

IOS (Release)	Software	Acquisition	Device ID	Calibration	Case selection	Scan protocol	Export
Omnica Sirona (2012)	Sirona Connect 4.5.0.105736	Optical triangulation and conofocal microscopy	Model 6371830	Sirona-ID 25782789	Acquisition No restoration	OLB	STL export on site
			RTC2017				
Itero Element (2015)	1.5.0.361	Parallel conofocal microscopy	W10A076 REF 102611 S/N 34862	No calibration presented by manufacturer	No restoration	OLBW	STL export of site
Planmeca Emerald (2017)	Planmeca Romexis 5.0.0.R	Multi-color laser scanning	REF 30006191 S/N 410405	No calibration (only color calibration required)	No Restoration	OLB	STL export on site
Carestream CS 3600 (2016)	CS Imaging Software 7.0.3	Active speed 3D video	S/N FHNB0033	No calibration presented by manufacturer	Standard scanning	OWOLB	STL export on site
Trios 3 (2015)	Trios 2015-1 Design studio 1.4.7.4	Conofocal microscopy	S/N 1WA1732S0 1015B	1AB1731TTA 080B and 1KA1731188 B (color)	Study model	OWOLB	STL export off site

RESULTS

Study I

Tables 7 and 8 show the measurements of the internal-hex and external-hex specimens and their respective virtual CAD specimens. M1 and M2 and M1CAD and M2CAD can be compared to calculate the differences between CAD measurements and subject measurements (Table 6 and 7) (Figure 12). The actual orientations of the different cuts can be seen in Figure 11. The groups with metallic components (PGC) showed the smallest difference versus the CAD models, ranging from -5 to 28 μm , and therefore the least deviation. In contrast, the PPC group measurements ranged from -89 to 47 (Table 6 and 7). The measurement outcome of the optimal theoretical cut orientation (M3CAD) (Figure 10) for the PGC groups showed a total machining tolerance of $58 \pm 28 \mu\text{m}$ for II and $44 \pm 9 \mu\text{m}$ for EI, whereas the PPC groups showed a total tolerance of $86 \pm 47 \mu\text{m}$ for IA and $12 \pm 89 \mu\text{m}$ for EA (Table 8).

Table 6.

Measurements (μm) of Samples and CAD Models for External-Connection Implants and Analogs							
	M1			M1CAD			Difference*
	Left	Right	Total	Left	Right	Total	Total
Implant + PGC							
EI 1	62	104	166	61	100	161	-5
EI 2	6	29	35	22	22	44	9
EI 3	29	35	64	23	33	56	-8
Analog + PPC							
EA 1	50	0	50	24	5	29	-21
EA 2	228	159	387	172	126	298	-89
EA 3	10	8	18	16	5	21	3

EA = external(-hex connection) analog; EI = external implant; M = measurement; PGC = prefabricated gold cylinder; PPC = prefabricated plastic cylinder. *Negative numbers indicate that the CAD measurement is smaller than the sample measurement.

Table 7.

Measurements (μm) of Samples and CAD Models for Internal-Connection Implants and Analogs							
	M2			M2CAD			Difference*
	Left	Right	Total	Left	Right	Total	Total
Implant + PGC							
II 1	23	178	201	34	193	227	26
II 2	138	43	181	149	58	207	26
II 3	63	173	236	74	190	264	28
Analog + PPC							
IA 1	72	28	100	47	39	86	-14
IA 1	65	50	115	79	55	134	19
IA 1	15	25	40	57	30	87	47

IA = internal(-hex connection) analog; II = internal implant; M = measurement; PGC = prefabricated gold cylinder; PPC = prefabricated plastic cylinder. *Negative numbers indicate that the CAD measurement is smaller than the sample measurement.

Table 8.

Optimal Theoretical Cut Orientations on CAD Models				
Model	M3CAD			CAD Deviation Total
	Left	Right	Total	
PGC				
IICAD	29	29	58	± 28
PPC				
IACAD	43	43	86	± 47
PGC				
EICAD	22	22	44	± 9
PPC				
EACAD	6	6	12	± 89

EA = external(-hex connection) analog; EI = external implant;
 IA = internal(-hex connection) analog; II = internal implant;
 M = measurement; PGC = prefabricated gold cylinder;
 PPC = prefabricated plastic cylinder.

Study II

The results of all measurements for mean, standard deviation and a comparison between CAD and mean values can be seen in Table 9.

x-axis

In the x-axis, EOS showed least accuracy when compared to the CAD dimension at -106 µm for object A and 84 µm for object B. Eden showed highest accuracy at 0 µm for object A and 12 µm for object B. The standard deviation (SD) for object A was highest for EOS at 61 µm and lowest for Projet at 11 µm. SD for object B was highest for Projet at 24 µm and least for Eden at 5 µm.

y-axis

In the y-axis, EOS showed least accuracy when compared to the CAD dimension at -201 µm for object A and Projet at -182 µm for object B. Projet showed highest accuracy at -7 µm for object A and EOS at -3 µm for object B. SD for object A was highest for EOS at 68 µm and lowest for Objet at 5 µm. SD for Object B was highest for Projet at 51 µm and least for Objet at 8 µm.

z-axis

In the z-axis, Objet showed least accuracy when compared to the CAD dimension at 43 μm for object A and EOS at 103 μm for object B. Eden showed highest accuracy at 1 μm for object A and Objet at 2 μm for object B. SD for object A was highest for Eden at 49 μm and lowest for Projet at 3 μm . SD for object B was highest for Eden at 24 μm and least for Objet at 6 μm .

Angle measurements and edge radius

The angle measurements for object A showed the least accuracy for Objet at 1.5° and the highest accuracy for Eden at -0.23°. Eden had the least accuracy for object B at -0.4° and EOS the highest at 0.06°. SD for object A was highest for Objet at 0.69° and lowest for EOS at 0.4°. For the edge radius measurement, Projet had the highest closeness to the CAD dimensions with a mean value of 96 μm for object A and 98 μm for object B.

Projet 3510 MP

For object A, the Projet machine displayed an overall accuracy of approximately 10 μm for all parameters except y, which was off by 61 μm . In the same axis, Projet had a standard deviation of <26 μm , for z <5 μm and for x <18 μm . The machine displayed similar results for the production of object B with an overall accuracy of <30 μm and the y parameter was off by -182 μm . The SD in the y parameter was 51 μm , for z 19 μm , and x <24 μm (Figure 16 and Table 9). The Projet device also showed an accuracy of approximately -0.5° with an SD of <0.6° for object A and less than -0.9° with an SD of <0.45° for object B (Table 9).

EOS Formiga P110

For object A the EOS machine presented an accuracy of 40 μm in the z parameters, <106 μm for the x parameters and <200 μm in the y parameters. The SD in the same parameters was <21 μm for z, <61 μm for x and <68 μm for the y parameters. The production of object B presented an accuracy of <103 μm for the z parameters, <84 μm for x and >-21 μm for y. The SD in the same parameters was <22 μm for z, <23 μm for x and <38 μm y (Figure 16 and Table 9). The EOS machine presented an angle accuracy <1.2° with an SD of <0.66° for object A and <0.28° for object B with an SD of <0.21° (Table 9).

Table 9.

Object A																	
Machine	(mm)	x	xac	xdb	za	zc	zd	z	zb	$y\bar{b}a$	$y\bar{c}d$	y	$aba(Degree)$	$ab\bar{b}(Degree)$	$acd(Degree)$	$aac(Degree)$	r
Objet	Standard d.	0.012	0.034	0.030	0.017	0.018	0.015	0.004	0.018	0.030	0.023	0.005	0.613	0.635	0.693	0.497	0.036
	Mean	16.060	4.916	4.953	7.038	7.040	7.042	2.033	7.043	4.978	4.962	16.024	17.282	16.589	17.504	16.555	0.288
	Accuracy	0.060	-0.084	-0.047	0.038	0.040	0.042	0.033	0.043	-0.022	-0.038	0.024	1.282	0.589	1.504	0.555	0.288
Eden	Standard d.	0.010	0.019	0.020	0.028	0.037	0.049	0.043	0.032	0.018	0.021	0.026	0.483	0.479	0.679	0.502	0.021
	Mean	16.000	4.977	4.968	6.974	6.980	6.975	2.001	6.972	4.931	4.944	16.092	16.949	16.267	17.051	16.226	0.251
	Accuracy	0.000	-0.023	-0.032	-0.026	-0.020	-0.025	0.001	-0.028	-0.069	-0.056	0.092	0.949	0.267	1.051	0.226	0.251
EOS	Standard d.	0.029	0.061	0.045	0.013	0.021	0.014	0.011	0.015	0.040	0.068	0.021	0.617	0.415	0.658	0.403	0.053
	Mean	15.929	4.911	4.894	7.041	7.029	7.035	2.030	7.036	4.803	4.799	16.021	17.049	16.339	17.225	16.464	0.253
	Accuracy	-0.071	-0.089	-0.106	0.041	0.029	0.035	0.030	0.036	-0.197	-0.201	0.021	1.049	0.339	1.225	0.464	0.253
Projet	Standard d.	0.011	0.018	0.017	0.004	0.005	0.004	0.003	0.005	0.021	0.015	0.026	0.413	0.613	0.499	0.609	0.025
	Mean	15.999	4.986	4.988	7.007	7.006	7.002	2.008	7.008	4.988	4.993	15.939	15.436	15.610	15.364	15.740	0.096
	Accuracy	-0.001	-0.014	-0.012	0.007	0.006	0.002	0.008	0.008	0.008	-0.012	-0.007	-0.061	-0.390	-0.636	-0.260	0.096

Object B														
Machine	(mm)	y	$y\bar{l}$	$y\bar{r}$	$z\bar{l}$	$z\bar{r}$	$c\bar{l}$	$c\bar{r}$	$x\bar{l}$	$x\bar{r}$	$a\bar{l}(Degree)$	$a\bar{r}(Degree)$	r	
Objet	Standard d.	0.028	0.008	0.009	0.010	0.006	0.010	0.007	0.011	0.011	0.248	0.204	0.028	
	Mean	44.041	14.021	14.025	13.996	14.002	10.035	10.030	14.054	14.052	15.890	15.776	0.303	
	Accuracy	0.041	0.021	0.025	-0.004	0.002	0.035	0.030	0.054	0.052	-0.110	-0.224	0.303	
Eden	Standard d.	0.050	0.024	0.031	0.024	0.021	0.017	0.016	0.006	0.005	0.444	0.350	0.028	
	Mean	44.064	14.015	14.066	13.947	13.944	10.085	10.085	14.015	14.012	15.699	15.588	0.303	
	Accuracy	0.064	0.015	0.066	-0.053	-0.056	0.085	0.085	0.015	0.012	-0.301	-0.412	0.303	
EOS	Standard d.	0.038	0.014	0.016	0.020	0.018	0.022	0.018	0.023	0.021	0.278	0.237	0.069	
	Mean	43.979	13.997	13.997	14.103	14.051	9.984	9.986	14.084	14.049	16.209	16.066	0.193	
	Accuracy	-0.021	-0.003	-0.003	0.103	0.051	-0.016	-0.014	0.084	0.049	0.209	0.066	0.193	
Projet	Standard d.	0.051	0.036	0.041	0.017	0.018	0.019	0.018	0.024	0.024	0.298	0.278	0.031	
	Mean	43.818	14.009	14.024	13.993	13.974	9.974	9.996	14.019	14.014	15.911	15.920	0.098	
	Accuracy	-0.182	0.009	0.024	-0.007	-0.026	-0.026	-0.004	0.019	0.014	-0.089	-0.080	0.098	

Stratasys Objet 30

The accuracy in the z parameters for object A was $<43 \mu\text{m}$, $<-84 \mu\text{m}$ for x and $<-38 \mu\text{m}$ for y. The SD for z was $<18 \mu\text{m}$, $<34 \mu\text{m}$ for x and $<30 \mu\text{m}$ for y. The measurements for object B resulted in a z-axis accuracy of $<35 \mu\text{m}$, $<54 \mu\text{m}$ for x, and $<41 \mu\text{m}$ for y. The SD results for object B were $<10 \mu\text{m}$ in z, $<11 \mu\text{m}$ in x and $<28 \mu\text{m}$ in y (Figure 16) and the Objet 30 machine presented an angle accuracy of $<1.5^\circ$ with a SD of $<0.69^\circ$ for object A and $>-0.21^\circ$ in accuracy for object B with a SD of <0.25 (Table 9).

Stratasys Objet Eden

The z-axis parameters for object A presented an accuracy of $>-28 \mu\text{m}$, $>-32 \mu\text{m}$ for x and $<92 \mu\text{m}$ for y. The SD for the z-axis parameters was $<49 \mu\text{m}$, $<20 \mu\text{m}$ for x and $<26 \mu\text{m}$ for y. The accuracy measurements for object B in the z-axis was $<85 \mu\text{m}$, $<15 \mu\text{m}$ for x and $<66 \mu\text{m}$ for y. The SD for the z-axis parameters was $<24 \mu\text{m}$, $<6 \mu\text{m}$ for x and $<50 \mu\text{m}$ for y (Figure 16 and table 9). The Objet Eden machine presented an angle accuracy of $<0.95^\circ$ with an SD of $<0.68^\circ$ for object A and $>-0.41^\circ$ in accuracy with an SD of $<0.44^\circ$ for object B (Table 9).

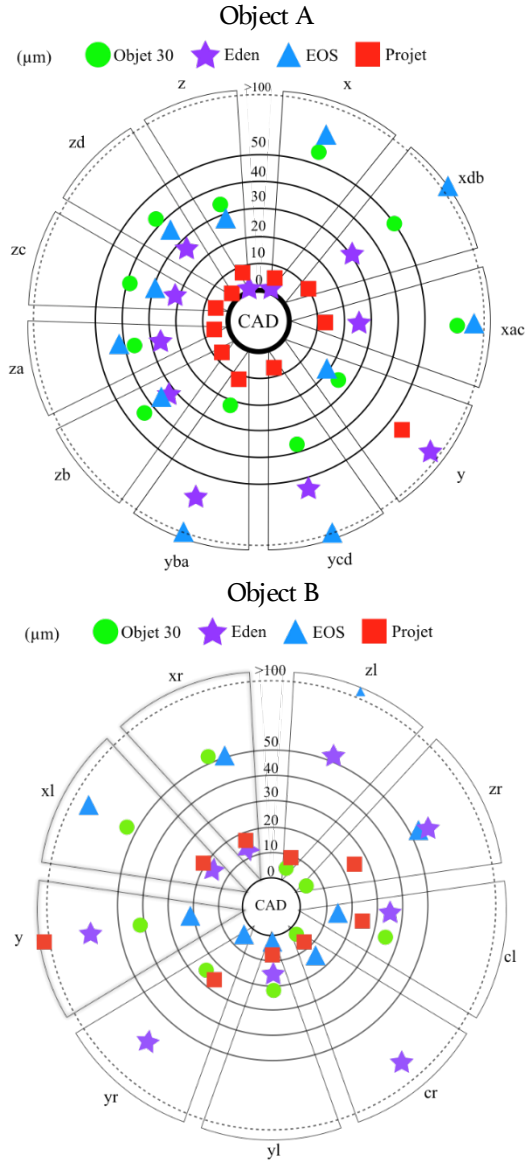


Figure 16. Bull's eye chart showing the mean values of the measurements for each parameter for all four machines, for both objects A and B. The closer the results are to the centre, the closer resemblance they have to the original CAD dimensions. This is an illustration of the machines' accuracy. It is important to notice that the illustration does not demonstrate if the results are bigger or smaller than zero, and that results past the 100 μm line could be more than 100 μm .

Study III

AM machines were compared with SM and CAD files with regard to measurements for standard deviation, accuracy, mean, angle measurements and corner radius (Tables 10 and 11).

Calibration and validation

According to Table 12, the precision for the calliper's validation in relation to gauge blocks measurements can be seen. Dahlberg's formula was used to calculate the inter-observatory variations using the digital calliper. The results shown in Table 13 demonstrate that the differences were minor for each measurement in general. Dahlberg's formula was also used to calculate the inter-observatory variations between the operators, taking the measurements from the microscope into consideration (Table 4).

Linear measurements

Object A – accuracy, precision and variance

X-axis

Arcam had the lowest x-axis precision, 0.078 mm, when compared to Mikron, which had the highest precision, 0.013 mm. Arcam also had the least accuracy, 0.176 mm in x-axis, when compared to the CAD file and Mikron had the highest accuracy, -0.012 mm.

Regarding the precision variance in the x-axis, xac and xdb Arcam had the highest variance, 0.039 – 0.078 mm, whereas EOS (CoCr) had the least variance, 0.013 – 0.019 mm. Accuracy variance for the same measurements showed that Mikron had most variation (-0.012) – (-0.173) and EOS had the lowest, 0.061 – 0.100. (Table 10, Figures 17 and 18).

Table 10. All the results from measuring object A, for orientation of the different measurements please see Figure 13. The results are presented in mm aside from the angle measurements; these are presented in degrees.

Object A Machine:	(mm)	x	xac	xdb	yba	yca	y	za	zc	zd	z	zb	(Degree) aba	(Degree) adb	(Degree) acd	(Degree) aac	(mm) I
Arcam®	Precision	0.078	0.039	0.049	0.071	0.045	0.117	0.148	0.208	0.184	0.020	0.158	0.422	0.546	0.332	0.579	0.078
	Mean	16.176	5.028	5.037	5.088	5.075	16.136	6.139	6.167	6.138	1.594	6.129	17.303	17.018	17.161	16.968	0.287
	Accuracy	0.176	0.028	0.037	0.088	0.075	0.136	-0.861	-0.833	-0.862	-0.406	-0.871	1.303	1.018	1.161	0.968	0.287
Concept laser®	Precision	0.045	0.045	0.017	0.021	0.027	0.043	0.109	0.082	0.092	0.088	0.105	0.209	0.074	0.043	0.089	0.041
	Mean	16.037	16.037	5.115	5.113	5.121	16.029	7.290	7.281	7.299	2.263	7.294	15.950	15.976	15.989	15.989	0.146
	Accuracy	0.037	0.013	0.115	0.113	0.121	0.029	0.290	0.281	0.299	0.263	0.294	-0.050	-0.024	-0.011	-0.011	0.146
EOS (CoCr)®	Precision	0.019	0.015	0.013	0.020	0.013	0.012	0.060	0.062	0.060	0.059	0.054	0.015	0.026	0.018	0.024	0.041
	Mean	15.971	5.089	5.081	5.082	5.080	15.970	7.069	7.086	7.081	2.061	7.058	16.004	15.994	16.000	15.992	0.155
	Accuracy	-0.029	0.089	0.081	0.082	0.080	-0.030	0.069	0.086	0.081	0.061	0.058	0.004	-0.006	0.000	-0.008	0.155
SLM®	Precision	0.023	0.015	0.015	0.018	0.020	0.029	0.061	0.042	0.041	0.054	0.038	0.170	0.035	0.113	0.089	0.060
	Mean	16.122	5.048	5.049	5.051	5.057	16.144	7.220	7.220	7.214	2.252	7.212	16.076	16.004	16.057	15.989	0.170
	Accuracy	0.122	0.048	0.049	0.051	0.057	0.144	0.220	0.220	0.214	0.252	0.212	0.076	0.004	0.057	-0.011	0.170
EOS®	Precision	0.022	0.037	0.030	0.020	0.023	0.027	0.268	0.251	0.253	0.264	0.282	0.039	0.035	0.028	0.028	0.040
	Mean	16.061	5.100	5.099	5.117	5.127	16.068	7.998	8.004	7.989	3.014	8.026	16.009	15.995	16.003	15.995	0.216
	Accuracy	0.061	0.100	0.099	0.117	0.127	0.068	0.998	1.004	0.989	1.014	1.026	0.009	-0.005	0.003	-0.005	0.216
Mikron®	Precision	0.009	0.048	0.054	0.038	0.041	0.009	0.013	0.012	0.015	0.034	0.017	0.017	0.017	0.013	0.015	0.034
	Mean	15.988	4.834	4.827	4.832	4.790	15.99	7.016	7.014	7.014	1.941	7.021	16.007	16.005	16.003	16.003	0.108
	Accuracy	-0.012	-0.166	-0.173	-0.168	-0.210	-0.010	0.016	0.014	0.014	-0.059	0.021	0.007	0.005	0.003	0.003	0.003

Table 11. All the results from measuring object B, for orientation of the different measurements please see Figure 14. The results are presented in mm aside from the angle measurements; these are presented in degrees.

Object B Machine:	(mm)	xl	xr	y	yl	yr	cl	cr	zl	zr	(Degree) al	(Degree) ar	(mm) r
Arcam®	Standard deviation	0.068	0.079	0.123	0.076	0.074	0.137	0.140	0.189	0.250	0.026	0.024	0.076
	Mean	14.144	14.161	44.243	14.135	14.118	10.102	10.161	13.027	13.025	15.982	15.995	0.153
	Accuracy	0.144	0.161	0.243	0.135	0.118	0.102	0.161	-0.973	-0.975	-0.018	-0.005	0.153
Concept laser®	Standard deviation	0.024	0.026	0.052	0.031	0.017	0.039	0.076	0.081	0.082	0.091	0.129	0.015
	Mean	13.946	13.948	43.990	13.971	13.974	9.985	9.945	14.268	14.208	15.924	15.896	0.084
	Accuracy	-0.054	-0.052	-0.010	-0.029	-0.026	-0.015	-0.055	0.268	0.208	-0.076	-0.104	0.084
EOS (GoCr)®	Standard deviation	0.020	0.014	0.030	0.013	0.014	0.044	0.034	0.117	0.071	0.019	0.022	0.020
	Mean	13.950	13.953	43.905	13.962	13.974	9.905	9.940	14.180	14.102	15.995	15.996	0.101
	Accuracy	-0.050	-0.047	-0.096	-0.038	-0.026	-0.095	-0.060	0.180	0.102	-0.005	-0.004	0.101
SLM®	Standard deviation	0.030	0.035	0.075	0.037	0.053	0.097	0.082	0.097	0.082	0.017	0.022	0.037
	Mean	14.017	14.026	44.022	14.063	14.071	9.912	9.995	14.043	14.060	16.003	16.001	0.059
	Accuracy	0.017	0.026	0.022	0.063	0.071	-0.088	-0.005	0.043	0.060	0.003	0.001	0.059
EOS®	Standard deviation	0.044	0.038	0.042	0.037	0.027	0.099	0.073	0.194	0.086	0.026	0.029	0.020
	Mean	14.005	14.005	44.154	14.020	14.017	9.942	10.050	14.683	14.683	15.982	15.987	0.117
	Accuracy	0.005	0.005	0.154	0.020	0.017	-0.058	0.050	0.683	0.683	-0.018	-0.013	0.117
Mikron®	Standard deviation	0.009	0.006	0.006	0.015	0.015	0.037	0.045	0.02	0.017	0.014	0.016	0.011
	Mean	14.008	14.007	44.005	13.958	14.06	10.082	10.127	13.984	13.955	16.000	16.008	0.032
	Accuracy	0.008	0.007	0.005	-0.042	0.060	0.082	0.127	-0.016	-0.045	0.000	0.008	0.032

Table 12. Calibration and validation of the digital calliper. This procedure was conducted before measuring each manufacturing group.

		Gauge block				
(n.50)		2 mm ± 0.15 µm	5 mm ± 0.22 µm	7 mm ± 0.15 µm	20 mm ± 0.32 µm	40 mm ± 0.35 µm
Machine	Arcam	1.993 ± 0.005	4.989 ± 0.008	6.993 ± 0.014	19.995 ± 0.020	39.998 ± 0.019
	Concept laser	1.990 ± 0.005	4.992 ± 0.008	6.992 ± 0.014	19.997 ± 0.020	39.997 ± 0.017
	EOS (CoCr)	1.999 ± 0.005	4.991 ± 0.005	6.993 ± 0.009	19.993 ± 0.011	39.997 ± 0.031
	SLM	1.999 ± 0.005	4.990 ± 0.007	6.991 ± 0.004	19.994 ± 0.015	40.002 ± 0.025
	EOS	1.995 ± 0.008	4.988 ± 0.015	6.990 ± 0.021	19.994 ± 0.020	39.993 ± 0.019
	Mikron	1.995 ± 0.008	4.988 ± 0.009	6.991 ± 0.011	19.995 ± 0.023	39.996 ± 0.020

Table 13. Inter-observatory variability between the operators using digital calliper, calculated with Dahlberg's formula.

		Gauge block				
		2 mm	5 mm	7 mm	20 mm	40 mm
Machine	Arcam	0.0022	0.0036	0.0026	0.0039	0.0116
	Concept laser	0.0013	0.0018	0.0041	0.0044	0.0035
	EOS (CoCr)	0.0008	0.0018	0.0026	0.0032	0.0046
	SLM	0.0014	0.0012	0.0021	0.0050	0.0072
	EOS	0.0014	0.0014	0.0026	0.0040	0.0044
	Mikron	0.0011	0.0029	0.0027	0.0053	0.0040

Y-axis

Arcam had the lowest precision, 0.117 mm, and Mikron had highest precision, 0.009 mm. Mikron showed highest accuracy, at -0.010 mm and, at the same time, the lowest accuracy at -0.0210 mm.

Regarding the precision variance in the y-axis, yba and ycd, Arcam had the highest, 0.045 – 0.117 mm, whereas EOS had the least variance, 0.020 – 0.027 mm. Accuracy variance for the same measurements showed that Mikron had the highest (-0.010) – (-0.210). Arcam and EOS shared the lowest with a difference of 0.059 mm (Table 10, Figures 17 and 18).

Z-axis

EOS had the lowest z-axis precision, 0.282 mm, while Mikron had the highest precision, 0.012 mm. Mikron also had the highest z-axis accuracy, 0.014 mm, while EOS had the lowest accuracy, at 1.026 mm.

Regarding the precision variance in the z-axis, za, zb, zc and zd, Arcam had the highest, 0.020 – 0.208 mm, whereas the least variance in the z-axis can be seen in EOS (CoCr) 0.054 – 0.062 mm. Accuracy variance for the same measurements showed that Mikron had least variation (-0.059) – 0.015 and Arcam had the most variation, ranging from (-0.871) – (-0.406) (Table 10, Figures 17 and 18).

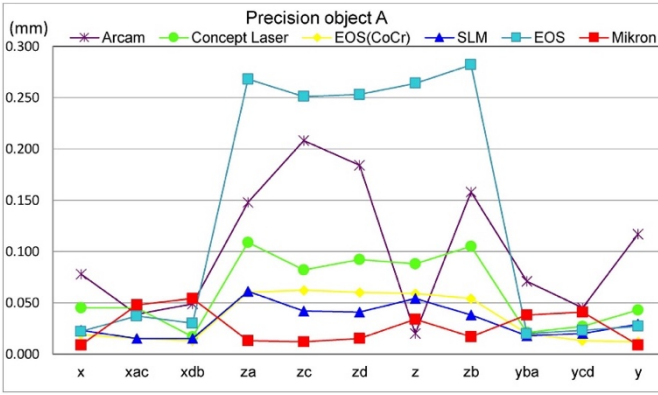


Figure 17. Precision chart for object A

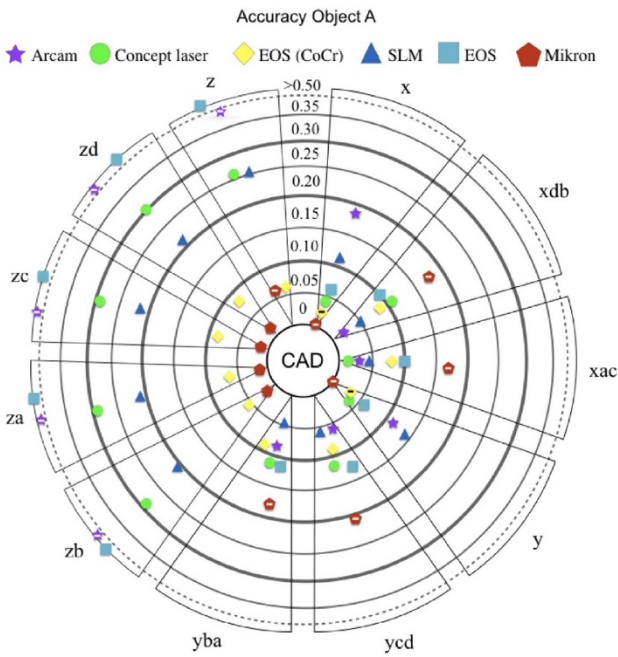


Figure 18. Bull's eye chart for object A showing mean values regarding accuracy for each machine. The minus sign represents a negative measurement value. All the markers that are outside of the dotted line have a number greater than 0.50 mm. The markers close to the bull's eye represent high accuracy or closeness to the original CAD design.

Object B - accuracy, precision and variance

X-axis

Arcam had lowest x-axis precision, 0.079 mm and Mikron had the highest precision, 0.006 mm. Mikron also had the highest accuracy, 0.007 mm whereas Arcam had the lowest accuracy, 0.161 mm.

Regarding the precision variance in xl and xr, Arcam had the highest, 0.068 – 0.079 mm, while Mikron had the least variance, 0.006 – 0.009 mm. Accuracy variance for the same measurements showed that EOS had the least variance at 0.005 mm and Arcam the highest at 0.144 – 0.161 mm (Table 11, Figures 19 and 20).

Y-axis

Mikron had the lowest precision, 0.153 mm in the y-axis and the highest precision at 0.006 mm. Arcam had the lowest accuracy, 0.243 mm and Mikron had the highest, at 0.005 mm.

Regarding the precision variance in y, yl and yr, Mikron had the highest variance, 0.006 – 0.153 mm, while EOS had the least variance, 0.027 – 0.042 mm. Accuracy variance for the same measurements showed that EOS had the highest variance, 0.005 – 0.154 mm. The Concept laser had the least variance (-0.029) – (-0.010) (Table 11, Figures 19 and 20).

Z-axis

Arcam had the lowest z-axis precision, 0.250 mm and Mikron had the highest precision at 0.017. Arcam had the lowest accuracy, -0.975 mm and SLM had the best accuracy, at -0.005 mm

Regarding the precision variance in zl, zr, cl, and cr, EOS had the highest variation, 0.073 – 0.194 mm, while Mikron showed the least variation, 0.045 – 0.017. Accuracy variance for the same measurements showed that Arcam ranged from -0.973 to 0.118 mm (Table 11, Figures 19 and 20).

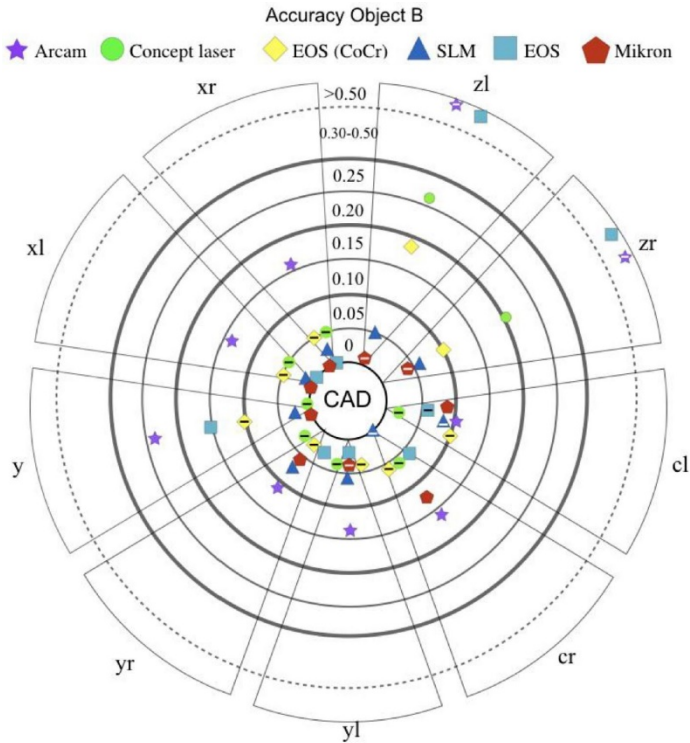


Figure 19. Bull's eye chart for object B showing mean values regarding accuracy for each machine. The minus sign represents a negative measurement value. All the markers that are outside of the dotted line have a number greater than 0.50 mm. The markers close to the bull's eye represent high accuracy or closeness to the original CAD design.

Objects A & B – angle measurements, precision and accuracy

The angle of objects A and B in the CAD was set to 16.000° (Figures 13 and 14). Mikron showed the highest precision for object A within 0.004° deviation, Mikron and Arcam had the highest precision for object B within 0.002° deviation. Arcam showed the lowest precision for object A of $>0.3^\circ$ and Concept Laser had the lowest precision for object B $>0.09^\circ$. Mikron had the highest accuracy for object A with a 0.004° deviation, while SLM had the highest accuracy at 0.002° deviation for object B. Arcam had the lowest accuracy for object A $>1.0^\circ$ and Concept laser for object B $>-0.07^\circ$. (Tables 10 and 11 and Figure 21).

Object A and B – corner radius, precision and accuracy

The corner radius for objects A and B in the CAD was set to 0.01 mm. Mikron showed the highest precision for objects A and B at 0.034 and 0.011 mm, and the highest accuracy at 0.108 and 0.032 mm. Arcam had the lowest precision form for objects A and B at 0.078 and 0.076 mm and the lowest accuracy at 0.287 and 0.153 mm (Tables 11 and 12).

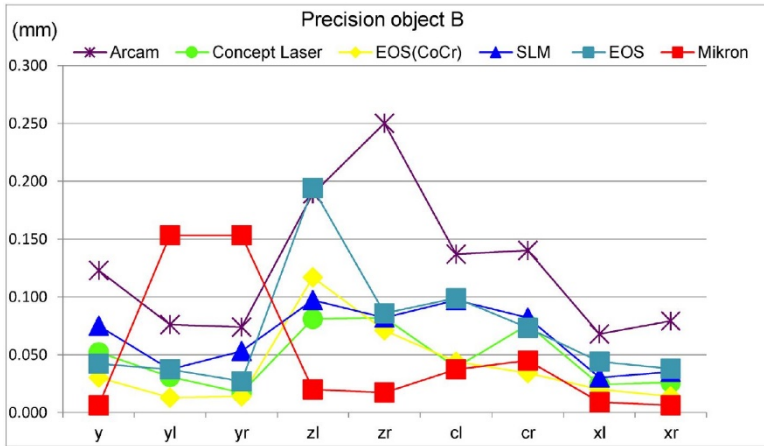


Figure 20. Precision chart for object B.

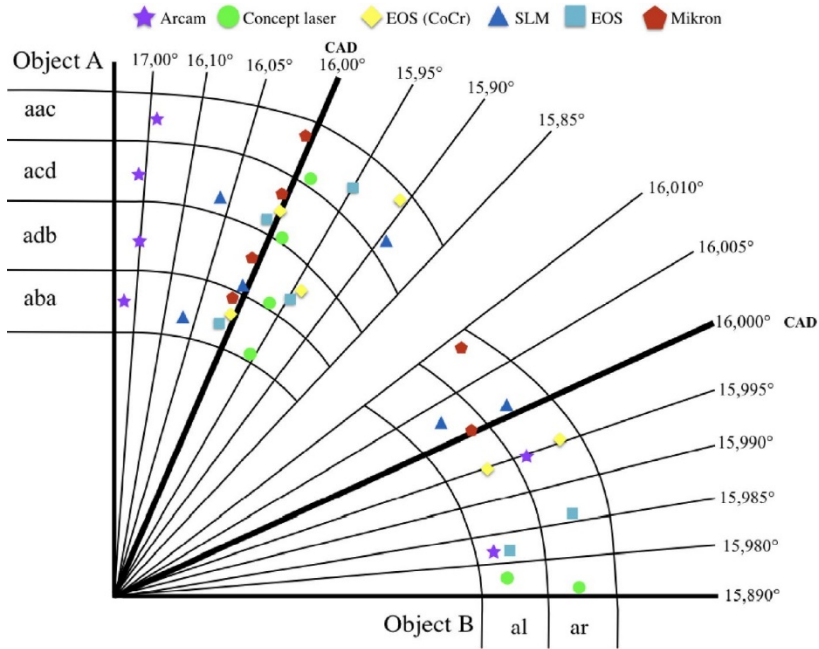


Figure 21. Precision chart for object B.

Study IV

The results and calculations were divided into two parts: in the first part, the calculations focused on the cross-arch measurements P1-P2, P1-P3, P1-P4, P1-P5 for both the edentulous and dentated cast, where point one was used as anchorage, or starting point. In the second part, the calculations were conducted in the inter-cylindrical measurements P1-P2, P2-P3, P3-P4, P4-P5. The measurement P1-P2 is the same for both groups. Table 15 presents the CMM data, the precision and trueness for both cross-arch and inter-cylindrical measurements for both the edentulous cast and the dentated cast. The Mann-Whitney test and the student t-test showed conclusive data for all the statistical tests except for Omnicam P1-P5 and P4-P5 and for CS 3600 P2-P3 ($P < .05$, Table 14).

Table 14. Results from the applied statistical methods. Numbers $< .05$ are highlighted in bold ($P < .05$)

		Statistical analysis for the comparison of edentulous models and dentated models ($<P .05$)							
		Cross arch				Inter cylindrical			
Omnicam	Mann-Whitney Sig. 2*(1-tailed Sig.)	.187	.187	.683	.021	.187	.137	.902	.026
	Student t-test Sig. (2-tailed)	.688	.168	.972	.101	.688	.207	.664	.945
	Levene's test for equality of variances	.001	.001	.005	.002	.001	.046	.062	.009
CS3600	Mann-Whitney Sig. 2*(1-tailed Sig.)	.000	.000	.217	.016	.000	.037	.000	.000
	Student t-test Sig. (2-tailed)	.000	.000	.449	.031	.000	.078	.000	.002
	Levene's test for equality of variances	.001	.000	.032	.011	.001	.007	.039	.027
Emerald	Mann-Whitney Sig. 2*(1-tailed Sig.)	.081	.174	.838	.539	.081	.026	.067	.098
	Student t-test Sig. (2-tailed)	.503	.245	.651	.453	.503	.012	.075	.125
	Levene's test for equality of variances	.009	.369	.876	.032	.009	1.000	.013	.004
Itero	Mann-Whitney Sig. 2*(1-tailed Sig.)	.010	.089	.325	.775	.010	.106	.002	.902
	Student t-test Sig. (2-tailed)	.023	.081	.636	.498	.023	.202	.001	.905
	Levene's test for equality of variances	.122	.225	.204	.760	.122	.902	.736	.000
Trios 3	Mann-Whitney Sig. 2*(1-tailed Sig.)	.000	.029	.174	.001	.000	.267	.217	.000
	Student t-test Sig. (2-tailed)	.000	.022	.113	.001	.000	.561	.196	.000
	Levene's test for equality of variances	.007	.018	.885	.390	.007	.626	.173	.029

Omnicam

Table 3 shows the results from a two-way independent student t-test in combination with a Mann-Whitney test and a Levene's variance test. When comparing the difference when scanning the dentated cast and the edentulous cast for cross-arch measurements for Omnicam, there was statistical significance for P1-P5 (Mann-Whitney .021) and there was statistical significance for P4-P5 (Mann-Whitney .026) in the inter-cylindrical measurements. All measurements for

both the cross-arch cast and the inter-cylindrical cast had statistical significance for Levene's test (except P3-P4 .062). The cross-arch trueness data for Omnicam E ranged from 23 μm (P1-P2) to 193 μm (P1-P5) with precision levels from 22 μm (P1P2) to 299 μm (P1-P5). The Inter-cylindrical trueness data ranged from 16 μm (P4-P5) to 23 μm (P1-P2) with precision levels from 93 μm (P4-P5) to 22 μm (P1-P2). The cross-arch trueness data for Omnicam D ranged from 25 μm (P1-P2) to 67 μm (P1-P3) with precision levels from 6 μm (P1P2) to 67 μm (P1-P5). The inter-cylindrical trueness data ranged from 14 μm (P4-P5) to 30 μm (P2-P3) with precision levels from 6 μm (P1-P2) to 16 μm (P2-P3 and P3-P4) (Table 15 and Figures 22 and 23).

CS 3600

When comparing the difference on scanning the dentated cast versus the edentulous cast for both cross-arch and inter-cylindrical measurements, there was statistical significance for all three statistical methods except for the t-test for P1-P4 (.449), the Mann-Whitney test (.217) and the t-test for P2-P3 (.078, Table 16). The cross-arch trueness data for CS 3600 E ranged from -103 μm (P1-P2) to 181 μm (P1-P5) with precision levels from 66 μm (P1-P2) to 247 μm (P1-P5). The inter-cylindrical trueness data ranged from -16 μm (P4-P5) to -103 μm (P1-P2) with precision levels from 42 μm (P2-P3) to 66 μm (P1-P2 and P3-P4). The cross-arch trueness data for CS 3600 D ranged from 6 μm (P1-P2) to 38 μm (P1-P4) with precision levels from 17 μm (P1-P2) to 82 μm (P1-P5). The inter-cylindrical trueness data ranged from 3 μm (P4-P5) to 33 μm (P3-P4) with precision levels from 16 μm (P2-P3) to 14 μm (P3-P4) (Table 15 and Figures 22 and 23).

Emerald

When comparing the difference on scanning the dentated cast and the edentulous cast for both the cross-arch and the inter-cylindrical group, only P2-P3 showed statistical significance for the t-test (.012) and the Mann-Whitney test (.026). With regard to the Levene's test, all measurements from the inter-cylindrical groups except P2-P3 (1.000) were significant (Table 14). For the cross-arch group, only P1-P2 (.009) and P1-P5 (.032) were significant (Table 14). The cross-arch trueness data for Emerald E ranged from 6 μm (P1-P2) to 163 μm (P1-P4) with precision levels from 96 μm (P1-P2) to 441 μm

(P1-P5). The inter-cylindrical trueness data ranged from 6 μm (P1-P2) to -67 μm (P3-P4) with precision levels from 38 μm (P2-P3) to 97 μm (P3-P4). The cross-arch trueness data for Emerald D ranged from -11 μm (P1-P2) to 129 μm (P1-P4) with precision levels from 17 μm (P1-P2) to 311 μm (P1-P5). The inter-cylindrical trueness data ranged from -11 μm (P1-P2) to -56 μm (P4-P5) with precision levels from 17 μm (P1-P2) to 54 μm (P3-P4) (Table 15 and Figures 22 and 23).

Table 15. Calculated data from all IOS devices for the edentulous and dentated cast.

		Edentulous					Dentated model				
	Measurement	N	CMM	Mean	Precision	Trueness	N	CMM	Mean	Precision	Trueness
OmnicaM											
Cross-arch	Point 1-Point 2	15	22.618	22.641	0.022	0.023	15	22.567	22.592	0.006	0.025
	Point 1-Point 3	15	35.020	35.061	0.070	0.042	15	34.986	35.053	0.015	0.067
	Point 1-Point 4	15	41.687	41.747	0.174	0.061	15	41.668	41.727	0.050	0.059
	Point 1-Point 5	15	39.566	39.759	0.299	0.193	15	39.626	39.685	0.067	0.059
Inter-cylinder	Point 1-Point 2	15	22.618	22.641	0.022	0.023	15	22.567	22.592	0.006	0.025
	Point 2-Point 3	15	16.536	16.556	0.028	0.020	15	16.544	16.575	0.016	0.030
	Point 3-Point 4	15	20.568	20.585	0.044	0.017	15	20.552	20.575	0.016	0.023
	Point 4-Point 5	15	21.591	21.607	0.093	0.016	15	21.544	21.558	0.009	0.014
CS 3600											
Cross-arch	Point 1-Point 2	15	22.618	22.515	0.066	-0.103	15	22.567	22.573	0.017	0.006
	Point 1-Point 3	15	35.020	34.895	0.074	-0.125	15	34.986	34.995	0.018	0.009
	Point 1-Point 4	15	41.687	41.702	0.111	0.015	15	41.668	41.706	0.044	0.038
	Point 1-Point 5	15	39.566	39.747	0.247	0.181	15	39.626	39.653	0.082	0.027
Inter-cylinder	Point 1-Point 2	15	22.618	22.515	0.066	-0.103	15	22.567	22.573	0.017	0.006
	Point 2-Point 3	15	16.536	16.520	0.042	-0.016	15	16.544	16.550	0.016	0.006
	Point 3-Point 4	15	20.568	20.508	0.066	-0.060	15	20.552	20.585	0.024	0.033
	Point 4-Point 5	15	21.591	21.537	0.061	-0.054	15	21.544	21.547	0.018	0.003
Emerald											
Cross-arch	Point 1-Point 2	15	22.618	22.624	0.096	0.006	15	22.567	22.556	0.017	-0.011
	Point 1-Point 3	15	35.020	35.099	0.115	0.079	15	34.986	35.025	0.061	0.039
	Point 1-Point 4	15	41.687	41.849	0.199	0.163	15	41.668	41.797	0.197	0.129
	Point 1-Point 5	15	39.566	39.711	0.441	0.145	15	39.626	39.665	0.311	0.039
Inter-cylinder	Point 1-Point 2	15	22.618	22.624	0.096	0.006	15	22.567	22.556	0.017	-0.011
	Point 2-Point 3	15	16.536	16.598	0.038	0.062	15	16.544	16.570	0.035	0.026
	Point 3-Point 4	15	20.568	20.501	0.097	-0.067	15	20.552	20.539	0.054	-0.013
	Point 4-Point 5	15	21.591	21.574	0.093	-0.017	15	21.544	21.487	0.027	-0.056
Itoro											
Cross-arch	Point 1-Point 2	15	22.618	22.588	0.017	-0.030	15	22.567	22.556	0.025	-0.011
	Point 1-Point 3	15	35.020	34.985	0.025	-0.035	15	34.986	34.971	0.037	-0.015
	Point 1-Point 4	15	41.687	41.628	0.053	-0.059	15	41.668	41.598	0.072	-0.070
	Point 1-Point 5	15	39.566	39.485	0.085	-0.081	15	39.626	39.569	0.105	-0.056
Inter-cylinder	Point 1-Point 2	15	22.618	22.588	0.017	-0.030	15	22.567	22.556	0.025	-0.011
	Point 2-Point 3	15	16.536	16.525	0.014	-0.011	15	16.544	16.539	0.014	-0.005
	Point 3-Point 4	15	20.568	20.566	0.017	-0.002	15	20.552	20.573	0.018	0.022
	Point 4-Point 5	15	21.591	21.593	0.030	0.002	15	21.544	21.547	0.010	0.004
Trios 3											
Cross-arch	Point 1-Point 2	15	22.618	22.712	0.023	0.094	15	22.567	22.607	0.012	0.040
	Point 1-Point 3	15	35.020	35.120	0.033	0.100	15	34.986	35.061	0.021	0.075
	Point 1-Point 4	15	41.687	41.803	0.045	0.117	15	41.668	41.811	0.046	0.143
	Point 1-Point 5	15	39.566	39.602	0.094	0.036	15	39.626	39.776	0.076	0.150
Inter-cylinder	Point 1-Point 2	15	22.618	22.712	0.023	0.094	15	22.567	22.607	0.012	0.040
	Point 2-Point 3	15	16.536	16.567	0.020	0.031	15	16.544	16.579	0.017	0.034
	Point 3-Point 4	15	20.568	20.605	0.023	0.037	15	20.552	20.598	0.015	0.046
	Point 4-Point 5	15	21.591	21.662	0.019	0.071	15	21.544	21.587	0.010	0.044

Itero

When comparing the difference in scanning the dentated cast and the edentulous cast for both the cross-arch and the inter-cylindrical group, only P1-P2 and P2-P3 showed statistical significance for the t-test (.023 and 0.001) and the Mann-Whitney test (.010 and .002). For the Levene's test, only P4-P5 (.000) from the inter-cylindrical measurement was significant (Table 14). The cross-arch trueness data for Itero E ranged from -30 μm (P1-P2) to -81 μm (P1-P5) with precision values from 17 μm (P1-P2) to 85 μm (P1-P5). The inter-cylindrical trueness data ranged from 2 μm (P4-P5) to -30 μm (P1-P2) with precision values from 14 μm (P2-P3) to 30 μm (P4-P5). The cross-arch trueness data for Itero D ranged from -11 μm (P1-P2) to -70 μm (P1-P4) with precision values from 25 μm (P1-P2) to 105 μm (P1-P5). The inter-cylindrical trueness data ranged from 4 μm (P4-P5) to 22 μm (P3-P4) with precision values from 10 μm (P4-P5) to 25 μm (P1-P2) (Table 15 and Figures 22 and 23).

Trios 3

When comparing the difference on scanning the dentated cast and the edentulous cast, there was statistical significance for P1-P2, P1-P3, P1-P5 and P4-P5 for both the t-test (.000, .022, .001 and .000) and the Mann-Whitney test (.000, .029, .001, .000). For the Levene's test there was statistical significance for P1-P2 (.007), P1-P3 (.018) and P4-P5 (.029, Table 14). The cross-arch trueness data for Trios 3 E ranged from 117 μm (P1-P4) to 36 μm (P1-P5) with precision values from 23 μm (P1-P2) to 94 μm (P1-P5). The inter-cylindrical trueness data ranged from 31 μm (P2-P3) to 94 μm (P1-P2) with precision values from 19 μm (P4-P5) to 23 μm (P1-P2 and P3-P4). The cross-arch trueness data for Trios 3 D ranged from 150 μm (P1-P5) to 40 μm (P1-P2) with precision values from 12 μm (P1-P2) to 76 μm (P1-P5). The inter-cylindrical trueness data ranged from 34 μm (P2-P3) to 46 μm (P3-P4) with precision values from 10 μm (P4-P5) to 17 μm (P2-P3) (Table 15 and Figures 22 and 23).

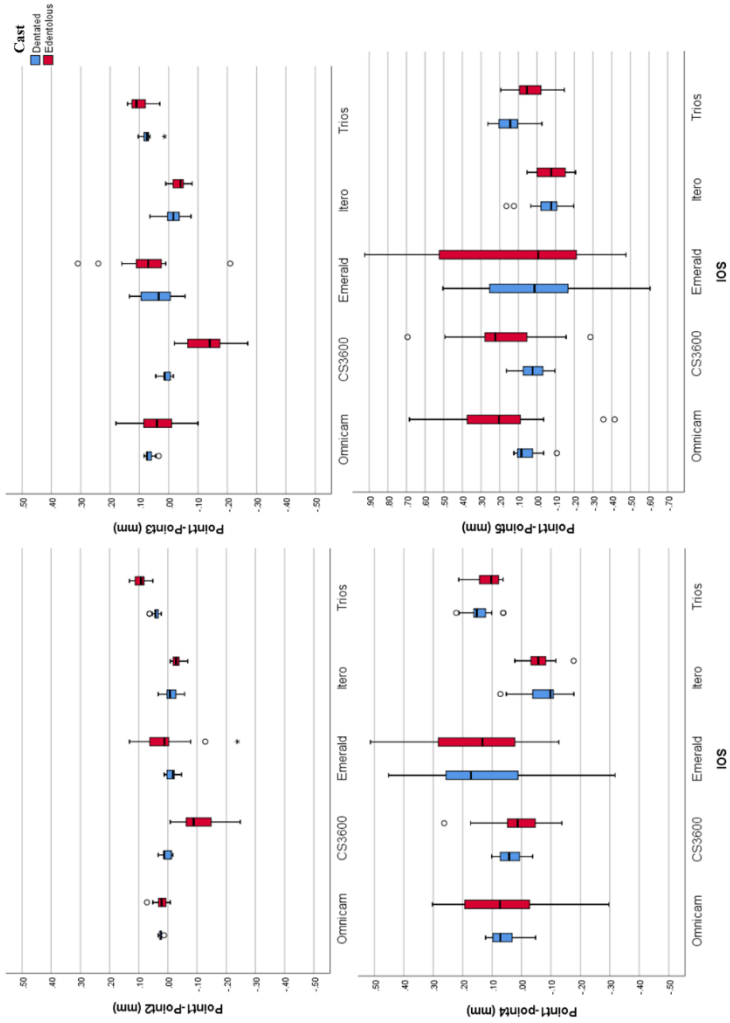


Figure 22. Boxplot illustration of the cross-arch measurement deviations from the CMM data (zero-line) for all IOS devices for both the edentulous and dentated cast.

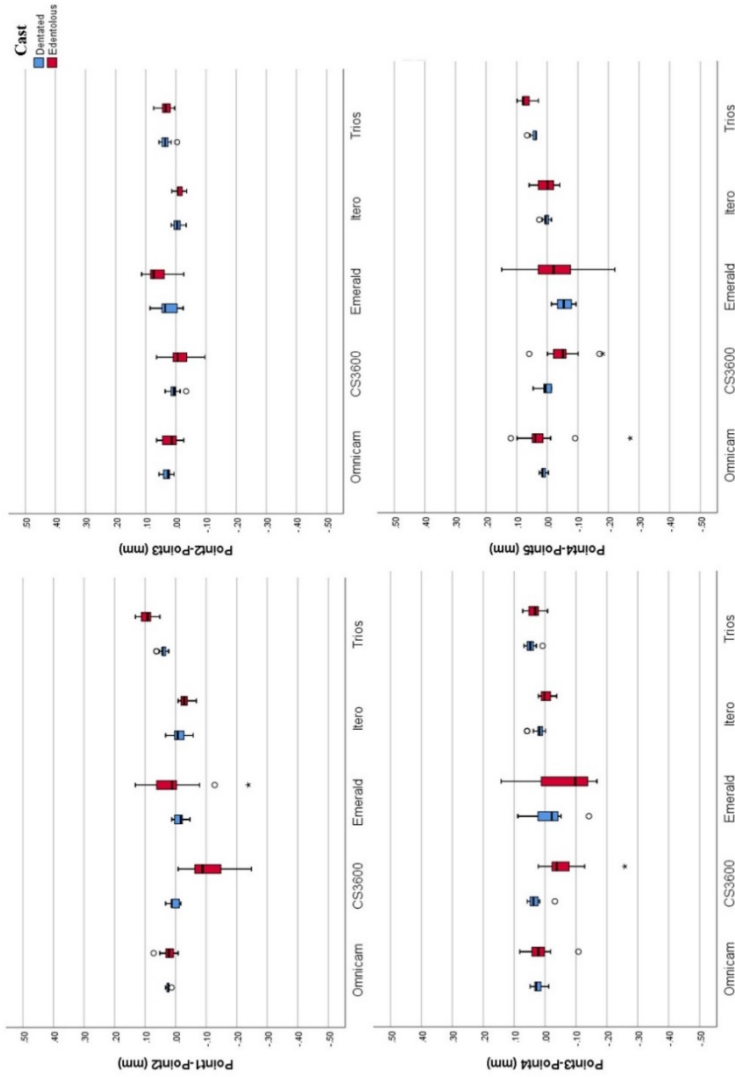


Figure 23. Boxplot illustration of the inter-cylindrical measurement deviations from the CMM data (zero-line) for all IOS devices for both the edentulous and dentated cast.

DISCUSSION

Discussion on methods

Study I

The main objective of the research was to measure implant components and the correlation between components in order to calculate the clearance. Clearance could be described as the air or space between two manufactured parts (Figure 3). The title of the first study is “Tolerance measurements on internal- and external-hexagon implants”. Tolerance, in engineering terms, refers to the manufacturing accuracy, answering the question “how accurately does the part need to be produced in order to function as intended”. The correct title for study I would be “Clearance measurements on internal- and external-hexagon implants”. Measuring components could be conducted in several ways, Tsun. Ma *et al.*[105] studied the centre point utilising a CMM to measure implant components. Hjalmarsson *et al.*[111] also studied the centre point of implant frameworks utilising a CMM. A CMM has the ability to measure x, y and z coordinates; with tactile movements they also have the ability to register geometries. The tactile touch of the probe to the object being measured results in 3D point cloud data. Depending on probe dimension the system’s ability to register shapes is limited. Thus, the tactile CMM technique is not optimal for registering shapes. Micro CT, optical 3D scanners are alternative ways to register three dimensional shapes of different components. These systems have the ability to scan physical components and present these as 3D models. Micro CT is often limited by material properties of the object being digitised, and 3D scanners sometimes struggle to scan reflective surfaces.

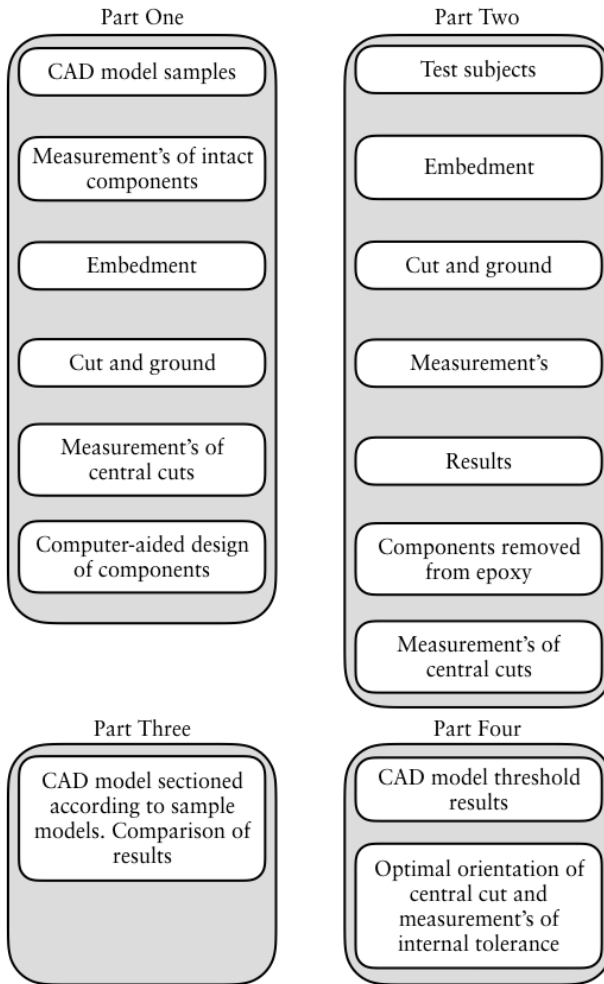


Figure 24. Workflow illustration for Study I.

Study one utilises linear and circular measurement to replicate the physical model, and the measurements are later used to design the components digitally (Figure 24). The downside of this method is the measurement procedure. Measurement errors of the physical object will affect the final design significantly. At the time, we had limited knowledge regarding equipment validation processes. The microscope that was utilised had a validation ruler; this ruler was measured in the microscope in a procedure that is referred to as calibration later in the text. One problem with this procedure was that the microscope had a focal depth of a couple of mm (Figure 25).

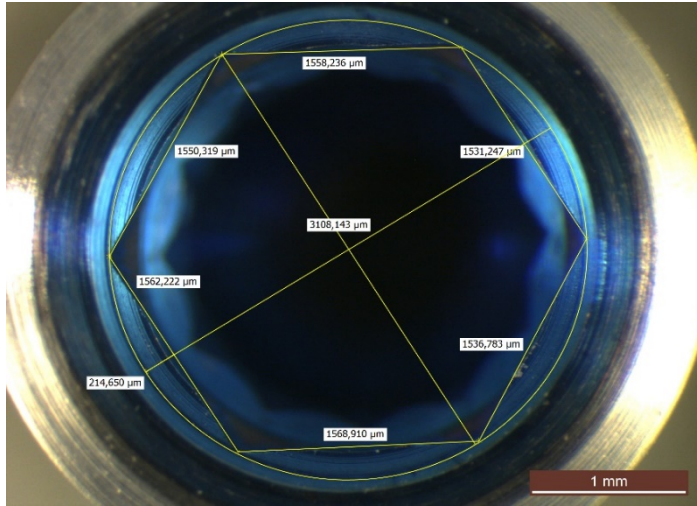


Figure 25. Image of the microscope measurements of the internal geometry of the implant. We tried to place the focal depth in the area of interest, but it is difficult to align the subject perfectly without the use of a tripod or something similar.

We had no standardised method while measuring the different geometries. Assembling the components in epoxy made it possible to section them in one piece; this procedure made it easier to measure some unreachable dimensions. The procedure also made it possible to measure the correlations between different components (Figure 26).

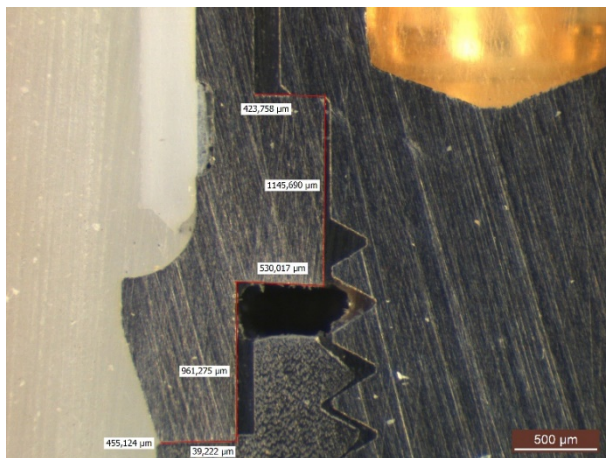


Figure 26. One of the sectioned assembled pieces that simplified measurements of difficult-to-reach geometries.

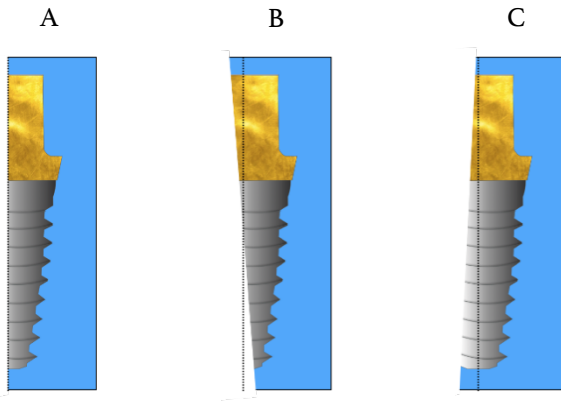


Figure 27. A) Ideal cut. B) Angulated cut. C) Angulated and not centred.

The micrometer was not validated in any way. Correspondingly, all measurements were performed on single components; because of manufacturing tolerances there are differences between every component that is produced (Figure 3). A more reliable version of this study would conduct measurements of several components of the same type, and then use the mean values for the computerised design. The grinding and cutting parts of the study also potentially cause errors. When grinding or cutting a metallic component embedded in epoxy it is a challenge to stop exactly in the centre while keeping the cut perpendicular (Figure 27 A). Upon submission of this paper, the reviewer questioned how we could be sure that the cut had been performed exactly in the middle of the implant. In order to answer that question, we had to separate the sectioned components and measure the cuts – almost none of the implants were cut exactly in the centre. Because we had the “original” data of the geometrical dimensions of all the components, we were able to measure the hexagon walls to estimate the orientation of each section (Figure 28). When this had been done we could section the digital version in the exact same place (virtually). Figure 29 illustrates the groups that were sectioned.

When conducting similar procedures, we have designed and additively manufactured a box that aligns the implant axially. This box is also composed of two straight gaps to assist the operator in the

perpendicular grinding (Figure 30). When the outer dimensions are known, the operator has the possibility to measure the box regularly to avoid stopping or passing the centre. Because of the flatness of the box, the object is well aligned when observed under the microscope, thus assisting the observer in keeping the magnification stable in between observations.

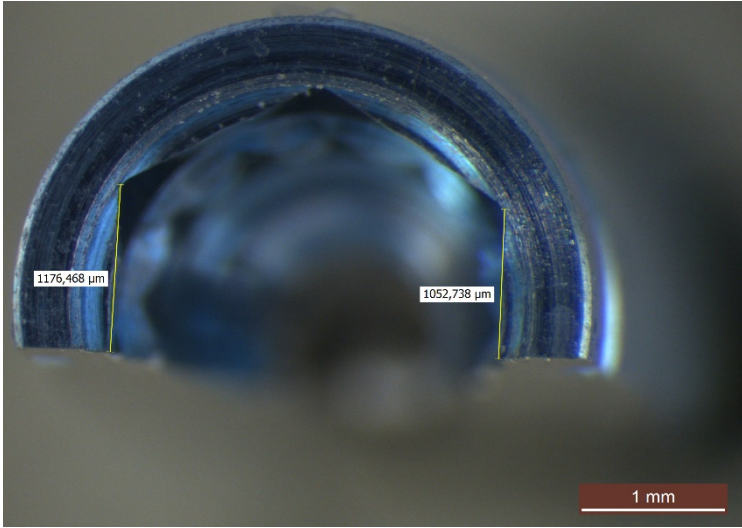


Figure 28. One dismantled implant component and the measurements of the remaining hexagonal walls.

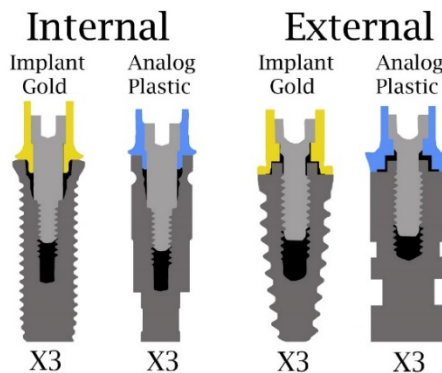


Figure 29. The grouping of the sectioned components in part two.



Figure 30. Grinding assistance box, the implant is placed in the cylinder and the box is filled with epoxy. The gap in the cylinder assists in achieving an aligned intersection.

Studies II and III

The main objective for Study II and Study III was to determine the production accuracy of models produced through AM for metals and polymers. When testing manufacturing technologies that are intended for dental applications, it is reasonable to choose a validation model that resembles a tooth or some other oral geometry. The biological shape of a tooth is challenging to measure, there are no fixed basic geometries from which to start and end the measure. It is also difficult for other researchers to verify or re-measure the biological shape without having that specific file available to them. There are several validation models available for assessing the geometrical accuracy of different manufacturing methods. Initially, we performed some pilot tests with some of the available designs[112]; however, regrettably these designs were difficult if not impossible to measure with tactile instruments. The validation models were also generally designed for industrial purposes (Figure 31).

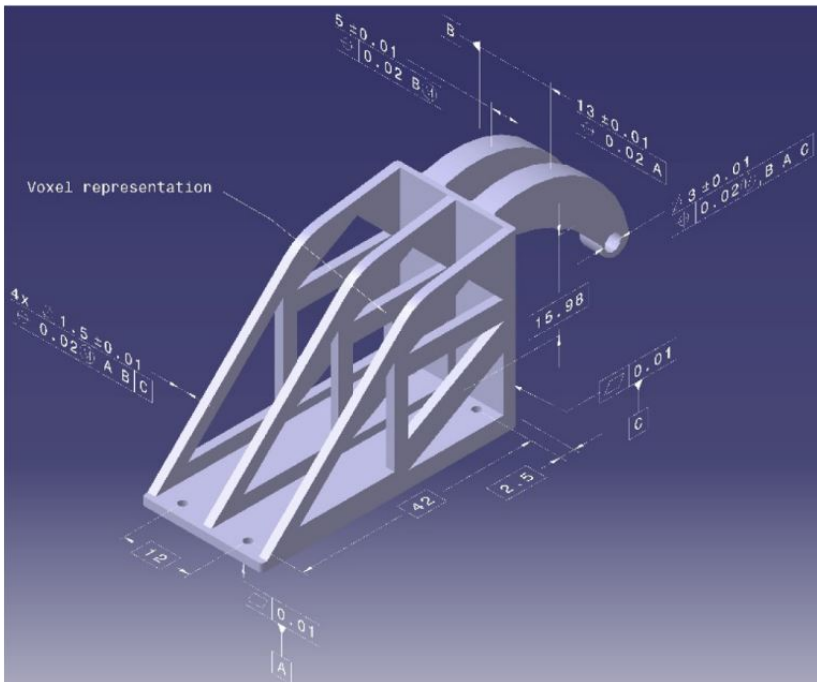


Figure 31. One of the validation models that were tested prior to ISO 12836. Image in courtesy of Moroni *et al.*

There are several reasons why we chose the ISO document as a reference for the study. The main reason was that others had the opportunity to purchase the ISO and use the designs. We also knew that the ISO comity had used these specific geometries for measurement purposes. The objects are easy to measure and the guidelines for producing and validating them are clearly stated in the document. One other reason for using this specific ISO was that the ISO contains production tolerances for the test objects that are going to be digitised. We were hoping that some of the objects manufactured in this study or the following study would be accepted by the ISO tolerances. If so, they could have been utilised in the fourth study to validate the intraoral scanners. Unfortunately, neither object A or B could be scanned with any intraoral scanner in any of our pilot tests. Even though the ISO 12836 clearly stated this in their instructions:

“This International Standard includes the measurement of the image that is digitized from dental scanners (**intraoral scanners**, **lab-based optical scanners and lab-based mechanical contact scanners**). Digitized images are not only used for the fabrication of restorative products but also applied to teaching and research in dentistry, in such areas as occlusion, tooth and gingival contour change measurements, and so forth.”[113]

One of the reasons why the objects could not be digitised with intraoral scanners was that the devices use a software algorithm that requires complicated and non-repeated geometries. Apparently, the ISO organisation figured this out and published a revised version of the ISO in 2015:

“This International Standard includes the measurement of the image that is digitized from dental scanners (lab-based optical scanners and lab-based mechanical contact scanners). Digitized images are not only used for the fabrication of restorative products but also applied to teaching and research in dentistry, in such areas as occlusion, tooth and gingival contour change measurements, and so forth.”[114]

In the 2015 version of the ISO, the intraoral scanning devices are no longer supported. In 2017, Uhm *et al.*[115] presented an interesting study that utilises object A and B to evaluate trueness and precision of four intraoral scanners. Their team also struggled to digitise the objects, but they found a solution. When the team reduced the size of the objects by 70%, they were able to digitise them. The size reduction enabled the IOS devices to digitise the entire object at once. They also added rubber impression material to the objects to provide non-symmetrical shapes, also aiding in the IOS acquisition process.

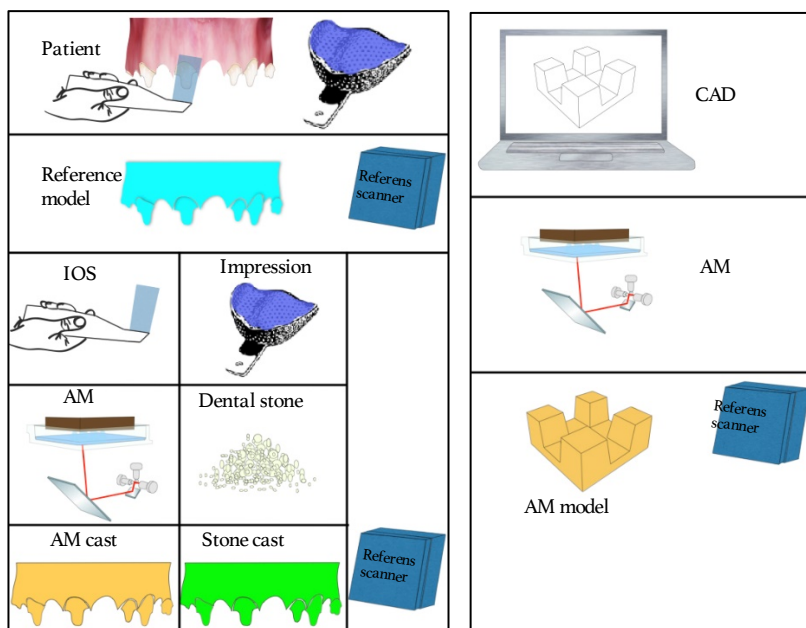


Figure 32. Left, a reference model is manufactured either from an intraoral scan or a conventional impression. The reference model is then scanned with a reference scanner. Furthermore, the reference model is scanned with one or more IOSs prior to the additive manufacturing of the model. The manufactured model is then scanned again with the same reference scanner and compared to the first scan. Right, a basic geometry is designed digitally, the design is then additively manufactured. The final object is then either scanned with a reference scanner or measured with other methods and compared to the original design.

Patzelt *et al.* [116] studied the accuracy of polymeric full-mouth models based on intraoral scans, concluding that all models had a clinically acceptable level of accuracy. They scanned one master model with a reference scanner before digitising it with the IOS devices. The files from three different IOSs were later used to additively manufacture models that were scanned with the reference scanner. Then they compared the first reference scans to the last ones. The method utilised by Patzel *et al.* and others [82, 110, 117, 118] studies the workflow of scanning and producing objects through AM, rather than focusing only on the production accuracy of the additive system. Figure 32 describes the difference further; the study workflow to the left illustrates the accuracy of additively manufactured objects post-digitisation, in this type of research the level of dimensional changes that the IOS device appends onto the model pre-production is unknown. The illustration to the right corresponds to the material and method utilised in Studies II and III. Instead of a reference scanner we utilised tactile measurement equipment. This type of research protocol focuses exclusively on the produced sample, and the computer-designed shape has digitally set dimensions and angles that serve as references. The tool utilised for measuring the produced object needs to be verified and of higher accuracy than the process in which it is going to be used (traceability). In the field of dentistry, it is difficult to specify the accuracy of different processes. The tactile instruments utilised in Studies II and III have been validated to $\pm 5 \mu\text{m}$ depending on gauge block dimension. Even if the operators have ensured repeatability conditions, and the instruments have been validated to a few microns, there still are several possible measurement errors. Some of the main handling errors when utilising tactile instruments are: alignment errors, pressure of contact point and to centralise the instrument onto the object being measured. Only flat surfaces of objects A and B (Figure 13 and 14) were measured utilising tactile instruments in Studies II and III. This minimises the alignment errors. Nevertheless, centralisation and pressure still remain as possible errors.

Initially, there were more measurements in the protocol. One interesting dimension that we measured was the distance between the cones in object B, as seen in Figure 33. The problem with these dimensions was that we had no reliable and reproducible way to

measure them with the equipment that was available to us. During the statistical analysis we noticed that there was a noteworthy difference in precision. Regarding the distance between the cones we had to use the microscope, and, with a binocular scope, the cones were not registered perpendicular to the scope. This resulted in unreliable measurements, thus all these dimensions were disregarded. We also measured the surface roughness of one part from each manufacturer, and the measurements were conducted utilising a surface roughness tester (Mitutoyo 178-561-02A, Takatsu-ku, Kawasaki, Japan). One measurement was along the print layers and the other one was cross-directional (Table 16). The surface roughness of additively manufactured parts for dental application is of importance when producing dental models or applications for intraoral use. The calculations were excluded during the review process.

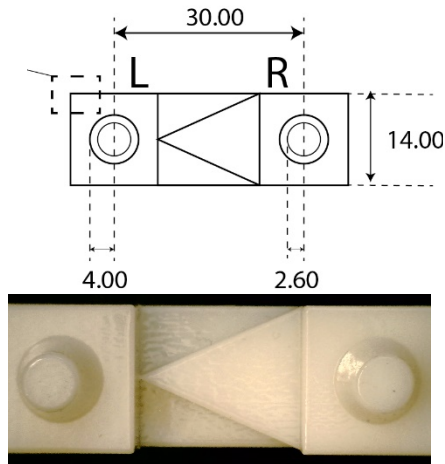


Figure 33. The distance between the cones of object B and the radius in the top and bottom of the cones.

The corner radius measurements were included in order to assess the manufacturing unit's ability to produce sharp edges. When producing objects intended for dental applications it is a necessity that the manufacturing unit has the ability to produce sharp edges and corners. A small corner radius pronounces a sharp edge, and vice versa. To the best of knowledge of the authors, the CAD software (Autocad 2013, version G.55.M.108 Mac, Autodesk Corp) that was utilised for designing the two objects in study one lacked the ability to

set edge radius. We only had the ability to set the edge to 90 degrees. The CAD files from Study II were re-designed in a different software (Solidworks educational edition 2013). All dimensions and designs are the same as for Study II, the only difference was that the edge radius was set to 0.01 mm. In addition, we thought that we had to use a different file format in order to utilise the subtractive manufacturing group (*.STEP, standard for the exchange of product model data). Later, it was clear that the STEP file was unnecessary, because the subtractive unit could utilise the STL files.

Table 16. Surface roughness measurements for the different manufacturers.

Roughness	Surface roughness (μm)				
	Machine	N	Mean	Std. Dev	Std Mean
Ra-x	Objet 30	50	1,25	0,40	,06
	Objet Eden	50	2,35	0,90	,13
	EOS	50	6,97	1,15	,16
	Projet	50	3,62	0,76	,11
Ra-z	Objet 30	50	4,80	1,45	,20
	Objet Eden	50	3,41	0,89	,13
	EOS	50	7,66	2,39	,34
	Projet	50	13,01	1,74	,25

One alternative way of checking the geometrical accuracy of a produced object is to digitise the object utilising a CMM system or optical 3D scanner. The same traceability requirements apply regardless of measuring equipment. A reliable digitised version of the produced object enables comprehensive measuring options, especially if the original CAD file is available. This powerful method enables the operator to either measure the digitised version or compare it to the original CAD file. The possibilities to measure flatness, roundness, tolerances, surface topologies, parallelism and so forth are countless. Figure 34 illustrates one of the dimensions that were of interest but unreliably measured in Study II, namely the distance between the cones of object B. This distance and many other factors are easily measured when utilising 3D analysing software. The fact that digital software applications were powerful measuring tools was known to the authors.

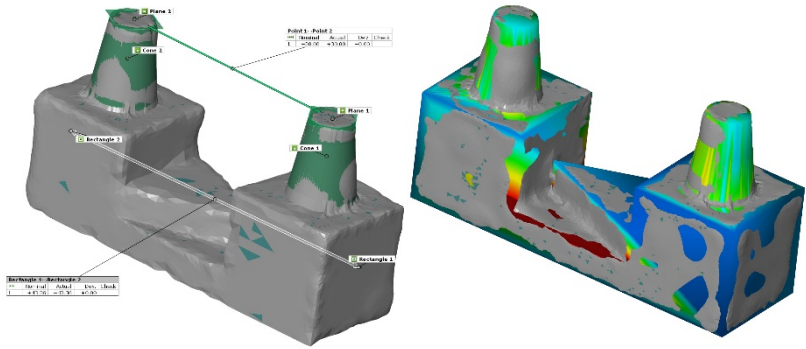


Figure 34. Left, inter-cone measurement. Right, tolerance illustration of the difference between CAD and the digitised version of the manufactured object.

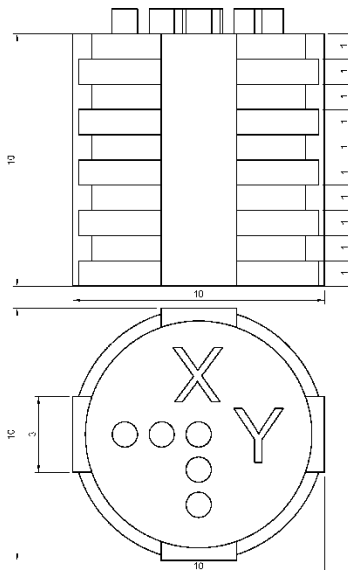


Figure 35. Technical drawing of the simplified validation design.

The reason why we chose tactile instruments was to simplify for technicians and dentists interested in conducting some in-house testing utilising object A and B before purchasing an additive system. That is also why we chose a microscope that was accessible to purchase and operate. Unfortunately, objects A and B had too many measuring dimensions to interest personnel without enthusiasm for research. This led to the design of an alternative object that was easy to produce, measure and orientate (Figure 35). In comparison with objects A and B the second design lacks cones, angles and inclinations. It must be emphasised that the geometry of object A was divided into four “cubes” (Figure 13). Therefore, for an object to be acceptable, it was of great importance that all four cubes presented comparable tolerance levels on all three axes. For instance, if the height of one of the four cubes in each object would show a difference of 100 μm , the produced inlay could be considered to have a non-passive fit. This is also the reason for conducting angle measurements for both objects A and B. Still, the second design assists in general x, y and z dimensions that aid in tolerance measurements of additive systems. When objects A and B were manufactured, the orientation onto the build plate of the tested machines was not controlled. Several of the AM machines that utilise optical solidification techniques could present tolerance differences on different parts of the build plate. Thus, the placement of the desired verification model should be controlled. In the second design we added this functionality, utilising five numbered objects. Four objects are placed in the corners of the build plate and the fifth in the middle (Figure 36). Furthermore, additional height was added in the lower part of the designs in order to compensate for compression layers that some AM systems produce in order to fixate the object to the build plate[119]. This feature was not designed in objects A and B. Figure 37 presents a microscope image of one object; the operator has the possibility to measure the x, y and z dimensions both with microscope and tactile instruments.

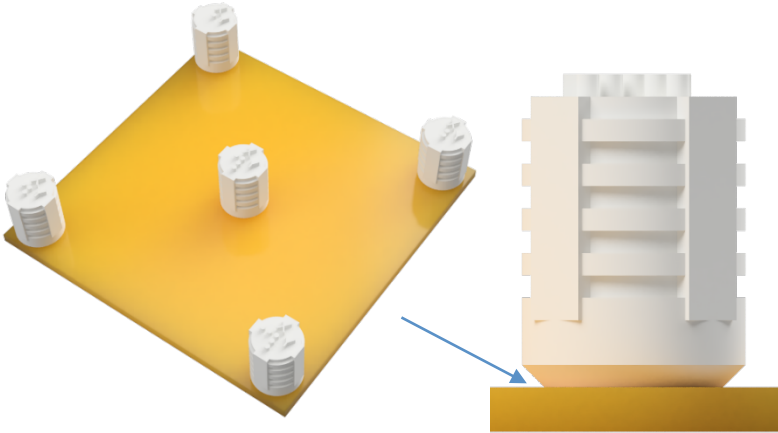


Figure 36. Left, build plate orientation of the five test objects. Right, an additional cylinder of 2 mm was added in the lower part, to compensate for possible compression layers.



Figure 37. Example of one of the five test objects, manufactured in polymer utilising a DLP system.

Study IV

Prior to the master model presented in this study, we performed several pilot studies on other master models. As previously described, we tried to scan objects A and B from Studies II and III. None of the IOS devices that we tested could digitise either object A or B properly, so we tried other alternatives. Figure 38 illustrates one of the designed master models that we tried to scan. The cubes in Figure 38 are 10*10*10 mm each. In the initial design different geometrical shapes were designed to the walls – these were difficult to digitise. We had to change the geometries to letters, as seen in Figure 38b. With this setup we were able to scan the female and male parts and the correlation (bite scan) between the two models. The downside with these cubes was that we were only able to study the behaviour of the IOS devices in a small area of approximately 10 mm. Figure 39 illustrates a larger version of the cube design. Unfortunately, the larger arch design was impossible to scan. It was clear to us that we had to utilise a geometrical shape that was similar to the oral environment regarding geometry; at the same time we needed measurable geometries. The pilot testing led to the hybrid model consisting of oral cavity geometries in combination with cylinders that are easy to measure.

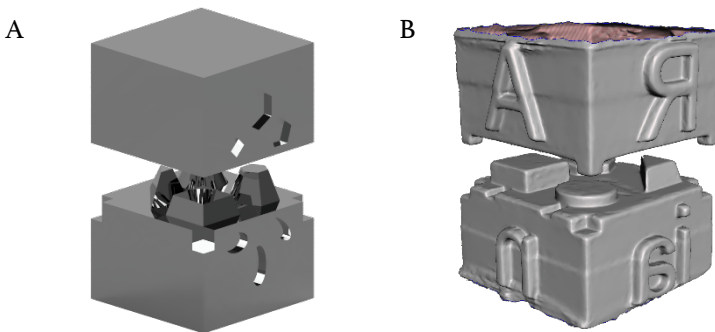


Figure 38. A The initial master design with one female (upper part) and male (lower part) model. B during the testing the wall geometries were changed to letters.

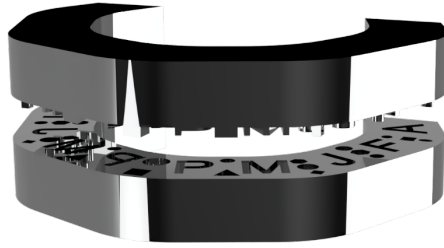


Figure 39. Upper and lower arch design utilising the same principle as the cubic design. With one female and one male part consisting of different measurable geometries.

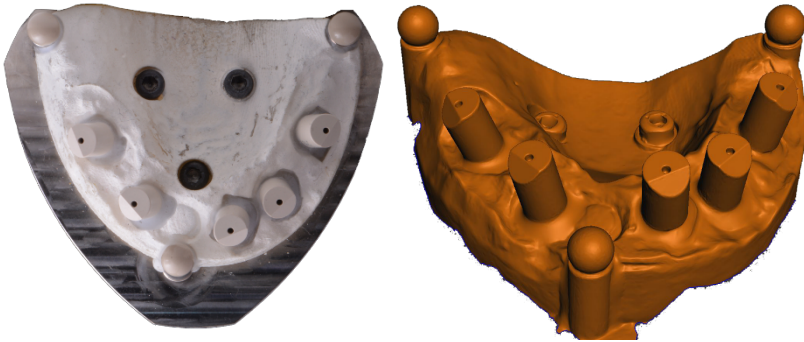


Figure 40. Left, a photograph of the actual implant master model. Right, a scanned version of the implant model.

The initial pilot test resulted in a master model (Figure 40) with a metallic base holding up 6 cylindrical peek objects, also known as scan bodies (intended for scanning implants). The base also consisted of three spheres and a gypsum model of a patient's maxilla wrapped around the implants. This implant master model had geometries from the oral cavity (gypsum part) cylindrical geometries for measurements, and spheres to assist in the measuring. It had all the necessary features, and it was fairly easy to digitise with IOS. The only downside of the implant model was that the spheres were glued in place and the cylindrical scan bodies were screw-retained to the implants. When scanning a master model more than 100 times it is important to have a model that is as rigid as possible. Moreover, we found that the height of the cylinders made it challenging to scan the cylinders and the gypsum

part at the same time. The master model utilised in Study III is the results of all previous pilot models (Figure 41). The dentated model consists of anatomical mandibular teeth and five shorter cylinders for measuring purposes. The physical model was manufactured through AM in cobalt chromium directly onto the build plate. For stability purposes, the models were never removed from the build plate. The models were sandblasted in order to achieve a non-reflective surface. Besides the removal of the teeth, the edentulous model was identical in regards of dimensions and production method.



Figure 41. Upper, dentated master model with a non-reflective surface. Lower, edentulous model with a non-reflective surface. Note that the models are attached to the build plate.

The validation technique utilised in Study IV consists of comparing known CMM measurements of the cylinders to the one calculated from the virtual scan file. Using a tactile probe, the CMM machine registers the diameter of the cylinder and the plane at the top of the

cylinder. The intersection between cylinder and plane results in an intersecting point (Figure 42).

The digital files acquired from different IOS devices are treated in a similar way in the GOM inspect software. Instead of a probe calculating the cylinder, the software utilises a Gaussian best-fit algorithm to calculate the cylindrical shape and the plane. The intersection between these two geometries results in a point (Figure 43). All five cylinders on both models are treated in the same way. This results in five points in each model; the linear distance between the five points are measured in the CMM and later compared to the same measurements on the IOS files. Figure 44 illustrates the linear distance between point one and two on the dentated model, the virtual file computes a dimension of 12.40 mm and the corresponding CMM measurements for the distance between point one and two was 12.43 mm.

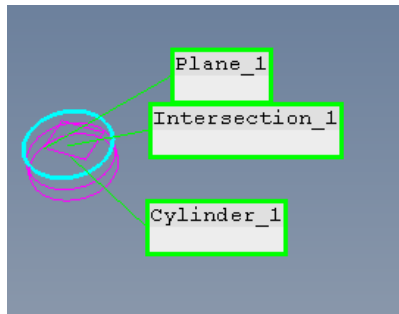


Figure 42. Image from the CMM software for the geometrical calculations to register the centre point of cylinder no. 1.

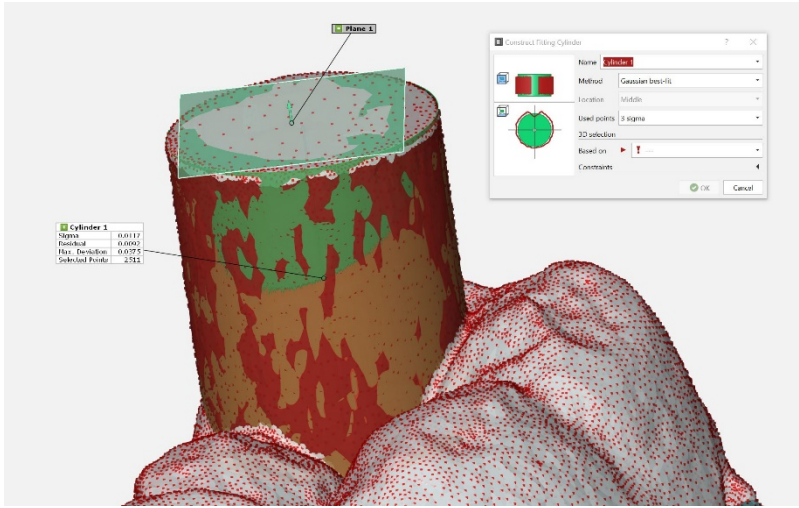


Figure 43. Image from the GOM inspect software when applying a cylinder and plane in order to calculate the centre point of cylinder no. 1.

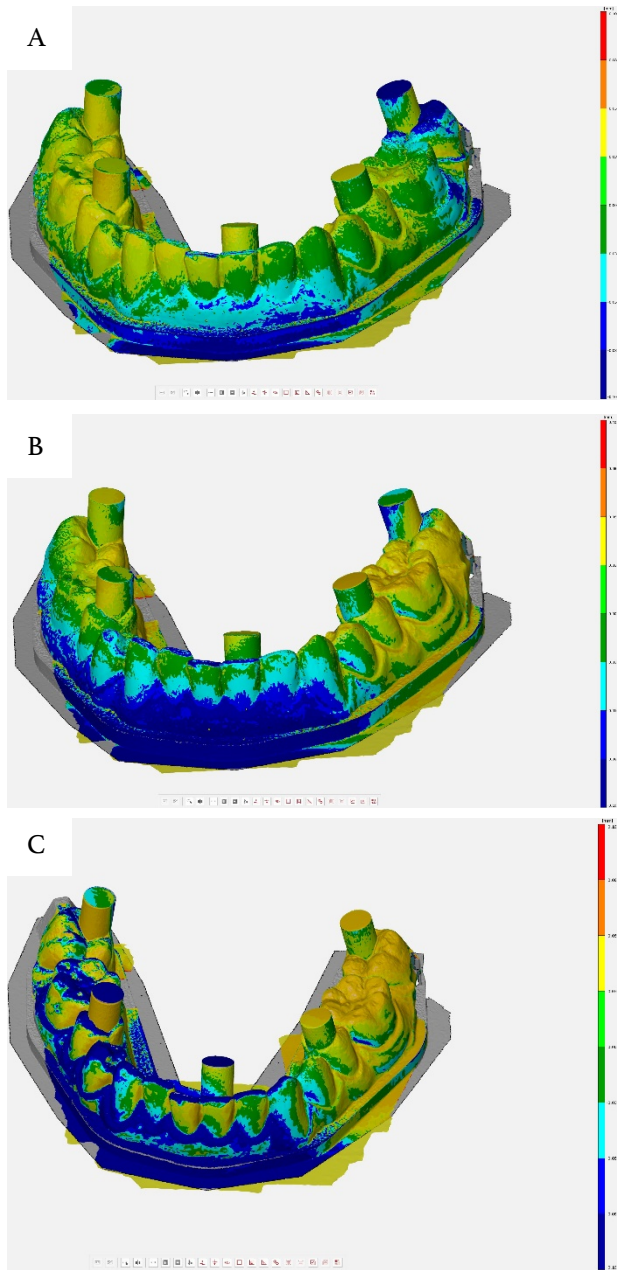


Figure 45. Blue = master scan, green = IOS scan. A) cylinder alignment. B) best fit alignment. C) alignment localises to 35, 36 and 37.

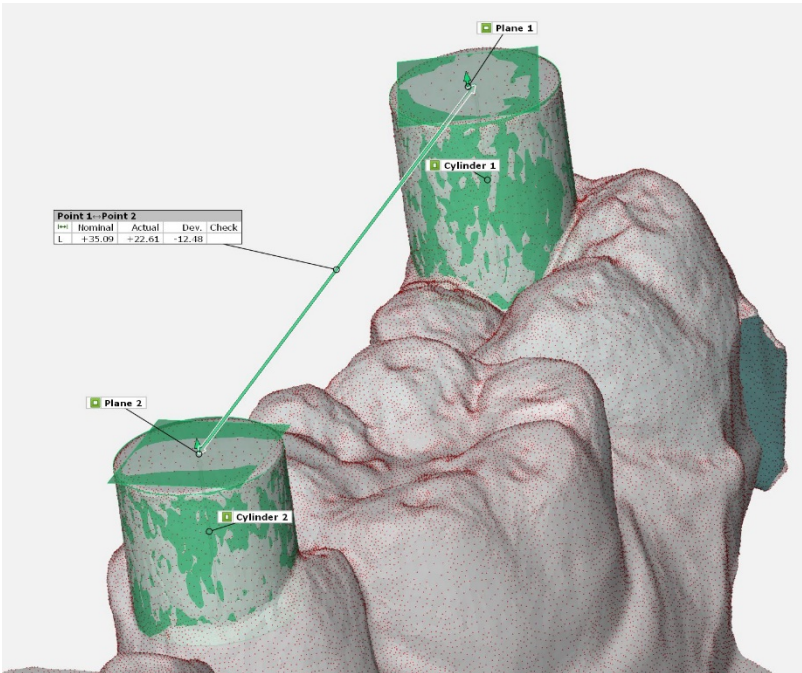


Figure 44. Software calculated linear distance between point one and two on the dentated model.

The point-to-point measurements conducted in Study IV are repeatable and simple to measure; the method utilises a software algorithm to calculate all cylinders in the same manner. The downside of the method is that only the points are calculated, thus the method would not be suitable for comparing geometrical shapes or rotations. One alternative way of comparing a virtual three-dimensional file to a known dimension consists of comparing two virtual files. One of the files originates from a 3D scanner with higher accuracy compared to the ones being tested. This method requires a point cloud to point cloud alignment. There are several ways to compare point cloud data, and, depending on method, the results will diverge significantly. Figure 45 illustrates three different types of alignments, the alignments in Figure 45a are localised to the cylinders only. The software calculates the local best fit between the two models comparing only the point cloud on the cylinders. Figure 45b illustrates the models when a local best fit is applied to the entire model and not only to the cylinders. Figure 45c illustrates when the local best fit is localised only to 35, 36 and 37. The downside of this type of alignment is that the operator

needs to understand how the different types of alignment methods affect the calculations. At the same time, this type of comparison enables the operator to study the IOS scan data freely. Moreover, the colourisation of the model enables the observer to clearly see differences between the compared models.

Discussions on results

Study I

The metallic components showed small differences, especially for the external hexagon connection (Table 6). When the external hex was cut according to optimal orientation, the virtual file presented a total clearance of 44 μm . Similar results could be found for the metallic components in the internal connection group, with a total clearance of 58 μm (Table 8). The prefabricated polymeric cylinders that were intended for casting procedures presented higher deviation when compared to the virtual files. The clearance of the polymeric components was around 90 μm (Table 8). The clear difference between the metallic and polymeric groups could be related to deformation of the polymeric cylinders. During tightening of the abutment screw, a degree of defatation of the cylinder occurs; with the external-hex implants, this causes the abutment to expand in width. The polymeric abutments in the external group showed horizontal misplacement at the abutment/implant margin, resulting in an overhang. According to the manufacturer, the Poisson ratio for the polymeric cylinder is 0.36. This ratio explains the volume changes in a material under stress. When a material is stretched in one direction, it will compress in the other direction; the Poisson ratio describes this compression. The subjects were only tightened once and with a very low force, whereas a dental technician typically tightens components a couple of times during fabrication of the framework. Study II focuses on the clearance between the implant/analogue and abutments, to estimate clearances between the components. The components are intended for screw-retained multi-unit constructions manufactured on an implant level. The results could not be used for constructions made on an abutment level, or as a standard for all implants. The results from Study I are only applicable to the specific components utilised. The findings from Study I and from other researchers[105, 106] suggest clearances ranging from 22-130 μm between different implant components.

Studies II and III

An important factor is the ability of the machine to produce the same objects every time, or, alternatively, to make the same consistent error. This means that the machine has continuity in its production and this, in turn, equals high precision. These characteristics can be evaluated by producing multiple objects from the same machine and thereafter repeating the measurements on each object. A comparison between all the measurements and the measurements of the CAD files is then needed in order to calculate the level of precision. If the precision of a measured object is low, this means that the machine manufactures the object differently each time; this lack of precision will undoubtedly affect trueness and the overall accuracy. However, if the level of precision is high, the manufacturing is consistent, but might not be close to the true value of the CAD file (Figure 1b). With this type of machine, which has a high level of precision, it is possible for the software to compensate for the CAD file in a different axis (X, Y or Z) in order to obtain greater accuracy. Bearing this in mind, the results from Studies II and III should be categorised in precision. One of the advantages with AM systems is the ability to manufacture several objects at once. All objects that were produced utilising AM technologies in Studies II and III were produced on one build plate per machine. The SM group in Study III produced each of the 20 objects one by one. When comparing the AM groups to the SM group, one should recognise that the AM groups actually are tested for repeatability and the SM group for reproducibility.

Linear measurements

Studies [106, 111, 120] have demonstrated that it can be impossible to obtain a passive fit and that a misfit always exists between implants and the manufactured superstructures they support. The lack of a reliable method to clinically evaluate the passive fit of implant restorations means that there is no consensus regarding the machine tolerance needed for a clinically acceptable fit for implant constructions[120]. Nevertheless, there is a need to produce dental reconstructions and models with high accuracy, in order to prevent technical and biological failures. As previously stated, process technologies in dentistry that have the capability to either digitise or manufacture reconstructions with a trueness of about 50-100 μm

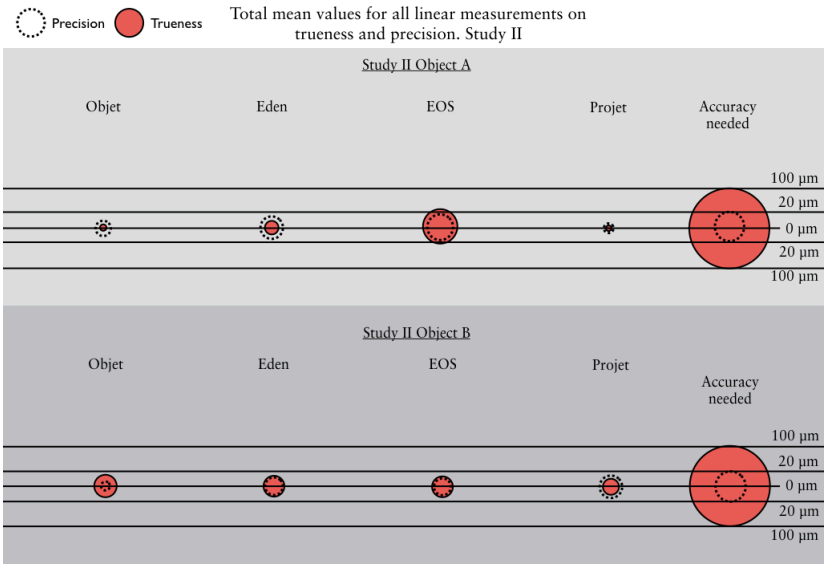


Figure 46. The calculated total mean values for all linear measurements in Study II. Dotted line = precision and filled circle = trueness. Illustration does not demonstrate if the results are bigger or smaller.

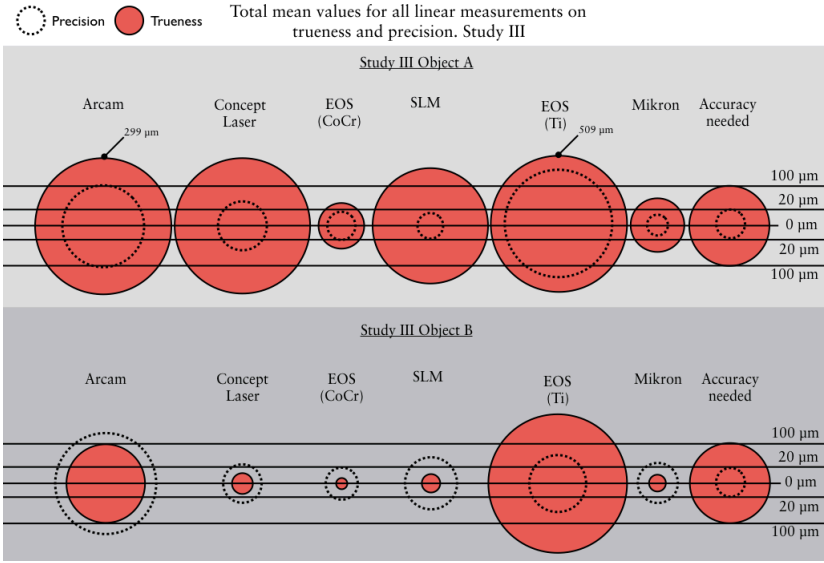


Figure 47. The calculated total mean values for all linear measurements in Study III. Dotted line = precision and filled circle = trueness. Illustration does not demonstrate if the results are bigger or smaller.

and with precision values about 20 μm would, in theory, be sufficient for dental applications. To facilitate the results from Studies II and III, the total accuracy (trueness) and precision have been calculated on all linear measurements in Figures 46 and 47. If the threshold value of $100 \mu\text{m} \pm 20$ is to be used, some of the AM technologies for producing metallic reconstructions would not have sufficient accuracy for dental application, even if precision is the considered feature for an acceptable and reliable production unit. One noticeable difference for the production of metallic versions of object A and B in Study III, is the difference in accuracy for the same machine but between the two objects. One example of this observation is the difference in linear production accuracy for ConceptLaser, EOS and Arcam when comparing object A and object B. One reason for this error could be that none of the objects produced with AM utilised supporting structures. Post-processing for all metallic objects involved cutting the metal object from the building platform. It is highly likely that the authorised personnel had difficulties removing the metallic and the polymeric objects from the build plate without affecting the z-axis dimensions. Human error can have a huge influence at this stage, resulting in low levels of trueness and precision. All the AM systems show lower levels of trueness and precision in the z-axis measurements, but Arcam and EOS had the lowest level of accuracy and precision of all AM systems in the z-axis. The measurements in the z-axis for these two machines do not represent the capability of the machine to produce the objects in that specific axis. Instead, this shows the importance of avoiding the build of important geometries directly on the build plate. When focusing on the capability of the machine to produce geometries, the measurements c_l and c_r (object B) are the more reliable measurements in the z-axis since these are not affected when they are removed from the build plate. Even if we only focus on c_l and c_r as z-axis measurements, Arcam would still have the lowest precision (c_r 140 μm), this might be due to the laser movement during processing, which results in an elevation on its perimeter.

Arcam uses high-electron beam energy and obtains a larger heat-affected zone (also known as melt pool) when compared to SLM, which uses a less powerful energy source. The melt pool also depends on the setting of the scan speed, beam diameter and bed temperature [121, 122]. Hence, the larger heat-affected zone in EBM

technology limits the recreation of the object's minimum features, inferior resolution and surface smoothness[123]. Arcam production can be simplified into three steps: the first step involves preheating powder, the second is the contouring step, where the machines melt the powder in the perimeter at a low beam ampere and speed, thereby maintaining the part accuracy. The third step is the melting step of the powder at high velocity, where the beam has a 'zigzag movement'. When the beam turns around in the perimeters, more heat is generated there. This results in a partial swelling at the perimeter due to the excessive heat generated there and consequently affects the dimension of the z-axis in objects A and B[124] (Figure 48).

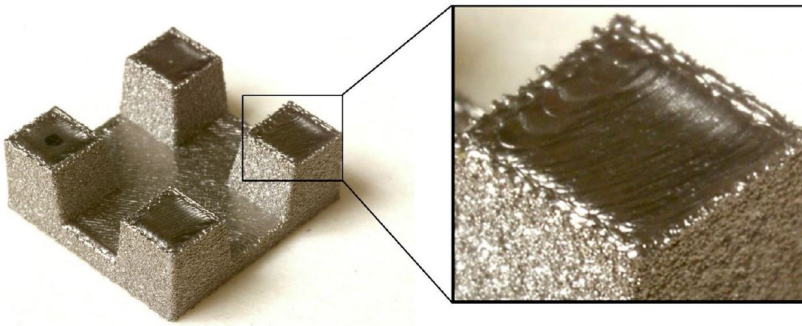


Figure 48. Photo of object A manufactured by EBM technology (Arcam), showing part-swelling at the perimeter of the "cubes".

Mikron showed constant lower values compared to the CAD file. The only dimensions that Micron struggled to produce accurately were xaz, xdb, yba and ycd. Due to the sharp internal corners of these measurements, the SM system had to compensate for the geometrical design. The SM machine was not able to reach the sharp internal corners without this drill compensation, which resulted in rounded corners that reduced distance for all four measurements (Figure 49). Some good examples of high-precision and high-trueness machines can be seen in Figure 46, where it is clear that all the machines from Study II had a total mean linear accuracy values in proximity or below the threshold values.

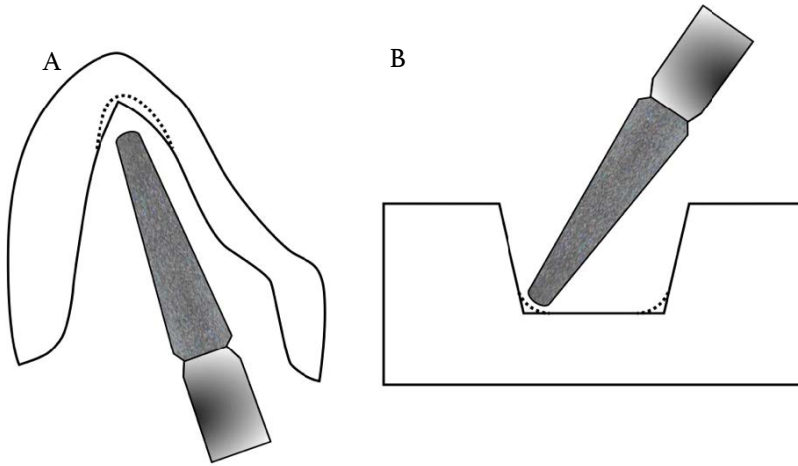


Figure 49. A, illustration of a designed crown in intersection. The black line illustrates the designed crown and the dashed line demonstrates the drill compensation. B, illustrates a side view of object A; the black line illustrates the designed object and the dashed lines demonstrates the drill compensation.

Degree and corner radius measurements

The CAD file had an angle set to 16.000° . The total mean precision and trueness for all angle measurements for both objects A and B for Studies II and III can be seen in Table 17. In addition, for Arcam, all the additive systems in Study II presented higher accuracy for the production of the 16° geometries. The system with highest overall accuracy was the Mikron system, presenting trueness values at 0.004° with a precision at 0.015° . The impact of an insufficient angle production is unknown, most likely an angle defect will affect the final geometries, but there are no threshold values with which to compare the results.

A possible cause is that SM can recreate the angles close to the CAD file's dimensions, possibly because of the simplicity of the periphery geometries, an outer-corner shaper in this case. This leads to an uncomplicated toolpath and easy accessibility for the burrs.

Table 17. Trueness and precision for all angle measurements for study III.

Total mean accuracy for all angle measurements for both Object A and B			Total mean accuracy for all angle measurements for both Object A and B		
Objet	Total mean precision	0.482	Arcam	Total mean precision	0.322
	Total mean trueness	0.599		Total mean trueness	0.738
Eden	Total mean precision	0.490	Concept Laser	Total mean precision	0.106
	Total mean trueness	0.297		Total mean trueness	-0.046
EOS	Total mean precision	0.435	EOS (CoCr)	Total mean precision	0.021
	Total mean trueness	0.559		Total mean trueness	-0.003
Projet	Total mean precision	0.452	SLM	Total mean precision	0.074
	Total mean trueness	-0.337		Total mean trueness	0.022
			EOS	Total mean precision	0.031
				Total mean trueness	-0.005
			Mikron	Total mean precision	0.015
				Total mean trueness	0.004

AM groups generally had poorer accuracy compared to SM in re-creating a 90° periphery corner radius from the CAD file. Arcam had the least accuracy for object A, with a corner radius of 0.287 mm, and object B, 0.153 mm. Arcam also had the lowest precision for object A, 0.078 and object B, 0.076 mm. The reason for this might be the surface roughness of the object, which made it difficult to see and measure the edges in the microscope (Figure 50). The main principle in AM technique is layer-by-layer build-up. When different geometries with angled or curved shapes are to be built in an AM machine, the ‘staircase shape’ is difficult to avoid and results in surface roughness and dimensional inaccuracy[125, 126]. Staircase shapes depend on the size of powder particles, layer thickness, surface angle to the building platform and melt pool temperature[126, 127]. This shape can be reduced if the layer thickness is thinner, if smaller powder particles are used or if a reduced surface angle of the object is utilised. Consequently, the building time will be affected as well as the cost. Arcam, which uses EBM technology, has the largest layer thickness and powder particle size. This results in poor surface smoothness and poorer dimensional accuracy, as shown in this study. One major difference of the EBM technology is the production speed; it is faster compared to other AM techniques because of its ability to melt each layer and the underlying layer during the build-up process. This results in lower residual stress of the manufactured object; therefore there is no need for post-processing and heat treatment[127-129].

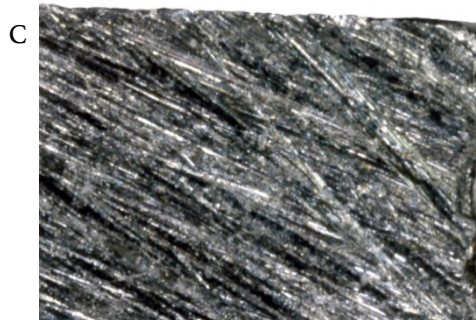


Figure 50. 250x magnification of one edge from object A manufactured by: A) Arcam machine, B) Concept laser and C) SM group, Mikron.

Inter-observatory variability

In Study II, two operators measured all the objects. It is of great importance to perform a calibration if more than one operator is executing the measurements in order to ensure that both operators are measuring correspondingly. This is of importance in order to achieve significant results as well as ensuring that a standardised method is used. Dahlberg's formula was chosen for calculating the calibration between the operators, due to the capability of the method to calculate small differences. Furthermore, this formula also provides the possibility of estimating inter-observatory variability, which is considered beneficial[130]. All the values received with Dahlberg's formula can be seen in Table 4 and Table 12. Furthermore, a standardised method for the measurements was used; thus all measurements were conducted in a temperature stable environment, 20 ± 1 °C [131].

Study IV

The hypothesis stating that there would be no significant differences within each IOS system when scanning the two different arches can be partially rejected. For the cross-arch measurements, three out of four measurements were statistically significant for Trios 3 and CS 3600, when comparing the edentulous cast with the dentated one. At the same time, the Emerald scanner had no significant difference for the cross-arch measurement. For the inter-cylindrical measurements, CS 3600 showed overall significant differences, while the other scanners were only partially significant. It is not clear how many of the comparing studies that have used Itero Elements and how many used the older generation Itero. The Itero Elements scanner was launched in March 2015; for comparison purposes studies pre-2015 should be disregarded. The same problem arises for Trios and the Planmeca plan scan. 3Shape has presented three generations of scanners and the one used in this study is Trios 3 (2015, third generation), Planmeca released the Emerald scanner in late 2017, and, to the best of the authors' knowledge, there are no similar studies available for comparison. Nevertheless, it is important to carry out a comparison of previous studies, even if there are limitations regarding conclusions. Ender *et al.* [35] studied conventional and digital full-arch impressions utilising the 3D superimposing technique. They found overall trueness data on the Omnicam to be 37.3 μm , while they also found that the same IOS showed increasing deviation toward the end of the arch, with a difference up to 100 μm . They also tested the Itero (pre-2015 version) scanner, with trueness data at 32.4 μm . The precision data from that study also showed that Omnicam differed partially on one side of the tested cast, with increasing deviation up to 130 μm . The Itero showed large deviations up to 120 μm . The data found from the current study on cross-arch measurements for Omnicam D showed trueness data from 25-67 μm and precision data ranging from 6-67 μm . The same data from Itero D showed trueness values ranging from -11 to -70 μm and precision values ranging from 30-81 μm . In a study by Muallah *et al.*[132] a method comparable to the current study was utilised, the authors measured the virtual files in a linear manner instead of superimposing 3D data. One of the linear measurements focuses on inter-molar width of a maxillary master cast; this measurement is

similar to P1-P5 in the current study. The trueness results for Trios (version unknown) presented were 29.160 μm with a precision of 52.872 μm , trueness for Itero (version unclear) -47.030 μm with a precision of 84.137 μm . The current study presents trueness data for Itero D (P1-P5) at -56 μm with a precision of 105 μm . Trueness for Trios D (P1-P5) 150 μm with a precision of 76 μm . Van der Meer *et al.*[133] utilised three cylinders on their master cast that were measured utilising tactile CMM. Two of the cylinders replaced the first molars and one replaced a mandibular front tooth; the measurements conducted in that study are comparable to P1-P3 and P1-P5 in the current study. The study concluded that trueness for Itero (pre-2015 version) was 70.5 μm (P1-P3) with precision values of 56.3 μm , and 61.1 μm in trueness for (P1-P5) with precision of 53.9 μm . These values could be compared to data from this article for trueness data at -15 μm (P1-P3) and -56 μm (P1-P5) with precision values of 37 μm (P1-P3) and 105 μm (P1-P5) for Itero D. Ender *et al.* [42] also tested the precision on digital quadrant scans. They scanned a master cast, third quadrant from molar to canine: a measurement comparable to P1-P2 in the current study. The mean percentage values of 26.1 μm for Trios color (second generation) with a SD of 3.8 μm , the same measurement for Itero (pre-2015) mean 49.0 μm SD 12.4 μm and mean values for Omnicam at 37.4 μm SD 8.1 μm . These could be compared to P1-P2 trueness for Itero D -11 μm and precision of 25 μm , trueness for Trios D 40 μm with precision of 12 μm and trueness of Omnicam D 25 μm with a precision of 6 μm . Giménez *et al.*[40] studied the Itero scanner (pre-2015 version) using a comparable master cast with cylinders as geometrical landmarks. They also used tactile CMM equipment to assess true values. Several factors were evaluated, one of them being comparable to the Itero E cross-arch data from the current study. They found that error increased with the increase in stitching, starting from -14.3 μm (mean deviation) with an SD of 25.6 μm to -32 μm (mean deviation) with an SD of 216.1 μm in the last quadrant scanned. The trueness data for similar measurements being P1-P2 and P1-P5 for Itero E ranged from 30 μm and -81 μm , with precision values of 17 μm (P1-P2) to 85 μm (P1-P5). The clear effect of the stitching processes producing errors proportional to the scan distance, as noted in this study, has also been documented in other studies [42, 134-136]. Even though

there are limitations for the comparison to other studies with regard to measuring methods, IOS versions and the shape, size, material of the validation casts, it is clear that full-arch scans pose a challenge to the IOS devices in regards of trueness but even more with regard to precision. The findings suggest that the trueness and precision of inter-cylindrical distances on the dentated cast for all IOS devices were $<50\ \mu\text{m}$ (except Emerald D P4-P5, $-56\ \mu\text{m}$) with precision data $\leq 35\ \mu\text{m}$ (except Emerald D, P3-P4, $54\ \mu\text{m}$). This suggests that the IOS devices are accurate for shorter arch acquisitions ranging from approximately 16 to 22 mm in length. When studying the cross-arch measurements it is clear that the results are not as favorable for the dentated validation cast. The trueness for all IOS devices was $\leq 129\ \mu\text{m}$ (except Trios D, P1-P5, $150\ \mu\text{m}$) and precision of $\leq 105\ \mu\text{m}$ (except Emerald D, P1-P5, $311\ \mu\text{m}$) suggesting that the cross-arch measurement is less reliable than the inter-cylindrical for the dentated casts. For the inter-cylindrical data on the edentulous validation cast, the IOS devices presented trueness values of $\leq 94\ \mu\text{m}$ (except CS 3600, P1-P2, $-103\ \mu\text{m}$) and precision of $\leq 97\ \mu\text{m}$. This indicates that the inter-cylindrical measurement on the dentated cast has almost twice the level of trueness and three times the level of precision when compared to the inter-cylindrical measurement on the edentulous cast. The trueness values for the cross-arch measurements on the edentulous cast presented values of $\leq 193\ \mu\text{m}$ and precision of $\leq 299\ \mu\text{m}$ (except Emerald E, P1-P5, $441\ \mu\text{m}$). In order to validate if these numbers are relevant or not for dentistry, there needs to be a threshold value for different dental applications. It has been suggested that an accuracy level of $<150[137]\ \mu\text{m}$ is favourable for fixed tooth supported prosthodontics. Ahrberg *et al.*[138] studied the digital workflow for all ceramic restorations for single units and three-unit bridges in vivo, with the conclusion that it was more accurate than the conventional workflow. Their findings could be supported by the data found in the current study suggesting that the IOS devices are accurate for shorter arches. If the findings from the current study also were to use $100\ \mu\text{m} \pm 20\ \mu\text{m}$ as a threshold, only short arch scans would be suitable for scanning the oral environment for further processing. Figure 51 Illustrates a similar comparison as for Studies II and III, where total mean trueness and precision has been calculated and compared to the theoretical threshold values. Studying Figure 51

it is clear that there are noteworthy differences between different IOS devices for the acquisition of edentulous, dentated and cross-arch, inter-cylindrical measurements.

The oral situation is affected by several factors that could not be included in the fourth study design, thus one can only speculate that saliva, light conditions, soft and hard tissue reflections, humidity, intermittent acquisition and movements from the soft tissue and tongue would affect the outcome of a similar study in vivo. Furthermore, an edentulous condition without implants would not consist of five cylinders aiding in the acquisition process. Therefore, further in vivo studies with a similar approach are needed.

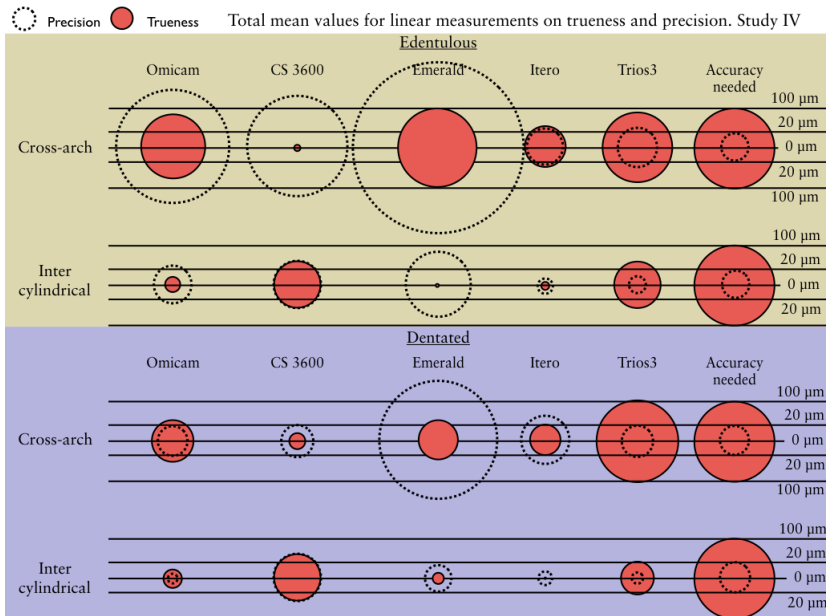


Figure 51. The calculated total mean values for measurements in Study IV. Dotted circle = precision and filled circle = trueness. Illustration does not demonstrate if the results are bigger or smaller.

CONCLUSIONS

The horizontal machining tolerances for prefabricated cylindric gold abutments on external implants with hexagonal connections showed the smallest machining tolerances, which were less than 50 μm . Prefabricated gold abutments on internal-hexagon implants showed tolerances $<90 \mu\text{m}$. In contrast, prefabricated plastic cylinders showed errors of $<100 \mu\text{m}$ for external-hex implants and $<130 \mu\text{m}$ for internal-hex implants.

The production accuracy for all four tested additive systems for producing polymeric objects were on average $<20 \mu\text{m}$ for both precision and trueness.

The production accuracy for all five tested additive systems for producing metallic objects ranged from $>500 \mu\text{m}$ to $<30 \mu\text{m}$ in trueness with precision values $<100 \mu\text{m}$. The subtractive system showed trueness values $<25 \mu\text{m}$ with a precision around $20 \mu\text{m}$.

For the cross-arch measurements on the edentulous scans, the trueness values ranged from $6 \mu\text{m}$ (Emerald P1-P2) to $193 \mu\text{m}$ (Omnicam P1-P5) and for the inter-cylindrical measurements, the results ranged from $2 \mu\text{m}$ (Itero P4-P5) to $-103 \mu\text{m}$ (CS 3600 P1-P2). For the dentated cast, the cross-arch trueness values ranged from $6 \mu\text{m}$ (CS3600 P1-P2) to $150 \mu\text{m}$ (Trios 3 P1-P5) and for the inter-cylindrical measurements, the results ranged from $4 \mu\text{m}$ (Itero P4-P5) to $-56 \mu\text{m}$ (Emerald P4-P5).

ACKNOWLEDGEMENTS

I would like to thank Malmö University and the faculty of odontology for giving me the opportunity to conduct my research. A special thanks to everyone at the department of fixed prosthodontics.

Professor Ann Wennerberg

For all the guidance during these eight years. You believed in my research from day one, and you supported me to explore a new world freely.

I would also like to thank everyone around me who has helped me to understand my own research better by critically reviewing my ideas, and giving me new ones.

Elisabeth Björnhammer

Without your love and support I would never have achieved anything that I have done today.

REFERENCES

1. ISO, I., 5725-1: 1994, *Accuracy (trueness and precision) of measurement methods and results-Part 1: General principles and definitions*. International Organization for Standardization, Geneva, 1994.
2. Carrotte, P.V., A. Johnson, and R.B. Winstanley, *The influence of the impression tray on the accuracy of impressions for crown and bridge work--an investigation and review*. Br Dent J, 1998. 185(11-12): p. 580-5.
3. Haralur, S.B., et al., *Accuracy of Multiple Pour Cast from Various Elastomer Impression Methods*. Int J Dent, 2016. 2016: p. 7414737.
4. Alkurt, M., Z. Yesil Duymus, and N. Dedeoglu, *Investigation of the effects of storage time on the dimensional accuracy of impression materials using cone beam computed tomography*. J Adv Prosthodont, 2016. 8(5): p. 380-387.
5. Anusavice, K.J., et al., *Phillips' science of dental materials*. 2013, St. Louis, Mo.: Elsevier/Saunders.
6. Serrano, J.G., et al., *An accuracy evaluation of four removable die systems*. J Prosthet Dent, 1998. 80(5): p. 575-86.
7. Swartz, M.L., et al., *Role of cavity varnishes and bases in the penetration of cement constituents through tooth structure*. The Journal of Prosthetic Dentistry, 1966. 16(5): p. 963-972.
8. Cho, S.H., et al., *Effect of die spacer thickness on shear bond strength of porcelain laminate veneers*. J Prosthet Dent, 2006. 95(3): p. 201-8.
9. Kotsiomiti, E. and A. Kaloyannides, *Crown pattern waxes: A study of their behavior on heating and cooling*. The Journal of Prosthetic Dentistry, 1994. 71(5): p. 511-516.
10. Zeltser, C., I. Lewinstein, and R. Grajower, *Fit of crown wax patterns after removal from the die*. The Journal of Prosthetic Dentistry, 1985. 53(3): p. 344-346.

11. Grajower, R. and I. Lewinstein, *Effect of manipulative variables on the accuracy of crown wax patterns*. The Journal of Prosthetic Dentistry, 1985. 53(2): p. 168-172.
12. Lloyd, C.H., et al., *Measurement of the setting expansion of phosphate-bonded investment materials: part II--An evaluation of the Casting-Ring Test at 10 laboratories*. J Oral Rehabil, 2004. 31(7): p. 703-9.
13. Hutton, J.E. and G.W. Marshall, *Expansion of phosphate-bonded investments: Part II—Thermal expansion*. The Journal of Prosthetic Dentistry, 1995. 73(2): p. 126-131.
14. Earnshaw, R., *The effect of casting ring liners on the potential expansion of a gypsum-bonded investment*. J Dent Res, 1988. 67(11): p. 1366-70.
15. Liu, Q., M.C. Leu, and S.M. Schmitt, *Rapid prototyping in dentistry: technology and application*. The International Journal of Advanced Manufacturing Technology, 2005. 29(3-4): p. 317-335.
16. Richert, R., et al., *Intraoral Scanner Technologies: A Review to Make a Successful Impression*. J Healthc Eng, 2017. 2017: p. 8427595.
17. Ireland, A.J., et al., *3D surface imaging in dentistry - what we are looking at*. Br Dent J, 2008. 205(7): p. 387-92.
18. Tapie, L., et al., *Understanding dental CAD/CAM for restorations--accuracy from a mechanical engineering viewpoint*. Int J Comput Dent, 2015. 18(4): p. 343-67.
19. Mandelli, F., et al., *Evaluation of the accuracy of extraoral laboratory scanners with a single-tooth abutment model: A 3D analysis*. J Prosthodont Res, 2017. 61(4): p. 363-370.
20. Luthardt, R.G., R. Loos, and S. Quaas, *Accuracy of intraoral data acquisition in comparison to the conventional impression*. Int J Comput Dent, 2005. 8(4): p. 283-94.
21. Su, T.S. and J. Sun, *Comparison of repeatability between intraoral digital scanner and extraoral digital scanner: An in-vitro study*. J Prosthodont Res, 2015. 59(4): p. 236-42.
22. Mormann, W.H., M. Brandestini, and F. Lutz, *The Cerec system: computer-assisted preparation of direct ceramic inlays in 1 setting*. Quintessenz, 1987. 38(3): p. 457-70.
23. Trifkovic, B., et al., *Comparative analysis on measuring performances of dental intraoral and extraoral optical 3D digitization systems*. Measurement, 2014. 47: p. 45-53.
24. da Costa, J.B., et al., *Evaluation of different methods of optical impression making on the marginal gap of onlays created with CEREC 3D*. Oper Dent, 2010. 35(3): p. 324-9.

25. El-Hakim, S.F., J.A. Beraldin, and F. Blais. *Comparative evaluation of the performance of passive and active 3D vision systems*. in *Digital Photogrammetry and Remote Sensing '95*. 1995. SPIE.
26. Logozzo, S., et al., *Recent advances in dental optics – Part I: 3D intraoral scanners for restorative dentistry*. Optics and Lasers in Engineering, 2014. 54: p. 203-221.
27. Remondino, F., *From point cloud to surface: the modeling and visualization problem*. International Archives of photogrammetry, Remote Sensing and spatial information sciences, 2003. 34.
28. Henriksen, L., *Polygon reduction process* M. Braian, Editor. 2018, Technical computersoftware product manager at 3Shape,.
29. Tapie, L., et al., *Understanding dental CAD/CAM for restorations-- the digital workflow from a mechanical engineering viewpoint*. Int J Comput Dent, 2015. 18(1): p. 21-44.
30. Flugge, T.V., et al., *Precision of intraoral digital dental impressions with iTero and extraoral digitization with the iTero and a model scanner*. Am J Orthod Dentofacial Orthop, 2013. 144(3): p. 471-8.
31. Ender, A. and A. Mehl, *Influence of scanning strategies on the accuracy of digital intraoral scanning systems*. Int J Comput Dent, 2013. 16(1): p. 11-21.
32. Muller, P., et al., *Impact of digital intraoral scan strategies on the impression accuracy using the TRIOS Pod scanner*. Quintessence Int, 2016. 47(4): p. 343-9.
33. Alikhasi, M., M.H.M. Alsharbaty, and M. Moharrami, *Digital Implant Impression Technique Accuracy: A Systematic Review*. Implant Dent, 2017. 26(6): p. 929-935.
34. Shim, J.S., et al., *Effect of software version and parameter settings on the marginal and internal adaptation of crowns fabricated with the CAD/CAM system*. J Appl Oral Sci, 2015. 23(5): p. 515-22.
35. Ender, A. and A. Mehl, *In-vitro evaluation of the accuracy of conventional and digital methods of obtaining full-arch dental impressions*. Quintessence Int, 2015. 46(1): p. 9-17.
36. Ender, A., T. Attin, and A. Mehl, *In vivo precision of conventional and digital methods of obtaining complete-arch dental impressions*. J Prosthet Dent, 2016. 115(3): p. 313-20.
37. Malik, J., et al., *Comparison of Accuracy Between a Conventional and Two Digital Intraoral Impression Techniques*. Int J Prosthodont, 2018. 31(2): p. 107-113.
38. Patzelt, S.B., et al., *Accuracy of full-arch scans using intraoral scanners*. Clin Oral Investig, 2014. 18(6): p. 1687-94.

39. Kim, J.E., et al., *Accuracy of intraoral digital impressions using an artificial landmark*. J Prosthet Dent, 2017. 117(6): p. 755-761.
40. Gimenez, B., et al., *Accuracy of a digital impression system based on parallel confocal laser technology for implants with consideration of operator experience and implant angulation and depth*. Int J Oral Maxillofac Implants, 2014. 29(4): p. 853-62.
41. Ajioka, H., et al., *Examination of the Position Accuracy of Implant Abutments Reproduced by Intra-Oral Optical Impression*. PLoS One, 2016. 11(10): p. e0164048.
42. Ender, A., et al., *In vivo precision of conventional and digital methods for obtaining quadrant dental impressions*. Clin Oral Investig, 2016. 20(7): p. 1495-504.
43. Nedelcu, R., et al., *Accuracy and precision of 3 intraoral scanners and accuracy of conventional impressions: A novel in vivo analysis method*. J Dent, 2017.
44. Mangano, F.G., et al., *Trueness and Precision of Four Intraoral Scanners in Oral Implantology: A Comparative in Vitro Study*. PLoS One, 2016. 11(9): p. e0163107.
45. Steinbrecher, T. and M. Gerth, *Dental Inlay and Onlay Construction by Iterative Laplacian Surface Editing*. Computer Graphics Forum, 2008. 27(5): p. 1441-1447.
46. Zheng, S.-X., J. Li, and Q.-F. Sun, *A novel 3D morphing approach for tooth occlusal surface reconstruction*. Computer-Aided Design, 2011. 43(3): p. 293-302.
47. Song, Y.-L., et al., *The feature-based posterior crown design in a dental CAD/CAM system*. The International Journal of Advanced Manufacturing Technology, 2006. 31(11-12): p. 1058-1065.
48. Mehl, A., V. Blanz, and R. Hickel, *Biogeneric tooth: a new mathematical representation for tooth morphology in lower first molars*. Eur J Oral Sci, 2005. 113(4): p. 333-40.
49. Vivadent, I. *Ivoclar Digital Software Parameter Chart Exocad*. 2018; Available from: <https://www.ivoclarvivadent.com/zoolu-website/media/document/40956/Ivoclar+Digital+Software+Parameter+Chart+Exocad>.
50. ISO, *ISO 2806:1994 Industrial automation systems -- Numerical control of machines -- Vocabulary*. 1994.
51. Lebon, N., et al., *Understanding dental CAD/CAM for restorations - dental milling machines from a mechanical engineering viewpoint. Part A: chairside milling machines*. Int J Comput Dent, 2016. 19(1): p. 45-62.
52. Kim, T., *Constant cusp height tool paths as geodesic parallels on an abstract Riemannian manifold*. Computer-Aided Design, 2007. 39(6): p. 477-489.

53. Llanos, I., et al., *Tool wear induced error avoidance on dental prosthesis manufacturing*. The International Journal of Advanced Manufacturing Technology, 2017. 95(1-4): p. 387-395.
54. Tinschert, J., et al., *Status of current CAD/CAM technology in dental medicine*. Int J Comput Dent, 2004. 7(1): p. 25-45.
55. Kirsch, C., et al., *Trueness of four different milling procedures used in dental CAD/CAM systems*. Clin Oral Investig, 2017. 21(2): p. 551-558.
56. Bosch, G., A. Ender, and A. Mehl, *A 3-dimensional accuracy analysis of chairside CAD/CAM milling processes*. J Prosthet Dent, 2014. 112(6): p. 1425-31.
57. Papadiochou, S. and A.L. Pissiotis, *Marginal adaptation and CAD-CAM technology: A systematic review of restorative material and fabrication techniques*. J Prosthet Dent, 2017.
58. W., H.C., *Apparatus for production of three-dimensional objects by stereolithography*. March 11, 1986, UVP, Inc. (San Gabriel, CA).
59. Noorani, R., *Rapid prototyping : principles and applications*. 2006, Hoboken, NJ: Wiley.
60. Wohlers, T., et al., *Wohlers report 2018 3D printing and additive manufacturing state of the industry ; annual worldwide progress report*. 2018.
61. Wohlers, T. and R.I. Campbell, *Wohlers report 2017 : 3D printing and additive manufacturing state of the industry : annual worldwide progress report*. 2017.
62. Hull, C.W., *Methods and apparatus for production of three-dimensional objects by stereolithography*, U.S. Patent, Editor. May 2, 1991 3-D Systems, Inc., Valencia, Calif. : U.S.
63. Kochan, D., *Solid freeform manufacturing : advanced rapid prototyping*. 1993, Amsterdam: Elsevier.
64. Vandenbroucke, B. and J.P. Kruth, *Selective laser melting of biocompatible metals for rapid manufacturing of medical parts*. Rapid Prototyping Journal, 2007. 13(4): p. 196-203.
65. Harun, W.S.W., et al., *A review of powdered additive manufacturing techniques for Ti-6al-4v biomedical applications*. Powder Technology, 2018. 331: p. 74-97.
66. Salmi, M., et al., *Accuracy of medical models made by additive manufacturing (rapid manufacturing)*. J Craniomaxillofac Surg, 2013. 41(7): p. 603-9.
67. Kasparova, M., et al., *Possibility of reconstruction of dental plaster cast from 3D digital study models*. Biomed Eng Online, 2013. 12: p. 49.

68. Tahayeri, A., et al., *3D printed versus conventionally cured provisional crown and bridge dental materials*. Dent Mater, 2018. 34(2): p. 192-200.
69. Reyes, A., I. Turkyilmaz, and T.J. Prihoda, *Accuracy of surgical guides made from conventional and a combination of digital scanning and rapid prototyping techniques*. J Prosthet Dent, 2015. 113(4): p. 295-303.
70. Martorelli, M., et al., *A comparison between customized clear and removable orthodontic appliances manufactured using RP and CNC techniques*. Dent Mater, 2013. 29(2): p. e1-10.
71. Barazanchi, A., et al., *Additive Technology: Update on Current Materials and Applications in Dentistry*. J Prosthodont, 2017. 26(2): p. 156-163.
72. Ye, H., et al., *Preliminary Clinical Application of Removable Partial Denture Frameworks Fabricated Using Computer-Aided Design and Rapid Prototyping Techniques*. Int J Prosthodont, 2017. 30(4): p. 348-353.
73. Turbush, S.K. and I. Turkyilmaz, *Accuracy of three different types of stereolithographic surgical guide in implant placement: An in vitro study*. The Journal of Prosthetic Dentistry, 2012. 108(3): p. 181-188.
74. Arnold, C., et al., *Accuracy of CAD-CAM-fabricated removable partial dentures*. J Prosthet Dent, 2018. 119(4): p. 586-592.
75. Fathi, H.M., et al., *The Accuracy of Fit of Crowns Made From Wax Patterns Produced Conventionally (Hand Formed) and Via CAD/CAM Technology*. Eur J Prosthodont Restor Dent, 2016. 24(1): p. 10-7.
76. Homsy, F.R., et al., *Marginal and internal fit of pressed lithium disilicate inlays fabricated with milling, 3D printing, and conventional technologies*. J Prosthet Dent, 2017.
77. Yau, H.T., T.J. Yang, and Y.K. Lin, *Comparison of 3-D Printing and 5-axis Milling for the Production of Dental e-models from Intra-oral Scanning*. Computer-Aided Design and Applications, 2015. 13(1): p. 32-38.
78. Berg, G.J., et al., *A Dual-Cure, Solid-State Photoresist Combining a Thermoreversible Diels–Alder Network and a Chain Growth Acrylate Network*. Macromolecules, 2014. 47(10): p. 3473-3482.
79. Alharbi, N., R.B. Osman, and D. Wismeijer, *Factors Influencing the Dimensional Accuracy of 3D-Printed Full-Coverage Dental Restorations Using Stereolithography Technology*. Int J Prosthodont, 2016. 29(5): p. 503-10.

80. Osman, R.B., N. Alharbi, and D. Wismeijer, *Build Angle: Does It Influence the Accuracy of 3D-Printed Dental Restorations Using Digital Light-Processing Technology?* Int J Prosthodont, 2017. 30(2): p. 182-188.
81. Huang, Z., et al., *Clinical marginal and internal fit of metal ceramic crowns fabricated with a selective laser melting technology.* J Prosthet Dent, 2015. 113(6): p. 623-7.
82. Kim, D.Y., et al., *Comparison and evaluation of marginal and internal gaps in cobalt-chromium alloy copings fabricated using subtractive and additive manufacturing.* J Prosthodont Res, 2018. 62(1): p. 56-64.
83. Bae, E.J., et al., *A comparative study of additive and subtractive manufacturing for dental restorations.* J Prosthet Dent, 2017. 118(2): p. 187-193.
84. Ortorp, A., et al., *The fit of cobalt-chromium three-unit fixed dental prostheses fabricated with four different techniques: a comparative in vitro study.* Dent Mater, 2011. 27(4): p. 356-63.
85. Sailer, I., et al., *Five-year clinical results of zirconia frameworks for posterior fixed partial dentures.* Int J Prosthodont, 2007. 20(4): p. 383-8.
86. Padbury, A., R. Eber, and H.-L. Wang, *Interactions between the gingiva and the margin of restorations.* Journal of Clinical Periodontology, 2003. 30(5): p. 379-385.
87. Lang, N.P., R.A. Kiel, and K. Anderhalden, *Clinical and microbiological effects of subgingival restorations with overhanging or clinically perfect margins.* Journal of Clinical Periodontology, 1983. 10(6): p. 563-578.
88. Wettstein, F., et al., *Clinical study of the internal gaps of zirconia and metal frameworks for fixed partial dentures.* Eur J Oral Sci, 2008. 116(3): p. 272-9.
89. Thompson, V.P. and D.E. Rekow, *Dental ceramics and the molar crown testing ground.* Journal of Applied Oral Science, 2004. 12: p. 26-36.
90. Hunter, A.J. and A.R. Hunter, *Gingival margins for crowns: A review and discussion. Part II: Discrepancies and configurations.* The Journal of Prosthetic Dentistry, 1990. 64(6): p. 636-642.
91. Hunter, A.J. and A.R. Hunter, *Gingival crown margin configurations: A review and discussion. Part I: Terminology and widths.* The Journal of Prosthetic Dentistry, 1990. 64(5): p. 548-552.
92. Bernhart, J., et al., *Cerec3D endocrowns--two-year clinical examination of CAD/CAM crowns for restoring endodontically treated molars.* Int J Comput Dent, 2010. 13(2): p. 141-54.
93. Keshvad, A., et al., *Marginal gap, internal fit, and fracture load of leucite-reinforced ceramic inlays fabricated by CEREC inLab and hot-pressed techniques.* J Prosthodont, 2011. 20(7): p. 535-40.

94. Martínez-Rus, F., et al., *Influence of CAD/CAM systems and cement selection on marginal discrepancy of zirconia-based ceramic crowns*. Am J Dent, 2012. 25(2): p. 67-72.
95. Colpani, J.T., M. Borba, and A. Della Bona, *Evaluation of marginal and internal fit of ceramic crown copings*. Dent Mater, 2013. 29(2): p. 174-80.
96. Moldovan, O., et al., *Three-dimensional fit of CAD/CAM-made zirconia copings*. Dent Mater, 2011. 27(12): p. 1273-8.
97. Pelekanos, S., et al., *Micro-CT evaluation of the marginal fit of different In-Ceram alumina copings*. Eur J Esthet Dent, 2009. 4(3): p. 278-92.
98. Martínez-Rus, F., et al., *Evaluation of the absolute marginal discrepancy of zirconia-based ceramic copings*. The Journal of Prosthetic Dentistry, 2011. 105(2): p. 108-114.
99. Renne, W., et al., *Predicting marginal fit of CAD/CAM crowns based on the presence or absence of common preparation errors*. The Journal of Prosthetic Dentistry, 2012. 108(5): p. 310-315.
100. Conrad, H.J., W.-J. Seong, and I.J. Pesun, *Current ceramic materials and systems with clinical recommendations: A systematic review*. The Journal of Prosthetic Dentistry, 2007. 98(5): p. 389-404.
101. Han, H.-S., et al., *Marginal accuracy and internal fit of machine-milled and cast titanium crowns*. The Journal of Prosthetic Dentistry, 2011. 106(3): p. 191-197.
102. McLean, J.W. and F. von, *The estimation of cement film thickness by an in vivo technique*. British Dental Journal, 1971. 131: p. 107.
103. Tan, K.B., et al., *Three-dimensional analysis of the casting accuracy of one-piece, osseointegrated implant-retained prostheses*. Int J Prosthodont, 1993. 6(4): p. 346-63.
104. Jemt, T., *Failures and complications in 391 consecutively inserted fixed prostheses supported by Branemark implants in edentulous jaws: a study of treatment from the time of prosthesis placement to the first annual checkup*. Int J Oral Maxillofac Implants, 1991. 6(3): p. 270-6.
105. Ma, T., J.I. Nicholls, and J.E. Rubenstein, *Tolerance measurements of various implant components*. Int J Oral Maxillofac Implants, 1997. 12(3): p. 371-5.
106. Braian, M., et al., *Tolerance measurements on internal- and external-hexagon implants*. Int J Oral Maxillofac Implants, 2014. 29(4): p. 846-52.
107. Boitelle, P., et al., *A systematic review of CAD/CAM fit restoration evaluations*. J Oral Rehabil, 2014. 41(11): p. 853-74.

108. Ueda, K., et al., *Fit of 4-unit FDPs from CoCr and zirconia after conventional and digital impressions*. Clin Oral Investig, 2016. 20(2): p. 283-9.
109. Ng, J., D. Ruse, and C. Wyatt, *A comparison of the marginal fit of crowns fabricated with digital and conventional methods*. J Prosthet Dent, 2014. 112(3): p. 555-60.
110. Pompa, G., et al., *Comparison of Conventional Methods and Laser-Assisted Rapid Prototyping for Manufacturing Fixed Dental Prostheses: An In Vitro Study*. Biomed Res Int, 2015. 2015: p. 318097.
111. Hjalmarsson, L., et al., *Precision of fit to implants: a comparison of Cresco and Procera(R) implant bridge frameworks*. Clin Implant Dent Relat Res, 2010. 12(4): p. 271-80.
112. Moroni, G., S. Petró, and W. Polini, *Geometrical product specification and verification in additive manufacturing*. CIRP Annals, 2017. 66(1): p. 157-160.
113. ISO, "*Dentistry - Digitizing devices for CAD/CAM systems for indirect dental restorations – Test methods for assessing accuracy*". International Organization for Standardization, Geneva, 2012.
114. ISO, "*Dentistry - Digitizing devices for CAD/CAM systems for indirect dental restorations — Test methods for assessing accuracy*". International Organization for Standardization, Geneva, 2015.
115. Uhm, S.H., et al., *Evaluation of the accuracy and precision of four intraoral scanners with 70% reduced inlay and four-unit bridge models of international standard*. Dent Mater J, 2017. 36(1): p. 27-34.
116. Patzelt, S.B., et al., *Accuracy of computer-aided design/computer-aided manufacturing-generated dental casts based on intraoral scanner data*. J Am Dent Assoc, 2014. 145(11): p. 1133-40.
117. Revilla-Leon, M., et al., *Position Accuracy of Implant Analogs on 3D Printed Polymer versus Conventional Dental Stone Casts Measured Using a Coordinate Measuring Machine*. J Prosthodont, 2017.
118. Kim, S.Y., et al., *Accuracy of dies captured by an intraoral digital impression system using parallel confocal imaging*. Int J Prosthodont, 2013. 26(2): p. 161-3.
119. Huang, Y.-M. and H.-Y. Lan, *Compensation of distortion in the bottom exposure of stereolithography process*. The International Journal of Advanced Manufacturing Technology, 2006. 27(11): p. 1101-1112.
120. Eliasson, A., et al., *The precision of fit of milled titanium implant frameworks (I-Bridge) in the edentulous jaw*. Clin Implant Dent Relat Res, 2010. 12(2): p. 81-90.
121. Murr, L.E., et al., *Metal Fabrication by Additive Manufacturing Using Laser and Electron Beam Melting Technologies*. Journal of Materials Science & Technology, 2012. 28(1): p. 1-14.

122. Puebla, K., et al., *Effect of melt scan rate on microstructure and macrostructure for electron beam melting of Ti-6Al-4V*. 2012.
123. Gong, H., et al. *Melt pool characterization for selective laser melting of Ti-6Al-4V pre-alloyed powder*. in *Solid Freeform Fabrication Proceedings*.
124. Algardh, J.K., et al., *Thickness dependency of mechanical properties for thin-walled titanium parts manufactured by Electron Beam Melting (EBM)* ©. Additive Manufacturing, 2016. 12: p. 45-50.
125. Murr, L.E., et al., *Microstructure and mechanical behavior of Ti-6Al-4V produced by rapid-layer manufacturing, for biomedical applications*. J Mech Behav Biomed Mater, 2009. 2(1): p. 20-32.
126. Mahamood, R.M., et al., *Revolutionary Additive Manufacturing: An Overview*. 2014. p. 161-178.
127. Gibson, I., D.W. Rosen, and B. Stucker, *Additive Manufacturing Technologies. [electronic resource] : Rapid Prototyping to Direct Digital Manufacturing*. 2010: Boston, MA : Springer Science+Business Media, LLC, 2010.
128. Rafi, H.K., et al., *Microstructures and mechanical properties of Ti6Al4V parts fabricated by selective laser melting and electron beam melting*. Journal of Materials Engineering and Performance, 2013. 22(12): p. 3872-3883.
129. Sochalski-Kolbus, L., et al., *Comparison of Residual Stresses in Inconel 718 Simple Parts Made by Electron Beam Melting and Direct Laser Metal Sintering*. Metallurgical and Materials Transactions A: Physical Metallurgy and Materials Science, 2015. 46(3): p. 1419-1432.
130. Kim, H.Y., *Statistical notes for clinical researchers: Evaluation of measurement error 2: Dahlberg's error, Bland-Altman method, and Kappa coefficient*. Restor Dent Endod, 2013. 38(3): p. 182-5.
131. Tipler, P.A. and G. Mosca, *Physics for scientists and engineers*. 2008: New York : W.H. Freeman, c2008; 6th ed.
132. Muallah, J., et al., *Accuracy of full-arch scans using intraoral and extraoral scanners: an in vitro study using a new method of evaluation*. Int J Comput Dent, 2017. 20(2): p. 151-164.
133. van der Meer, W.J., et al., *Application of intra-oral dental scanners in the digital workflow of implantology*. PLoS One, 2012. 7(8): p. e43312.
134. Gimenez, B., et al., *Accuracy of two digital implant impression systems based on confocal microscopy with variations in customized software and clinical parameters*. Int J Oral Maxillofac Implants, 2015. 30(1): p. 56-64.
135. Flugge, T.V., et al., *Precision of Dental Implant Digitization Using Intraoral Scanners*. Int J Prosthodont, 2016. 29(3): p. 277-83.

136. Patzelt, S.B.M., et al., *Assessing the feasibility and accuracy of digitizing edentulous jaws*. The Journal of the American Dental Association, 2013. 144(8): p. 914-920.
137. Boitelle, P., et al., *Evaluation of the marginal fit of CAD-CAM zirconia copings: Comparison of 2D and 3D measurement methods*. J Prosthet Dent, 2018. 119(1): p. 75-81.
138. Ahrberg, D., et al., *Evaluation of fit and efficiency of CAD/CAM fabricated all-ceramic restorations based on direct and indirect digitalization: a double-blinded, randomized clinical trial*. Clin Oral Investig, 2016. 20(2): p. 291-300.

I

Tolerance Measurements on Internal- and External-Hexagon Implants

Michael Braian, DDS, CDT¹/Hugo De Bruyn, DDS, PhD²/Håkan Fransson³/
Cecilia Christersson, DDS, PhD⁴/Ann Wennerberg, DDS, PhD⁵

Purpose: To measure the horizontal machining tolerances of the interface between internal- and external-hexagon implants and analogs with corresponding components after delivery from the manufacturer. These values may be a valuable tool for evaluating increasing misfit caused by fabrication, processing, and wear.

Materials and Methods: Seven implants and seven analogs with external- and internal-hexagon connections (Biomet 3i) with corresponding prefabricated gold cylinders and gold screws, prefabricated cylindrical plastic cylinders, and laboratory screws were studied. One set of components from the external and internal groups was measured manually and digitally. Measurements from the test subjects were compared with identical measurements from the virtual model to obtain threshold values. The virtual model was then used to obtain optimally oriented cuts. **Results:** The horizontal machining tolerances for castable plastic abutments on external implants were $12 \pm 89 \mu\text{m}$, and for internal implants they were $86 \pm 47 \mu\text{m}$. Tolerance measurements on prefabricated gold abutments for external implants were $44 \pm 9 \mu\text{m}$, and for internal implants they were $58 \pm 28 \mu\text{m}$. **Conclusion:** The groups with metallic components showed the smallest tolerance at $< 50 \mu\text{m}$ for the external group and $< 90 \mu\text{m}$ for the internal group. The prefabricated plastic cylinder groups ranged from $< 100 \mu\text{m}$ for external and $< 130 \mu\text{m}$ for internal connection. *INT J ORAL MAXILLOFAC IMPLANTS* 2014;29:846–852. doi: 10.11607/jomi.3242

Key words: dental implants, external-connection implant, internal-connection implant, machining tolerances, misfit

The modern era of implant dentistry began in 1965, when Brånemark treated the first patient with oral implants and a fixed denture in the edentulous mandible.¹ During the 1980s, treatment with mandibular implants developed into a popular option. Among the implant-related complications that have been observed are the biomechanical problems that occur after loading; marginal bone loss is one of those^{2–5} and has an etiology that is not fully understood. Problems

can occur independent of the prosthodontic solution. In an implant-supported fixed dental prosthesis (FDP), problems can occur with acrylic/ceramic veneer fractures, abutment or prosthetic screw loosening, porcelain fractures, and metal framework complications.^{5–8} During a 5-year period, the most common technical complications for implant-supported FDPs were veneer fractures (11.9%), abutment and screw loosening (5.6%), and loss of retention (5.7%).^{6,7} The incidence of technical complications for implant-supported FDPs is reported to be higher than for tooth-supported FDPs.^{6,7} The higher incidence of technical complications for implant-supported FDPs could be explained by the type of screw material, preload, abutment material, and connection configuration.^{9–11}

Many studies have demonstrated that there is a marginal gap and a horizontal/vertical discrepancy between implants and the superstructures they support.^{12–22} Although misfit may exist, there is still no definition of the threshold that distinguishes misfit from acceptable fit.¹³ It was suggested that a cement layer would compensate for any inaccuracies if a prosthesis was cemented instead of retained by screws.^{23,24} However, Karl and associates found no significant difference in the strains measured in screw-retained and cemented five-unit FDPs.²¹

¹PhD Student, Department of Prosthodontics, Faculty of Odontology, Malmö University, Malmö, Sweden.

²Chairman and Professor, Periodontology and Oral Implantology, Faculty of Medicine and Health Sciences, University of Ghent, Ghent, Belgium; Visiting Professor, Department of Prosthodontics, University of Malmö, Malmö, Sweden.

³Engineer, Department of Technology, Malmö University, Malmö, Sweden.

⁴Vice Chancellor, Malmö University, Malmö, Sweden.

⁵Professor, Department of Prosthodontics, Faculty of Odontology, Malmö University, Malmö, Sweden.

Correspondence to: Dr Michael Braian, Department of Prosthodontics, Faculty of Odontology, Malmö University, Malmö, 205 06 Sweden. Fax: +46-40-6658503. Email: Michael.Braian@mah.se

©2014 by Quintessence Publishing Co Inc.

846 Volume 29, Number 4, 2014

© 2014 BY QUINTESSENCE PUBLISHING CO, INC. PRINTING OF THIS DOCUMENT IS RESTRICTED TO PERSONAL USE ONLY. NO PART MAY BE REPRODUCED OR TRANSMITTED IN ANY FORM WITHOUT WRITTEN PERMISSION FROM THE PUBLISHER.

Implant-supported FDPs require a manufacturing process with high accuracy. To create an accurate framework, the dental technician uses one of two methods: casting or computer-aided design/computer-assisted manufacture (CAD/CAM). Studies have indicated that CAD/CAM frameworks show significantly higher precision than cast frameworks.^{25,26} The accuracy of cast constructions is affected by parameters such as operator handling and dimensional changes in wax, dental stone, and metal alloys.²⁷⁻³⁰ CAD/CAM systems are not affected by dimensional changes during the milling process of metal alloys; on the contrary, there are many other variables to consider. The accuracy of a CAD/CAM system could be measured by reverse engineering. This is done by scanning or modeling a standardized object; the object is then fabricated with CAM and rescanned. The original scan is then compared to the manufactured scan. A system with high accuracy will show smaller differences between the two virtual objects compared to a less accurate system. Constructions demanding great precision will require a CAD/CAM system with high accuracy, but no threshold values for the precision of different implant systems and manufacturers are available.

For treatment of single-tooth cases, many implant systems provide prefabricated components. For multiple-unit cases, the fabrication process becomes more complicated, depending on the number of implants, their angulations, the use of abutments, and the complexity of the connecting components. To date, the different manufacturers have provided no information regarding the precision required between implants and frameworks/abutments. Such dimensions would help dentists and technicians to understand and appreciate the precision that is needed to manufacture and fit prosthodontic components.

The aim of this paper, therefore, is to present the horizontal machining tolerances of the interface between internal-hexagon and external-hexagon implants and analogs with corresponding cylindrical gold and plastic abutments upon delivery from the implant manufacturer.

MATERIALS AND METHODS

Part One

One implant with an internal-connection interface (Biomet 3i) with a corresponding prefabricated gold cylinder (PGC) and gold screw; an internal-connection implant analog, prefabricated cylindrical plastic cylinder (PPC), and laboratory screw; one implant with an external-connection interface (Biomet 3i), corresponding PGC, and gold screw; and an external-connection implant analog, PPC, and laboratory screw were used

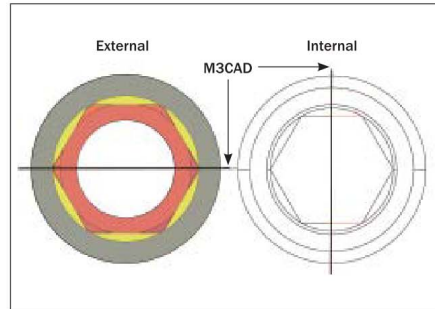


Fig 1. Optimal cut orientation on external- and internal-hexagon-connection implants and analogs.

for this part of the study. These implant and analog parts were used to capture the raw data needed to create CAD models. The implants' cylindrical parts were measured manually using a micrometer instrument (CEJ 101) and digitally with a Leica microscope using a $\times 50$ magnification and Leica computer software (Leica application suite version 3.7.0 2010). All specimens were then embedded in epoxy (EpoFix Resin Hardener, Struers). After 24 hours, each specimen was cut and ground to the center point using a grinder (Phoenix 4000 sample preparation system, Buehler), with the alignment centered and carefully controlled according to prior cylindrical measurements. On the implants and analogs, the center point was located according to Fig 1. Digital measurements of all the connecting parts were made with a Leica microscope under $\times 50$ magnification and Leica computer software (Leica application suite, version 3.7.0 2010), and the equipment was calibrated before each measurement. The dimensions of all 12 components were then used to model 12 virtual three-dimensional objects using Autocad 2013 (Autocad 2013, version G.55.M.108 Mac, Autodesk Corp). In Part One, each component was measured separately, whereas in Part Two the fully assembled implant (analog)/cylinder/screw specimens were measured.

Part Two

In this portion of the study, 12 actual implant (analog)/abutment connections were measured, six with external-hexagon connections and six with internal-hexagon connections. Each group included three implants and three analogs: internal implant (II) and internal analog (IA) in the internal-hex group, and external implants (EI) and external analogs (EA) in the external-hex group. A total of 12 cylindrical abutments were

retained with gold screws; on the implants, PGC abutments were used and on the analogs, PPC abutments were used. All the abutments were retained carefully with finger pressure calculated to 5 Ncm (W&H Elcomet), simulating the force a dental technician uses when making a framework. All specimens were then embedded in epoxy and positioned vertically. After 24 hours, each specimen was cut and ground to the center point. A central position was regarded to be most representative of the fit of the connection. Digital measurements were made with a Leica microscope using $\times 50$ magnification. The distances between each abutment and its corresponding implant/analog were measured on the left and right sides of all the samples. Measurements for EA and EI were designated M1, and for IA and II the measurements were designated M2. The epoxy, abutments, and abutment screws were then removed from the implants/analog, and measurements of the external hexagon and internal hexagon were made to orientate the direction of the cut (Fig 2).

Part Three

The measurements of the cut assemblies obtained in Part Two were then used on the CAD objects to orientate and replicate the different cuts (Fig 3). The virtual objects were then cut digitally, and M1 and M2 were compared with the digital measurements (M1CAD and M2CAD). Threshold results were calculated from this comparison.

Part Four

The virtual model was then used to obtain optimally oriented cuts (Fig 1). M3CAD and measurements of the theoretical machining tolerances were made.

RESULTS

Tables 1 and 2 show the measurements of the internal-hex and external-hex specimens and their respective virtual CAD specimens. M1 and M2 and M1CAD and M2CAD can be compared to calculate the differences between CAD measurements and subject measurements (Tables 1 and 2) (Fig 3). The actual orientations of the different cuts can be seen in Fig 2. The groups with metallic components (PGC) showed the smallest difference versus the CAD models, ranging from -5 to $28 \mu\text{m}$, and therefore the least deviation. In contrast, the PPC group measurements ranged from -89 to $47 \mu\text{m}$ (Tables 1 and 2). The measurement outcome of the optimal theoretical cut orientation (M3CAD) (Fig 1) for the PGC groups showed a total machining tolerance of $58 \pm 28 \mu\text{m}$ for II and $44 \pm 9 \mu\text{m}$ for EI, whereas the PPC groups showed a total tolerance of $86 \pm 47 \mu\text{m}$ for IA and $12 \pm 89 \mu\text{m}$ for EA (Table 3).

DISCUSSION

Deformation of Plastic Cylinders

The clear difference between the PGC and PPC groups could be related to deformation of the plastic cylinders. During tightening of the abutment screw, a degree of deformation of the plastic cylinder occurs; with the external-hex implants, this causes the abutment to expand in width (Fig 4a). The PPC abutments in the external group showed horizontal misplacement at the abutment/implant margin, resulting in an overhang. According to the manufacturer, the Poisson ratio for the plastic cylinder is 0.36. This ratio explains the volume changes in a material under stress. When a material is stretched in one direction, it will compress in the other direction; the Poisson ratio describes this compression. The subjects in the present investigation were only tightened once and with a very low force, whereas a dental technician typically tightens components a couple of times during fabrication of the framework. The cylindrical gold abutments did not deform during the tightening, which is in accordance with the findings of Carr and associates.³¹ They analyzed preload of fixation screws in single-crown restorations when tightening various cylinders and found that the prefabricated gold cylinders were superior to the plastic cylinders. The deformation of the plastic cylinders could be an important observation regarding the significantly higher rotational misfit in castable abutments compared to machined abutments.³²

Platform Step

In studying the horizontal machining tolerance, the authors noted one interesting observation in the external-hexagon assemblies. At the junction between the hexagon and the flat platform is a step approximately $20 \mu\text{m}$ in height (Figs 4b and 4c). The step does not exceed the edges of the hexagon; thus, no effect on the fit of cylindrical abutments could be seen (Fig 4d). This observation could be useful for further studies of prefabricated abutments on single-implant cases because of the noncylindrical hexagon-abutment connection.

Passive Fit

Passive fit or stress-free fit is believed to be of great importance for implant components and the surrounding bone. In theory, components seated on implants should transfer no strain to the implants and surrounding bone under unloaded conditions. Any lack of passive fit could result in prosthodontic complications, such as fractures of abutment screws, fixation screws, frameworks, and veneers.³³⁻³⁶ However, there are no clinical studies reporting the correlation between misfit and the effects on the biologic tissues surrounding implants. Obtaining a passive fit may, in fact, be

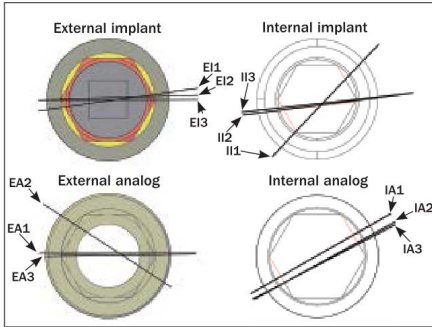


Fig 2 Orientation of cuts of specimens for internal- and external-hexagon implants and analogs. Note the divergence of EA2 and IA1.

Table 1 Measurements (µm) of Samples and CAD Models for External-Connection Implants and Analogs

	M1			M1CAD			Difference* Total
	Left	Right	Total	Left	Right	Total	
Implant + PGC							
EI 1	62	104	166	61	100	161	-5
EI 2	6	29	35	22	22	44	9
EI 3	29	35	64	23	33	56	-8
Analog + PPC							
EA 1	50	0	50	24	5	29	-21
EA 2	228	159	387	172	126	298	-89
EA 3	10	8	18	16	5	21	3

EA = external(-hex connection) analog; EI = external implant; M = measurement; PGC = prefabricated gold cylinder; PPC = prefabricated plastic cylinder. *Negative numbers indicate that the CAD measurement is smaller than the sample measurement.

impossible and the impact of such precision has been questioned.^{15,21,34,37} The lack of a definition of passive fit and a method to evaluate it clinically makes this issue even more difficult and unpredictable. According to the current results, a horizontal displacement of the connecting components above a range of 50 µm (PGC group) will lead to contact with the hexagon, which could lead to increased stress and displacement of the framework. However, discrepancies in this range are not visible to the naked eye and are therefore almost impossible to detect without the use of expensive and time-consuming methods.

Impression, Fabrication, and Precision

From the perspective of mechanical stability, replication, and the prognosis of prosthodontic components, the issue of passively fitting constructions is considered of high importance. The accuracy of a definitive implant superstructure is influenced by a number of factors. Impression method and impression material

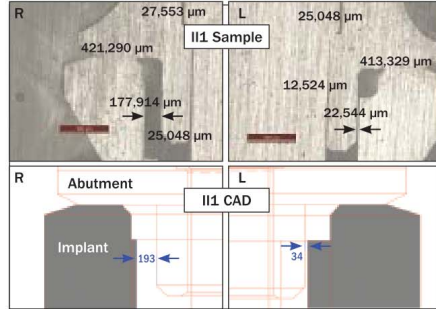


Fig 3 Comparison of left and right sides of an internal-hex implant sample and internal-hex implant CAD model.

Table 2 Measurements (µm) of Samples and CAD Models for Internal-Connection Implants and Analogs

	M2			M2CAD			Difference* Total
	Left	Right	Total	Left	Right	Total	
Implant + PGC							
II 1	23	178	201	34	193	227	26
II 2	138	43	181	149	58	207	26
II 3	63	173	236	74	190	264	28
Analog + PPC							
IA 1	72	28	100	47	39	86	-14
IA 1	65	50	115	79	55	134	19
IA 1	15	25	40	57	30	87	47

IA = internal(-hex connection) analog; II = internal implant; M = measurement; PGC = prefabricated gold cylinder; PPC = prefabricated plastic cylinder. *Negative numbers indicate that the CAD measurement is smaller than the sample measurement.

Table 3 Optimal Theoretical Cut Orientations on CAD Models

Model	M3CAD			CAD Deviation Total
	Left	Right	Total	
PGC				
II CAD	29	29	58	± 28
PPC				
IACAD	43	43	86	± 47
PGC				
EI CAD	22	22	44	± 9
PPC				
EACAD	6	6	12	± 89

EA = external(-hex connection) analog; EI = external implant; IA = internal(-hex connection) analog; II = internal implant; M = measurement; PGC = prefabricated gold cylinder; PPC = prefabricated plastic cylinder.

are the first critical steps affecting the outcome of the final product and can result in precision errors ranging from 20 to 180 µm.^{30,38-41} This is followed by dental

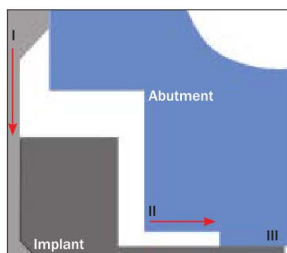


Fig 4a The force from the abutment screw (I) deforms the plastic abutment, resulting in an increased distance between the abutment and the implant (II). The displaced/deformed abutment therefore juts out horizontally (III).



Figs 4b and 4c External-hexagon implant. Red arrow = the platform step.

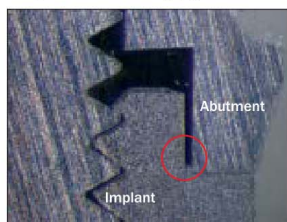


Fig 4d The implant and prefabricated cylindrical gold abutment in contact. The red circle highlights the platform step. Note that this cut is not oriented on the edge of the hexagon.

stone expansion, the use of wax or resin, investment material/investment technique, type of alloy, and any differences between implant components and their corresponding analogs.^{27–30}

The modern implant-supported prosthodontic armament consists mostly of prefabricated, machined components. Ma et al³⁰ studied machining tolerances on Noble Biocare implants in 1997 to identify the amount of horizontal shifting between abutment, gold cylinder, impression coping, and abutment replica. They compared circumference measurements of the components and then paired these to measure the tolerances. The differences ranged from 22 to 100 μm . Jemt et al⁴² studied conventional frameworks and compared them to computer numerically controlled (CNC)-milled frameworks on Nobel Biocare implants using a photogrammetric technique. They compared a central orientation between frameworks and implants and observed a mean difference of 16 to 80 μm in three dimensions. In a study by Al-Fadda et al,²⁵ conventional frameworks were compared to CNC-milled frameworks on Nobel Biocare implants. The measurements were performed with a coordinate measurement machine. They found mean horizontal distortions of 56 μm for CNC frameworks and 85 μm for conventional frameworks. Takahashi and Gunne¹⁷ measured the interfaces between abutments and frameworks using

a silicone impression technique for conventional and CNC-milled constructions. The silicone material was then cut and measured; a total mean value of 26.9 μm was seen for CNC frameworks and 46.8 μm for conventional frameworks.

The present study demonstrates the interface between prefabricated cylindrical abutments connected to implants with internal-hex and external-hex designs. The measurements show the actual interface designed by the manufacturer. The test subjects were not cast, milled, or treated in any way before being tightened; thus, any handling errors that might occur clinically were not taken into account. The results demonstrated an optimal fit situation. Prefabricated components are manufactured in advanced CAD/CAM factories, where the manufacturers are aware of the machining tolerances between different components, and it is possible to achieve a high level of accuracy. With this in mind, implant components made by different manufacturers in attempts to duplicate implant components from another manufacturer might not have the same accuracy. Today, screw-retained multiunit frameworks at the implant level can be manufactured in much smaller and less accurate CAD/CAM systems. According to the present findings, and keeping the earlier findings of Rubenstein and Ma⁴³ and Ma et al³⁰ in mind, CAD/CAM should possibly have an accuracy of 20 to 100 μm .

The degree of precision that is needed to achieve a passive fit is not clear and varies between different manufacturers and connection designs. However, there should be a balance between internal tolerance and areas in contact. Dental loads must be transferred through the framework and implant to the surrounding biologic tissue, especially to the bone; to achieve this, the components must be in close contact. Machining tolerances will decrease the connection area; the greater the tolerance, the smaller the area of framework and implant that will be in contact. The diameter of the implant is a key factor in increasing the connection area.⁴⁴⁻⁴⁶ Many studies have shown horizontal and vertical discrepancies, which are usually called gaps; however, the definition of a gap is not clear.^{14,16,17,21,30,47-49} If machining tolerances are required to achieve passive fit, three-dimensional deviations may be inevitable. Knowledge of the machining tolerances for the specific implant systems studied in scientific papers could be necessary before fit measurements are made of the finished framework. The information could also be useful for clinicians to understand and respect the level of precision that is needed for implant-supported prosthodontics on the implant level. The expanding CAD/CAM market with its variety of manufacturing methods and precision, in conjunction with the increased amount of copycats on the implant market, makes this knowledge even more important.

Possible Measurement Errors

The CAD model used in this study was based on components originally measured individually, not assembled; thus, there was no influence of preload/compression or seating forces. To observe the internal design and the noncylindrical parts, the subjects were ground to the center, with the process controlled by a micrometer. The precision of the cuts affects the measurements and, later, the modeling of the CAD objects. When the distance between two objects is measured in a microscope, the measurement points will vary, depending on focus and angulation of the measured objects. The effect of this measurement error is dependent on magnification and handling errors. The measurement accuracy between CAD models and PGC test subjects in this study was approximately 30 μm in the internal implant group versus the external implant group. The components used in this study were prefabricated, and one could emphasize that these deviations would be 0 μm if optimal measurements had been performed. Although the consistency of fabrication is not known, there will inevitably be some degree of deviation in the replication of components. Because a limited number of samples were used for the present study, a proper statistical analysis could not be made; thus, more extensive studies are required.

CONCLUSION

The horizontal machining tolerances for prefabricated cylindrical gold abutments on external implants with hexagonal connections showed the smallest machining tolerances, which were less than 50 μm . Prefabricated gold abutments on internal-hexagon implants showed tolerances < 90 μm . In contrast, prefabricated plastic cylinders showed errors of < 100 μm for external-hex implants and < 130 μm for internal-hex implants.

ACKNOWLEDGMENTS

The authors reported no conflicts of interest related to this study.

REFERENCES

1. Brånemark PI, Hansson BO, Adell R, et al. Osseointegrated implants in the treatment of the edentulous jaw. Experience from a 10-year period. *Scand J Plast Reconstr Surg Suppl* 1977;16:1-132.
2. Cox JF, Zarb GA. The longitudinal clinical efficacy of osseointegrated dental implants: A 3-year report. *Int J Oral Maxillofac Implants* 1987;2:91-100.
3. Adell R, Lekholm U, Rockler B, et al. Marginal tissue reactions at osseointegrated titanium fixtures (I). A 3-year longitudinal prospective study. *Int J Oral Maxillofac Surg* 1986;15:39-52.
4. van Steenberghe D, Lekholm U, Bolender C, et al. Applicability of osseointegrated oral implants in the rehabilitation of partial edentulism: A prospective multicenter study on 558 fixtures. *Int J Oral Maxillofac Implants* 1990;5:272-281.
5. Goodacre CJ, Kan JY, Rungcharassaeng K. Clinical complications of osseointegrated implants. *J Prosthet Dent* 1999;81:537-552.
6. Pjetursson BE, Bragger U, Lang NP, Zwahlen M. Comparison of survival and complication rates of tooth-supported fixed dental prostheses (FDPs) and implant-supported FDPs and single crowns (SCs). *Clin Oral Implants Res* 2007;18(suppl 3):97-113.
7. Bragger U, Aeschlimann S, Burgin W, Hammerle CH, Lang NP. Biological and technical complications and failures with fixed partial dentures (FPD) on implants and teeth after four to five years of function. *Clin Oral Implants Res* 2001;12:26-34.
8. Krennmair G, Waldenberger O. Clinical analysis of wide-diameter Frialit-2 implants. *Int J Oral Maxillofac Implants* 2004;19:710-715.
9. Ortop A, Jemt T, Wennerberg A, Berggren C, Brycke M. Screw preloads and measurements of surface roughness in screw joints: An in vitro study on implant frameworks. *Clin Implant Dent Relat Res* 2005;7:141-149.
10. Tsuge T, Hagiwara Y. Influence of lateral-oblique cyclic loading on abutment screw loosening of internal and external hexagon implants. *Dent Mater J* 2009;28:373-381.
11. Vigolo P, Fonzi F, Majzoub Z, Cordioli G. Evaluation of gold-machined UCLA-type abutments and CAD/CAM titanium abutments with hexagonal external connection and with internal connection. *Int J Oral Maxillofac Implants* 2008;23:247-252.
12. Oyama K, Kan JY, Kleinman AS, Rungcharassaeng K, Lozada JL, Goodacre CJ. Misfit of implant fixed complete denture following computer-guided surgery. *Int J Oral Maxillofac Implants* 2009;24:124-130.
13. Hjalmarsson L, Ortop A, Smedberg JJ, Jemt T. Precision of fit to implants: A comparison of Cresco and Procera implant bridge Frameworks. *Clin Implant Dent Relat Res* 2010;12(4):271-280.
14. Mitha T, Owen CP, Howes DG. The three-dimensional casting distortion of five implant-supported frameworks. *Int J Prosthodont* 2009;22:248-250.

15. Sahin S, Cehreli MC. The significance of passive framework fit in implant prosthodontics: Current status. *Implant Dent* 2001;10:85–92.
16. Jemt T, Rubenstein JE, Carlsson L, Lang BR. Measuring fit at the implant prosthodontic interface. *J Prosthet Dent* 1996;75:314–325.
17. Takahashi T, Gunne J. Fit of implant frameworks: An in vitro comparison between two fabrication techniques. *J Prosthet Dent* 2003;89:256–260.
18. Tosches NA, Bragger U, Lang NP. Marginal fit of cemented and screw-retained crowns incorporated on the Straumann (ITI) Dental Implant System: An in vitro study. *Clin Oral Implants Res* 2009;20:79–86.
19. Scarano A, Assenza B, Piattelli M, et al. A 16-year study of the micro-gap between 272 human titanium implants and their abutments. *J Oral Implantol* 2005;31:269–275.
20. Tsuge T, Hagiwara Y, Matsumura H. Marginal fit and microgaps of implant-abutment interface with internal anti-rotation configuration. *Dent Mater J* 2008;27:29–34.
21. Karl M, Winter W, Taylor TD, Heckmann SM. In vitro study on passive fit in implant-supported 5-unit fixed partial dentures. *Int J Oral Maxillofac Implants* 2004;19:30–37.
22. Cheshire PD, Hobkirk JA. An in vivo quantitative analysis of the fit of Nobel Biocare implant superstructures. *J Oral Rehabil* 1996;23:782–789.
23. Pietrabissa R, Gionso L, Quaglini V, Di Martino E, Simion M. An in vitro study on compensation of mismatch of screw versus cement-retained implant supported fixed prostheses. *Clin Oral Implants Res* 2000;11:448–457.
24. Guichet DL, Caputo AA, Choi H, Sorensen JA. Passivity of fit and marginal opening in screw- or cement-retained implant fixed partial denture designs. *Int J Oral Maxillofac Implants* 2000;15:239–246.
25. Al-Fadda SA, Zarb GA, Finer Y. A comparison of the accuracy of fit of 2 methods for fabricating implant-prosthodontic frameworks. *Int J Prosthodont* 2007;20:125–131.
26. Ortorp A, Jemt T, Back T, Jalevik T. Comparisons of precision of fit between cast and CNC-milled titanium implant frameworks for the edentulous mandible. *Int J Prosthodont* 2003;16:194–200.
27. Tan KB, Rubenstein JE, Nicholls JI, Yuodelis RA. Three-dimensional analysis of the casting accuracy of one-piece, osseointegrated implant-retained prostheses. *Int J Prosthodont* 1993;6:346–363.
28. Ness EM, Nicholls JI, Rubenstein JE, Smith DE. Accuracy of the acrylic resin pattern for the implant-retained prosthesis. *Int J Prosthodont* 1992;5:542–549.
29. Vigolo P, Millstein PL. Evaluation of master cast techniques for multiple abutment implant prostheses. *Int J Oral Maxillofac Implants* 1993;8:439–446.
30. Ma T, Nicholls JI, Rubenstein JE. Tolerance measurements of various implant components. *Int J Oral Maxillofac Implants* 1997;12:371–375.
31. Carr AB, Brunski JB, Hurler E. Effects of fabrication, finishing, and polishing procedures on preload in prostheses using conventional “gold” and plastic cylinders. *Int J Oral Maxillofac Implants* 1996;11:589–598.
32. Kano SC, Binon PP, Bonfante G, Curtis DA. The effect of casting procedures on rotational misfit in castable abutments. *Int J Oral Maxillofac Implants* 2007;22:575–579.
33. Sones AD. Complications with osseointegrated implants. *J Prosthet Dent* 1989;62:581–585.
34. Taylor TD, Agar JR, Vogiatzi T. Implant prosthodontics: Current perspective and future directions. *Int J Oral Maxillofac Implants* 2000;15:66–75.
35. Kohavi D. Complications in the tissue integrated prostheses components: Clinical and mechanical evaluation. *J Oral Rehabil* 1993;20:413–422.
36. Kallus T, Bessing C. Loose gold screws frequently occur in full-arch fixed prostheses supported by osseointegrated implants after 5 years. *Int J Oral Maxillofac Implants* 1994;9:169–178.
37. Jemt T, Book K. Prosthesis misfit and marginal bone loss in edentulous implant patients. *Int J Oral Maxillofac Implants* 1996;11:620–625.
38. Singh K, Sahoo S, Prasad KD, Goel M, Singh A. Effect of different impression techniques on the dimensional accuracy of impressions using various elastomeric impression materials: An in vitro study. *J Contemp Dent Pract* 2012;13:98–106.
39. Al Quran FA, Rashdan BA, Zomar AA, Weiner S. Passive fit and accuracy of three dental implant impression techniques. *Quintessence Int* 2012;43:119–125.
40. Spector MR, Donovan TE, Nicholls JI. An evaluation of impression techniques for osseointegrated implants. *J Prosthet Dent* 1990;63:444–447.
41. Humphries RM, Yaman P, Bloem TJ. The accuracy of implant master casts constructed from transfer impressions. *Int J Oral Maxillofac Implants* 1990;5:331–336.
42. Jemt T, Back T, Petersson A. Precision of CNC-milled titanium frameworks for implant treatment in the edentulous jaw. *Int J Prosthodont* 1999;12:209–215.
43. Rubenstein JE, Ma T. Comparison of interface relationships between implant components for laser-welded titanium frameworks and standard cast frameworks. *Int J Oral Maxillofac Implants* 1999;14:491–495.
44. Jarvis WC. Biomechanical advantages of wide-diameter implants. *Compend Contin Educ Dent* 1997;18:687–692, 694.
45. Ivanoff CJ, Sennerby L, Johansson C, Rangert B, Lekholm U. Influence of implant diameters on the integration of screw implants. An experimental study in rabbits. *Int J Oral Maxillofac Surg* 1997;26:141–148.
46. Graves SL, Jansen CE, Siddiqui AA, Beaty KD. Wide diameter implants: Indications, considerations and preliminary results over a two-year period. *Aust Prosthodont J* 1994;8:31–37.
47. de Torres EM, Barbosa GA, Bernardes SR, de Mattos Mda G, Ribeiro RF. Correlation between vertical misfits and stresses transmitted to implants from metal frameworks. *J Biomech* 2011;44:1735–1739.
48. de Torres EM, Rodrigues RC, de Mattos Mda G, Ribeiro RF. The effect of commercially pure titanium and alternative dental alloys on the marginal fit of one-piece cast implant frameworks. *J Dent* 2007;35:800–805.
49. Koke U, Wolf A, Lenz P, Gilde H. In vitro investigation of marginal accuracy of implant-supported screw-retained partial dentures. *J Oral Rehabil* 2004;31:477–482.

II

Available online at www.sciencedirect.com

ScienceDirect

journal homepage: www.intl.elsevierhealth.com/journals/dema

Production tolerance of additive manufactured polymeric objects for clinical applications

Michael Braian*, Ryo Jimbo, Ann Wennerberg

Department of Prosthodontics, Faculty of Odontology, Malmö University, Smedjegatan 16, 214 21 Malmö, Sweden

ARTICLE INFO

Article history:

Received 16 June 2015

Received in revised form

21 March 2016

Accepted 22 March 2016

Keywords:

Additive manufacturing

Rapid prototyping

Accuracy

Stereolithography

Selective laser sintering

Dentistry

ABSTRACT

Objectives. To determine the production tolerance of four commercially available additive manufacturing systems.

Methods. By reverse engineering annex A and B from the ISO.12836:2012, two geometrical figures relevant to dentistry was obtained. Object A specifies the measurement of an inlay-shaped object and B a multi-unit specimen to simulate a four-unit bridge model. The objects were divided into x, y and z measurements, object A was divided into a total of 16 parameters and object B was tested for 12 parameters. The objects were designed digitally and manufactured by professionals in four different additive manufacturing systems; each system produced 10 samples of each objects.

Results. For object A, three manufacturers presented an accuracy of <100 μm and one system showed an accuracy of <20 μm. For object B, all systems presented an accuracy of <100 μm, and most parameters were <40 μm. The standard deviation for most parameters were <40 μm.

Significance. The growing interest and use of intra-oral digitizing systems stresses the use of computer aided manufacturing of working models. The additive manufacturing techniques has the potential to help us in the digital workflow. Thus, it is important to have knowledge about production accuracy and tolerances. This study presents a method to test additive manufacturing units for accuracy and repeatability.

© 2016 The Academy of Dental Materials. Published by Elsevier Ltd. All rights reserved.

1. Introduction

The application of computer aided design (CAD) and computer aided manufacturing (CAM) in dentistry has evolved over the last two decades. Today, what was originally inspired by the industry has changed the treatment modalities in many clinical situations. The methodology for dental applications starts from the dental technicians scanning conventional plaster models to obtain virtual models or, more recently, the clinicians digitizing the oral cavity with an intra-oral

scanner. By using computer software, the technicians have the capability to virtually design crowns and bridges on the virtual models. In this way, it has been suggested that the human errors that could occur during the laboratory procedures can be reduced, therefore leading to a passive fitness of the prosthetic construction [1]. Until recently, the majority of these prosthodontic constructions have been manufactured using subtractive computer numerically controlled (CNC) techniques, better known as milling techniques possible for a wide variety of materials.

* Corresponding author. Tel.: +46 737088584; fax: +46 40 665 8521.

E-mail addresses: Michael.Braian@mah.se (M. Braian), Ryo.Jimbo@mah.se (R. Jimbo), Ann.Wennerberg@mah.se (A. Wennerberg).

<http://dx.doi.org/10.1016/j.dental.2016.03.020>

0109-5641/© 2016 The Academy of Dental Materials. Published by Elsevier Ltd. All rights reserved.

Subtractive manufacturing is a process in which a piece of material is cut into its final geometry by removing the unnecessary bulk material [2]. From an ecological viewpoint, it can be suggested that the method is rather wasteful since more material is removed than used in the final product. Moreover, the subtractive technique also has a limitation in the amount of objects it can produce per milling procedure, the inability to manufacture complex geometries and the fact that these machines use drills and burrs that wear.

An alternative way of manufacturing the CAD-based construction is the so-called additive manufacturing process [3]. The basic concept of all additive production methods is to apply sequentially thin layers of material (layering), which are then solidified through computer control layers. A plethora of additive manufacturing (AM) methods is available on the market, which in a collective term can be called rapid prototyping/manufacturing (RP/RM) [4]. In contrast to the subtractive manufacturing, it can be suggested that the AM methods generate less material waste since unnecessary structures will not be created unless so designed. There is no use of drills and burrs that wear, and the systems have a superior capability to produce complex geometries, which makes the production technique a suitable solution for the dental field. For instance, additive manufacturing process has the possibility to be utilized for model production, fixed/removable prosthodontics, diagnostic and treatment planning for oral and maxillofacial surgery, as well as for orthodontics [5,6]. With regards to the production of polymeric products, there exist mainly two AM systems that are actively utilized in dentistry, namely stereolithography (SLA), and the selective laser melting/sintering (SLM/SLS).

Stereolithography is a method, which involves a computer aided design (CAD) model communicating through a Standard Tessellation Language (STL) file extension with a manufacturing machine (CAM) that produces the intended object [7]. The SLA method could be utilized with the platform covered by liquid resin that is cured according to computer-controlled layers with UV light or laser while the platform is moving in the z-direction (vertically). The SLA in dentistry is used during the prosthodontic laboratory procedure replacing wax models with lost wax investment casting capable photopolymers. Moreover, the method is used for manufacturing intra-oral provisional restorations, laboratory models replacing dental stone models, and for diagnostic models (made from computer tomography) in the fields of orthodontics and oral and maxillofacial surgery.

Selective laser melting (SLM) is a fabrication method that communicates with the CAD using the same file system STL. The method uses a powder as layering material that is sintered/melted with a laser according to computer-controlled layers onto a platform [8].

There exist numerous studies with regards to the accuracy and precision of the SLA systems, mostly focusing on biomodels for treatment planning and diagnostics in the fields of oral and maxillofacial surgery and orthodontics [6,9–12]. The drawback of these different studies is that the methods and objects to determine the accuracy and precision of SLA products are unique for each study, which makes it difficult to compare and to reproduce data. Lamentably, at present there is no industry standard for assessing the accuracy and precision of objects

made from additive CAD/CAM systems in dentistry. It must be noted here that in 2012, an ISO standard for assessing accuracy of digitizing devices was published, however, this ISO (12836:2012) is mainly focused on testing intra-oral and laboratory digital scanners. Therefore, it is of utmost importance to obtain information with regards to the production tolerance (accuracy and precision) of the products generated from different AM systems, which could provide information necessary for a universal calibration of them.

Thus, the aim of this current study was to determine the production tolerance of four commercially available AM systems by reverse engineering annex A and B from the ISO.12836:2012.

2. Materials and methods

2.1. ISO reference

The ISO 12836 “Dentistry – Digitizing devices for CAD/CAM systems for indirect dental restorations – Test methods for assessing accuracy”. The ISO describes three geometrical figures, described as Annex A, B and C the present study has utilized Annex A and B as reference, the former specifying the measurement of an inlay-shaped object and the latter a multi-unit specimen to simulate a four-unit bridge model. Annex A and from the ISO was the reference for the design of object A and B in the present study (Figs. 1 and 2). The CAD was designed as solids using 3D modeling software (Solidworks educational edition 2013) with an edge radius of 0.01 mm. Both CAD models were exported as standard tessellation language files (STL) and delivered together with production information to the manufacturers.

2.2. CAM

A total of four additive manufacturing units were tested EOS (Formiga P110) 3D Systems (Projet MP 3510), Stratasys (Objet 30) and Stratasys (Objet Eden) (Table 1). Authorized personnel from each company manufactured all objects. All producers manufactured 10 sets for object A and 10 sets for object B on separate build plates. The geometries of both object A and B have no undercuts, thus there was no need for support structures, allowing the objects to be manufactured directly onto the build plate. The person responsible for each production unit decided material and software settings to achieve accurate samples. All manufacturers had seen the protocol ahead of initiating the present study. It was clear that all objects would be tested for geometrical accuracy. The manufacturers decided the best parameters for their specific machine, price was not an evaluated parameter (Table 1). The material of choice was then specified together with information about the print resolution, specification of the production unit, software, and the manufacturing time (Table 1). The test samples went through the same process as for clinical dental products, regarding both production and shipment.

2.3. Measurements

The measurements for the inlay shaped geometry of object A was divided in x, y and z-axis. The geometrical measurements

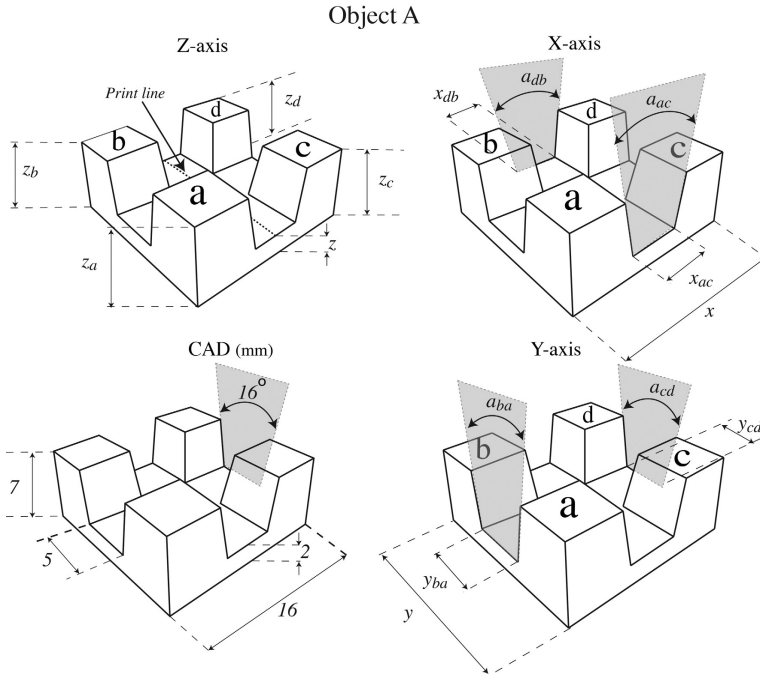


Fig. 1 – Figure illustrates object A (inlay shaped), the CAD illustration describes the dimensions designed in the computer, the x, y and z illustrations shows the abbreviation measurements.

that were conducted consisted of linear parameters, angles and corner radius. Object A was divided in a total of 16 parameters (Fig. 1) and object B was tested for 12 parameters (Fig. 2). Each manufacturing unit produced 10 objects from each group; all parameters were measured five times for a total of 5600 measurements. All the objects were measured within 7 days from arrival. All the measurements were conducted by one investigator.

2.4. Measurements parameters

The z-axis describes the height of the objects, this vertical dimension was perpendicular to the layering orientation and consisted of 5 linear measurements for object A and 4 for object B. The x and y-axis describe the horizontal dimensions and consists of 3 linear x-axis dimensions for object A and 2 for object B. Both object A and B consisted of three y-axis dimensions. To orientate object A, the four cubic forms were named a–d, the placement of a was orientated in the top left corner in relation to the horizontal print lines (surface lines see Fig. 1) on each object. Object B was divided in a left and right side, the tip of the triangle shaped geometry in the middle of the object points on the right side (Fig. 2). All linear parameters

were measured using tactile measurement equipment (digital micrometer C.E Johansson Jomic IP67, Eskilstuna, Sweden, and digital caliper Sylvac S_Cal Pro IP67, Crissier, Switzerland). All the measurements were conducted in a stable temperature environment 20 ± 1 °C.

2.5. Angle parameters/corner radius

A total of four angle parameters were measured for object A and two for object B. These measurements were conducted using a digital microscope (Dino-Lite Premier2 HR, polarisator, AM5018MT, Hsinchu, Taiwan) and computer software (DinoCapture 2.0 Version 1.5.5). The same method was conducted to measure corner radius.

2.6. Measurement equipment validation and test conditions

Validation of the micrometer and the caliper were conducted using measurement gauge blocks (Passbitsats Limit, Sweden, DIN 861/2, DIN 861/1). The micrometer equipment was validated with gauge blocks for 2, 5, 7 mm and the caliper for 20, 30 and 40 mm. These tests were conducted in a stable

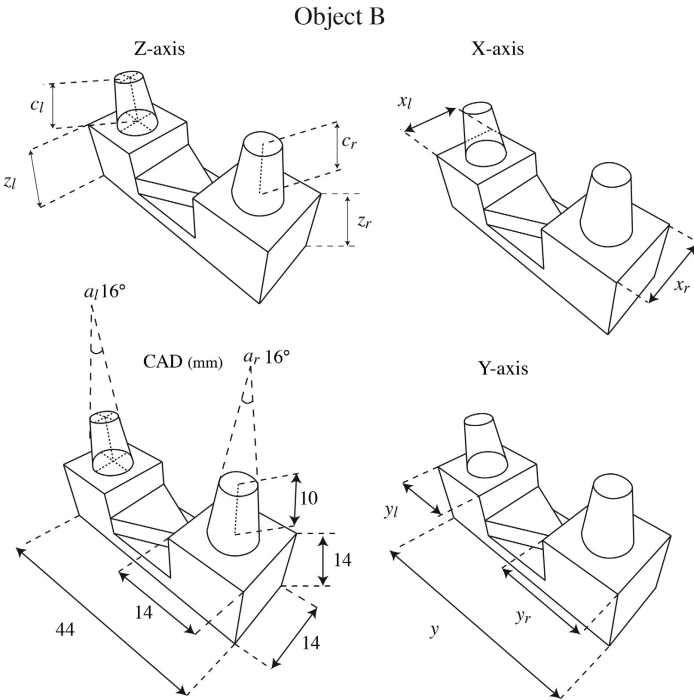


Fig. 2 – Illustration of object B (four unit bridge model) CAD describes the dimensions designed in the computer, the x, y and z axis illustrates the abbreviation measurements.

temperature environment $20 \pm 1^\circ\text{C}$, the gauges were stabilized in a silicone form to avoid body heat transferred to the test objects. Each block was measured 50 times. Results for caliper validation for 20 mm blocks mean 20.001 ± 0.002 , for 30 mm blocks mean 29.998 ± 0.001 and for 40 mm blocks mean 30.998 ± 0.002 . Validation of the micrometer instrument showed mean 2.001 ± 0.001 for the 2 mm block, mean 5.003 ± 0.0005 for 5 mm block and mean 7.006 ± 0.001 for the 7 mm block

3. Results

The results of all measurements for mean, standard deviation and a comparison between CAD and mean values can be seen in Table 2.

3.1. x-axis

In the x-axis, EOS showed least accuracy when compared to the CAD dimension at $-106 \mu\text{m}$ for object A and $84 \mu\text{m}$ for object B. Eden showed highest accuracy at $0 \mu\text{m}$ for object A

and $12 \mu\text{m}$ for object B. The standard deviation (SD) for object A was highest for EOS at $61 \mu\text{m}$ and lowest for Projet at $11 \mu\text{m}$. SD for object B was highest for Projet at $24 \mu\text{m}$ and least for Eden at $5 \mu\text{m}$.

3.2. y-axis

In the y-axis, EOS showed least accuracy when compared to the CAD dimension at $-201 \mu\text{m}$ for object A and Projet at $-182 \mu\text{m}$ for object B. Projet showed highest accuracy at $-7 \mu\text{m}$ for object A and EOS at $-3 \mu\text{m}$ for object B. SD for object A was highest for EOS at $68 \mu\text{m}$ and lowest for Object at $5 \mu\text{m}$. SD for Object B was highest for Projet at $51 \mu\text{m}$ and least for Object at $8 \mu\text{m}$.

3.3. z-axis

In the z-axis, Object showed least accuracy when compared to the CAD dimension at $43 \mu\text{m}$ for object A and EOS at $103 \mu\text{m}$ for Object B. Eden showed highest accuracy at $1 \mu\text{m}$ for object A and Object at $2 \mu\text{m}$ for object B. SD for object A was highest

Table 1 – Information about the four additive manufacturing units.

Manufacturer	EOS	3D Systems	Stratasys	Stratasys
Material	PA 2105	VISIJET PEARLSTONE	VeroWhite	VeroWhite
Layer thickness/printing resolution	60 μm	HIGH DEFINITION PLASTER (HDP) x-axis 375 dpi, y-axis 375 dpi, z-axis 790 dpi	28 μm x-axis 600 dpi, y-axis 600 dpi, z-axis 900 dpi	16 μm x-axis 600 dpi, y-axis 600 dpi, z-axis 1600 dpi
Machine/model	FORMIGA P110	3D SYSTEMS PROJET MP 3510	Objet 30	Objet Eden 260 V
Production year	2013	2013	2013	2013
Firmware	PSW 3.6.62	CONTROL VERSION 5.2.3540	V30.2.1.10908	V 27.0.1.16
Software/data preparation	Magics/Materialize 17.02.00, RPTools/EOS 06.01.08	PRINT3D 5.2.3540	Objet Studio 9.1.1.0	Objet Studio 9.2.8.10
Build time (Part A – 10 parts)	3 h	2 h 8 min	1 h 10 min	34 min
Build time (Part B – 10 parts)	6 h 30 min	6 h 3 min	3 h 40 min	1 h 43 min
Effective build volumex, y, z in mm	200 \times 250 \times 330	298 \times 185 \times 203	300 \times 200 \times 150	255 \times 252 \times 200
Production technique	Selective Laser Sintering	Multi jet printing	Polyjet	Polyjet

for Eden at 49 μm and lowest for Projet at 3 μm . SD for object B was highest for Eden at 24 μm and least for Objet at 6 μm .

3.4. Angle measurements and edge radius

The angle measurements for object A showed the least accuracy for Objet at 1.5° and the highest accuracy for Eden at –0.23°. Eden had the least accuracy for object B at –0.4° and EOS the highest at 0.06°. SD for object A was highest for Objet at 0.69° and lowest for EOS at 0.4°. For the edge radius measurement, Projet had the highest closeness to the CAD dimensions with a mean value of 96 μm for object A and 98 μm for object B.

3.5. Projet 3510 MP

For object A, the Projet machine displayed an overall accuracy of approximately 10 μm for all parameters besides y, which was off by 61 μm . In the same axis, Projet had a standard deviation of <26 μm , for z < 5 μm and for x < 18 μm . The machine displayed similar results for the production of object B with an overall accuracy of <30 μm and the y parameter was off by –182 μm . The SD in the y parameter was 51 μm , for z < 19 μm , and x < 24 μm (Fig. 3 and Table 2). The Projet device also showed an accuracy of approximately –0.5° with an SD of <0.6° for object A and less than –0.9° with an SD of <0.45° for object B (Table 2).

3.6. EOS Formiga P110

For object A the EOS machine presented an accuracy of 40 μm in the z parameters, <106 μm for the x parameters and <200 μm in the y parameters. The SD in the same parameters was

<21 μm for z, <61 μm for x and <68 μm for the y parameters. The production of object B presented an accuracy of <103 μm for the z parameters, <84 μm for x and >–21 μm for y. The SD in the same parameters was <22 μm for z, <23 μm for x and <38 μm y (Fig. 3 and Table 2). The EOS machine presented an angle accuracy <1.2° with an SD of <0.66° for object A and <0.28° for object B with an SD of <0.21° (Table 2).

3.7. Stratasys Objet 30

The accuracy in the z parameters for object A was <43 μm , <–84 μm for x and <–38 μm for y. The SD for z was <18 μm , <34 μm for x and <30 μm for y. The measurements for object B resulted in a z-axis accuracy of <35 μm , <54 μm for x, and <41 μm for y. The SD results for object B was <10 μm in z, <11 μm in x and <28 μm in y (Fig. 3 and Table 2). The Objet 30 machine presented an angle accuracy of <1.5° with a SD of <0.69° for object A and >–0.21° in accuracy for object B with a SD of <0.25 (Table 2).

3.8. Stratasys Objet Eden

The z-axis parameters for object A presented an accuracy of >–28 μm , >–32 μm for x and <92 μm for y. The SD for the z-axis parameters was <49 μm , <20 μm for x and <26 μm for y. The accuracy measurements for object B in the z-axis was <85 μm , <15 μm for x and <66 μm for y. The SD for the z-axis parameters was <24 μm , <6 μm for x and <50 μm for y (Fig. 3 and Table 2). The Objet Eden machine presented an angle accuracy of <0.95° with an SD of <0.68° for object A and >–0.41° in accuracy with an SD of <0.44° for object B (Table 2).

Table 2 – Results for all measurements.

Object A																			
Machine	(mm)	x	xac	xzb	za	zc	zd	z	zb	zr	cl	cr	xl	xr	al(Degree)	ar(Degree)	accl(Degree)	acc(Degree)	r
Objet	Standard d.	0.012	0.034	0.030	0.017	0.018	0.015	0.004	0.018	0.030	0.018	0.030	0.005	0.613	0.635	0.693	0.697	0.497	0.036
	Mean	16.060	4.916	4.953	7.038	7.040	7.042	2.033	7.043	4.978	4.962	16.024	17.282	16.589	17.504	16.589	17.504	16.555	0.288
	Accuracy	0.060	-0.084	-0.047	0.038	0.040	0.042	0.033	0.043	-0.022	-0.038	0.024	1.282	0.589	1.504	0.589	1.504	0.555	0.288
Eden	Standard d.	0.010	0.019	0.020	0.028	0.037	0.049	0.043	0.032	0.018	0.021	0.026	0.483	0.479	0.679	0.679	0.502	0.502	0.021
	Mean	16.000	4.977	4.968	6.974	6.980	6.975	2.001	6.972	4.931	4.944	16.092	16.949	16.267	17.051	16.267	17.051	16.226	0.251
	Accuracy	0.000	-0.023	-0.032	-0.026	-0.020	-0.025	0.001	-0.028	-0.069	-0.056	0.092	0.949	0.267	1.051	0.267	1.051	0.226	0.251
EOS	Standard d.	0.029	0.061	0.045	0.013	0.021	0.014	0.011	0.015	0.049	0.068	0.021	0.617	0.415	0.658	0.658	0.403	0.403	0.053
	Mean	15.929	4.911	4.894	7.041	7.029	7.035	2.030	7.036	4.803	4.799	16.021	17.049	16.339	17.225	16.339	17.225	16.464	0.253
	Accuracy	-0.071	-0.089	-0.106	0.041	0.029	0.035	0.030	0.036	-0.197	-0.201	0.021	1.049	0.339	1.225	0.339	1.225	0.464	0.253
Projet	Standard d.	0.011	0.018	0.017	0.004	0.005	0.004	0.003	0.005	0.021	0.015	0.026	0.413	0.613	0.499	0.499	0.609	0.609	0.025
	Mean	15.999	4.986	4.988	7.007	7.006	7.002	2.008	7.008	4.988	4.993	15.939	15.436	15.610	15.364	15.610	15.364	15.740	0.096
	Accuracy	-0.001	-0.014	-0.012	0.007	0.006	0.002	0.008	0.008	-0.012	-0.007	-0.061	-0.564	-0.390	-0.636	-0.390	-0.636	-0.260	0.096
Object B																			
Machine	(mm)	y	yl	yl	yr	zl	zl	zr	zr	cl	cr	xl	xr	al(Degree)	ar(Degree)	ar(Degree)	ar(Degree)	r	
Objet	Standard d.	0.028	0.008	0.009	0.010	0.010	0.006	0.010	0.007	0.010	0.007	0.011	0.011	0.248	0.204	0.204	0.204	0.028	
	Mean	44.041	14.021	14.025	13.996	14.002	14.002	14.002	10.035	10.035	10.030	14.054	14.052	15.890	15.776	15.776	15.776	0.303	
	Accuracy	0.041	0.021	0.025	-0.004	0.002	0.002	0.002	0.035	0.030	0.030	0.054	0.052	-0.110	-0.224	-0.224	-0.224	0.303	
Eden	Standard d.	0.050	0.024	0.031	0.024	0.021	0.021	0.017	0.016	0.006	0.006	0.444	0.005	0.444	0.350	0.350	0.350	0.028	
	Mean	44.064	14.015	14.066	13.947	13.944	13.944	10.085	10.085	10.085	14.015	14.012	15.699	15.699	15.588	15.588	15.588	0.303	
	Accuracy	0.064	0.015	0.066	-0.053	-0.056	-0.056	0.085	0.085	0.085	0.015	0.012	-0.301	-0.301	-0.412	-0.412	-0.412	0.303	
EOS	Standard d.	0.038	0.014	0.016	0.020	0.018	0.020	0.018	0.022	0.018	0.023	0.021	0.278	0.237	0.237	0.237	0.237	0.069	
	Mean	43.979	13.997	13.997	14.103	14.051	14.051	9.984	9.986	9.986	14.084	14.049	16.209	16.209	16.066	16.066	16.066	0.193	
	Accuracy	-0.021	-0.003	-0.003	0.103	0.051	0.051	-0.016	-0.014	-0.014	0.084	0.049	0.209	0.209	0.066	0.066	0.066	0.193	
Projet	Standard d.	0.051	0.036	0.041	0.017	0.018	0.018	0.019	0.018	0.024	0.024	0.298	0.024	0.298	0.278	0.278	0.278	0.031	
	Mean	43.818	14.009	14.024	13.993	13.974	13.974	9.974	9.996	9.996	14.019	14.014	15.911	15.911	15.920	15.920	15.920	0.098	
	Accuracy	-0.182	0.009	0.024	-0.007	-0.026	-0.026	-0.026	-0.004	-0.004	0.019	0.014	-0.089	-0.089	-0.080	-0.080	-0.080	0.098	

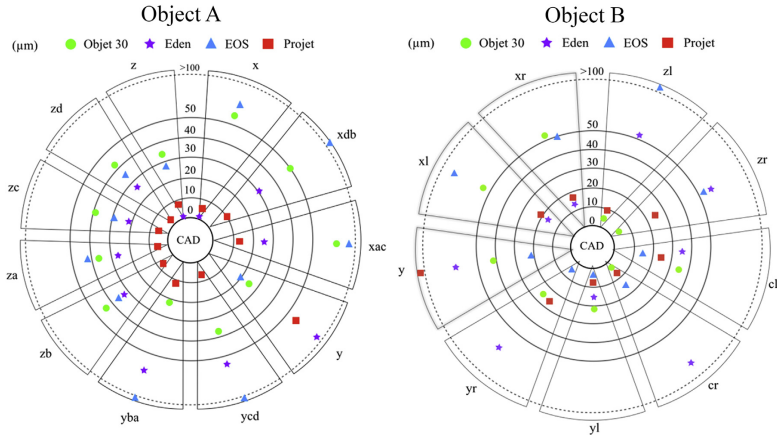


Fig. 3 – Bulls eye chart showing the mean values of the measurements for each parameter for all four machines, for booth object A and B. The closer the results are to the center, the closer resemblance they have to the original CAD dimensions. This is an illustration of the machines accuracy. It is important to notice that the illustration does not demonstrate if the results are bigger or smaller than zero, and that results past the 100 μm line could be more than 100 μm .

4. Discussion

If focusing on the x , y and z parameters (for object A), the results would have shown an accuracy of 0 μm (x), 92 μm (y) and 1 μm (z) for Objet Eden, 60 μm (x), 24 μm (y) and 33 μm (z) for Objet 30, -71 μm (x), 21 μm (y) and 30 μm (z) for the EOS machine and -1 μm (x), -61 μm (y) and 8 μm (z) for the Projet machine. One could emphasize that it would be satisfactory only to use these three parameters in the shape of a cube to determine the production tolerances. However, it must be emphasized that the primary reason for selecting complex geometries in the current study was that the geometries that need to be manufactured in dentistry are unique thus using a cube was not clinically relevant. The “inlay shaped” object, referred as object A was divided into four “cubes”. Therefore, for an object to be acceptable, it is of great importance that these four cubes present comparable tolerance levels in all three axes (Fig. 3 and Table 2 parameter z_a , z_b , z_c and z_d). For instance if the height of one of the four cubes in each object would show a difference of 100 μm , the produced inlay can be considered to have a non-passive fit. This is also the reason for conducting angle measurements from different directions.

It is of great importance to make a distinction between resolution, accuracy and repeatability. Resolution refers to the fineness of the production technology or the smallest feature the system can produce. A system with high resolution might be capable of producing objects with small details however, this does not imply that these details are accurately manufactured. The Objet Eden machine presents the highest resolution specifications (Table 1) with a layer thickness (z -axis) of 16 μm , DPI specifications of 600 and 1600 (z , x , y -

axis). These numbers should not be regarded or interpreted as the ability of the machine to produce accurate samples, however this might imply that the systems has the ability to manufacture objects with high resolution. ISO describes accuracy as the closeness of agreement between a measured quantity value and a true quantity value of a measured object (ISO/IEC GUIDE 99:2007(E/F)). A system with high accuracy has the capability to produce an object that is closely comparable to the CAD file. However, it can be said that if the same production unit lacks high resolution, the production of fine details and surface finish will not be possible. Reproducibility can be described as the systems ability to produce consistent output time after time. It must be noted that a system with high accuracy and high resolution does not automatically have high reproducibility. There are several aspects to address regarding reproducibility in additive manufacturing, all additive systems produce objects on some platform also referred as a build envelope or build platform [4]. The manufacturing systems capability to produce several consistent parts within one build envelope (repeatability as tested in this study), or the parts consistency in between several build envelopes are of interest (reproducibility) [13].

Additive manufacturing technologies have the capability to produce objects with various geometries and with various materials suitable for dental applications. However, it must be noted that the production tolerances would naturally be different depending on different applications; therefore a universal calibration is essential before manufacturing. Hence, the results of the current study provide information with regards to the axis by axis tolerance errors for the operator to calibrate and to compensate for the deviation, which could result in a product with a higher resemblance to the original

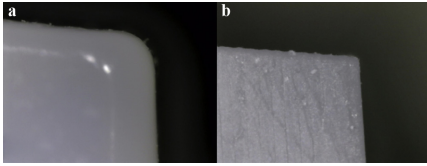


Fig. 4 – (a) 250× magnification of one edge from object B manufactured by the Objet 30 machine. (b) The same geometry manufactured by the Projet 3510MP. The CAD file has a 90° angle in this area thus the edge radius in the CAD file is 0.01 mm.

CAD file. For instance, if one manufacturing unit has produced objects that are 1% larger than that of the CAD file in the y-axis, this error could be compensated in the software to manufacturing the object 1% smaller only in the necessary axis.

One of the most important aspects of additive manufacturing is the degree of deviation within a single system (repeatability) in relation to the specific geometry designed. If one system is supposed to produce a cube that is 30 μm in all directions, and the result is approximately 25 μm and the standard deviation 10 μm then that system is probably not accurate enough for producing an object of that size. On the contrary, if the result is 28 μm and the standard deviation 2 μm the systems accuracy and repeatability would be more reliable. Therefore, it is of utmost importance to carefully observe the standard deviation of each system, since this could significantly influence the reliability of the calibration. Thus, in the current study, the degree of mean deviation from the original CAD file for each system was not ranked in any way, and should be discussed as a separate issue because this can easily be calibrated if the repeatability (standard deviation) of the manufacturing system is good.

4.1. Object A

The system that produced object A with the least standard deviation and highest overall accuracy was Projet 3510 MP, it showed an SD < 20 μm for all parameters besides y (26 μm). The systems produced object A with an accuracy of approximately 10 μm for all parameters besides y (61 μm), it also had the sharpest edge, with an edge radius at 96 μm. All the angle measurements on the Projet objects were smaller than the CAD file with approximately –0.4° to –0.6°.

4.2. Object B

The system that produced object B with the least standard deviation and highest overall accuracy was Objet 30, it showed an SD of approximately 10 μm for all parameters besides y (28 μm). The unit produced object B with an over all accuracy of around 50 μm. On the other hand, the Objet 30 machine did not have the best edge radius at 303 μm and the angle parameters were approximately –0.1° to –0.2° whereas the Projet machine had an edge radius of 98 μm (Fig. 4) and an angle accuracy of –0.08 to –0.09°.

Before we can reflect on the results of studies like this, we need to know what level of production tolerances we are looking for in dentistry. One of the most demanding prosthodontic applications is probably implant supported fixed prosthodontics. Several studies have shown that the production tolerances for implant supported fixed prosthodontics would be in the range of 20–100 μm [14–17]. Bearing this in mind, the accuracy results from the current study would be in the same production tolerance range. One good example is the Projet machine for object A. It shows an accuracy of approximately 10 μm in all parameters but y (–61 μm), on the other hand the same machine had accuracy results of around 25 μm (y –182 μm) for object B. The correlation between standard deviation and accuracy is an important aspect in choosing the suitable machine for the intended application. One other important aspect is the production time, the Objet Eden machine produced object B four times faster than the EOS machine, and at the same time the accuracy results are comparable.

4.3. Limitations of the study

Neither object A or B has any overhanging structures, so there is no need for supporting materials, the object production starts from the base and builds upwards in the z-direction. A geometry with overhangs would need supporting material to keep the structure from collapsing. Further tests need to be done on objects with support structures.

Acknowledgements

We would like to thank M-Tec, SIGNCOM and EOS for providing us with all the samples.

REFERENCES

- [1] Thalji G, Bryington M, De Kok IJ, Cooper LF. Prosthodontic management of implant therapy. *Dent Clin N Am* 2014;58:207–25. <http://dx.doi.org/10.1016/j.cden.2013.09.007>.
- [2] van Noort R. The future of dental devices is digital. *Dent Mater* 2012;28:3–12. <http://dx.doi.org/10.1016/j.dental.2011.10.014>.
- [3] Silva NRFA, Witek L, Coelho PG, Thompson VP, Rekow ED, Smay J. Additive CAD/CAM process for dental prostheses. *J Prosthodont* 2011;20:93–6. <http://dx.doi.org/10.1111/j.1532-849X.2010.00623.x>.
- [4] Torabi K, Farjood E, Hamedani S. Rapid prototyping technologies and their applications in prosthodontics, a review of literature. *J Dent (Shiraz)* 2015;16:1–9.
- [5] Germani M, Raffaelli R, Mazzoli A. A method for performance evaluation of RE/RP systems in dentistry. *Rapid Prototyp J* 2010;16:345–55. <http://dx.doi.org/10.1108/13552541011065740>.
- [6] Salmi M, Paloheimo K-S, Tuomi J, Wolff J, Mäkitie A. Accuracy of medical models made by additive manufacturing (rapid manufacturing). *J Cranio-Maxillofac Surg* 2013;1:7. <http://dx.doi.org/10.1016/j.jcms.2012.11.041>.
- [7] UVP, Inc. Apparatus for production of three-dimensional objects by stereolithography; 1984.
- [8] Pérez CJL. Analysis of the surface roughness and dimensional accuracy capability of fused deposition

- modelling processes. *Int J Prod Res* 2002;40:2865–81, <http://dx.doi.org/10.1080/00207540210146099>.
- [9] Katatny El I, Masood SH, Morsi YS. Error analysis of FDM fabricated medical replicas. *Rapid Prototyp J* 2010;16:36–43, <http://dx.doi.org/10.1108/13552541011011695>.
- [10] Choi JY, Choi JH, Kim NK, Kim Y, Lee JK, Kim MK, et al. Analysis of errors in medical rapid prototyping models. *Int J Oral Maxillofac Surg* 2002;31:23–32, <http://dx.doi.org/10.1054/ijom.2000.0135>.
- [11] Ibrahim D, Broilo TL, Heitz C, de Oliveira MG, de Oliveira HW, Nobre SMW, et al. Dimensional error of selective laser sintering, three-dimensional printing and PolyJet™ models in the reproduction of mandibular anatomy. *J Cranio-Maxillofac Surg* 2009;37:167–73, <http://dx.doi.org/10.1016/j.jcms.2008.10.008>.
- [12] Silva DN, de Oliveira MG, Meurer E, Meurer MI, da Silva JVL, Santa-Bárbara A. Dimensional error in selective laser sintering and 3D-printing of models for craniomaxillary anatomy reconstruction. *J Cranio-Maxillofac Surg* 2008;36:443–9, <http://dx.doi.org/10.1016/j.jcms.2008.04.003>.
- [13] Pinto JM, Arrieta C, Andia ME, Uribe S, Ramos-Grez J, Vargas A, et al. Sensitivity analysis of geometric errors in additive manufacturing medical models. *Med Eng Phys* 2015;37:328–34, <http://dx.doi.org/10.1016/j.medengphy.2015.01.009>.
- [14] Örtorp A, Jemt T, Bäck T, Jälevik T. Comparisons of precision of fit between cast and CNC-milled titanium implant frameworks for the edentulous mandible. *Int J Prosthodont* 2003;16:194–200.
- [15] Ma T, Nicholls JL, Rubenstein JE. Tolerance measurements of various implant components. *JoMI* 1997;12:371–5.
- [16] Braian M, Bruyn H, De Bruyn H, Fransson H, Christersson C, Wennerberg A. Tolerance measurements on internal- and external-hexagon implants. *JoMI* 2014;29:846–52, <http://dx.doi.org/10.11607/jomi.3242>.
- [17] Rubenstein JE, Ma T. Comparison of interface relationships between implant components for laser-welded titanium frameworks and standard cast frameworks. *JoMI* 1999;14:491–5.

III

Available online at www.sciencedirect.com

ScienceDirect

journal homepage: www.intl.elsevierhealth.com/journals/dema

Geometrical accuracy of metallic objects produced with additive or subtractive manufacturing: A comparative in vitro study

Michael Braian*, David Jönsson, Mir Kevci, Ann Wennerberg

Department of Prosthodontics, Faculty of Odontology, Malmö University, Smedjegatan 16, 214 21 Malmö, Sweden

ARTICLE INFO

Article history:

Received 20 September 2017

Received in revised form

19 December 2017

Accepted 23 March 2018

Available online xxx

Keywords:

Additive manufacturing

Subtractive manufacturing

3D printing

Accuracy

Precision

Dentistry

Metals

ABSTRACT

Objective. To evaluate the accuracy and precision of objects produced by additive manufacturing systems (AM) for use in dentistry and to compare with subtractive manufacturing systems (SM).

Methods. Ten specimens of two geometrical objects were produced by five different AM machines and one SM machine. Object A mimics an inlay-shaped object, while object B imitates a four-unit bridge model. All the objects were sorted into different measurement dimensions (x, y, z), linear distances, angles and corner radius.

Results. None of the additive manufacturing or subtractive manufacturing groups presented a perfect match to the CAD file with regard to all parameters included in the present study. Considering linear measurements, the precision for subtractive manufacturing group was consistent in all axes for object A, presenting results of <0.050 mm. The additive manufacturing groups had consistent precision in the x-axis and y-axis but not in the z-axis. With regard to corner radius measurements, the SM group had the best overall accuracy and precision for both objects A and B when compared to the AM groups.

Significance. Within the limitations of this in vitro study, the conclusion can be made that subtractive manufacturing presented overall precision on all measurements below 0.050 mm. The AM machines also presented fairly good precision, <0.150 mm, on all axes except for the z-axis. Knowledge regarding accuracy and precision for different production techniques utilized in dentistry is of great clinical importance. The dental community has moved from casting to milling and additive techniques are now being implemented. Thus all these production techniques need to be tested, compared and validated.

© 2018 The Academy of Dental Materials. Published by Elsevier Inc. All rights reserved.

1. Introduction

Metal is used in dentistry for different applications, such as fixed partial dentures (FPD), implant-supported super-

structures, dental implants and removable partial dentures (RPD). Since their introduction in dentistry, metals have been produced by casting using the lost-wax technique [1]. This manufacturing technique has been improved and computer-aided design and computer-aided manufacturing (CAD/CAM)

* Corresponding author.

E-mail addresses: Michael.Braian@mah.se (M. Braian), david.jonsson@folktandvardenskane.se (D. Jönsson),

Lewend.kevci@folktandvarden.se (M. Kevci), Ann.Wennerberg@mah.se (A. Wennerberg).

<https://doi.org/10.1016/j.dental.2018.03.009>

0109-5641/© 2018 The Academy of Dental Materials. Published by Elsevier Inc. All rights reserved.

have had a huge influence on the quality of the metal frameworks. Compared to the lost wax technique, CAD/CAM is both time-saving and efficient due to the reduction in human errors [1,2]. Modern prosthetic constructions are produced utilizing CAD/CAM with established [1] subtractive manufacturing (SM) techniques. The method uses Computer Numerical Controlled (CNC) machining technology and often consists of a milling machine that removes bulk material from solid blocks in order to shape the desired object from the CAD. The blocks used in SM are industrially produced under highly standardized conditions, reducing the risk of defects and residual stresses in the material [1,2]. One of the drawbacks of SM is that most of the material becomes waste and there is significant wear on the burrs [2,3]. The high waste ratio is also unfavourable for the environment [4]. Another limitation of this technique is the inability to create organic geometries such as complex occlusal anatomy [5,6]. This is due to the restricted accessibility of the burrs [2,7]. Surface details of less than the diameter of the smallest milling burr will not be produced. Dental CAM software counterbalance for this with drill-compensating features that could affect the fit of the object being produced [8].

Recently a new production technique known as additive manufacturing (AM) or 3D printing has been introduced to dentistry. Some of the AM techniques for metal production used in dentistry are: selective laser melting (SLM), selective laser sintering (SLS) or electron beam melting (EBM). When using the AM technique, the CAD object is sliced into multiple layers along the vertical axis with a pre-set layer thickness. Each layer contains information about the object's profile in that specific layer. The profile information from each layer is used to control the laser movement, which moves selectively over an alloy powder bed [9]. The beam transfers heat to the powder bed particles, resulting in local fusing or melting of the particles on a build platform. When a layer is completed, the platform is lowered by a one-layer thickness. Another layer of powder is then deposited on top and the procedure is repeated for the next layer. Depending on the type of AM technique, the applied powder particles fuse or melt together, not only in the new layer, but also with the previous layer, allowing the different layers to form a 3D object designed from the CAD model [5,10]. When compared to the SM technique, the AM technique is not dependent on tool axes to produce the desired object. Since various layers are built up without the object penetrating the powder bed, the laser itself is not blocked. Hence, there are basically no restrictions to building complex shapes [1]. The powder granules that were unexposed to the laser beam can be reused [1,6], consequently making a significant reduction in waste material. [8,11]. Furthermore, it is environmentally beneficial and reduces production costs [12]. One more advantage to the AM technique is its ability to produce several prosthetic units at the same time [1,5], unlike the SM technique, where only one part can be machined at a time.

One known disadvantage of metallic objects produced by AM is the build-up of tensions in the material due to uneven heat distribution during the manufacturing process. These tensions may lead to deformation at a later date and possibly affect the final product [11,13]. In order to reduce these tensions, the object should be exposed to a post-production

heat treatment [10]. If porosity arises in the material during fabrication, this can also be considered a disadvantage as this might affect the material properties [14].

Many AM production techniques produce objects with a rough surface topography because of un-melted or partially melted powder particles. The speed of the laser as well as the laser beam itself and the size of the powder particles has great significance for the roughness of the end product [15–19]. For instance, today the implant connection of FDPs must be post-processed with SM to get a smooth, well-fitting contact surface, making the finalized object an AM and SM hybrid [20].

The SLS technique uses a high-energy carbon dioxide laser beam that fuses the outer surface of the grains and forms a solid mass when the temperature decreases [5,6], while the SLM technique often uses a more powerful type of laser that melts the outer surfaces of the grains together. The temperature never reaches melting temperature in SLS, resulting in one of the most important differences to SLM. The SLM technique was developed to avoid time-consuming post-processing processes and to produce almost completely dense objects with better mechanical properties [10].

A third way for AM to process metallic objects is electron beam melting (EBM). This technique is similar to SLM, but represents the joining of powder particles by selectively melting them with an electron beam instead of a laser. The energy density of the electron beam is higher compared to the laser beam, thus generating a higher temperature output and making it possible to use alloys that have a higher melting range [21].

These new manufacturing techniques need to be evaluated in vitro and in vivo to ensure the quality is equal or better than production with conventional production techniques. This is necessary to protect patients from complications and failed restorations [2,6].

1.1. Hypothesis

Subtractive manufacturing is superior to additive manufacturing regarding accuracy and precision of the final product.

1.2. Aim

The aim of this in vitro study was to evaluate the production accuracy and precision of AM and SM techniques through reverse engineering, considering production tolerance for usage in dentistry.

2. Materials and method

2.1. ISO reference

The ISO (the International Organization for Standardization) is an international federation of standardized ISO bodies. This paper utilizes ISO 12836:2015 'Dentistry – Digitizing devices for CAD/CAM systems for indirect dental restorations – Test methods for assessing accuracy'. Three geometrical figures were described by ISO as Annex A, B and C. In this paper, the Annex A and B were utilized but not the method in the ISO (see Figs. 1 and 2). Annex A simulates the structures of an

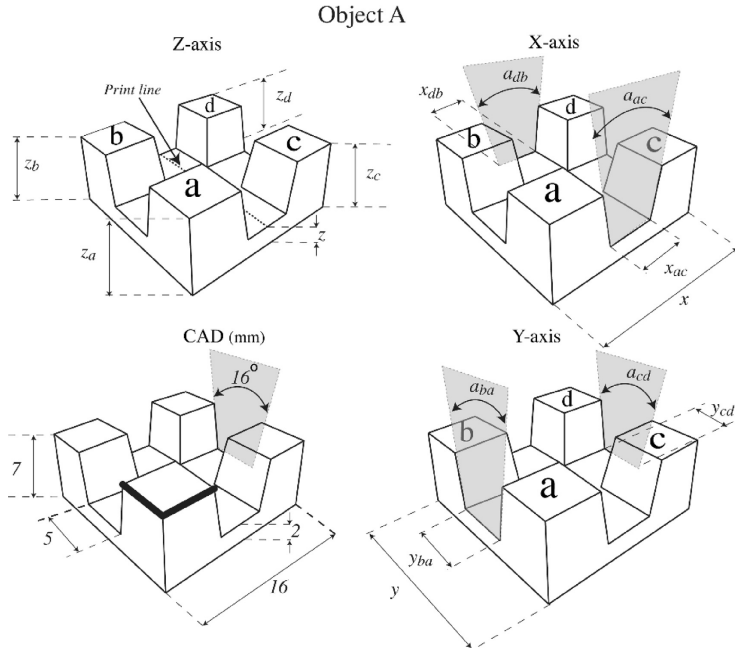


Fig. 1 – Inlay-shaped object, illustration of the CAD dimensions of the object and all the measurements in xyz direction. The marked corner describes where the edge radius was measured.

inlay-shaped object and Annex B simulates the structures of a four-unit bridge model. The CAD object was designed using 3D software (Solidworks educational edition 2013) with a corner radius of 0.01 mm set as 90° (Figs. 1 and 2). The purpose of the objects' geometry was to mimic linear, angle and corner radius measurements. Object A contained 16 measurements and object B 12 measurements. The standard tessellation language files (STL) for Annex A and B were exported and delivered to the manufactures with information about the products and production.

2.2. Fabrication of specimens

Five additive manufacturing units and one subtractive machine were tested. The additive machines tested were: Arcam[®], Concept laser[®], EOS[®], SLM Solutions[®] and the subtractive machine was Mikron[®]. Every company manufacturing the objects and all their personnel were authorized and included in the protocol sent out at the start of the project. Ten sets were manufactured for object A and object B. The software settings were decided by authorized personnel for each production unit in order to achieve accurate samples. Arcam, Mikron, SLM solutions, Concept laser and EOS manufactured

the objects in titanium. EOS also manufactured the objects in chrome cobalt. Upon delivery, the manufacturer decided the print resolution, specification of production unit, software and manufacturing time, based on the choice of alloy. All the samples went through the same process with regard to the delivery and manufacturing that is utilized for dental products.

2.3. Linear measurements

All the objects were divided into three different axes: X, Y and Z. The X-axis describes one of the horizontal dimensions for both objects. A total of three linear dimensions were measured in object A and two for object B. The Y-axis also measured horizontal dimensions for objects A and B, which consisted of three linear dimensions for each object. The Z-axis describes the vertical dimensions of the objects and a total of five linear measurements were performed for object A and four for object B. The linear dimensions of the objects were perpendicular to the layering orientation. To ease the orientation of object A, the four cubic forms were named a–d (see Fig. 1). The placement of the cube form a was orientated in the top-left corner in relation to the horizontal print lines on each object. Object B has a triangle shape in the middle; the tip of the triangle

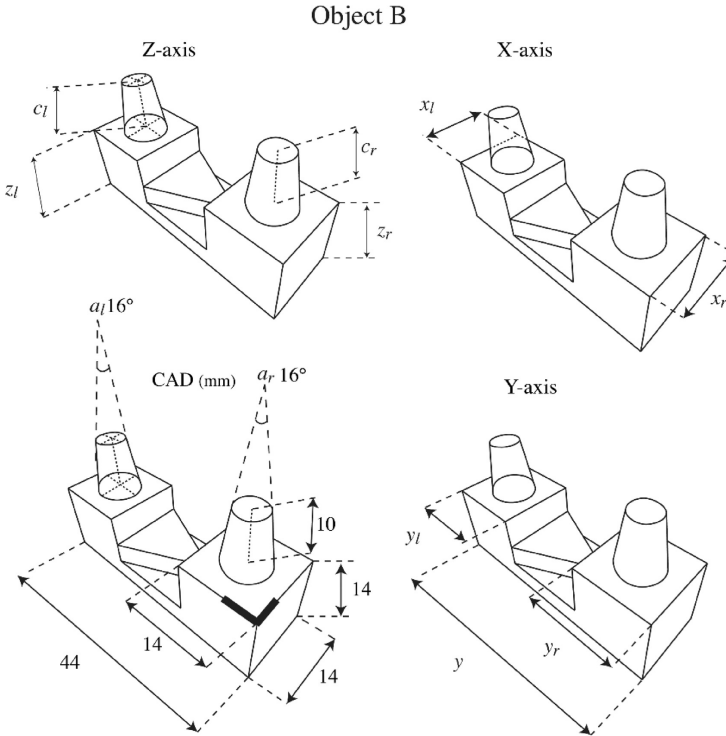


Fig. 2 – Four-unit bridge model, illustration of the CAD dimensions and all the measurements in xyz direction. The marked corner describes where the edge radius was measured.

was defined as the right-hand side of the object and the opposite as the left-hand side (Fig. 2). The tool for measuring all linear measurements was executed with a validated and calibrated digital calliper (Digital Sylvac S Cal Pro IP67, Crissier, Switzerland). While measuring the linear measurements of the objects, the examiner validated the digital calliper by using gauge blocks (Passbitsats Limit, Sweden, DIN 861/2, DIN 861/1). The digital calliper measured gauge blocks of 2, 5, 7, 20 and 40 mm in order to calibrate between the operators and the validation of the instrument. Each gauge block was measured 50 times. A calculation was then performed with standard error of measurement using Dahlberg's formula in order to control inter-observatory variations. This was done for all manufacturing groups before measuring objects A and B. In order to keep dimensional stability, the objects were placed on a silicone form and the measuring process was executed in a room with a stable temperature of $20 \pm 1^\circ\text{C}$; all the linear measurements were measured five times.

2.4. Angle parameters and corner radius

There were four measurements of angles for object A and two for object B. The angles and corner radius were measured using a validated and calibrated digital microscope (Dino-Lite Premier2 HR, polarisator, AM5018MT, DinoXcope Version 1.12, Hsinchu, Taiwan). Before measuring the angle parameters and corner radius of the objects, a validation of the microscope was performed using a Dino-Lite calibration sample (Dino-lite calibration sample P/N TC2001Aug 2013). The validation sample had known measurements, with 1 mm intervals and a line was drawn on the validation sample in the measurement software to calibrate the microscope against the sample. In the computer software (DinoCapture 2.0), all the calibrations were saved in a calibration manager and were later used for each magnification (X30, X50 and X250). During the angle and corner radius measurements, a calibration was performed between the operators (see Table 3). The result from Dahlberg's formula indicates that

Table 1 – Calibration and validation of the digital calliper. This procedure was conducted before measuring each manufacturing group.

		Gauge block				
	(n.50)	2 mm ± 0.15 µm	5 mm ± 0.22 µm	7 mm ± 0.15 µm	20 mm ± 0.32 µm	40 mm ± 0.35 µm
Machine	Arcam	1.993 ± 0.005	4.989 ± 0.008	6.993 ± 0.014	19.995 ± 0.020	39.998 ± 0.019
	Concept laser	1.990 ± 0.005	4.992 ± 0.008	6.992 ± 0.014	19.997 ± 0.020	39.997 ± 0.017
	EOS (CoCr)	1.999 ± 0.005	4.991 ± 0.005	6.993 ± 0.009	19.993 ± 0.011	39.997 ± 0.031
	SLM	1.999 ± 0.005	4.990 ± 0.007	6.991 ± 0.004	19.994 ± 0.015	40.002 ± 0.025
	EOS	1.995 ± 0.008	4.988 ± 0.015	6.990 ± 0.021	19.994 ± 0.020	39.993 ± 0.019
	Mikron	1.995 ± 0.008	4.988 ± 0.009	6.991 ± 0.011	19.995 ± 0.023	39.996 ± 0.020

Table 2 – Inter-observatory variability between the operators using digital calliper, calculated with Dahlbergs formula.

		Gauge block				
		2 mm	5 mm	7 mm	20 mm	40 mm
Machine	Arcam	0.0022	0.0036	0.0026	0.0039	0.0116
	Concept laser	0.0013	0.0018	0.0041	0.0044	0.0035
	EOS (CoCr)	0.0008	0.0018	0.0026	0.0032	0.0046
	SLM	0.0014	0.0012	0.0021	0.0050	0.0072
	EOS	0.0014	0.0014	0.0026	0.0040	0.0044
	Mikron	0.0011	0.0029	0.0027	0.0053	0.0040

Table 3 – Inter-observatory variability between the operators using microscope, calculated with Dahlbergs formula.

	X30	X50	X250
Error of measurement	0.0103	0.0050	0.0023

the error of measurement between the operators is negligible.

3. Results

AM machines were compared with SM and CAD files with regard to measurements for standard deviation, accuracy, mean, angle measurements and corner radius (see Tables 4 and 5).

3.1. Calibration and validation

According to Table 1, the precision for the calliper's validation in relation to gauge blocks measurements can be seen.

Dahlberg's formula was used to calculate the inter-observatory variations using the digital calliper. The results shown in Table 2 demonstrate that the differences were minor for each measurement in general.

Dahlberg's formula was also used to calculate the inter-observatory variations between the operators, taking the measurements from the microscope into consideration (see Table 3).

3.2. Linear measurements

3.2.1. Object A — accuracy, precision and variance

3.2.1.1. X-axis. Arcam had the lowest x-axis precision, 0.078 mm, when compared to Mikron, which had the highest precision, 0.013 mm. Arcam also had the least accuracy, 0.176 mm in x-axis, when compared to the CAD file and Mikron had the highest accuracy, -0.012 mm.

Regarding the precision variance in the x-axis, xac and xdb Arcam had the highest variance, 0.039–0.078 mm, whereas EOS (CoCr) had the least variance, 0.013–0.019 mm. Accuracy variance for the same measurements showed that Mikron had most variation (-0.012)–(-0.173) and EOS had the lowest, 0.061–0.100 (Table 4, Figs. 3 and 4).

3.2.1.2. Y-axis. Arcam had the lowest precision, 0.117 mm, and Mikron had highest precision, 0.009 mm. Mikron showed highest accuracy at -0.010 mm and, at the same time, the lowest accuracy at -0.0210 mm.

Regarding the precision variance in the y-axis, yba and ycd, Arcam had the highest, 0.045–0.117 mm, whereas EOS had the least variance, 0.020–0.027 mm. Accuracy variance for the same measurements showed that Mikron had the highest (-0.010)–(-0.210). Arcam and EOS shared the lowest with a difference of 0.059 mm (Table 4, Figs. 3 and 4).

3.2.1.3. Z-axis. EOS had the lowest z-axis precision, 0.282 mm, while Mikron had the highest precision, 0.012 mm. Mikron also had the highest z-axis accuracy, 0.014 mm, while EOS had the lowest accuracy at 1.026 mm.

Regarding the precision variance in the z-axis, za, zb, zc and zd, Arcam had the highest, 0.020–0.208 mm, whereas the least variance in the z-axis can be seen in EOS (CoCr) 0.054–0.062 mm. Accuracy variance for the same measurements showed that Mikron had least variation (-0.059)–0.015 and Arcam had the most variation, ranging from (-0.871)–(-0.406) (Table 4, Figs. 3 and 4).

3.2.2. Object B — accuracy, precision and variance

3.2.2.1. X-axis. Arcam had lowest x-axis precision, 0.079 mm and Mikron had the highest precision, 0.006 mm. Mikron also had the highest accuracy, 0.007 mm whereas Arcam had the lowest accuracy, 0.161 mm

Regarding the precision variance in xl and xr, Arcam had the highest, 0.068–0.079 mm, while Mikron had the least variance, 0.006–0.009 mm. Accuracy variance for the same

Table 4 – All the results from measuring object A, for orientation of the different measurements please see Fig. 1. The results are presented in mm besides the angle measurements, these are presented in degrees.

Object A Machine:	(mm)	x	xac	xdb	yba	yca	y	za	zc	zd	z	zb	(Degree) aba	(Degree) adb	(Degree) acd	(Degree) aac	(mm) r
Arcam®	Precision	0.078	0.039	0.049	0.071	0.045	0.117	0.148	0.208	0.184	0.020	0.158	0.422	0.546	0.332	0.579	0.078
	Mean	16.176	5.028	5.037	5.088	5.075	16.136	6.139	6.167	6.138	1.594	6.129	17.303	17.018	17.161	16.968	0.287
	Accuracy	0.176	0.028	0.037	0.088	0.075	0.136	-0.861	-0.833	-0.862	-0.862	-0.406	-0.871	1.303	1.018	1.161	0.968
Concept laser®	Precision	0.045	0.045	0.017	0.021	0.027	0.043	0.109	0.082	0.092	0.088	0.105	0.209	0.074	0.043	0.089	0.041
	Mean	16.037	16.037	5.115	5.113	5.121	16.029	7.290	7.281	7.299	2.263	7.294	15.950	15.976	15.989	15.989	0.146
	Accuracy	0.037	0.013	0.115	0.113	0.121	0.029	0.290	0.281	0.299	0.263	0.294	-0.050	-0.024	-0.011	-0.011	0.146
EOS (CoCr)®	Precision	0.019	0.015	0.013	0.020	0.013	0.012	0.060	0.062	0.060	0.059	0.054	0.015	0.026	0.018	0.024	0.041
	Mean	15.971	5.089	5.081	5.082	5.080	15.970	7.069	7.086	7.081	2.061	7.058	16.004	15.994	16.000	15.992	0.155
	Accuracy	-0.029	0.089	0.081	0.082	0.080	-0.030	0.069	0.086	0.081	0.061	0.058	0.004	-0.006	0.000	-0.008	0.155
SLM®	Precision	0.023	0.015	0.015	0.018	0.020	0.029	0.061	0.042	0.041	0.054	0.038	0.170	0.035	0.113	0.089	0.060
	Mean	16.122	5.048	5.049	5.051	5.057	16.144	7.220	7.220	7.214	2.252	7.212	16.076	16.004	16.057	15.989	0.170
	Accuracy	0.122	0.048	0.049	0.051	0.057	0.144	0.220	0.220	0.214	0.252	0.212	0.076	0.004	0.057	-0.011	0.170
EOS®	Precision	0.022	0.037	0.030	0.020	0.023	0.027	0.268	0.251	0.253	0.264	0.282	0.089	0.035	0.028	0.028	0.040
	Mean	16.061	5.100	5.099	5.117	5.127	16.068	7.998	8.004	7.989	3.014	8.026	16.009	15.995	16.003	15.995	0.216
	Accuracy	0.061	0.100	0.099	0.117	0.127	0.068	0.998	1.004	0.989	1.014	1.026	0.009	-0.005	0.003	-0.005	0.216
Mikron®	Precision	0.009	0.048	0.054	0.038	0.041	0.009	0.013	0.012	0.015	0.034	0.017	0.017	0.017	0.013	0.015	0.034
	Mean	15.988	4.824	4.827	4.832	4.790	15.999	7.016	7.014	7.014	1.941	7.021	16.007	16.005	16.003	16.003	0.108
	Accuracy	-0.012	-0.166	-0.173	-0.168	-0.210	-0.010	0.016	0.014	0.014	-0.059	0.021	0.007	0.005	0.003	0.003	0.108

Please cite this article in press as: Braian M, et al. Geometrical accuracy of metallic objects produced with additive or subtractive manufacturing: A comparative in vitro study. Dent Mater (2018), <https://doi.org/10.1016/j.dental.2018.03.009>

Table 5 – All the results from measuring object B, for orientation of the different measurements please see Fig. 2. The results are presented in mm besides the angle measurements, these are presented in degrees.

Object B Machine:	(mm)	xl	xr	y	yl	yr	cl	cr	zl	zr	(Degree) al	(Degree) ar	(mm) r
Arcam®	Standard deviation	0.068	0.079	0.123	0.076	0.074	0.137	0.140	0.189	0.250	0.026	0.024	0.076
	Mean	14.144	14.161	44.243	14.135	14.118	10.102	10.161	13.027	13.025	15.982	15.995	0.153
	Accuracy	0.144	0.161	0.243	0.135	0.118	0.102	0.161	-0.973	-0.975	-0.018	-0.005	0.153
Concept laser®	Standard deviation	0.024	0.026	0.052	0.031	0.017	0.039	0.076	0.081	0.082	0.091	0.129	0.015
	Mean	13.946	13.948	43.990	13.971	13.974	9.985	9.945	14.268	14.208	15.924	15.896	0.084
	Accuracy	-0.054	-0.052	-0.010	-0.029	-0.026	-0.015	-0.055	0.268	0.208	-0.076	-0.104	0.084
EOS (CoCr)®	Standard deviation	0.020	0.014	0.030	0.013	0.014	0.044	0.034	0.117	0.071	0.019	0.022	0.020
	Mean	13.950	13.953	43.905	13.962	13.974	9.905	9.940	14.180	14.102	15.995	15.996	0.101
	Accuracy	-0.050	-0.047	-0.096	-0.038	-0.026	-0.095	-0.060	0.180	0.102	-0.005	-0.004	0.101
SLM®	Standard deviation	0.030	0.035	0.075	0.037	0.053	0.097	0.082	0.097	0.082	0.017	0.022	0.037
	Mean	14.017	14.026	44.022	14.063	14.071	9.912	9.995	14.043	14.060	16.003	16.001	0.059
	Accuracy	0.017	0.026	0.022	0.063	0.071	-0.088	-0.005	0.043	0.060	0.003	0.001	0.059
EOS®	Standard deviation	0.044	0.038	0.042	0.037	0.027	0.099	0.073	0.194	0.086	0.026	0.029	0.020
	Mean	14.005	14.005	44.154	14.020	14.017	9.942	10.050	14.683	14.683	15.982	15.987	0.117
	Accuracy	0.005	0.005	0.154	0.020	0.017	-0.058	0.050	0.683	0.683	-0.018	-0.013	0.117
Mikron®	Standard deviation	0.009	0.006	0.006	0.153	0.153	0.037	0.045	0.02	0.017	0.014	0.016	0.011
	Mean	14.008	14.007	44.005	13.958	14.06	10.082	10.127	13.984	13.955	16.000	16.008	0.032
	Accuracy	0.008	0.007	0.005	-0.042	0.060	0.082	0.127	-0.016	-0.045	0.000	0.008	0.032

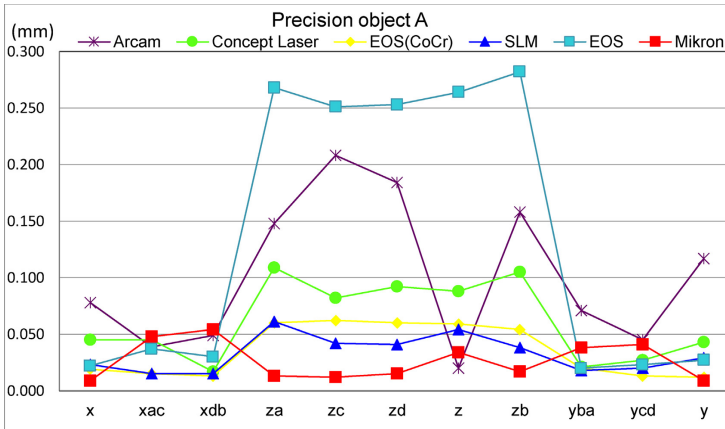


Fig. 3 – Precision chart for object A.

measurements showed that EOS had the least variance at 0.005 mm and Arcam the highest at 0.144–0.161 mm (Table 5, Figs. 5 and 6).

3.2.2.2. Y-axis. Mikron had the lowest precision, 0.153 mm in the y-axis and the highest precision at 0.006 mm. Arcam had the lowest accuracy, 0.243 mm and Mikron had the highest at 0.005 mm.

Regarding the precision variance in y, yl and yr, Mikron had the highest variance, 0.006–0.153 mm, while EOS had the least variance, 0.027–0.042 mm. Accuracy variance for the same measurements showed that EOS had the highest variance, 0.005–0.154 mm. The Concept laser had the least variance (–0.029)–(–0.010) (Table 5, Figs. 5 and 6).

3.2.2.3. Z-axis. Arcam had the lowest z-axis precision, 0.250 mm and Mikron had the highest precision at 0.017. Arcam had the lowest accuracy, –0.975 mm and SLM had the best accuracy at –0.005 mm.

Regarding the precision variance in zl, zr, cl, and cr, EOS had the highest variation, 0.073–0.194 mm, while Mikron showed the least variation, 0.045–0.017. Accuracy variance for the same measurements showed that Arcam ranged from –0.973 to 0.118 mm (Table 5, Figs. 5 and 6).

3.3. Objects A & B — angle measurements, precision and accuracy

The angle of objects A and B in the CAD was set to 16.000° (Figs. 1 and 2). Mikron showed the highest precision for object A within 0.004° deviation, Mikron and Arcam had the highest precision for object B within 0.002° deviation. Arcam showed the lowest precision for object A of >0.3° and Concept laser had the lowest precision for object B >0.09°. Mikron had the highest accuracy for object A with a 0.004° deviation, while

SLM had the highest accuracy at 0.002° deviation for object B. Arcam had the lowest accuracy for object A >1.0° and Concept laser for object B >–0.07°. (Tables 4 and 5, Fig. 7).

3.4. Object A & B — corner radius, precision and accuracy

The corner radius for objects A and B in the CAD was set to 0.01 mm. Mikron showed the highest precision for objects A and B at 0.034 and 0.011 mm, and the highest accuracy at 0.108 and 0.032 mm. Arcam had the lowest precision form for objects A and B at 0.078 and 0.076 mm and the lowest accuracy at 0.287 and 0.153 mm. (Tables 4 and 5, Fig. 7).

4. Discussion

Studies [22–25] have demonstrated that it can be impossible to obtain a passive fit and that a misfit always exists between implants and the manufactured superstructures they support. The lack of a method to clinically evaluate the passive fit of implant restorations means that there is no consensus regarding the machine tolerance needed for a clinically acceptable fit for implant constructions [23,25]. According to in vitro studies [27–30] discrepancy above a range of 0.100 mm could result in increased stress and the displacement of the implant superstructures. This demonstrates that implant-supported FDPs require a manufacturing process with an accuracy of <0.100 mm.

4.1. Accuracy and precision

An important factor is the ability of the machine to produce the same objects every time or to make the same consistent error. This means that the machine has continuity in

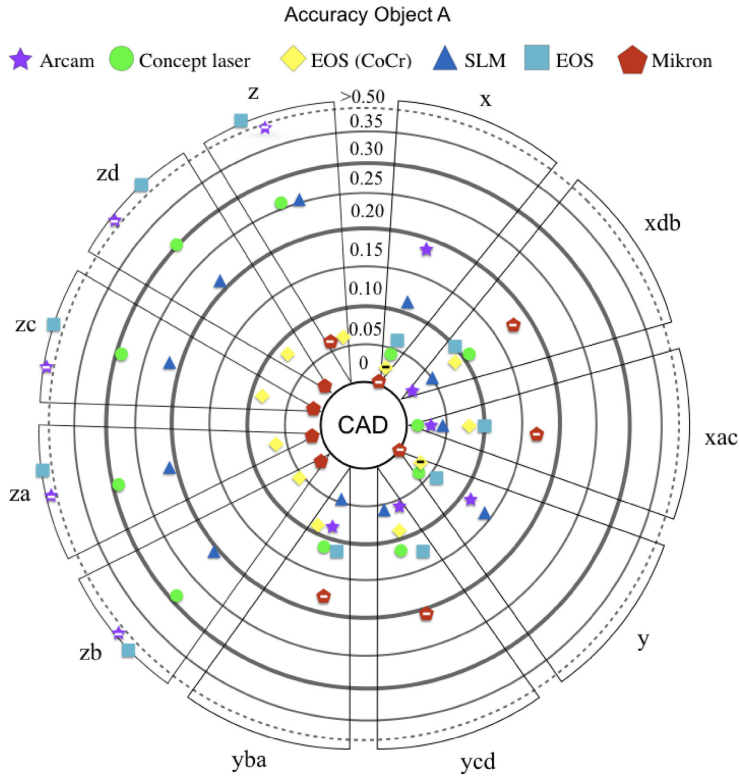


Fig. 4 – Bullseye chart for object A showing mean values regarding accuracy for each machine. The minus sign represents a negative measurement value. All the markers that are outside of the dotted line have a number greater than 0.050 mm. The markers close to the bulls-eye represent high accuracy or closeness to the original CAD design.

its production and this, in turn, equals high precision. These characteristics can be evaluated by producing multiple objects from the same machine and thereafter repeating the measurements on each object. A comparison between all the measurements and the measurements of the CAD files is then needed in order to calculate the level of precision. If the precision of a measured object is low, this means that the machine manufactures the object differently each time; this lack of precision will undoubtedly effect accuracy. However, if the level of precision is high, the manufacturing is consistent, but might not be as accurate as a CAD file. With this type of machine, which has a high level of precision, it is possible for the software to compensate for the CAD file in a different axis (X, Y or Z) in order to obtain greater accuracy. A good example of a high-precision and high-accuracy machine in the present study can be seen in Fig. 3, where it is clear that Mikron has high precision in x, and Fig. 4 shows that the same machine

also has high accuracy in x. However the same machine has a lower level of precision for xac and also lower accuracy for the same measurement.

4.2. Z-axis error

None of the objects produced with AM utilized supporting structures. Post-processing for all these objects involved cutting the metal object from the building platform. It is highly likely that the authorized personnel had difficulties removing the objects from the build plate without affecting the z-axis dimensions. Human error can have a huge influence at this stage, resulting in low levels of accuracy and precision. All the AM systems show lower levels of accuracy and precision in the z-axis measurements, but Arcam and EOS had the lowest level of accuracy and precision of all AM systems in the z-axis. The measurements in the z-axis for these two machines

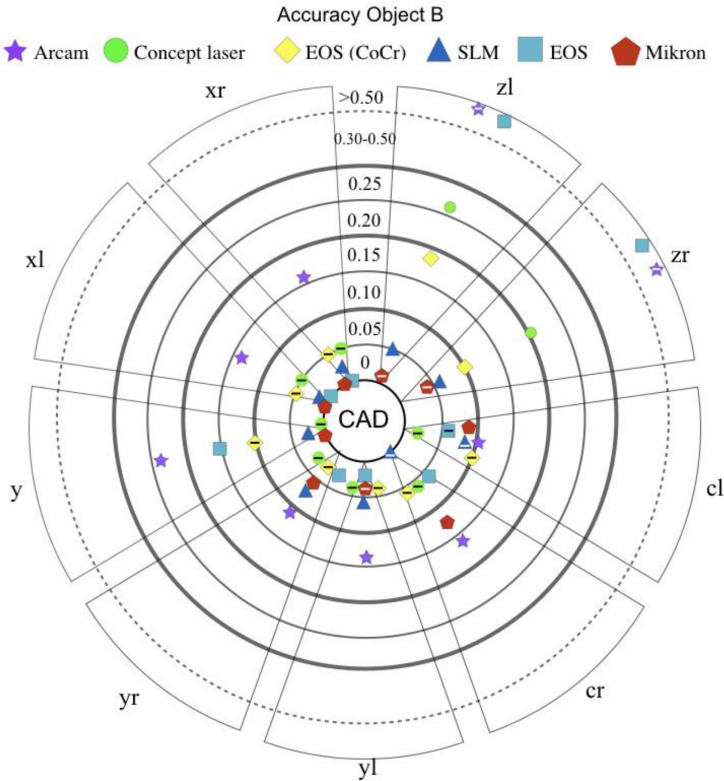


Fig. 5 – Bullseye chart for object B showing mean values regarding accuracy for each machine. The minus sign represents a negative measurement value. All the markers that are outside of the dotted line have a number greater than 0.050 mm. The markers close to the bullseye represent high accuracy or closeness to the original CAD design.

do not represent the capability of the machine to produce the objects in that specific axis, rather this shows the importance of avoiding the build of important geometries directly on the build plate. When focusing on the capability of the machine to produce geometries, the measurements cl and cr are the more reliable measurements in the z-axis since these are not affected when they are removed from the build plate. Even if we only focus on cl and cr as z-axis measurements, Arcam would still have the lowest precision (cr 0.140 mm), this might be due to the laser movement during processing, which results in an elevation on its perimeter. Arcam uses high electron beam energy and obtains a larger heat-affected zone (also known as melt pool) when compared to SLM, which uses a less powerful energy source. The melt pool also depends on the setting of the scan speed, beam diameter and bed temperature [21,26,27]. Hence, the larger heat-affected zone in EBM technology limits the recreation of the object's minimum fea-

tures, inferior resolution and surface smoothness [26,28,29]. Arcam production can be simplified into three steps: the first step involves preheating powder, the second is the contouring step, where the machines melts the powder in the perimeter at a low beam ampere and speed, thereby maintaining the part accuracy. The third step is the melting step of the powder at high velocity, where the beam has a 'zigzag-movement'. When the beam turns around in the perimeters, more heat is generated there. This results in a partial swelling at the perimeter due to the excessive heat generated there and consequently affects the dimension of the z-axis in objects A and B [30] (Fig. 9).

4.3. Calibration and validation

It is essential that the values of an object that the instruments measure are as true as possible. A non-validated instrument

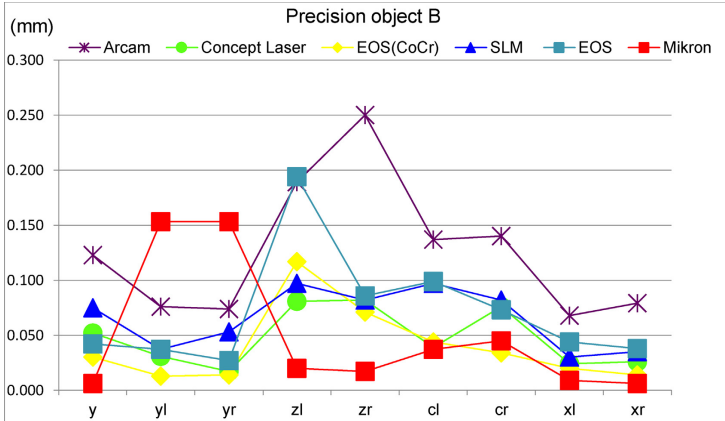


Fig. 6 – Precision chart for object B.

risks providing measurements that deviate from the actual values. This means that the instrument shows incorrect values with regard to the known distance of an object. As seen in Table 1, the calibration measurements of the calliper are

within the acceptable range of maximal deviation according to the recommendation of the gauge block fabricant.

It is of great importance to perform a calibration if more than one operator is executing the measurements in order

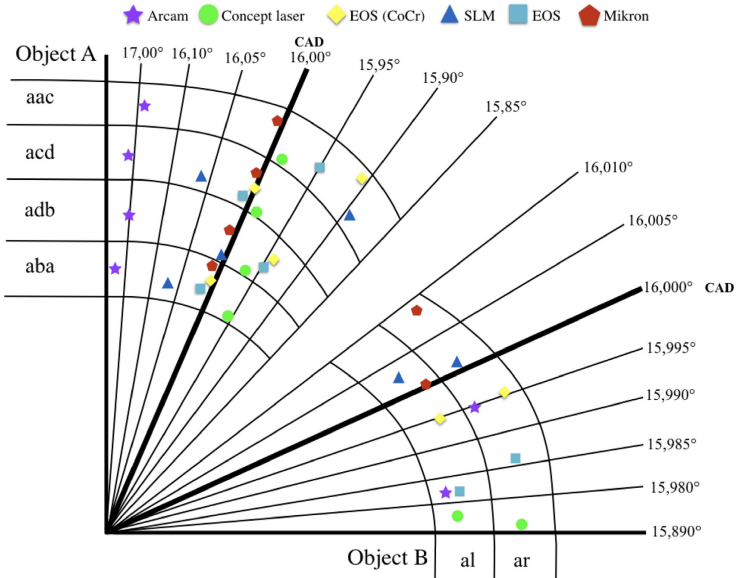


Fig. 7 – An overview of object A and B's mean values of angle measurements. The closer the markers are to the thick CAD line the higher accuracy.

Please cite this article in press as: Braian M, et al. Geometrical accuracy of metallic objects produced with additive or subtractive manufacturing: A comparative in vitro study. Dent Mater (2018), <https://doi.org/10.1016/j.dental.2018.03.009>

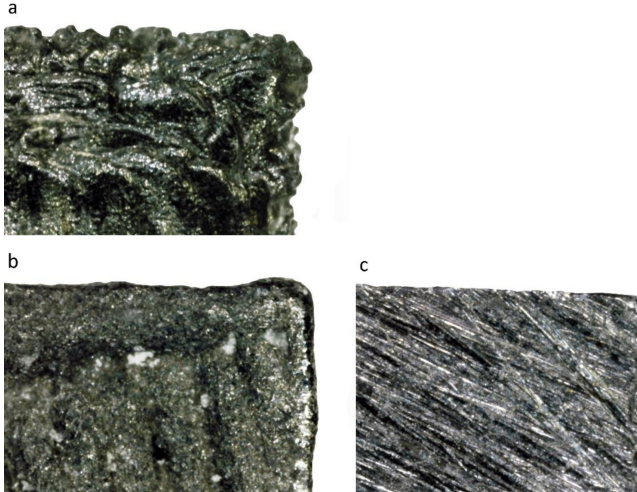


Fig. 8 – 250x magnification of one edge from object A manufactured by; (a) Arcam machine, (b) Concept laser and (c) SM group, Mikron. The CAD file has a 90° angle in this area.

to assure that both operators are measuring correspondingly. This is of importance in order to achieve significant results as well as assuring that a standardized method is used. Dahlberg's formula was chosen for calculating the calibration between the operators, due to the capability of the method to calculate small differences as shown in the present study. Furthermore, this formula also provides the possibility of estimating inter-observatory variability, which is considered beneficial [31]. All the values received with Dahlberg's formula can be seen in Tables 2 and 3. These values imply that the results are acceptable for the measurements carried out in the present study.

Moreover, a standardized method for the measurements was used; thus all measurements were conducted in a temperature stable environment, 20 ± 1 °C. The reason for using this method is its potential ability to control the expansion

and contraction of the metal material in the instruments as well as in the objects [32].

4.4. Linear measurements

With regard to objects A and B, Arcam had the highest variance in precision in all axes, ranging between 0.020–0.250 mm. EOS (CoCr) had the highest precision among all AM machines, 0.012–0.117 mm. Accuracy for Mikron demonstrates a consistency in almost all axes, except for some of the linear measurements on the x-axis and y-axis deviating from 0.005 to –0.210 mm. Mikron had a variance in precision within a range of 0.006–0.153 mm.

Regarding the measurement distances for object A, xac, xdb, yba and ycd Mikron showed constant lower values compared to the CAD file. Due to the sharp internal corners of

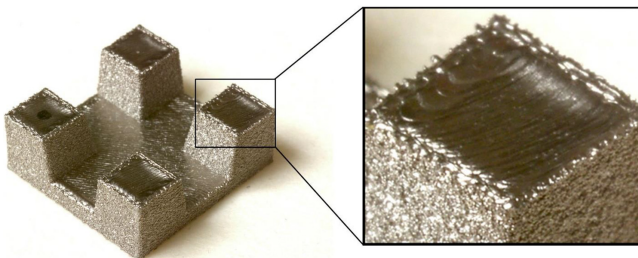


Fig. 9 – Photo of object A manufactured by EBM technology (Arcam), showing part-swelling at the perimeter of the “cubes”.

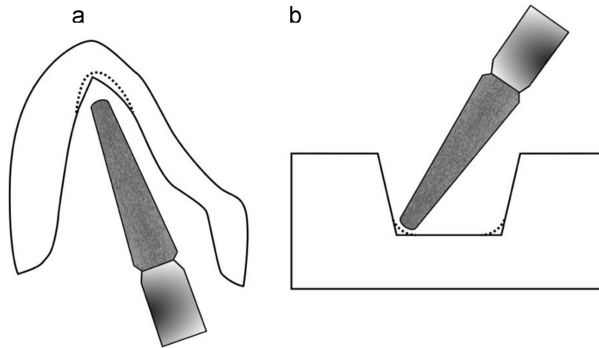


Fig. 10 – (a) Illustration of a designed crown in intersection. The black line illustrates the designed crown and the dashed line demonstrates the drill compensation. (b) Illustrates a side view of object A, the black line illustrates the designed object and the dashed lines demonstrate the drill compensation.

these measurements, the SM system had to compensate for the geometrical design. The SM machine was not able to reach the sharp internal corner without this drill compensation, which resulted in rounded corners that reduced distance for all four measurements (Fig. 10).

4.5. Degree and corner radius — additive manufacturing

The CAD file had an angle set to 16.000° . In this case, none of the AM groups had a substantial deviation from the CAD file, except for Arcam on object A; it was approximately $+1^\circ$ off in every angle measurement. Mikron showed an insignificant angle deviation. Mikron had highest corner radius precision: object A: 0.034 mm and object B: 0.011 mm. Mikron also had the highest accuracy for object A, 0.108 mm, and object B, 0.032 mm. A possible cause is that SM can recreate the angles close to the CAD file's dimensions, possibly because of the simplicity of the periphery geometries, an outer-corner shaper in this case. This leads to an uncomplicated toolpath and easy accessibility for the burrs.

AM groups generally had poorer accuracy compared to SM in re-creating a 90° periphery corner radius from the CAD file. Arcam had the least accuracy for object A, with a corner radius of 0.287 mm, and object B, 0.153 mm. Arcam also had the lowest precision for object A, 0.078 and object B, 0.076 mm. The reason for this might be the surface roughness of the object, which made it difficult for the person carrying out the test to see and measure the edges in the microscope (Fig. 8). The main principle in AM technique is layer-by-layer build up. When different geometries with angled or curved shapes are to be built in an AM machine, the 'staircase shape' (Fig. 11) is difficult to avoid and results in surface roughness and dimensional inaccuracy [33,34]. Staircase shapes depend on the size of powder particles, layer thickness, surface angle to the building platform and melt pool temperature [34,35]. This shape can be reduced if the layer thickness is thinner, if smaller powder

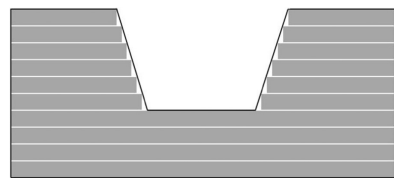


Fig. 11 – Illustration of object A in cross-section manufactured by AM technique. The black frame presenting the CAD-file boundary and the white triangles within showing the "stair case effect".

particles are used or if a reduced surface angle of the object is utilized. Consequently, the building time will be affected as well as the cost. Arcam, which uses EBM technology, has the largest layer thickness and powder particle size. This results in poor surface smoothness and poorer dimensional accuracy, as shown in this study. One major difference of the EBM technology is the production speed; it is faster compared to other AM techniques because of the ability to melt each layer and the underlying layer during the build process. This results in lower residual stress of the manufactured object; therefore there is no need for post-processing and heat treatment [33,35–37].

4.6. Production parameters for AM and SM

Both AM and SM machines requires setup before production. AM can produce multiple objects at the same time, utilizing a single setting. In the case of SM, the production of multiple objects requires several settings. These repeated settings increase the risk for production error. This is a possible scenario outcome for one sample in the SM group (object B), regarding the yl and yr linear measurements. AM machines also need to be optimized before usage of a specific pow-

der particle alloy size to avoid the decrease in resolution, strength properties, and production speed of the end product [36,38–40]. Layer thickness varies between different additive manufacturing units. It takes less time to manufacture objects built with thicker layers, nonetheless this could be less precise and accurate. However, smaller powder particles might generate higher accuracy, smoother surface and thinner layers [40,41]. Small powder particles may however generate other problems. For example, the powder can lose its flowability or become airborne, which, in turn, affects the AM machine's optics as well as deflecting the laser beam and damaging other moving parts [35]. The z-axis in AM corresponds to the layer thickness and has lower resolution compared to the x-axis and y-axis (build plane). The accuracy on the x-axis and y-axis depends on the build mechanism, which involves the machine's mirrors and the energy of the beam. The resolution of the mirrors determines the minimal dimension of the building parts, while the laser's diameter determines the minimum thickness [35].

Important parameters for SM settings are: approach position, angle of the burr, machine speed settings and tool selection [35,42]. Subsequently, the accuracy of a SM machine is determined by the diameter of the burrs and is similar in the x-, y- and z-axes. Subtractive methods can produce thin walls, however extreme vibrations and mechanical stress during milling process can cause dimensional distortions on thin edges [43,44].

Different parameters among AM machines can affect the end product. Low laser power in combination with low bed temperature results in better dimensional accuracy, but may also reduce the density and increase delamination. However, using a lower laser power requires a slower scan speed to assure fusion of the powder particles. All these parameters could potentially influence the dimensional accuracy, surface morphology, build rate and mechanical properties of the end product [35].

4.7. Geometries

An advantage of AM is the possibility of creating complex geometrics. AM has the capability to create hollow structures and sharp internal corners resulting in a geometry that is impossible to manufacture with SM [45,46]. This is due to burr size of the milling machine and the fact that it must be carried in a spindle. This, in turn, creates limited access for the burrs to the object's surface [47,48]. AM is not limited in the same way as SM and can easily create hollow and complex geometrical structures; a simple geometry like a cube would take the same production time to fabricate as other complex structures. AM techniques can split a complex 3D image from the CAD into a series of simple 2D cross-sectional images, interpretation consequently becomes easier [5]. This cannot be done as easily in SM as in AM, therefore the object is interpreted and machined in 3D. Simple geometries in objects A and B, such as cuboids and cone structures, can be relatively easy to process with SM. A more complex tool path is generated if the geometry becomes more complex. Such complex geometry can be, for example, undercuts and sharp internal corners. This can be difficult to produce with a milling machine, even with five or more axes [35]. Preparations in dentistry can contain com-

plex geometries such as sharp edges and thin structures. AM can create individual and customized geometries for every preparation, while the SM drill compensates for the complex geometries. For example, an abutment seat has geometries that are linear and regular. This type of geometry is more suitable for production with SM in order to obtain an acceptable fit between the fixture and abutment [28]. One other production parameter to consider is the software setting utilized by the authorized production personnel. The software functions and the operator experience could effect the outcome considerably.

4.8. Previous studies

A previous study [49] used the same method of measurement and had the same shaped objects. The previous study used plastic as the material of choice when producing the objects, while metal was the material of choice in the current study. Overall, results from the previous study compared with results from the current study show that the production of linear distances are produced more accurately and precisely in comparison to metal objects. However, the corner radius and the angle of the objects were more accurate and precise in the metal production.

5. Conclusion

Within the limitations of this *in vitro* study, the conclusion can be made that subtractive manufacturing presented overall precision on all measurements below 0.050 mm. If measurements za, zb, zc, zd z, zl and zr are disregarded, due to possible handling errors when removing the objects from the build plate, all the additive systems would have an overall precision below 0.140 mm, and the additive system with highest overall precision would be EOS (CoCr) with an overall precision below 0.050 mm. Bearing this in mind, the hypothesis was rejected and AM technologies could achieve precision and accuracy results close that of subtractive systems when creating geometries that are difficult to manufacture with SM technology. Due to the z-axis errors seen in the AM group, operators should avoid placing sensitive geometries directly on the build plate when utilizing additive manufacturing for metallic objects.

Acknowledgements

The authors report no conflict of interest related to this study.

We would like to thank: Arcam, Concept laser, EOS, SLM Solutions and Creatch medical for providing us with all the samples.

REFERENCES

- [1] van Noort R. The future of dental devices is digital. *Dent Mater* 2012;28:3–12.
- [2] Beuer F, Schweiger J, Edelhoff D. Digital dentistry: an overview of recent developments for CAD/CAM generated restorations. *Br Dent J* 2008;204:505–11.

- [3] Lebon N, Tapie L, Vennat E, Mawussi B. Research and education: influence of CAD/CAM tool and material on tool wear and roughness of dental prostheses after milling. *J Prosthet Dent* 2015;114:236–47.
- [4] Kikuchi M. The use of cutting temperature to evaluate the machinability of titanium alloys. *Acta Biomater* 2009;5:770–5.
- [5] Liu Q, Leu MC, Schmitt SM. Rapid prototyping in dentistry: technology and application. *Int J Adv Manuf Technol* 2006;29:317–35.
- [6] Koutsoukis T, Zinelis S, Eliades G, Al-Wazzan K, Rifaiy MA, Al Jabbari YS. Selective laser melting technique of Co–Cr dental alloys: a review of structure and properties and comparative analysis with other available techniques. *J Prosthodont* 2015;24:303–12.
- [7] Abduo J, Lyons K, Bennamoun M. Trends in computer-aided manufacturing in prosthodontics: a review of the available streams. *Int J Dent* 2014;2014(2014).
- [8] Örtorp A, Jonsson D, Moushen A, Vult von Steyern P. The fit of cobalt–chromium three-unit fixed dental prostheses fabricated with four different techniques: a comparative in vitro study. *Dent Mater* 2011;27:356–63.
- [9] Guo N, Leu MC. Additive manufacturing: technology, applications and research needs. *Front Mech Eng* 2013;8:215–43.
- [10] Kruth J, Mercelis P, Van Vaerenbergh J, Froyen L, Rombouts M. Binding mechanisms in selective laser sintering and selective laser melting. *Rapid Prototyp J* 2005;11:26–36.
- [11] Kruth JP, Levy G, Klocke F, Childs THC. Consolidation phenomena in laser and powder-bed based layered manufacturing. *CIRP Ann Manuf Technol* 2007;56:730–59.
- [12] Le Bourhis F, Kerbrat O, Hascoet JY, Mognol P. Sustainable manufacturing: evaluation and modeling of environmental impacts in additive manufacturing. *Int J Adv Manuf Technol* 2013;69:1927–39.
- [13] Al Jabbari YS, Koutsoukis T, Barmagadaki X, Zinelis S. Metallurgical and interfacial characterization of PFM Co–Cr dental alloys fabricated via casting, milling or selective laser melting. *Dent Mater* 2014;30:679.
- [14] Ivanova O, Williams C, Campbell T. Additive manufacturing (AM) and nanotechnology: promises and challenges. *Rapid Prototyp J* 2013;19:353–64.
- [15] Murr LE, Gaytan SM, Martinez E, Hernandez DH, Martinez L, Lopez MI, et al. Effect of build parameters and build geometries on residual microstructures and mechanical properties of Ti–6Al–4V components built by electron beam melting (EBM). 20th Annual International Solid Freeform Fabrication Symposium, SFF 2009 2009:374–97.
- [16] Chan KS, Koike M, Mason RL, Okabe T. Fatigue life of titanium alloys fabricated by additive layer manufacturing techniques for dental implants. *Metall Mater Trans A Phys Metall Mater Sci* 2013;44A:1010–22.
- [17] Murr LE, Gaytan SM, Ceylan A, Martinez E, Martinez JL, Hernandez DH, et al. Characterization of titanium aluminide alloy components fabricated by additive manufacturing using electron beam melting. *Acta Mater* 2010;58:1887–94.
- [18] Bian L, Thompson SM, Shamsaei N. Mechanical properties and microstructural features of direct laser-deposited Ti–6Al–4V. *JOM* 2015, 10p.
- [19] Thijs L, Verhaeghe F, Craeghs T, Humbeck JV, Kruth J. A study of the microstructural evolution during selective laser melting of Ti–6Al–4V. *Acta Mater* 2010;58:3303–12.
- [20] Fernández M, Delgado L, Molmeneu M, García D, Rodríguez D. Analysis of the misfit of dental implant-supported prostheses made with three manufacturing processes. *J Prosthet Dent* 2014;111:116–23.
- [21] Murr LE, Gaytan SM, Ramirez DA, Martinez E, Hernandez J, Amato KN, et al. Metal fabrication by additive manufacturing using laser and electron beam melting technologies. *J Mater Sci Technol* 2012;28:1–14.
- [22] Braian M, De Bruyn H, Fransson H, Christerson C, Wennerberg A. Tolerance measurements on internal- and external-hexagon implants. *Int J Oral Maxillofac Implants* 2014;29:846–52.
- [23] Eliasson A, Wennerberg A, Johansson A, Örtorp A, Jemt T, Faculty of Odontology, et al. The precision of fit of milled titanium implant frameworks (I-Bridge) in the edentulous jaw. *Clin Implant Dent Relat Res* 2010;12:81–90.
- [24] Hjalmarsson L, Örtorp A, Smedberg J, Jemt T, Institute of Odontology, Institutionen för odontologi, et al. Precision of fit to implants: a comparison of Cresco™ and ProCera™ implant bridge frameworks. *Clin Implant Dent Relat Res* 2010;12:271.
- [25] Örtorp A, Jemt T, Bäck T, Jälevik T, Sahlgrenska akademien, Institute of Odontology, et al. Comparisons of precision of fit between cast and CNC-milled titanium implant frameworks for the edentulous mandible. *Int J Prosthodont* 2003;16:194–200.
- [26] Cheng B, Chou K. Melt pool evolution study in selective laser melting. 26th annual international solid freeform fabrication symposium — an additive manufacturing conference, 2015. p. 1182–94.
- [27] Murr LSM, Gaytan E, Martinez F, Medina RB. Effect of melt scan rate on microstructure and macrostructure for electron beam melting of Ti–6Al–4V. *Mater Sci Appl* 2018;3:259–64.
- [28] H Gong, H Gu, K Zeng, J Dilip, D Pal, B Stucker. Melt pool characterization for selective laser melting of Ti–6Al–4V Pre-alloyed Powder. January 2014 solid freeform fabrication symposium. 256–267.
- [29] Thompson SM, Bian L, Shamsaei N, Yadollahi A. An overview of direct laser deposition for additive manufacturing: part I: transport phenomena, modeling and diagnostics. *Addit Manuf* 2015;8:36–62.
- [30] Algardh JK, Lausmaa J, Horn T, West H, Aman R, Harrysson O, et al. Thickness dependency of mechanical properties for thin-walled titanium parts manufactured by electron beam melting (EBM)®. *Addit Manuf* 2016;12:45–50.
- [31] Kim H. Statistical notes for clinical researchers: evaluation of measurement error 2: Dahlberg's error, Bland–Altman method, and Kappa coefficient. *Restor Dent Endod* 2013;38:182–5.
- [32] Tipler PA, Mosca G. Physics for scientists and engineers, 2008, 6th ed. New York: W.H. Freeman; 2008.
- [33] Murr LE, Quinones SA, Gaytan SM, Lopez MI, Rodela A, Martinez EY, et al. Microstructure and mechanical behavior of Ti–6Al–4V produced by rapid-layer manufacturing, for biomedical applications. *J Mech Behav Biomed Mater* 2009;2:20–32.
- [34] Mahamood RM, Akinlabi ET, Shukla M, Pityana S. Revolutionary additive manufacturing: an overview. *Lasers Eng* 2014;27:161–78.
- [35] Gibson J, Rosen DW, Stucker B. Additive manufacturing technologies [electronic resource]: rapid prototyping to direct digital manufacturing. 2010. Boston, MA: Springer Science + Business Media, LLC; 2010.
- [36] Rafi HK, Karthik NV, Gong H, Starr TL, Stucker BE. Microstructures and mechanical properties of Ti6Al4V parts fabricated by selective laser melting and electron beam melting. *J Mater Eng Perform* 2013;22:3872–83.
- [37] Sochalski-Kolbus L, Payzant EA, Cornwell PA, Watkins TR, Dehoff RR, Duty C, et al. Comparison of residual stresses in inconel 718 simple parts made by electron beam melting and direct laser metal sintering. *Metall Mater Trans A Phys Metall Mater Sci* 2015;46:1419–32.
- [38] Biamino S, Penna A, Ackelid U, Sabbadini S, Tassa O, Fino P, et al. Electron beam melting of Ti–48Al–2Cr–2Nb alloy:

- microstructure and mechanical properties investigation. *Intermetallics* 2011;19:776–81.
- [39] Song B, Dong S, Zhang B, Liao H, Coddet C. Effects of processing parameters on microstructure and mechanical property of selective laser melted Ti6Al4V. *Mater Des* 2012;35:120–5.
- [40] Safdar A, He HZ, Wei LY, Snis A, de Paz L. Effect of process parameters settings and thickness on surface roughness of EBM produced Ti-6Al-4V. *Rapid Prototyp J* 2012;18:401–8.
- [41] Farzadi A, Solati-Hashjin Mehran, Asadi-Eydivand Mitra, Noor Azuan AO. Effect of layer thickness and printing orientation on mechanical properties and dimensional accuracy of 3D printed porous samples for bone tissue engineering. *PLoS One* 2014;9(9):e108252, e108252.
- [42] Kruth J, Vandenbroucke B, Vaerenbergh VJ, Mercelis P. Benchmarking of different SLS/SLM processes as rapid manufacturing techniques. 2005.
- [43] Bravo U, Altuzarra O, López DL, Sánchez JA, Campa FJ. Stability limits of milling considering the flexibility of the workpiece and the machine. *Int J Mach Tools Manuf* 2005;45:1669–80.
- [44] Davies MA, Balachandran B. Impact dynamics in milling of thin-walled structures. *Nonlinear Dyn* 2000;22:375–92.
- [45] Upcraft S, Fletcher R. The rapid prototyping technologies. *Assem Autom* 2003;23:318–30.
- [46] Thompson MK, Moroni G, Vaneker T, Fadel G, Campbell RI, Gibson I, et al. Design for additive manufacturing: trends, opportunities, considerations, and constraints. *CIRP Ann Manuf Technol* 2016;65:737–60.
- [47] Zębala W, Plaza M. Comparative study of 3- and 5-axis CNC centers for free-form machining of difficult-to-cut material. *Int J Prod Econ* 2014;158:345–58.
- [48] So BS, Jung YH, Kurfess TR, Hwang SM. 5-Axis machining speed enhancement by step length optimization. *J Mater Process Technol* 2007;187–188:2–5.
- [49] Braian M, Jimbo R, Wennerberg A. Production tolerance of additive manufactured polymeric objects for clinical applications. *Dent Mater* 2016;32:853–61.

IV

JPD-18-334

RESEARCH AND EDUCATION

Trueness and precision of five intraoral scanners for scanning edentulous and dentate complete-arch mandibular casts: A comparative in vitro study

ABSTRACT

Statement of problem. Limited information is available on the trueness and precision of intraoral scanners (IOSs) for scanning dentate and edentulous casts.

Purpose. The purpose of this in vitro study was to evaluate the trueness and precision of 5 different IOS devices for scanning a dentate and an edentulous cast in a standardized way for short arches and complete arches.

Material and methods. Five IOS devices were used to scan 2 computer metric-measured (CMM) casts. Both were scanned 15 times. All scans were done by 1 experienced operator in a standardized way. One cast was edentulous, and 1 was dentate. Five cylindrical landmarks were added to each cast. These cylinders made the measurement of point-to-point distances possible, dividing the tests into cross-arch measurements and intercylindrical (short-arch) measurements. The Student *t* test, Mann-Whitney test, and Levene test for equality were used to calculate the difference between the edentulous and dentate scans for both cross-arch and intercylindrical measurements ($\alpha=.05$).

Results. For the cross-arch measurements on the edentulous scans, the trueness values ranged between 6 μm (Emerald P1-P2) and 193 μm (Omnicaam P1-P5) and for the intercylindrical measurements, between 2 μm (Itero P4-P5) and -103 μm (CS 3600 P1-P2). For the dentate cast, the cross-arch trueness values ranged between 6 μm (CS3600 P1-P2) and μm (TRIOS 3 P1-P5)

and for the intercylindrical measurements, between 4 μm (Itero P4-P5) and -56 μm (Emerald P4-P5).

Conclusions. Significant differences were found in scanning edentulous and dentate scans for short arches and complete arches. Trueness for complete-arch scans were <193 μm for edentulous scans and <150 μm for dentate scans. Trueness for short-arch scans were <103 μm for edentulous scans and <56 μm for dentate scans.

CLINICAL IMPLICATIONS

Care should be taken with complete-arch scans, since the precision is low for dentate scans and particularly low for edentulous scans. One observation from this in vitro study suggests that the tested IOS devices are reliable for digitizing short arches (16 to 22 mm) for both edentulous and dentate situations.

INTRODUCTION

Digital workflows in dentistry rely on different techniques: from data acquisition of the oral cavity with intraoral scanners (IOSs), to computer-aided design (CAD) in dental modeling software, to the use of additive and subtractive manufacturing systems for manufacturing restorations in materials ranging from polymers to monolithic ceramics. To control or adapt to errors in this workflow, each process in the workflow should be carefully studied. The current study focused on the trueness and precision of 5 IOSs used on a dentate cast and an edentulous cast. ISO 5725-1¹ was used as a reference for describing the terms accuracy, trueness, and precision. Trueness is described as the closeness of agreement between the arithmetic mean of a measured subject to a known or true value. Precision is described as the closeness of agreement

between test results. Test results that justify both trueness and precision are regarded as accurate. Precision is divided into 2 different groups: in the first group the subject is tested in the same way by the same operator and measuring equipment under the same conditions. This first version of precision tests repeatability. In the second version of precision, the conditions change. Thus, this part tests reproducibility. The combination of trueness and precision describes the accuracy of the test subject.

Several studies have shown that IOS devices have difficulty in scanning complete-arches accurately²⁻¹⁰ and this is even more problematic for edentulous areas.⁹ The main reason for enhanced errors on longer span scans could be the acquisition method found in most IOS devices. The scanners acquire images that are matched; a software process known as the best-fit algorithm stitches the images. To achieve a proper alignment, the scanned object needs a suitable geometry. If the scanned area has a simple geometry, the alignment of the images could cause errors. Typically, occlusal surfaces on molars and premolars present complex geometries with many anatomic details. Thus, these areas are easier to align compared with edentulous areas or the incisal edge of the mandibular anterior teeth.

As every overlapping image aligned with best-fit stitching could lead to an error, scanning longer spans would require more stitching and possibly lead to more errors.¹¹ To simplify the scanning of edentulous areas, landmarks can be added or objects with complicated geometries attached to the edentulous area to simplify the scanning procedure and improve the trueness of the virtual cast.¹² Several in vitro and in vivo studies have shown that prostheses made on shorter span scans could achieve trueness levels comparable with those of conventional impressions.¹³⁻¹⁷

The methods used to study the trueness and precision of IOS devices have varied, making comparison between studies difficult. Most of the studies used a master model that had been digitized either with tactile computer metric measurements (CMM) or with an optical reference scanner to obtain reference data as a virtual 3-dimensional (3D) file or as raw data. The physical cast was then scanned by the test scanners to obtain virtual casts, which were later compared with the virtual master model, and the measurements were recorded. Some studies present color map data with threshold colors to visualize and measure differences between 2 scans.

The current study used a different method: 5 cylinders were made as landmarks, making it possible to calculate only 5 points in the scan, instead of comparing thousands of points from the scan data. The cylinders were divided across 2 complete-arch mandibles; the first cast was dentate and the second edentulous. The purpose of this in vitro study was to measure the trueness and precision of the scanners for the 2 different arches; the null hypothesis was that no significant differences would be found within each IOS system for the 2 different arches.

MATERIAL AND METHODS

Two validation casts of a mandible were designed: one dentate and one edentulous. Each cast was supplied with 5 cylindrical landmarks. The casts were manufactured additively and measured with a computer metric measurement (CMM) system. From this step on, the casts were regarded as validation casts and were scanned using different IOSs; the virtual files from the scans were later measured, analyzed, and compared with the CMM data.

An intraoral scan of a complete-arch mandible was made with an IOS (TRIOS 3; 3Shape). The scan was exported as a standard tessellation language (STL) file and imported into CAD modeling software (Fusion 360 2017 v2.0.3800; Autodesk). In Fusion 360, 5 cylinders

were designed and placed axially onto the occlusion (Fig. 1A, B). The locations of the cylinders were as follows: second molars, second premolars, and one was placed lingually to the anterior teeth (Fig. 1C). The same cylinders were used for the edentulous mandible, and the teeth were removed using mesh modeling software (Fig. 1D) (Autodesk Meshmixer 2017 v3.4.35; Autodesk).

Before manufacturing, the validation casts were hollowed and evaluated for errors using data preparation software (Materialise Magics v13; Materialise). The casts were produced additively (ConceptLaser M-lab 100W; GE Additive) and manufactured directly on the build plate without support structures, at a layer height set to 30 μm . Remanium-Star-CL (Co 60.5%, Cr 28%, W 9%, Si15%) material powder was used. The casts were treated according to ConceptLaser recommendations for heat treatment after processing. The casts were not removed from the 90 \times 90 mm build plate. Finally, the casts were airborne-particle abraded with 250- μm aluminum oxide until a nonreflective surface was achieved.

The validation casts were measured with CMM equipment (O-inspect, 153862; Zeiss) by authorized personnel at an ISO 13485:2016 validated institution (Elos MedTech). The CMM machine registered the diameter of each cylinder and the plane at the top of the cylinders. The intersection between cylinder and plane results in an intersecting point. Furthermore, the CMM device measured the distances between each intersecting point for cross-arch P1-P2, P1-P3, P1-P4, P1-P5, and intercylindrical P1-P2, P2-P3, P3-P4, P4-P5 (Fig. 1A). The CMM measurements were regarded as true values (Supplemental Table 1).

Table 1 shows the scanners tested and provides information on the scan conditions, equipment, and software. Each system was used to scan each cast 15 times (n=15 for the dentate cast and n=15 for the edentulous cast) by the same operator (MB). Although some difference was

found between the scan protocols of the systems, all scans started at position 1 (Fig. 1C) and continued through positions 2, 3, 4, and 5. On some occasions, a corrective scan was needed to achieve a watertight (that is, data without holes) scan file. Usually these corrections correlated with the cylinders. The validation casts were fixed; only the ISO device was moved during scanning; there was a 10-minute interval between each scan. Three-dimensional measuring data were used for the quality control software (Gom Inspect 2017 Hotfix 4 Rev v106794; Gom). All 150 intraoral scans were measured in the same way. Figure 1D illustrates the construction of the fitting cylinders, fitting planes, and the intersecting point between the constructed cylinders, planes, and the 2-point measurements between the intersecting points. The best Gaussian fit was used as the fitting algorithm for the cylinders and planes.

The measurement data were exported to statistical software (IBM SPSS Statistics v25; IBM Corp) where calculations for the mean, precision, trueness, the 2-tailed independent Student *t* test, and the Mann-Whitney test ($\alpha=.05$) were carried out.

RESULTS

The results and calculations were divided into 2 parts: in the first part, the calculations focused on the cross-arch measurements P1-P2, P1-P3, P1-P4, and P1-P5 for both the edentulous and dentate cast, where point 1 was used as the anchorage, or starting point. In the second part, the calculations were conducted in the intercylindrical measurements P1-P2, P2-P3, P3-P4, and P4-P5. The measurement P1-P2 is the same for both groups. Supplemental Table 1 presents the CMM data, the precision and trueness for both cross-arch, and intercylindrical measurements for both the edentulous cast and the dentate cast. The Mann-Whitney test and the Student *t* test

showed conclusive data for all the statistical tests except for Omnicam P1-P5, P4-P5, and for CS 3600 P2-P3 ($P < .05$, Table 2).

For Omnicam, the cross-arch trueness data for Omnicam E ranged from 23 μm (P1-P2) to 193 μm (P1-P5), with precision levels from 22 μm (P1-P2) to 299 μm (P1-P5). The intercyindrical trueness data ranged from 16 μm (P4-P5) to 23 μm (P1-P2), with precision levels from 93 μm (P4-P5) to 22 μm (P1-P2). The cross-arch trueness data for Omnicam D ranged from 25 μm (P1-P2) to 67 μm (P1-P3), with precision levels from 6 μm (P1-P2) to 67 μm (P1-P5). The intercyindrical trueness data ranged from 14 μm (P4-P5) to 30 μm (P2-P3), with precision levels from 6 μm (P1-P2) to 16 μm (P2-P3 and P3-P4) (Supplemental Table 1, Figs. 2 and 3).

For CS 3600, the cross-arch trueness data for CS 3600 E ranged from -103 μm (P1-P2) to 181 μm (P1-P5), with precision levels from 66 μm (P1-P2) to 247 μm (P1-P5). The intercyindrical trueness data ranged from -16 μm (P4-P5) to -103 μm (P1-P2), with precision levels from 42 μm (P2-P3) to 66 μm (P1-P2 and P3-P4). The cross-arch trueness data for CS 3600 D ranged from 6 μm (P1-P2) to 38 μm (P1-P4), with precision levels from 17 μm (P1-P2) to 82 μm (P1-P5). The intercyindrical trueness data ranged from 3 μm (P4-P5) to 33 μm (P3-P4), with precision levels from 16 μm (P2-P3) to 14 μm (P3-P4) (Supplemental Table 1, Figs. 2 and 3).

For Emerald, the cross-arch trueness data for Emerald E ranged from 6 μm (P1-P2) to 163 μm (P1-P4) with precision levels from 96 μm (P1-P2) to 441 μm (P1-P5). The intercyindrical trueness data ranged from 6 μm (P1-P2) to -67 μm (P3-P4,) with precision levels from 38 μm (P2-P3) to 97 μm (P3-P4). The cross-arch trueness data for Emerald D ranged from -11 μm (P1-P2) to 129 μm (P1-P4), with precision levels from 17 μm (P1-P2) to 311 μm (P1-

P5). The intercyindrical trueness data ranged from -11 μm (P1-P2) to -56 μm (P4-P5), with precision levels from 17 μm (P1-P2) to 54 μm (P3-P4) (Supplemental Table 1, Figs. 2 and 3)

For Itero, the cross-arch trueness data for Itero E ranged from -30 μm (P1-P2) to -81 μm (P1-P5), with precision values from 17 μm (P1-P2) to 85 μm (P1-P5). The intercyindrical trueness data ranged from 2 μm (P4-P5) to -30 μm (P1-P2), with precision values from 14 μm (P2-P3) to 30 μm (P4-P5). The cross-arch trueness data for Itero D ranged from -11 μm (P1-P2) to -70 μm (P1-P4), with precision values from 25 μm (P1-P2) to 105 μm (P1-P5). The intercyindrical trueness data ranged from 4 μm (P4-P5) to 22 μm (P3-P4), with precision values from 10 μm (P4-P5) to 25 μm (P1-P2) (Supplemental Table 1, Figs. 2 and 3).

For TRIOS 3, the cross-arch trueness data for TRIOS 3 E ranged from 117 μm (P1-P4) to 36 μm (P1-P5), with precision values from 23 μm (P1-P2) to 94 μm (P1-P5). The intercyindrical trueness data ranged from 31 μm (P2-P3) to 94 μm (P1-P2), with precision values from 19 μm (P4-P5) to 23 μm (P1-P2 and P3-P4). The cross-arch trueness data for TRIOS 3 D ranged from 150 μm (P1-P5) to 40 μm (P1-P2), with precision values from 12 μm (P1-P2) to 76 μm (P1-P5). The intercyindrical trueness data ranged from 34 μm (P2-P3) to 46 μm (P3-P4), with precision values from 10 μm (P4-P5) to 17 μm (P2-P3) (Supplemental Table 1, Figs. 2 and 3).

DISCUSSION

The null hypothesis that no significant differences would be found for the 2 different arches in each IOS system was partially rejected. For the cross-arch measurements, 3 of 4 measurements were statistically significant for TRIOS 3 and CS 3600 when the edentulous cast was compared with the dentate one. At the same time, the Emerald scanner showed no significant difference for

the cross-arch measurement. For the intercylindrical measurements, CS 3600 showed overall significant differences, while differences for the other scanners only were partially significant. How many of the comparison studies used Itero Elements and how many used the older generation Itero is not clear. The Itero Elements scanner was launched in March 2015; for comparison purposes, studies before 2015 should be disregarded. The same problem arises for TRIOS and the Planmeca plan scan. 3Shape has released 3 generations of scanners and the one used in this study was TRIOS 3 (2015, third generation), Planmeca released the Emerald scanner in late 2017, and, to the best of the authors' knowledge, no similar studies are available for comparison.

A method comparable with that of the current study was used in a study by Muallah et al,¹⁸ where the authors measured the virtual files in a linear manner instead of superimposing 3D data. One of the linear measurements focused on the intermolar width of a maxillary master model; this measurement is similar to P1-P5 in the current study. The presented trueness results for TRIOS (version unreported) were 29.160 μm with a precision of 52.872 μm ; trueness for Itero (version unreported) was -47.030 μm with a precision of 84.137 μm . The current study found trueness data for Itero D (P1-P5) at -56 μm with a precision of 105 μm . Trueness for TRIOS D (P1-P5) was 150 μm with a precision of 76 μm . Van der Meer et al⁶ used 3 cylinders on their master model that were measured using tactile CMM. Two of the cylinders replaced the first molars and 1 replaced a mandibular anterior tooth; the measurements conducted in that study were comparable with P1-P3 and P1-P5 in the current study. The study concluded that trueness for Itero (pre-2015 version) was 70.5 μm (P1-P3) with precision values of 56.3 μm , and 61.1 μm in trueness for (P1-P5) with precision values of 53.9 μm . These values could be compared with data from this article for trueness data at -15 μm (P1-P3) and -56 μm (P1-P5),

with precision values of 37 μm (P1-P3) and 105 μm (P1-P5) for Itero D. Giménez al¹¹ studied the Itero scanner (pre-2015 version) using a comparable master model with cylinders as geometric landmarks. They also used tactile CMM equipment to assess true values. Several factors were evaluated, one of them being comparable to the Itero E cross-arch data from the current study. They reported that error increased with the increase in stitching, starting from -14.3 μm (mean deviation) with an $\pm\text{SD}$ of 25.6 μm to -32.0 μm (mean deviation) with an $\pm\text{SD}$ of 216.1 μm in the last quadrant scanned. The clear effect of the stitching processes producing errors proportional to the scan distance, as noted in this study, has also been documented in other studies.¹⁹⁻²¹

Even though there are limitations to the comparison with other studies with regard to measuring methods, IOS versions, and the shape, size, and material of the validation casts, it is clear that complete-arch scans pose a challenge to the IOS devices with regard to trueness but even more with regard to precision. The findings suggest that the trueness and precision of intercylindrical distances on the dentate cast for all IOS devices were $<50 \mu\text{m}$ (except Emerald D, P4-P5, -56 μm), with precision data $\leq 35 \mu\text{m}$ (except Emerald D, P3-P4, 54 μm). This suggests that the IOS devices are accurate for shorter arch acquisitions ranging from approximately 16 to 22 mm in length. In studying the cross-arch measurements, it is clear that the results are not as favorable for the dentate validation cast. The trueness for all IOS devices was $\leq 129 \mu\text{m}$ (except TRIOS D, P1-P5, 150 μm) and the precision $\leq 105 \mu\text{m}$ (except Emerald D, P1-P5, 311 μm), suggesting that the cross-arch measurement is less reliable than the intercylindrical measurement for the dentate cast. For the intercylindrical data on the edentulous validation cast, the IOS devices presented trueness values $\leq 94 \mu\text{m}$ (except, CS 3600, P1-P2, -103 μm) and precision values $\leq 97 \mu\text{m}$. This indicates that the intercylindrical measurement on

the dentate cast has almost twice the level of trueness and 3 times the level of precision when compared with the intercylindrical measurement on the edentulous cast. The trueness values for the cross-arch measurements on the edentulous cast were $\leq 193 \mu\text{m}$ and the precision values $\leq 299 \mu\text{m}$ (except Emerald E, P1-P5, $441 \mu\text{m}$). To validate whether these numbers are relevant for dentistry, a threshold value for different dental applications needs to be established. An accuracy level of $< 150 \mu\text{m}^1$ may be favorable for fixed tooth-supported prosthodontics. Ahrberget al¹⁵ studied the digital workflow for ceramic restorations for single units and 3-unit fixed partial dentures in vivo, concluding that it was more accurate than the conventional workflow. Their findings were supported by the data found in the current study, suggesting that the IOS devices are sufficiently accurate for shorter spans. Clinically acceptable tolerances for implant-supported, multi-unit restorations should be between 50 and 90 μm .²² This study focused on the accuracy of IOS devices but did not compensate for the computer-aided design of implant restorations or the manufacturing tolerances of selected manufacturing equipment, factors that will add dimensional changes to the definitive restoration. If 50 to 90 μm were used as a threshold, only short-arch spans would be suitable for scanning implants.

To calculate the fit of implant restorations, accuracy measurements of the total digital workflow are needed for IOS, CAD, and CAM. As the oral situation is affected by factors that could not be included in the current study design, one can only speculate that saliva, light conditions, soft and hard tissue reflections, humidity, intermittent acquisition, and movement of the soft tissue and tongue would affect the outcome of a similar study in vivo. Furthermore, an edentulous condition without implants would not have 5 cylinders aiding in the acquisition process. Therefore, in vivo studies with a similar approach are needed.

CONCLUSIONS

Within the limitations of this in vitro study, the following conclusions were drawn:

1. Complete-arch scanning had low precision, suggesting that the intraoral scanning devices are less reliable for complete-arch scans, especially for edentulous patients.
2. All scanners presented better accuracy compared with the complete-arch measurements when distances of approximately 16 to 22 mm were measured.

REFERENCES

1. International Organization for Standardization, ISO I. 5725-1: 1994, Accuracy (trueness and precision) of measurement methods and results – Part 1: General principles and definitions. Geneva. International Organization for Standardization 1994. Available at:
<https://www.iso.org/standard/11833.html>
2. Nedelcu R, Olsson P, Nystrom I, Ryden J, Thor A. Accuracy and precision of 3 intraoral scanners and accuracy of conventional impressions: A novel in vivo analysis method. *J Dent* 2018;69:110-8.
3. Imburgia M, Logozzo S, Hauschild U, Veronesi G, Mangano C, Mangano FG. Accuracy of four intraoral scanners in oral implantology: A comparative in vitro study. *BMC Oral Health* 2017;17:92.
4. Patzelt SB, Emmanouilidi A, Stampf S, Strub JR, Att W. Accuracy of full-arch scans using intraoral scanners. *Clin Oral Investig* 2014;18:1687-94.
5. Andriessen FS, Rijkens DR, van der Meer WJ, Wismeijer DW. Applicability and accuracy of an intraoral scanner for scanning multiple implants in edentulous mandibles: A pilot study. *J Prosthet Dent* 2014;111:186-94.
6. Van der Meer WJ, Andriessen FS, Wismeijer D, Ren Y. Application of intra-oral dental scanners in the digital workflow of implantology. *PLoS One* 2012;7:e43312.
7. Su TS, Sun J. Comparison of repeatability between intraoral digital scanner and extraoral digital scanner: An in-vitro study. *J Prosthodont Res* 2015;59:236-42.
8. Alikhasi M, Alsharbaty MHM, Moharrami M. Digital implant impression technique accuracy: a systematic review. *Implant Dent* 2017;26:929-35.

9. Ender A, Mehl A. In-vitro evaluation of the accuracy of conventional and digital methods of obtaining full-arch dental impressions. *Quintessence Int* 2015;46:9-17.
10. Mangano FG, Veronesi G, Hauschild U, Mijiritsky E, Mangano C. Trueness and precision of four intraoral scanners in oral implantology: A comparative in vitro study. *PLoS One* 2016;11:e0163107.
11. Gimenez B, Ozcan M, Martinez-Rus F, Pradies G. Accuracy of a digital impression system based on parallel confocal laser technology for implants with consideration of operator experience and implant angulation and depth. *Int J Oral Maxillofac Implants* 2014;29:853-62.
12. Kim JE, Amelya A, Shin Y, Shim JS. Accuracy of intraoral digital impressions using an artificial landmark. *J Prosthet Dent* 2017;117:755-61.
13. Ng J, Ruse D, Wyatt C. A comparison of the marginal fit of crowns fabricated with digital and conventional methods. *J Prosthet Dent* 2014;112:555-60.
14. Ueda K, Beuer F, Stimmelmayer M, Erdelt K, Keul C, Guth JF. Fit of 4-unit FDPs from CoCr and zirconia after conventional and digital impressions. *Clin Oral Investig* 2016;20:283-9.
15. Ahrberg D, Lauer HC, Ahrberg M, Weigl P. Evaluation of fit and efficiency of CAD/CAM fabricated all-ceramic restorations based on direct and indirect digitalization: a double-blinded, randomized clinical trial. *Clin Oral Investig* 2016;20:291-300.
16. Pradies G, Zarauz C, Valverde A, Ferreiroa A, Martinez-Rus F. Clinical evaluation comparing the fit of all-ceramic crowns obtained from silicone and digital intraoral impressions based on wavefront sampling technology. *J Dent* 2015;43:201-8.
17. Zarauz C, Valverde A, Martinez-Rus F, Hassan B, Pradies G. Clinical evaluation comparing the fit of all-ceramic crowns obtained from silicone and digital intraoral impressions. *Clin Oral Investig* 2016;20:799-806.

18. Muallah J, Wesemann C, Nowak R, Robben J, Mah J, Pospiech P, et al. Accuracy of full-arch scans using intraoral and extraoral scanners: an in vitro study using a new method of evaluation. *Int J Comput Dent* 2017;20:151-64.
19. Gimenez B, Pradies G, Martinez-Rus F, Ozcan M. Accuracy of 2 digital implant impression systems based on confocal microscopy with variations in customized software and clinical parameters. *Int J Oral Maxillofac Implants* 2015;30:56-64.
20. Flugge TV, Att W, Metzger MC, Nelson K. Precision of dental implant digitization using intraoral scanners. *Int J Prosthodont* 2016;29:277-83.
21. Patzelt SBM, Vonau S, Stampf S, Att W. Assessing the feasibility and accuracy of digitizing edentulous jaws. *J Am Dent Assoc* 2013;144:914-20.
22. Braian M, De Bruyn H, Fransson H, Christersson C, Wennerberg A. Tolerance measurements on internal- and external-hexagon implants. *Int J Oral Maxillofac Implants* 2014;29:846-52.

TABLES

Table 1. IOS related specifications. IOS, intraoral scanner; O, occlusal; L, lingual; B, buccal; W, wiggling (scanning in rocking manner)

IOS (Release)	Software	Acquisition	Device ID	Calibration	Case selection	Scan protocol	Export	Conditions	Notes
Omnicam Sirona (2012)	Sirona Connect 4.5.0.105736	Optical triangulation and confocal microscopy	Model 6371830	Sirona-ID	Acquisition	OLB	STL export on site	200 ansi lumen \pm 50 lumen. 21 \pm 1 degree	High resolution STL export
			S/N 138016	25782789					
Itero Element (2015)	Itero Element 1.5.0.361	Parallel confocal microscopy	RTC2017	No calibration presented by manufacturer	No restoration	OLBW	STL export of site	200 ansi lumen \pm 50 lumen. 21 \pm 1 degree	
			W10A076						
Planmeca Emerald (2017)	Planmeca Romexis 5.0.0.R	Multi-color laser scanning	REF 30006191	No calibration (only color calibration required)	No restoration	OLB	STL export on site	200 ansi lumen \pm 50 lumen. 21 \pm 1 degree	Model mode scanning
			S/N 410405						
Carestream CS 3600 (2016)	CS Imaging Software 7.0.3	Active speed 3D video	S/N FHNB0033	No calibration presented by manufacturer	Standard scanning	OWOLB	STL export on site	200 ansi lumen \pm 50 lumen. 21 \pm 1 degree	To finish the scan all mandibular teeth were selected
TRIOS 3 (2015)	TRIOS 2015-1 Design studio 1.4.7.4	Confocal microscopy	S/N 1WA1732S01015B	1AB1731TTA080B and 1KA1731188B (color)	Study model	OWOLB	STL export off site	200 ansi lumen \pm 50 lumen. 21 \pm 1 degree	

Table 2. Applied statistical methods. Significant difference in bold font ($P < .05$)

Statistical analysis for comparison of each cast ($P < .05$)									
		Cross-arch				Intercylindrical			
		P1- P2	P1- P3	P1- P4	P1- P5	P1- P2	P2-P3	P3- P4	P4- P5
Omnica	Mann-Whitney Sig. 2×(1-tailed Sig.)	.187	.187	.683	.021	.187	.137	.902	.026
	Student <i>t</i> test Sig. (2-tailed)	.688	.168	.972	.101	.688	.207	.664	.945
	Levene test for equality of variances	.001	.001	.005	.002	.001	.046	.062	.009
CS3600	Mann-Whitney Sig. 2×(1-tailed Sig.)	<.001	<.001	.217	.016	<.001	.037	<.001	<.001
	Student <i>t</i> test Sig. (2-tailed)	<.001	<.001	.449	.031	<.001	.078	<.001	.002
	Levene test for equality of variances	.001	<.001	.032	.011	.001	.007	.039	.027
Emerald	Mann-Whitney Sig. 2×(1-tailed Sig.)	.081	.174	.838	.539	.081	.026	.067	.098
	Student <i>t</i> test Sig. (2-tailed)	.503	.245	.651	.453	.503	.012	.075	.125
	Levene test for equality of variances	.009	.369	.876	.032	.009	<.001	.013	.004
Itero	Mann-Whitney Sig. 2×(1-tailed Sig.)	.010	.089	.325	.775	.010	.106	.002	.902
	Student <i>t</i> test Sig. (2-tailed)	.023	.081	.636	.498	.023	.202	.001	.905
	Levene test for equality of variances	.122	.225	.204	.760	.122	.902	.736	<.001
TRIOS 3	Mann-Whitney Sig. 2×(1-tailed Sig.)	<.001	.029	.174	.001	<.001	.267	.217	<.001
	Student <i>t</i> test Sig. (2-tailed)	<.001	.022	.113	.001	<.001	.561	.196	<.001
	Levene test for equality of variances	.007	.018	.885	.390	.007	.626	.173	.029

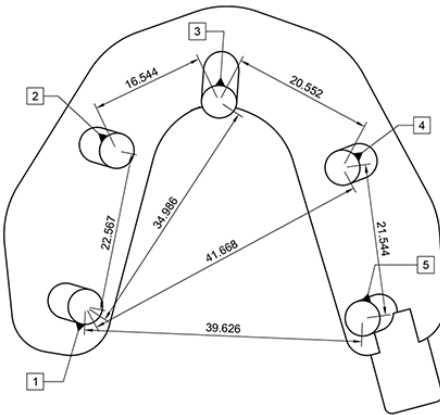
Supplementary Table 1. Calculated data from IOS devices for both casts

Units (mm)		Edentulous					Dentate				
Measurement	N	CMM	Mean	Precision	Trueness	N	CMM	Mean	Precision	Trueness	
Omnica											
Cross-arch	Point 1-Point 2	15	22.618	22.641	0.022	0.023	15	22.567	22.592	0.006	0.025
	Point 1-Point 3	15	35.020	35.061	0.070	0.042	15	34.986	35.053	0.015	0.067
	Point 1-Point 4	15	41.687	41.747	0.174	0.061	15	41.668	41.727	0.050	0.059
	Point 1-Point 5	15	39.566	39.759	0.299	0.193	15	39.626	39.685	0.067	0.059
Inter-cylindrical	Point 1-Point 2	15	22.618	22.641	0.022	0.023	15	22.567	22.592	0.006	0.025
	Point 2-Point 3	15	16.536	16.556	0.028	0.020	15	16.544	16.575	0.016	0.030
	Point 3-Point 4	15	20.568	20.585	0.044	0.017	15	20.552	20.575	0.016	0.023
	Point 4-Point 5	15	21.591	21.607	0.093	0.016	15	21.544	21.558	0.009	0.014
CS 3600											
Cross-arch	Point 1-Point 2	15	22.618	22.515	0.066	-0.103	15	22.567	22.573	0.017	0.006
	Point 1-Point 3	15	35.020	34.895	0.074	-0.125	15	34.986	34.995	0.018	0.009
	Point 1-Point 4	15	41.687	41.702	0.111	0.015	15	41.668	41.706	0.044	0.038
	Point 1-Point 5	15	39.566	39.747	0.247	0.181	15	39.626	39.653	0.082	0.027
Inter-cylindrical	Point 1-Point 2	15	22.618	22.515	0.066	-0.103	15	22.567	22.573	0.017	0.006
	Point 2-Point 3	15	16.536	16.520	0.042	-0.016	15	16.544	16.550	0.016	0.006
	Point 3-Point 4	15	20.568	20.508	0.066	-0.060	15	20.552	20.585	0.024	0.033
	Point 4-Point 5	15	21.591	21.537	0.061	-0.054	15	21.544	21.547	0.018	0.003
Emerald											
Cross-arch	Point 1-Point 2	15	22.618	22.624	0.096	0.006	15	22.567	22.556	0.017	-0.011
	Point 1-Point 3	15	35.020	35.099	0.115	0.079	15	34.986	35.025	0.061	0.039
	Point 1-Point 4	15	41.687	41.849	0.199	0.163	15	41.668	41.797	0.197	0.129
	Point 1-Point 5	15	39.566	39.711	0.441	0.145	15	39.626	39.665	0.311	0.039
Inter-cylindrical	Point 1-Point 2	15	22.618	22.624	0.096	0.006	15	22.567	22.556	0.017	-0.011
	Point 2-Point 3	15	16.536	16.598	0.038	0.062	15	16.544	16.570	0.035	0.026
	Point 3-Point 4	15	20.568	20.501	0.097	-0.067	15	20.552	20.539	0.054	-0.013
	Point 4-Point 5	15	21.591	21.574	0.093	-0.017	15	21.544	21.487	0.027	-0.056
Itero											
Cross-arch	Point 1-Point 2	15	22.618	22.588	0.017	-0.030	15	22.567	22.556	0.025	-0.011

	Point 1-Point 3	15	35.020	34.985	0.025	-0.035	15	34.986	34.971	0.037	-0.015
	Point 1-Point 4	15	41.687	41.628	0.053	-0.059	15	41.668	41.598	0.072	-0.070
	Point 1-Point 5	15	39.566	39.485	0.085	-0.081	15	39.626	39.569	0.105	-0.056
Inter-cylindrical	Point 1-Point 2	15	22.618	22.588	0.017	-0.030	15	22.567	22.556	0.025	-0.011
	Point 2-Point 3	15	16.536	16.525	0.014	-0.011	15	16.544	16.539	0.014	-0.005
	Point 3-Point 4	15	20.568	20.566	0.017	-0.002	15	20.552	20.573	0.018	0.022
	Point 4-Point 5	15	21.591	21.593	0.030	0.002	15	21.544	21.547	0.010	0.004
TRIOS 3											
Cross-arch	Point 1-Point 2	15	22.618	22.712	0.023	0.094	15	22.567	22.607	0.012	0.040
	Point 1-Point 3	15	35.020	35.120	0.033	0.100	15	34.986	35.061	0.021	0.075
	Point 1-Point 4	15	41.687	41.803	0.045	0.117	15	41.668	41.811	0.046	0.143
	Point 1-Point 5	15	39.566	39.602	0.094	0.036	15	39.626	39.776	0.076	0.150
Inter-cylindrical	Point 1-Point 2	15	22.618	22.712	0.023	0.094	15	22.567	22.607	0.012	0.040
	Point 2-Point 3	15	16.536	16.567	0.020	0.031	15	16.544	16.579	0.017	0.034
	Point 3-Point 4	15	20.568	20.605	0.023	0.037	15	20.552	20.598	0.015	0.046
	Point 4-Point 5	15	21.591	21.662	0.019	0.071	15	21.544	21.587	0.010	0.044

FIGURES

Figure 1. A, Occlusal view of CAD illustrating cylinder orientation. Dimensions from CMM measurements. B, Lateral view of CAD sketch illustrating cylinder design without cast. C, Profile view of assembled dentate CAD cast with cylinder abbreviations. D, Profile view of assembled edentulous CAD cast. Illustration of intersections between cylinders, planes, and intersecting points. CAD, computer-aided design; CMM, computer metric-measured.



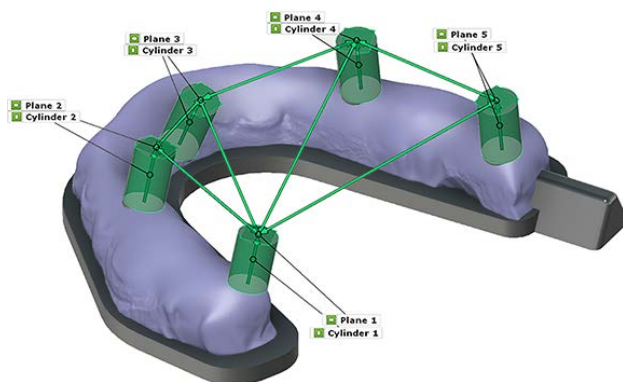
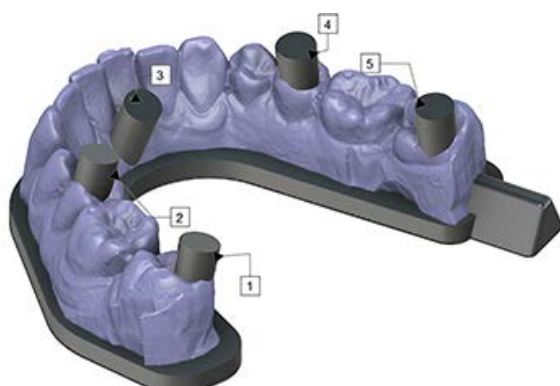
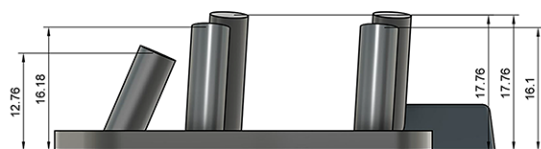


Figure 2. Cross-arch measurement deviations from CMM data (zero-line) for all IOS devices for each cast. CMM, computer metric-measured; IOS, intraoral scanner.

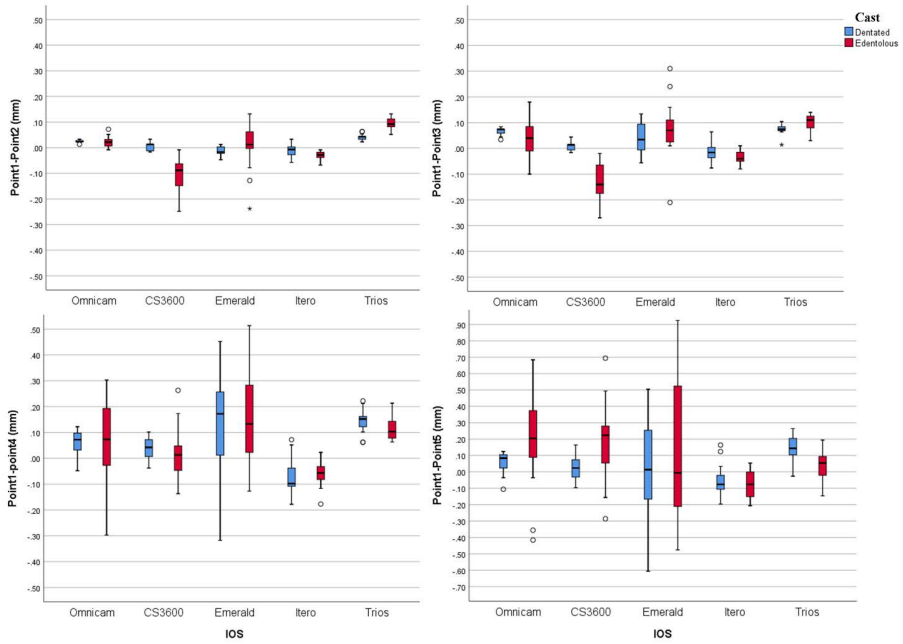
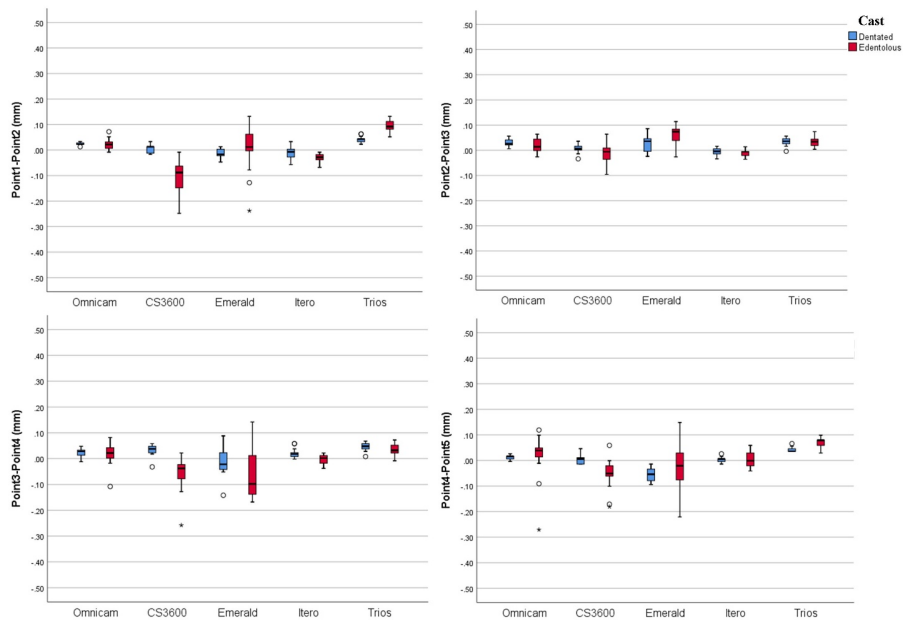


Figure 3. Intercylindrical measurement deviations from CMM data (zero-line) for IOS devices for each cast. CMM, computer metric-measured; IOS, intraoral scanner.



ISBN 978-91-7104-940-7 (print)

ISBN 978-91-7104-941-4 (pdf)

MALMÖ UNIVERSITY
205 06 MALMÖ, SWEDEN
WWW.MAU.SE